A RADIO SURVEY OF THE ORBITS OF METEORS

by

Carl Sigurd Nilsson

B.Sc.(Hons)

A Thesis

presented for the degree of

DOCTOR of PHILOSOPHY

at the

UNIVERSITY of ADELAIDE

(Physics Department)

October 1962

and May 1963

LIST OF PLATES

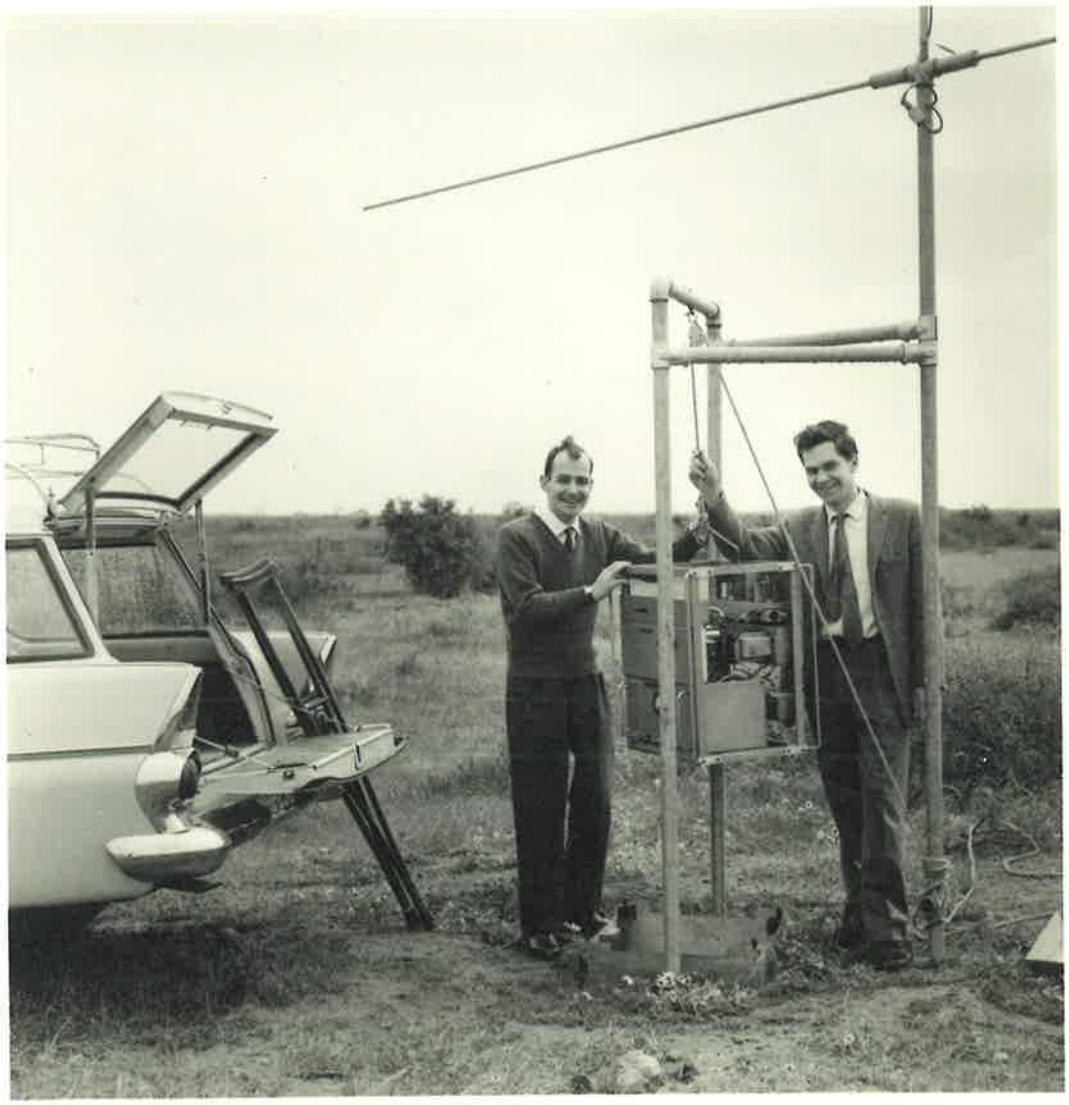

plate 1

CONTENTS

SUMMARY

This thesis presents the results of a radio survey of the orbits of 2101 meteors carried out at Adelaide during 1961. The limit of the survey was radio magnitude +6. To date it is the only survey in the Southern Hemisphere that has measured the orbits of individual meteors. A spaced-station c.w. technique was used which not only determines the direction of the meteor trail in space, but also its absolute position and motion under the influence of atmospheric winds. The presence of groundwave complicates the diffraction waveform observed with each echo, which is analogous to the optical diffraction pattern due to a moving straight edge. New reduction methods have been developed for these waveforms which take advantage of the availability of a large digital computer. Considerable attention has been paid to the accuracy of the results, especially with regard to the use of redundant data, and methods of improving on previous techniques have been developed. The output data from this survey is listed in detail in the Appendices.

In order to correct the observed results for observational selection it was necessary to determine the polar diagrams of the receiving and transmitting aerials. A method of doing this and the results so obtained are given in some detail. Methods of correcting the radiant for atmospheric retardation, trail drift due to winds, and the diurnal motion of the observer, are also presented.

The distribution of the meteor orbits in space is compared to the faint radio data of Davies and Gill (1960), whose survey in the Northern Hemisphere of meteors of radio magnitude +8 was the first to utilise radio methods of measuring the orbits of individual meteors, and the faint photographic data of McCrosky and Posen, which extends to magnitude +3. Considerable differences are found in the spatial distributions of the three surveys, which may be attributed to the different magnitude ranges observed. At magnitude +6 the orbits can be roughly divided into two classes. There is a large proportion of high eccentricity, direct, short-period orbits of low inclination with aphelia between Mars and Jupiter. There

is also a class of low eccentricity, short-period orbits with inclinations centred on 60° and 150°. The latter class becomes more pronounced with fainter magnitudes.

It was found that about 25% of the meteors observed could be classified as members of major or minor streams. The author has carefully considered the statistical significance of the small groups of meteors. All the groups observed are contained in the first class of meteors, i.e. those travelling in highly eccentric, low inclination orbits of short period. No streams were observed in the second class. In order to account for the observed features of the spatial distribution of the second class of meteors, the author has put forward the hypothesis that these meteors have resulted from ejection from long-period comets.

A possible association is advanced for a minor shower in Scorpius during December with the lost comet Lexell 1770 I. Some of the streams listed in this thesis with radiants south of the ecliptic have not been previously detected.

In addition to the Adelaide survey, the author has included the results of astronomical interest obtained from a meteor radar he installed and operated during 1957 at Mawson, on the Antarctic continent.

ORIGINALITY

To the best of the author's knowledge this thesis contains no material previously published or written by another person, except where due reference is made. It contains no material which has been accepted for the award of any other degree or diploma in any University, except where due reference is made.

Adelaide University

8/5/63

(Carl Nilsson)

ACKNOWLEDGEMENTS

The two projects discussed in this thesis required the work and help of many people. Professor L.G.H. Huxley was responsible for both the Mawson and the early stages of the Adelaide survey, and the author would like to acknowledge the interest and help given by him. The study of upper atmospheric winds at Mawson was a joint undertaking by the University of Adelaide and the Australian National Antarctic Research Expedition, who under Mr. P.G. Law, provided both facilities and finance as well as the difficult logistics for such an experiment. The latter were so important to the success of the project, and are so often taken for granted. The Radio Research Board also provided finance to build and maintain the equipment. The design and construction were undertaken by Dr. W.G. Elford and Mr. E.L. Murray, of the University of Adelaide, and the author also wishes to thank Messrs. E. Burnett, I. Bird and G. Cresswell for operating the equipment during parts of 1958 and 1960.

The Adelaide survey was planned and initiated by Dr. A.A. Weiss, C.S.I.R.O., who has maintained an unfailing interest in all stages of the survey, despite his shift to Sydney at the end of 1960. The second Chapter of this thesis is virtually a copy of a paper presented jointly by him and the author in the Australian Journal of Physics, 1962. His knowledge and experience in many phases of meteor astronomy has guided the author from the very beginning of this thesis. Dr. W.G. Elford heads the Adelaide Meteor Group, and as the author's supervisor for this project he deserves especial thanks. His ever friendly help and advice were appreciated more deeply by the author than he probably realises. The author also appreciates the help given to the project by Professor J.H. Carver, appointed to the Chair of Physics at Adelaide in 1961.

The building of the equipment for the Adelaide survey was very much a group effort, in which the author but played a part.

Dr. W.G. Elford, Dr. E.L. Murray and Mr. R.G. Roper were responsible for the design and construction of the receiving station, the larger portion of the equipment being built by Mr. J. Welsby. The author's particular thanks must go to Mr. R.G. Roper, who as a fellow research student, was jointly concerned with the outstations and the running of the equipment. The electrical design and construction of the two outstations and attendant V.H.F. links must be credited to him. The film reading and computing facilities provided by the Weapons Research Establishment made the data reduction methods given in this thesis possible. Thanks are also due to Mr. J.R.G. Morris of Armstrong-Whitworth Aircraft Ltd., who developed a solution to the spaced-station problem.

Credit must be given to the work of J.H. Mainstone, who presented the basic c.w. reduction principles in his thesis, 'Radio Measurements of Meteor Velocities', and to Mr. J. Gascoigne, who was responsible for the mechanical construction of the Tape Delay Unit. Credit too, must be given to the members of staff who worked on the data reduction, particularly to Miss M. Chapman whose careful film reading was much appreciated. The endless task of punching data cards was performed so cheerfully by the staff of the University Computing Centre, under Mr. D. Simmonds, that their names are perpetuated by the subroutines of the main reduction program.

Finance for the Adelaide survey was provided by the Radio Research Board and a University Research Grant. The author worked on a General Motors-Holden's Pty. Ltd. Post-Graduate Research Fellowship for the period 1959-61, and a C.S.I.R.O. Senior Fellowship for the first six months of 1962.

CHAPTER 1

INTRODUCTION

The current expansion of Sun-Earth astronomy has led to a relatively recent increase in interest being taken in the distribution of dust particles in the Solar system. Besides the continued need for this knowledge to augment and satisfy theories concerning the evolution of the earth and its environment, adequate mapping of meteoroid streams is necessary for the planning of interplanetary space probes.

Dust particles range in size from the large meteorites which occasionally strike the Earth to the large quantities of submicron dust which is continually settling on our planet. By studying the orbital distributions of the particles which encounter the Earth we can hope to build up a picture of the distribution of this matter in interplanetary space. Due to their large surface area/mass ratio, particles less than about 10μ decelerate in the Earth's atmosphere without being evaporated by the influx of kinetic energy from molecular collision. Particles much larger than 1 inch in diameter can also often reach the ground with only superficial melting. These are known as meteorites. The comparative rarity of the latter makes it extremely difficult to obtain any significant information concerning their distribution in space. It is only with the recent advent of satellite detectors that the micrometeoroid orbits can be studied, and even now, such study can only be done on a statistical basis. Individual micrometeoroid orbits have not yet been determined.

The intermediate particles which evaporate before reaching the Earth have, paradoxically, been the easiest to study. These are known as meteors, and visual observations of the trails of ionised gas trails they leave in the nighttime sky date back to biblical times.

The most spectacular displays of meteors occur when the Earth encounters meteor streams, and most of the early studies were

concentrated on these so called "showers". Professor Olmstead of Yale University was one of the observers of the famous Leonid shower of 1833. It was he who noted that all the meteors appeared to emanate from the same part of the sky, in the constellation Leo, from which the stream now gets its name. He concluded that the meteors must be travelling in parallel paths, and the apparent divergence in the sky was an effect of perspective.

The point in the sky from which the meteors appear to come is known as the "radiant", and visual and telescopic observations of meteor radiants have now been systematically made for over one hundred years. In the few cases where the periodicity of a shower is apparent, the orbit can be determined. During the last century the orbit of the Leonid meteors was noted to coincide closely with that of Comet 1866 I, and so began the long and still present questioning into the precise nature of the association between comets and meteor streams. Photographic observations now enable both the radiant and the velocity of individual meteors to be determined, and in the last few decades considerable knowledge has been accumulated concerning the orbits of meteors. One of the most controversial issues has been whether or not sporadic meteors (the term loosely applied to those meteors that do not appear to be members of a stream) move in elliptical orbits and are members of the solar system or move in hyberbolic orbits and thus come from another star. Present evidence is that no meteors have yet been detected that were not members of our solar system, although slightly hyperbolic orbits do exist due to perturbations from planets such as Jupiter.

In recent years the development of radio techniques has greatly extended the study of meteors. The trail of ionised gas left by the passage of the meteor is quite an efficient reflector of high frequency radio energy. Range can be easily determined from a single station radar, whereas a parallactic technique is necessary for range determination in photographic studies. Most important of all, radio observations can be made not only at night, but also during the day, and the observations are independent of

the prevailing weather conditions.

This thesis presents the results of the radio survey of the orbits of meteors undertaken at Adelaide during 1961. The survey is unique in a number of ways, but primarily in that it is the only survey in the Southern Hemisphere that has measured the orbits of individual meteors. Several surveys of this type have been undertaken in the Northern Hemisphere, but these have not been able to include the radiants much south of the Equator. The survey is also unique in that it is the only one that has utilised c.w. techniques rather than using radar equipments. The observational method is basically as follows: The trail of ionised gas left by the meteor is an effective reflector of r.f. energy at 27 mc/s. The echo received at a ground station as the trail is being formed is analogous to the optical diffraction pattern due to a moving straight edge. The diffraction waveform can be used to determine the velocity of the meteor, while the precise time of arrival of the echo at each of three receiving stations depends on the ground geometry of the transmitter - receiver system. Thus the direction cosines of the meteor path can be obtained by measuring the time differences between the echoes at the various receiving sites. The point on the trail such that the r.f. path length is a minimum is known as the specular reflection point, and has the same properties as the analogous point in optical theory, viz, the integrated reflected radiation from the trail can be considered to emanate from this point. In this thesis it is often referred to as the 't_o' point (see Figure 3.2).

Davies and Gill (1960) at Jodrell Bank used a 100 kW radar, and with no groundwave injection at the receiving sites they were not able to determine the position of the specular reflection point in space; that is, they did not know exactly where each echo came from. The Adelaide survey is similar to theirs in that it makes use of the diffraction echo at three spaced stations to determine the direction cosines and velocity of the meteor trail; however, it has the added advantage of being able to uniquely determine the

position of each specular reflection point in space. Thus not only the direction, but also the absolute position in space of the ionised trail left by the meteor is known. This is being utilised in the study of upper atmospheric winds, the study of turbulence and the study of the ionisation distribution along the trail.

Whipple (1954) published the orbit of 144 meteors of magnitude zero and brighter. He found that there were no meteors for which the semi-major axis was less than 1 a.u. and that the orbits were predominantly direct and of low inclination. More than 50% of the orbits were associated with showers.

A survey of 300 meteors photographed at Harvard by a Super-Schmidt camera has been published by Hawkins and Southworth (1958). Because these observations could only be made at night, a large part of the celestial sky was not available for observation. However, the data showed a marked concentration of radiants approximately opposite the Sun on the ecliptic, besides an apparent concentration at the apex of the Earth's Way. The data also gave valuable information concerning the physical processes acting during the ablation of the meteor in the atmosphere. Hawkins (1956) used the early Jodrell Bank radar data to fill in the region near the Sun. He found that the daylight meteor activity provided a third concentration of radiant on the ecliptic near the longitude of the Sun. The survey of 2,500 meteor orbits undertaken at Jodrell Bank by Davies and Gill was a major advance, and covered meteors down to the eighth radio magnitude. In many respects this survey confirmed the photographic results of Hawkins and Southworth, particularly in the distribution of meteor radiants with ecliptic longitude. As other workers had found (e.g. Weiss 1957) using various statistical techniques, the distribution could be approximated by three sources on the ecliptic: one at the Apex of the Earth's Way, due to the motion of the Earth, and two sources symmetrically placed 68° either side of the Apex. These were known as the Sun and Antisun sources. Of these, the visual observers could only study the Apex and Antisun components. The results of Davies and Gill differed from the optical results, however, in that they found a large proportion of echoes were of short period, with the reciprocal of

the semi-major axis, 1/a, between 1.0 and 2.0 a.u.$^{-1}$. The brighter photographic meteors were all of longer period, 1/a<1.0 a.u^{-1}.

McCrosky and Posen (1961) have given the distribution of 1/a for 2529 Super Schmidt meteors of third magnitude and brighter. The distribution extends a little beyond 1/a = 1.0 a.u.$^{-1}$, showing that the proportion of short period orbits increases with fainter magnitudes. The Adelaide survey covered meteors of radio magnitude +6, and the limit of the distribution of 1/a is between that of the photographic observations and those of Davies and Gill. The latter have just completed a survey extending to magnitude +4. The distribution of 1/a, together with the distribution for this survey, shows that there is a smooth transition between the photographic distributions and those for eight radio magnitude meteors. A detailed examination of the orbital distributions is made in Chapter 10 and 13, and we are able to show that some differences do exist between the various surveys, particularly between the photographic and radio results. The question of whether these differences are due to observational selection or are real differences due to the varying magnitudes of the meteors observed is also discussed in these chapters.

The survey of the various shower radiants given in Chapter 11 is of particular interest. The conclusion that about 25% of the total number of meteors observed can be associated with streams is in direct comparison to the figure of 3% suggested by Davies and Gill. It has been noted, however, by previous workers (e.g. Kaiser 1953) that the importance of showers diminishes with fainter magnitudes. The Adelaide results emphasise the need for more sophisticated analysis in classifying meteors as members of a stream. The terms 'sporadic' and 'shower type' meteors do not appear to have much meaning if one takes the picture of an isolated meteor being the only member detected of a minor stream, rather than being in an isolated orbit all by itself. The results presented here show an ever increasing number of orbit groups with smaller numbers, down to many pairs of meteors with nearly identical

orbits. The necessity to consider the statistical significance of these small groups led the author to the method of grouping considered in Section 11.3. This, with the consideration of chance groups, is probably the most sophisticated search for minor showers yet conducted for radio data. The final analysis of these minor showers has not yet been completed, but the tentative lists given in Chapter 11 certainly contain all the more intense streams detected by this survey during 1961.

The early chapters of this thesis are devoted to outlining the equipment used and explaining the methods of reduction employed. Considerable attention is given to the methods of 'improving' the data by making use of redundant information. Any future work of this type should use four out-stations, rather than merely the three essential for the unique reduction of the trail direction cosines. The added accuracy the extra information would provide to the data would more than outweigh the additional expense and effort required to maintain the equipment. The receiving site used for the Adelaide survey was very good and the receivers were able to operate near their optimum noise levels; the employment of c.w. techniques meant that narrow bandwidths could be used. However, the transmitter power was low by contempory standards, only about 250 W into a low gain antenna. This meant that in order to collect a statistically significant number of meteors the equipment had to run for over a week every month, and more important still, the reduction had to include many poor quality echoes with barely distinguishable diffraction waveforms. It speaks highly for the power of the reduction methods used that the system was able to cope successfully with echoes such as the one shown in Figure 5.6a. However, including echoes of this quality must invariably cause the accuracy of the output data to deteriorate, no matter how one makes use of redundant information in their reduction.

Although a c.w. equipment for measuring meteor orbits is simpler than the equivalent radar, the reduction of the echoes obtained is much more complicated. This is due to the presence of groundwave, which is usually lacking in the radar observations.

Consequently , the radar Fresnel diffraction waveform is essentially the same for every meteor of a given velocity and range. Not so in the c.w. case with direct groundwave present, however, as the diffraction waveform depends quite strongly on the relative phase between the skywave and groundwave (McKinley 1951). As this phase angle is dependent on time and on the upper atmospheric winds present, each echo must be considered individually. The author feels that he has made considerable progress in this field by utilising the whole waveform, and making a least - squares fit to the data in the manner described in Chapter 5, rather than merely choosin several points as has been done in the past. This improved analysis is the result of having available a modern computor such as the I.B.M 7090; one would never attempt to use these procedures with only a desk calculator.

In Chapter 7 the author describes an attempt to measure the polar diagram of the transmitting antenna. There was nothing remarkable about the antenna itself, a three element Yagi pointing at the zenith, but the necessity to keep it low to limit the groundwave at the receiving site also necessitated the antenna being in close proximity with the guttering and other metallic incidentals attached to the Physics department. In such circumstances it has been normal practice to assume the polar diagram and hope for the best. The author is not sure that he has improved on this procedure by a great deal, but at least the attempt was made and the detailed results are set out for the reader in this chapter. Certainly as a result of the experiment more reliance can be placed on the weighting program that corrects the observed results for observational selection.

Chapter 2 refers to data on meteor rates which were gathered outside this survey. These are the results of astronomical interest obtained so painstakingly by the author from a meteor radar at Mawson, on the Antarctic continent. The equipment was designed by Murray (1961) to measure winds in the upper atmosphere. The author helped build the equipment, took it down and installed it on the Antarctic coast during 1957, and,with the help of A.A.Weiss , was

able to show that the diurnal rate variation was not inconsistent with a three source distribution of meteor radiants on the ecliptic. These results have been published in a paper by Weiss and the author (1961). The study was plagued by an unfortunate variation from the normal in the antenna polar diagrams, which only became apparent after the data had been reduced. The local noise level at Mawson was so high that in spite of the much greater (5 kW) transmitter power, the limiting line density of detectable meteor trails was about 3.10^{11} electrons/cm. This corresponds to radio magnitude +6, so, rather fortuitously, both surveys cover the same magnitude range of meteors, and the Adelaide survey results can be immediately applied retrospectively to the Mawson data. The theoretical rates predicted in Chapter 2 for Mawson were based on the assumed equality of the Sun and Antisun sources on the ecliptic. This assumption has been strikingly invalidated by the results shown in Chapter 10, at least for the months July to October. As McKinley (1961) has remarked in discussing this approach to the meteor distribution problem:

> "..... the answer, when compared with observations, tends to indicate what the distribution is not, rather than to determine what it is."

However, despite the somewhat disparaging remarks about the Mawson data, the author feels that it is certainly worth including, even if only for the data concerning the possible action of the ionosphere on the observed meteor rate. The observations of T.C. Poulter (ref. McKinley 1961) of Stanford Research Institute during the second Byrd Antarctic Expedition 1933-1935, who observed visual rates varying from 30 to 1000 meteors/hr, are brought to mind when the Mawson radio rates for the summer of 1957-58 are studied. The sudden increases in rate during that period were certainly not observed at Adelaide.

Finally, as this thesis is being submitted for a Ph.D. degree, the author would like to state that all the work contained herein is his own, except where otherwise acknowledged. A.A. Weiss wrote Section 4 of Chapter 2, but it is included for completeness. The author spent part of 1956 helping to build the Mawson

equipment, and all of 1957 installing and operating it. Part of 1959 and 1960 was taken in presenting the data from Mawson, but in the main those years were spent in building the Adelaide equipment and in initiating the reduction procedures. The Adelaide observations were made during 1961 and the main reduction program listed in Appendix 5 for the I.B.M. 7090 computor was developed during this year. All the programs in Appendix 5 were written by the author for this computor. The bulk of the data was read during the first half of 1962 and computed shortly afterwards.

All aspects of the survey have not been completed. The author is at present (April 1963) continuing the work on the accurate delineation of the minor streams. Also, estimates of mass for about 50% of the meteors detected in this survey will shortly be available, and some of the distributions discussed in Chapter 10 and 13 will be further analysed with the aid of this extra information.

CHAPTER 2

RADIO-ECHO OBSERVATIONS OF METEORS IN THE ANTARCTIC

2.1 Introduction.

Radio observations of meteors have been made at Mawson (68°S., 67°E.) on the Antarctic coast between 1957 and 1961. The equipment used is a coherent pulse radar with the following characteristics:

p.r.f. = 750 c/s	f = 34 Mc/s
pulse length = 15 μs	peak pulse power = 5 kW.

The antennas are $\frac{1}{2}\lambda$ dipoles $\frac{1}{4}\lambda$ above an earth mesh, and supported near the ends by vertical piping. A double pulse discriminator system is used to improve the signal/noise ratio, but the local noise level is so high that the maximum usable receiver sensitivity gives a limiting power at the receiver of $\bar{\omega} = 4 \times 10^{-12}$ W. This is equivalent to a limiting line density of $\alpha_o = 3 \times 10^{11}$ electrons/cm.

The equipment is basically designed to measure winds in the meteor region by comparing, at various spaced antennas, the phases of the signal returned from a meteor trail (Robertson, Liddy, and Elford 1953). Thus the direction cosines and heights of the reflection points are known for about 10% of the echoes. As has already been shown (Weiss 1957, 1959), analysis of these characteristics of the reflection points provides information on the distribution of meteor radiants.

This chapter presents the results of astronomical interest so far obtained from the Mawson recordings, with particular emphasis on the distribution of the radiants of sporadic meteors. The basic data are the characteristics of reflection points just mentioned, and the temporal variations in the total rate of echoes detected by the equipment. In interpreting these data we adopt the now well-established distribution of sporadic radiants based on three sources, all of which lie on the ecliptic, namely, a broad apex source and more concentrated sources near the Sun and antisun. Our results

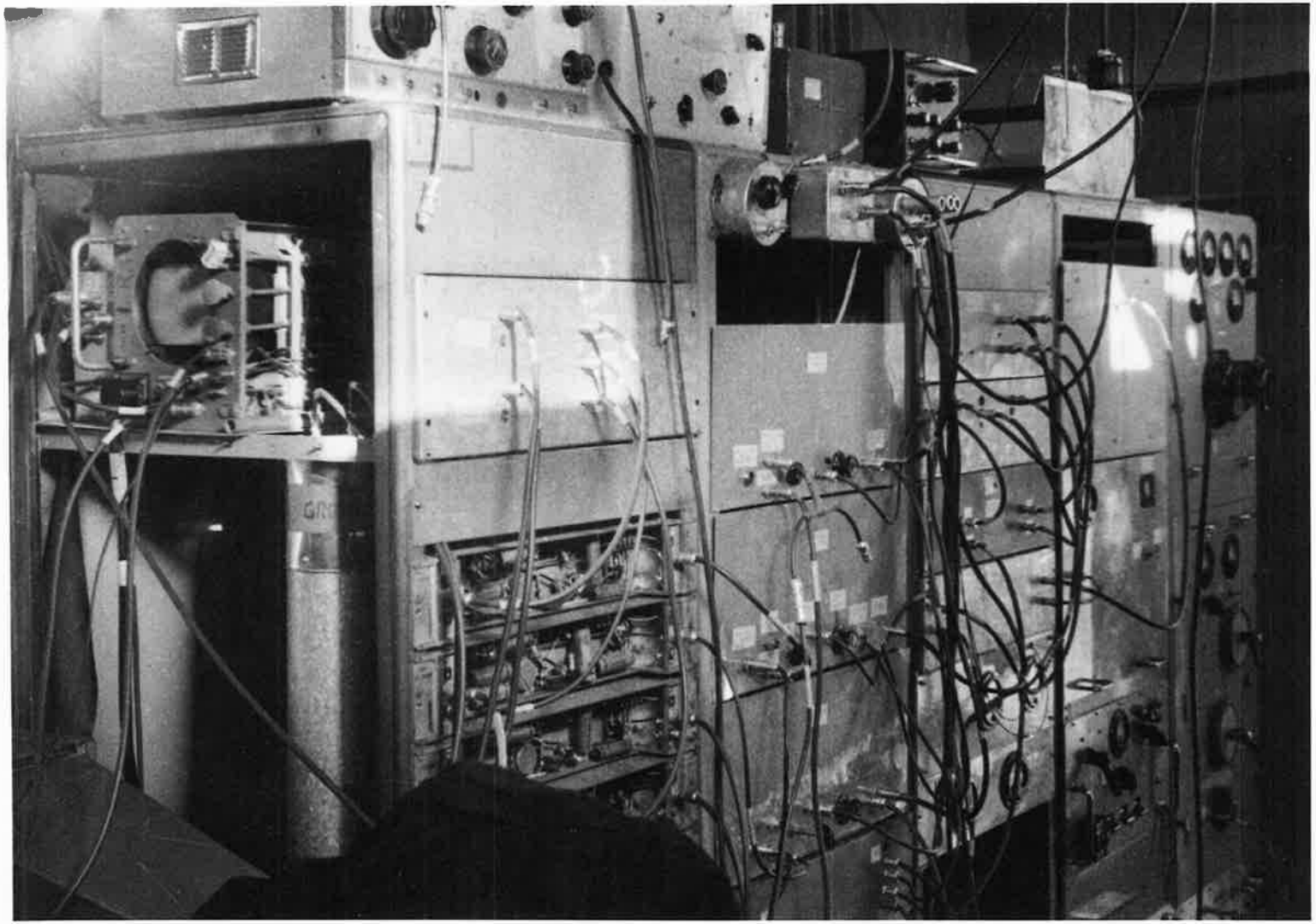

The Mawson Meteor Radar

plate 2

suggest that the integrated intensities of all three sources are approximately equal.

The symbols used in this paper are defined in the Appendix. All times quoted in this chapter are in Local Time (L.T. = U.T.+4 hr).

TABLE 1
SUMMARY OF HEIGHT DATA ANALYSED

Month	Number of Meteors	Mean Height (km)	r.m.s. Deviation (km)
Oct.–Nov. 1957 ..	135	95·2	13·1
Dec. 1957 ..	296	96·0	10·4
Jan. 1958 ..	145	92·8	10·1
Feb. 1958 ..	118	91·2	9·4
Mar.–Apr. 1958 ..	81	91·7	12·0
Dec. 1958 ..	342	95·4	10·0
Jan. 1959 ..	317	95·3	9·6

2.2 Azimuthal Distribution of Reflection Points

We shall first ascertain the information on the source distribution of the radiants of sporadic meteors which is contained in the azimuth data. Weiss (1957) has shown that this can be achieved through use of the property of specular

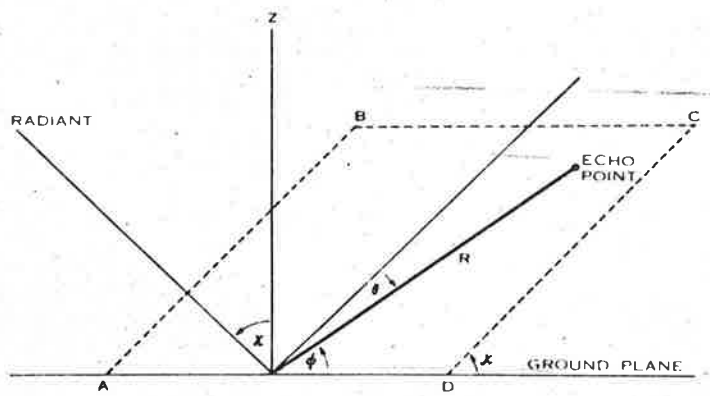

Fig. 1.—The geometry of echo detection. The echo plane *ABCD* is normal to the radiant direction. $\frac{1}{2}\pi - \theta$ is the direction of the echo, at slant range R, in the echo plane measured from the horizontal, and φ is the elevation of the echoing point.

reflection of the meteor trail. The reflection points for trails proceeding from a given radiant of zenith angle χ must all lie in a plane perpendicular to the observer-radiant line and have an elevation less than or equal to χ. Since the antennas have maximum gain vertically overhead, it follows that the most likely

azimuth for the reflection points is 180° removed from that of the radiant. This corresponds to $\theta = 0$ in Figure 1.

The echoes analysed (see Table 1) were recorded during the summers of 1957/58 and 1958/59. Figure 2 shows the azimuthal distribution of reflection

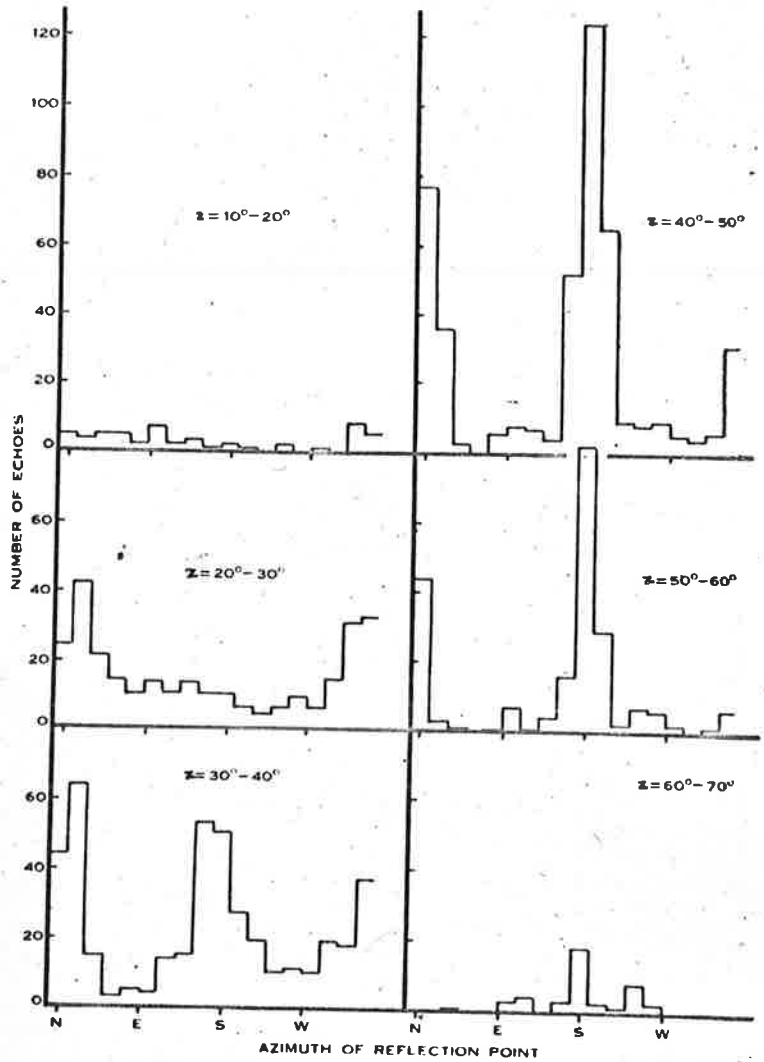

Fig. 2.—The observed azimuthal distributions of reflection points for 10° intervals of zenith angle.

points for 10° intervals of zenith angle. The obvious preference for reflection points to lie in the north or south can be explained by the form of the antenna polar diagram. The end supports of the dipoles are conducting waterpipe and presumably give the antennas loop characteristics. The dipoles are aligned on

the east-west line, hence we have in effect a broad figure-of-eight beam to the north and south.

Figure 3 shows the diurnal variation of the numbers of echoes in each of the four azimuthal groups centred on north, south, east, and west. The diurnal variation of the total number of echoes of quality sufficient to give reflection point direction cosines is given in Figure 3 (*e*). This variation, which applies to only 10% of the total echoes detected, is not the same as the overall diurnal variation for December–January given in Section 5, a fact undoubtedly due to the selection processes involved in choosing echoes for detailed analysis, as opposed to the requirements for the recognition of echoes.

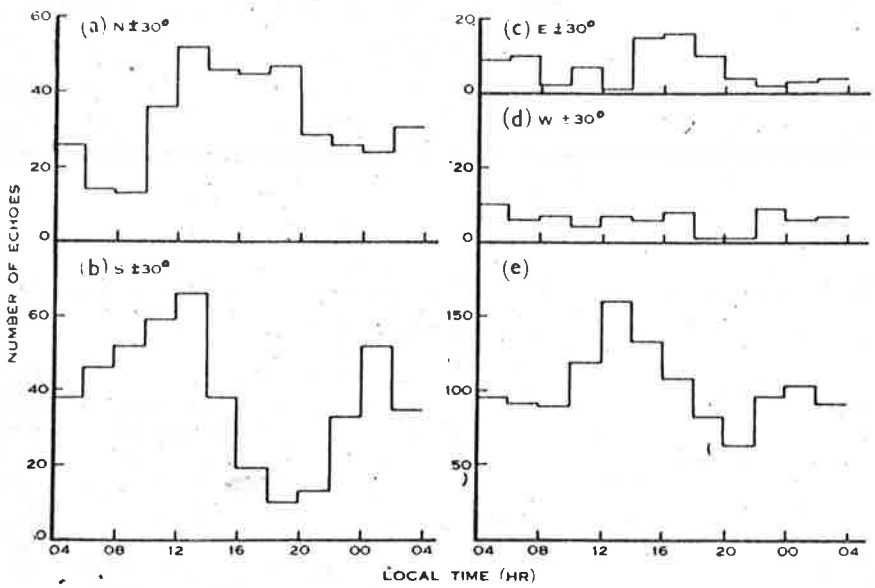

Fig. 3.—The diurnal variations of the numbers of echoes. (*a*)–(*d*) In different azimuth groups, (*e*) the diurnal variation of all echoes without regard to azimuth.

We will now show that these diurnal variations in azimuth distribution can be explained by assuming a distribution of sporadic radiants based on three sources, namely, a broad apex source and more concentrated sources near the Sun and antisun. All three are taken to lie on the ecliptic, the latter two having ecliptic longitudes 70° removed from the apex. This source model is based on the radio results of Hawkins (1956) and of Weiss (1960*b*), and the visual results of Hawkins and Prentice (1957).

There is a peak in Figure 3 (*e*) between 14 and 19 hr which can possibly be attributed to the Sun source at low elevation (about 20°) in the west, but the antenna polar diagram is too uncertain to permit a useful discussion of the east-west results.

The ratio of the numbers of northern to southern reflection points is more useful. Figure 4 is a logarithmic plot of the north/south ratio obtained from the data presented in Figure 3. Upper and lower transit times of the three sources

are shown, with the exception of the lower transit of the antisun source, which does not contribute to the echo rate at lower transit during the summer months. At apex lower transit in January the apex source is centred on zenith angle $Z=104°$ in the south, and from the arguments advanced in the first paragraph of this section we can expect a concentration of echoing points in the north at this time (18 hr). The observations (see Fig. 4) conform to this expectation. The upper transit of the apex at 06 hr should be marked by a concentration of reflection

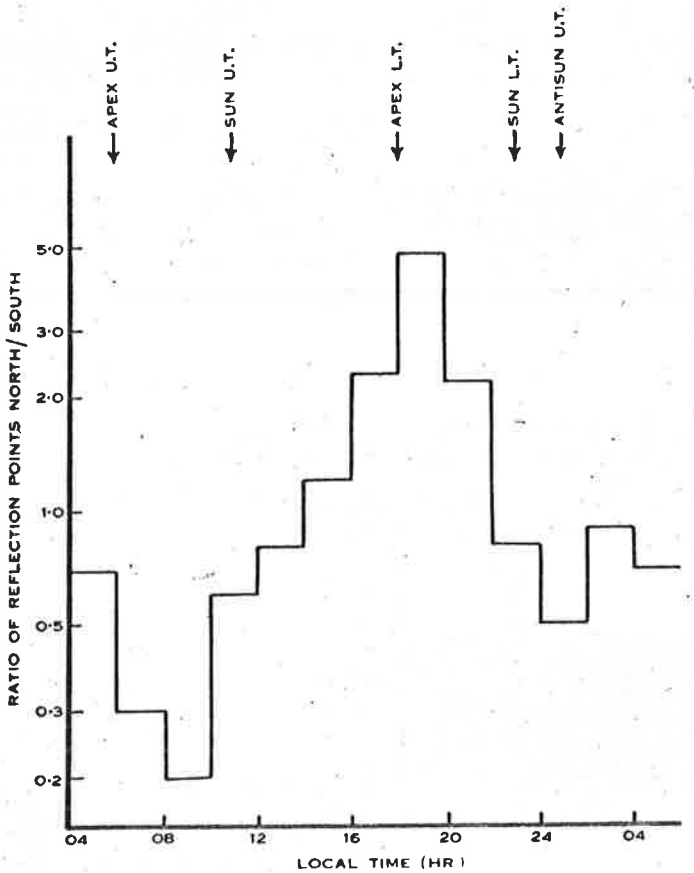

Fig. 4.—The diurnal variation of the ratio of northern to southern reflection points. The transit times of the various sources are indicated near the top of the diagram (U.T.=upper transit, L.T.=lower transit).

points in the south, which should appear as a minimum in Figure 4. Actually, the minimum is seen to fall midway between the upper transit of the apex and the upper transit of the Sun source at 11 hr. Since the strengths of the Sun and antisun sources are approximately equal, this result implies that these sources are stronger than indicated by the visual results of Hawkins and Prentice (which applied only to the antisun source). This conclusion as to the relative strengths of the sources is substantiated by the observed diurnal rate variations analysed later in Section 5.

The antisun source does not rise far above the horizon in January, but at upper transit near 01 hr should give echoes in the south. However, the lower transit of the Sun source near 23 hr should give about the same number of echoes in the north. The step near 00 hr in Figure 4 is not inconsistent with contributions from these two sources.

2.3 Zenith Angle Distribution of Reflection Points

Figure 5 (*a*) shows the distribution in zenith angle of the reflection points of all echoes, without regard to azimuth. This distribution has a broad maximum between zenith angles 30 and 50°, and there are very few reflection points with zenith angles exceeding 50°. These observed features may be compared with the result of Kaiser (1953), who showed that for a $\frac{1}{2}\lambda$ dipole $\frac{1}{4}\lambda$ above ground, and a uniform radiant distribution, the peak of the zenith angle distribution is fairly sharp and occurs at $z=50°$. The differences between our observed distribution and the theoretical one can be fully accounted for by the departure of the assumed

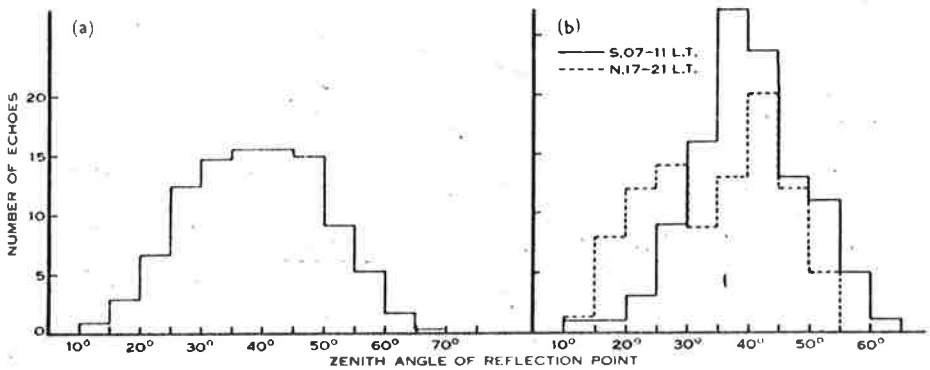

Fig. 5.—The zenith angle distribution of (*a*) all echoes without regard to time or azimuth; (*b*) of two groups of echoes: —— those with southern reflection points received between 07 and 11 hr, --- those with northern reflection points received between 17 and 21 hr.

radiant distribution from uniformity; in fact, our assumed radiant distribution implies that the elevation of any of the source centres never exceeds 45°. The lack of reflection points with zenith angles exceeding 50° is consistent with this source distribution and the geometry of specular reflection. There is thus no evidence that the distortion of the antenna polar diagram, inferred from the azimuth distributions, extends to the variation of the antenna gain with zenith angle.

With this assurance, we now proceed to examine the zenith angle distribution of selected groups of echoes for agreement with predictions based on our assumed source function.

The northern echoes detected between 17 and 21 hr have been associated with the apex source at lower transit, and the southern echoes detected between 07 and 11 hr with the apex and Sun sources at upper transit. As a group, the reflection points of the former echoes should have smaller zenith angles than the latter. The zenith angle distributions for the appropriate groups of echoes,

plotted in Figure 5 (*b*), indicate that this is the case; the mean zenith angle for northern echoes is 40°, for southern echoes 45°.

Further confirmation that the sources in the south (which produce echoes in the north) are lower in the sky than the sources in the north (which produce echoes in the south) is afforded by a detailed examination of Figure 2. We observe that (*a*) there is no peak in the south for z less than 30°, and (*b*) no peak in the north for z greater than 60°. From Figure 1, the zenith angle of the reflection point, z, is greater than or equal to the elevation of the radiant, 90-χ. From (*a*) we infer that there are not many radiants in the north for which $\chi > 60°$. This argument is only strictly true for a point radiant, but in fact can be extended to a source of radiants with maximum density in the centre. There is thus no source in the north for which $Z > 60°$, i.e. no source of low elevation. Again, from the argument of Section 2, paragraph 1, we use the most probable relation, $90 - Z = z$, and infer from (*b*) that there is no source in the south for which $Z < 30°$, i.e. no source of high elevation. For $30 < z < 60$, there are peaks both in the north and south, indicating both southern and northern sources of reasonable elevation.

We thus conclude that both azimuth and zenith angle data are consistent with our assumed source distribution. It is possible to go a little further, and to use the data of Figure 2 to obtain an estimate of the diameter of the apex source. Between $z = 50$ and 60° there is still a pronounced peak in the north. If we assume that this is due to the lower transit of the apex source, for which $Z = 104°$ in January, the source must extend for at least $104° - (90° - 55°) = 70°$ approximately from the centre. According to the apex source density distribution function derived from the radio results of Weiss and illustrated in Fig.A1.2, the source density is reduced by a factor of only from 2 to 3 at 70° from the centre.

2.4 Height Distribution

The heights of the echoing points of the sporadic meteors whose azimuths and zenith angles have been discussed in the preceding sections have also been measured. Heights were determined from zenith angles and slant ranges. The error in the slant range is of the order of 1%, but the errors in the heights are determined largely by the errors in the azimuth measurements. These are rather difficult to assess, but we estimate an error of ± 5 km in the individual heights.

The mean height, and the r.m.s. deviation from the mean, of the height distributions for each month separately are listed in Table 1. There is no evidence that the low mean heights found for January–April 1958 result from errors in equipment calibration, and data for all months have been combined on the assumption that the variations in mean height from month to month are real. There is no apparent seasonal variation in the mean height, in agreement with measurements made at Adelaide over a more extended period with similar equipment (Weiss 1959), but the possibility of a seasonal variation in the r.m.s. deviation, with a minimum in February, cannot be dismissed.

The overall height distribution for all Mawson echoes is sketched in Figure 6 (*a*), where it is compared with the height distribution measured at Adelaide (Weiss 1959). Both distributions have been normalized to equal areas under the histograms. The higher mean height at Mawson is probably a latitude effect. At Mawson the minimum zenith angles of the sources of sporadic meteors are some 30° greater than at Adelaide, and a simple calculation shows that this is quite adequate to explain the difference of 2 km or so in the mean heights recorded at the two stations. The long tails of the Mawson height distribution, which are responsible for the high value of the r.m.s. deviation, are real, as will be shown presently. Similar tails are not present in the Adelaide distribution, but it is thought that this is a consequence of selection of echoes for analysis rather than an indication of their absence from the Adelaide recordings.

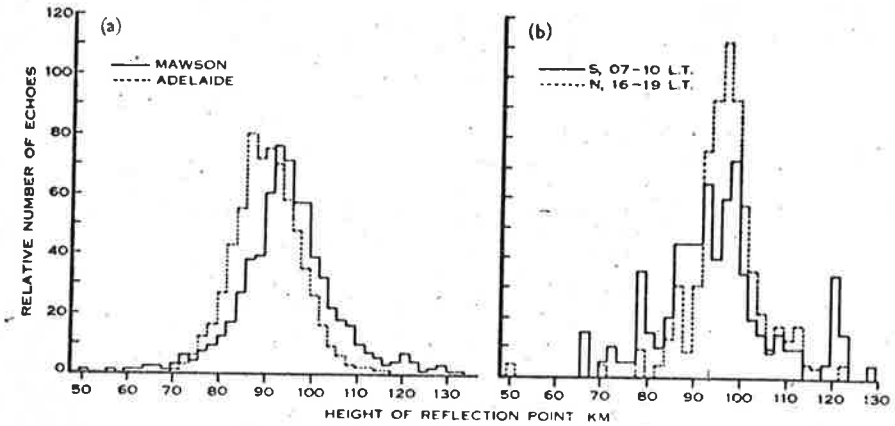

Fig. 6 (*a*).—The height distribution of reflection points for Adelaide and Mawson.
Fig. 6 (*b*).—The height distribution of two groups of echoes : —— those with southern reflection points received between 07 and 10 hr ; --- those with northern reflection points received between 16 and 19 hr.

The diurnal variations in the mean height and the r.m.s. deviation from the mean have been ascertained for each month separately. There are no strong variations from month to month and the data have been pooled. The average diurnal variation in each parameter over the summer months is illustrated in Figure 7.

As already found from the Adelaide measurements, the diurnal variation in the mean height is small. Maximum height occurs at 17 hr when the apex is near lower transit ; this is the only indication that the mean height is influenced to any extent by the position in the sky of the sources of sporadic meteors.

On the other hand, the diurnal variation in the r.m.s. deviation is large, and its reality is made more plausible by the excellent agreement between its phase and the phases of the azimuthal diurnal variations presented in Figure 4. The r.m.s. deviation of the height distribution is largest at a time midway between the upper transits of the apex and Sun sources, and smallest near the lower

transit of the apex source. Further information on the nature of the diurnal variation in width of the height distribution is contained in Figure 6 (*b*), in which we have drawn height distributions for two selected groups of meteors. These two groups dominate the total echo rate and so largely determine the properties of the height distribution, at the respective times. The first group, comprising all meteors detected between 07–10 hr with echoing points located to the south, presumably originates from the combined Sun and apex sources near upper transit. The second group, which includes all meteors detected from 16–19 hr with echoing points to the north, proceeds from the apex source near lower transit. It will be seen that the latter distribution is much narrower than,

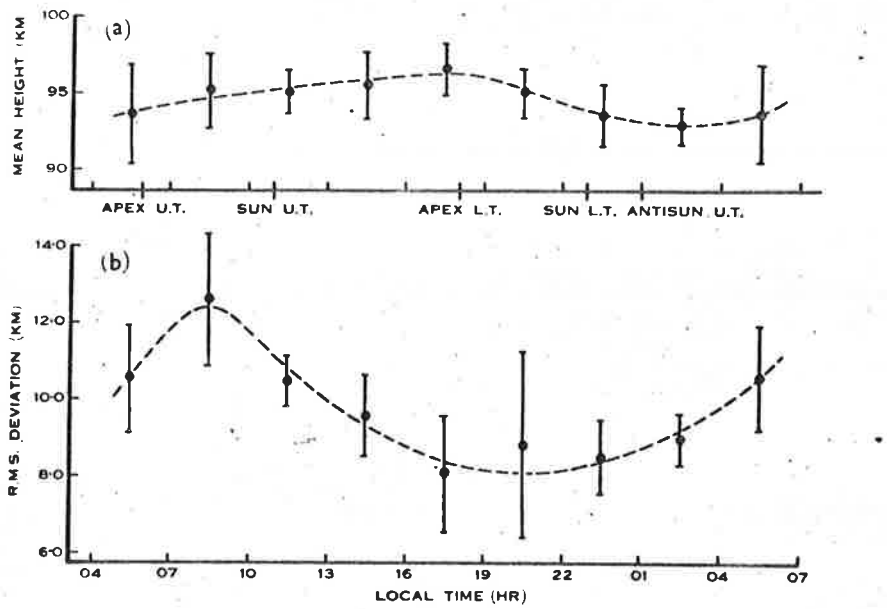

Fig. 7 (*a*).—The diurnal variation of the mean height for the summer months.
Fig. 7 (*b*).—The diurnal variation of the r.m.s. deviation from the mean height.
The vertical lines represent the r.m.s. deviations of mean values which are indicated by dots. The transit times of the various sources are indicated (U.T. = upper transit, L.T. = lower transit).

and lacks the long initial tail of, the former. From the times of occurrence of the maximum and minimum of Figure 7 (*b*), in relation to the times of upper and lower transit of the apex and Sun sources, it is clear that the Sun source can make little contribution to the narrow height distribution found for the apex source at lower transit, whereas it does contribute strongly to the wider distribution found at 07–10 hr. The inference is that trails of Sun source meteors are formed lower in the atmosphere than apex source meteors. Since the heights of formation of trails of meteors which differ only in velocity v depend on $\ln v$, this suggests that Sun source meteors possess lower speeds than apex source meteors. The occurrence of maximum mean height at apex lower transit could then be due

simply to the low relative number of detectable Sun source meteors at that time, but the large zenith angle of the apex source may also be a contributing factor.

Incidentally, the absence of the long tail of low heights at apex lower transit suggests that the tails in the overall Mawson distribution (Fig. 6 (*a*)) are real.

2.5 The Diurnal Rate Variation

In this section we discuss the calculation of the theoretical diurnal variation in the echo rate and compare it with the observed results.

A table of α_0, the line density of a barely detectable echo, can be prepared as a function of the zenith angle and azimuth of the reflection point from the formulae for Lovell-Clegg and persistent scattering given in the Appendix. The table, which is not reproduced, predicts a cut-off of echoes at zenith angles larger than 65°, where $\alpha_0 \simeq 10^{14}$ electrons/cm. This corresponds to a maximum range of detectable echoes of 250 km, and this was observed in practice. Also, Figure 5 (*a*) shows a cut-off around $z = 65°$, and we conclude that the sensitivity figures used are reasonable.

To use this table of α_0-values for a determination of the sporadic diurnal rate variation, we first assume independence of the antenna polar diagram on azimuth, an assumption which is modified at the end of the calculations.

The first step is to calculate the response of the equipment, $f(\chi)$, to a point radiant at zenith angle χ. Kaiser (1953) has given a formula for the echo rate, which is equivalent to

$$f(\chi) = \cos\chi \int_{\theta=0}^{\frac{1}{2}\pi} \frac{R\,d\theta}{R/R_E + \sin\varphi} \cdot \frac{1}{\alpha(\theta)^s}, \qquad (1)$$

where the mass distribution parameter s is assumed to have the value $s = 2$ for sporadics. Here R_E is the radius of the Earth, φ is the elevation of the echo, and θ is as shown in Figure 1. Because of the cut-off in echo rate at $z = 65°$, $R/R_E \ll \sin\varphi$, and it is adequate to use flat earth geometry for which $h = R\sin\varphi$. Also $\sin\varphi = \sin\chi\cos\theta$. Introducing a mean height, $\bar{h}$, for reflection points, (1) may be written

$$f(\chi) = \frac{\bar{h}\cos\chi}{\sin^2\chi} \int_{\theta=0}^{\frac{1}{2}\pi} \frac{d\theta}{\alpha(0)^s \cdot \cos^2\theta}, \qquad (2)$$

from which $f(\chi)$ may be found, making use of the table of α_0 already prepared. $f(\chi)$ for the Mawson equipment is illustrated in Figure 8 (*a*).

The next step, the calculation of the echo rate as a function of the zenith angle of the source, is quite general and applicable to any function $f(\chi)$ and to any extended source whose density is a function only of the elongation from the centre of the source. It is described in the Appendix, together with the details of the apex, Sun, and antisun source distributions.

For any one of the sources, therefore, we have now established the variation of the echo rate as a function of the zenith angle of the source. This variation $F(z)$ for the Mawson equipment is shown in Figure 8 (*b*), where the contributions from each source have been normalized to give the same peak rate within the range of the zenith angles of the sources expected at Mawson. This corresponds

to the maximum density of the Sun and antisun sources being 4·5 times that of the apex source. The visual results of Hawkins and Prentice indicated a ratio of only 1·5, but the Mawson diurnal sporadic rate variation best fits the theoretical predictions if a larger ratio is used. This is discussed more fully later in this section.

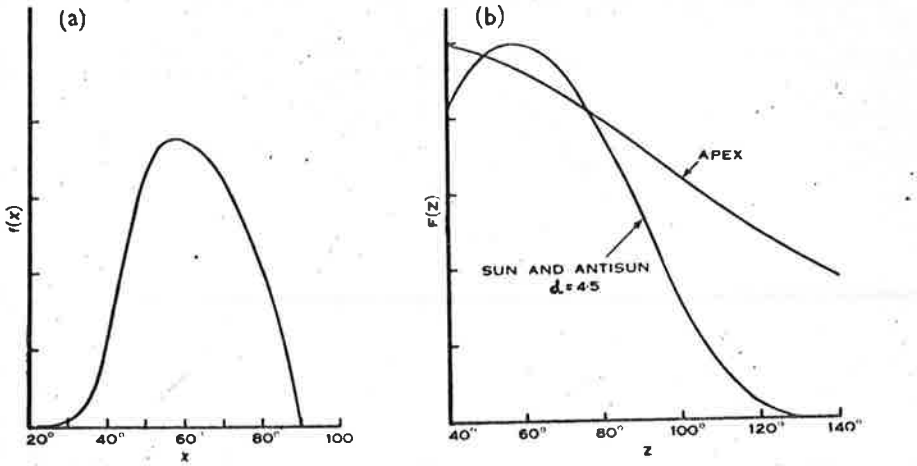

Fig. 8 (*a*).—The equipment response function, $f(\chi)$ (see Section V) plotted against the zenith angle χ of a radiant.

Fig. 8 (*b*).—The rate variation function, $F(Z)$ (see Appendix) plotted against the zenith angle Z of the three sources. d is the ratio of the peak source density of the Sun and antisun sources to that of the apex source.

It remains to allow for the azimuth variation of the aerial polar diagram. The assumption that the azimuth of the radiant is 180° removed from that of the reflection point is valid *only on the average* for either a point radiant or an extended source of radiants. With this limitation in mind, we can weight the source distribution as a function of azimuth of the source, although in reality all we should weight are the reflection points. The weighting function is based on the data from Figure 2 and is set out in Table 2.

TABLE 2

AZIMUTH WEIGHTING FUNCTION

Hour Angle of Source ..	0– 2 12–14	3– 4 15–16	5– 7 17–19	8– 9 20–21	10–12 22–24
Weight	1	½	¼	½	1

The only means of verifying this procedure was afforded by the δ-Aquarid shower of July–August. Figure 9 shows that the theoretical temporal variation in echo rate, based on the known movement of the radiant, fits the observations more closely when the dependence of the antenna polar diagram on azimuth is taken into account in this way.

plate 3a

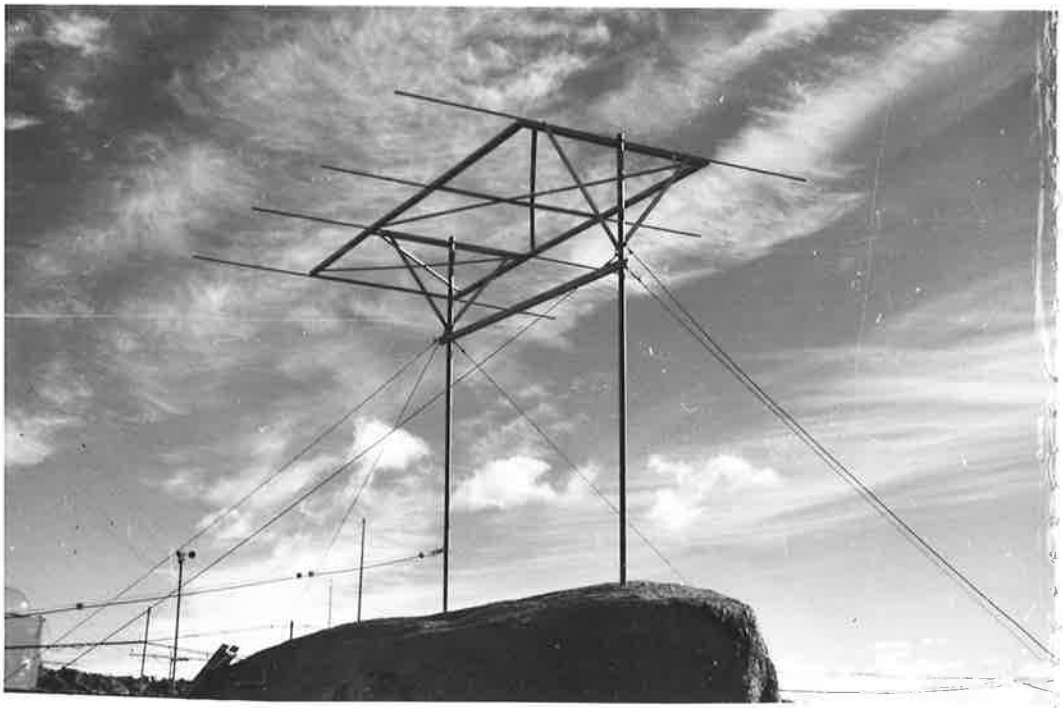

plate 3

Finally, we calculate the zenith angles of the three sources as a function of time, substitute for the zenith angle the appropriate echo rate from Figure 8 (*b*), weight this with the azimuth function, and add together the rates for all three sources. This has been done for each month separately and the resulting theoretical echo rates are shown in Figure 10.

Apex upper transit occurs at 06 hr, lower transit at 18 hr. The use of the azimuth weighting function and a Sun source to apex source peak density ratio as low as 1·5 results in a noticeable peak at 18 hr in the predicted echo rate, due to the apex source at lower transit. This is illustrated in Figure 10 for October and the summer months of December and January. There is no sign of such a peak in any of the observations for any months (see Fig. 11), so we conclude that

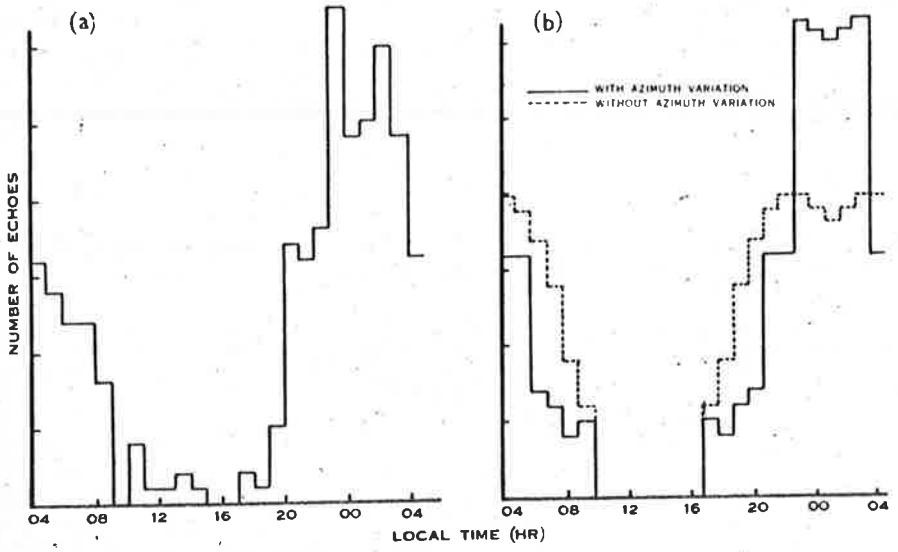

Fig. 9.—The temporal variation in the echo rate for the δ-Aquarid shower of July–August, 1957. (*a*) Observed, normalized to a mean rate of 11 echoes/hr. (*b*) Theoretical, plotted with and without allowance for the azimuth variation in the antenna polar diagram. The theoretical rates have been normalized to the same mean rate as the observations.

the Sun and antisun components are large enough to mask the effect. We have therefore used a peak density ratio of 4·5 in calculating the theoretical rates. This implies that the integrated contributions from the three sources are approximately equal, as the lower peak apex density is compensated by the greater extent of this source. Meek and James (1959), in the predictions for their forward-scatter experiments, used a three-point radiant model, weighting each radiant equally. This is approximately equivalent to assuming the integrated response from each source to have the same maximum value, as we have done in normalizing Figure 8 (*b*).

During the summer, when the azimuth and height data require a strong Sun source, the observed diurnal echo rate is high (even to the extent of showing a second peak, as in December 1958 and January 1959) from apex upper transit

at 06 hr to Sun source upper transit at 11 hr. Choosing a value of peak density ratio of 4·5 leads to broader maxima in the theoretical rate curves than does a smaller value. These broad maxima are thus supported by the observations, which are shown in Figure 11.

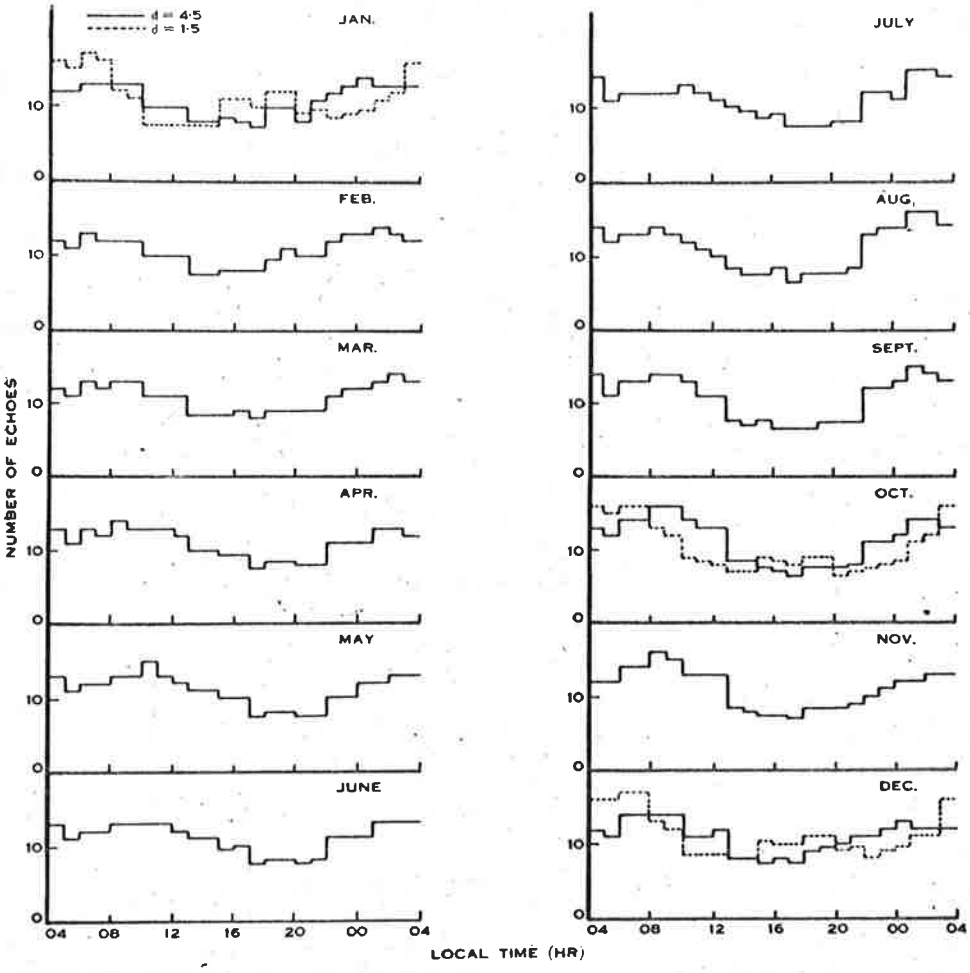

Fig. 10.—The theoretical diurnal rate variations of sporadic meteors at Mawson based on a distributed three-source model. *d* is the ratio of the peak source density of the Sun and antisun sources to that of the apex source. The echo rates have all been normalized to a mean rate of 11 echoes/hr.

The observed rates have been normalized to a mean echo rate of 11 per hour. The data have also been corrected as far as possible for equipment-off periods, but the high noise level introduces some uncertainty. This should not change the form of the diurnal variation, but it does necessitate the equipment operating at a rate as low as 2–3 echoes per hour for some periods. This leads to considerable scatter in the records. November 1957 and all 1960 rates are in this category.

Close examination shows that, while the general features of the observed and predicted rates are in agreement, there are certain dissimilarities. Between July and December the predicted minimum shifts from 19 hr to 16 hr, whereas the observed rates show the reverse effect, the minimum shifting from 17 hr in August to 20 hr in December. It is shown in Section 6, however, that ionospheric conditions appear to affect the echo rate, and this disagreement could

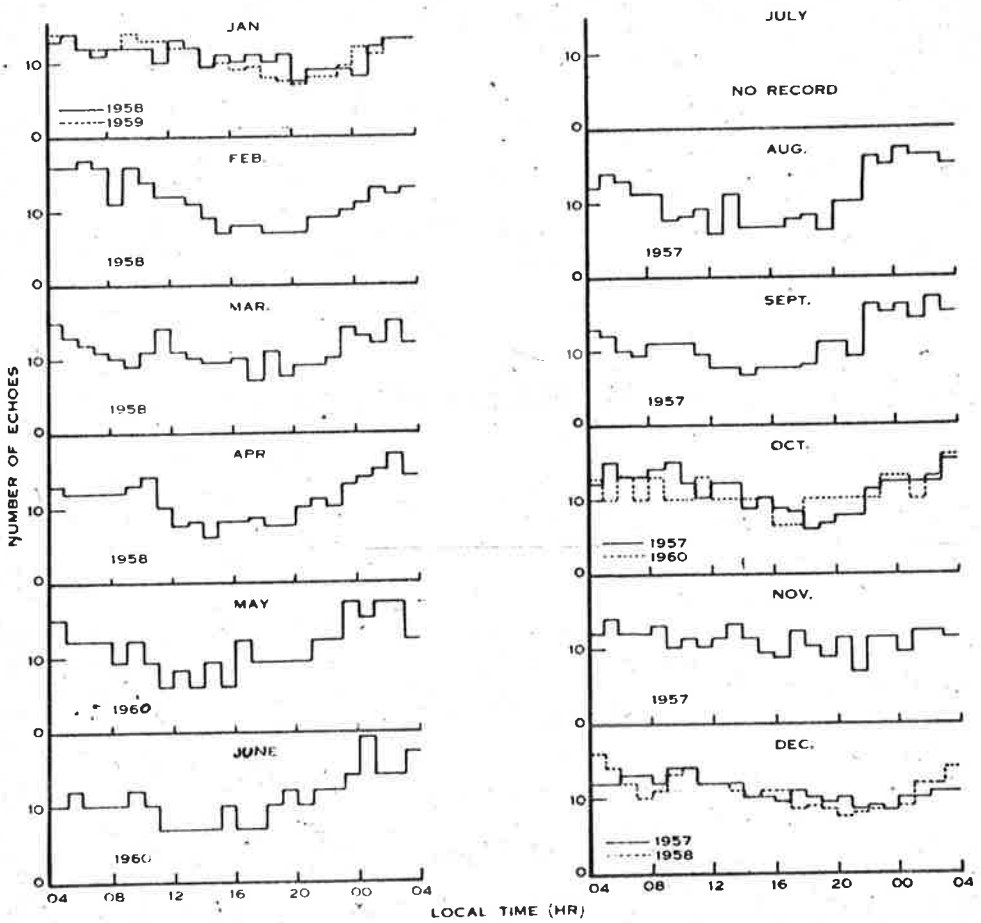

Fig. 11.—The observed diurnal rate variations of sporadic meteors, normalized to a mean rate of 11 echoes/hr.

well be due to some diurnal ionospheric effect, rather than an actual difference between our model and the true distribution of sporadic meteors. In view of the uncertainties in both the observed rate due to the high noise level at Mawson, and the predicted rate due to the variation in response with azimuth, the significance of minor features should not be overstressed.'

The major features of the diurnal variation have repeated from year to year. Several repetitions are shown in Figure 11 for comparison.

Echo rates for July have been omitted because of the difficulty in separating the sporadic background from the δ-Aquarid shower activity. Both sets of activity have maxima occurring between 00 and 04 hr.

2.6 The Daily and Seasonal Variation in Echo Rate

Because of unusually large variations in equipment sensitivity, introduced by severe operating conditions and large fluctuations in noise level, the seasonal variation in the total daily echo rate could not be determined. However, the variation in daily total echo rate, after smoothing out gross equipment changes and any possible seasonal variation, is plotted in Figure 12. The data have been smoothed by plotting in running groups of three.

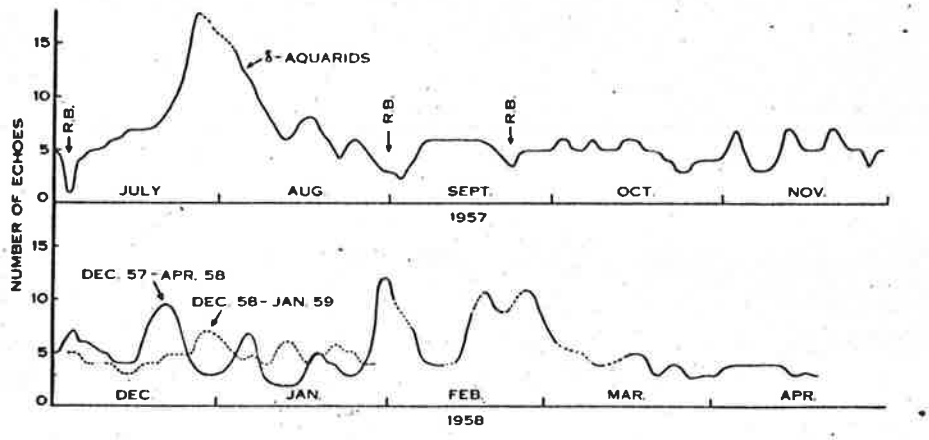

Fig. 12.—The fluctuations in daily echo rate, after correction for equipment and possible seasonal changes in the echo rate. R.B.=radio communication black-out.

The δ-Aquarid shower is the only major shower expected to be detected; it is prominent in July–August. There is also marked correlation between short periods of low rate and poor radio communications between Mawson and the rest of the world, known as "radio black-outs".* (Our records of radio black-outs at Mawson do not extend beyond September 1957.) The summer of 1957–58 has large variations in total daily rate. The increases from December 15 to December 24, January 26 to February 6, and February 12 to February 28 are probably significant. These increases do not show any shower characteristics, nor have they any tendency to repeat from year to year, as the months of December 1958 and January 1959 show. Any attempt to separate a presumed base level of sporadic activity from these periods of high count leaves a residual diurnal rate variation similar to the predicted and observed sporadic rate; the periods of low activity on either side of the high activity periods in question have been taken to represent the true observed sporadic rate for this test. Our conclusion is that these are real increases in the sporadic background rate. They

* McNamara (1961) has given a similar example of a marked decrease in the meteor echo rate during 12/13 November 1960, which he attributed to low-level absorption during a PCA event.

could be due either to true increases in the influx of meteors or to increases in the detection rate due to changes in the ionosphere. The latter hypothesis is supported by the absence of any abnormal activity in echo counts made at Adelaide with the high resolution radiant equipment (Weiss 1960*a*) over this period. The radio black-out periods indicate that ionospheric changes can inhibit the rate and it is conceivable that other changes could increase it. This possibility is enhanced by the fact that Mawson is located in the belt of maximum auroral frequency.

2.7. Conclusions

Experience with the interpretation of the Mawson records has confirmed the opinion, reached in the analysis of records obtained with Adelaide equipments, that broad-beam antenna systems are not the most suitable for measuring the distribution of meteor radiants over the sky. Extraction of data from the Mawson records was hampered by the unfortunate azimuth variation in the antenna polar diagram, which basically arose from the necessity for mechanical stability of the antennas in the inclement environment of the Antarctic continent, and by the unusually high and varying receiver noise level of local origin.

Despite these severe limitations, we have been able to show that azimuths, zenith angles, and heights of reflection points can be explained satisfactorily by a source distribution for sporadic meteors which consists of an extended source centred on the apex of the Earth's way, together with more concentrated sources located on the ecliptic near the Sun and antisun. The direction and height data, together with the diurnal variation in the echo rate, require that the integrated strengths of the three sources be approximately the same.

Of particular interest is our conclusion that large increases in the sporadic echo rate observed during the summer months could be caused by abnormal ionospheric conditions. Should this be the case, it is not impossible that ionospheric conditions in the auroral zone could also influence the diurnal echo rate variation in some regular way.

CHAPTER 3

THE METHOD AND GROUND GEOMETRY OF THE ADELAIDE SURVEY

3.1 Fresnel Zone Diffraction Theory.

Consider a transmitted wave of the form

$$A_t = F_t e^{i\omega t}$$

The amplitude of the reflected wave from an element ds of the trail at range R can be written as

$$dA_r = g(R,\alpha)e^{i(\omega t-(4\pi R/\lambda)-\beta)}ds \quad \ldots \quad (1)$$

where β is the phase change on reflection, α is the electron line density, $g(R,\alpha)$ is a real scattering function which only varies slowly over the trail in the vicinity of the reflection point. In this analysis any dependence of β on α and hence on time is ignored. The total reflected wave from the portion of the trail $-s_1$ to s_1 is given by

$$A_r = g(R,\alpha)\int_{-s_1}^{s_1} \exp\, i(\omega t-(4\pi R/\lambda)-\beta)ds. \quad \ldots \quad (2)$$

Write $\phi = \omega t - 4\pi R_o/\lambda - \beta$ * ... (3a)

and $\pi x^2/2 = 2\pi s^2/R_o\lambda$ ... (3b)

where R_o is given by $R = R_o + s^2/2R_o$ in the vicinity of the reflection point. The distance, s, along the trail is measured from the reflection point. The expression for A_r now becomes

$$A_r = F_r \int_{-x_1}^{x_1} \exp i(\phi - \pi x^2/2)\,dx \qquad \ldots (4)$$

where F_r is a constant for a given meteor. (4) reduces to

$$A_r = F_r(C - iS)e^{i\phi} \qquad \ldots (5)$$

where C and S are the usual Fresnel integrals

$$C = \int_{-x_1}^{x_1} \cos \pi x^2/2 \qquad S = \int_{-x_1}^{x_1} \sin \pi x^2/2$$

If A_r is plotted in amplitude and phase the familiar Cornu's spiral results, with however, the usual orientation reversed. The usual orientation corresponds to a function

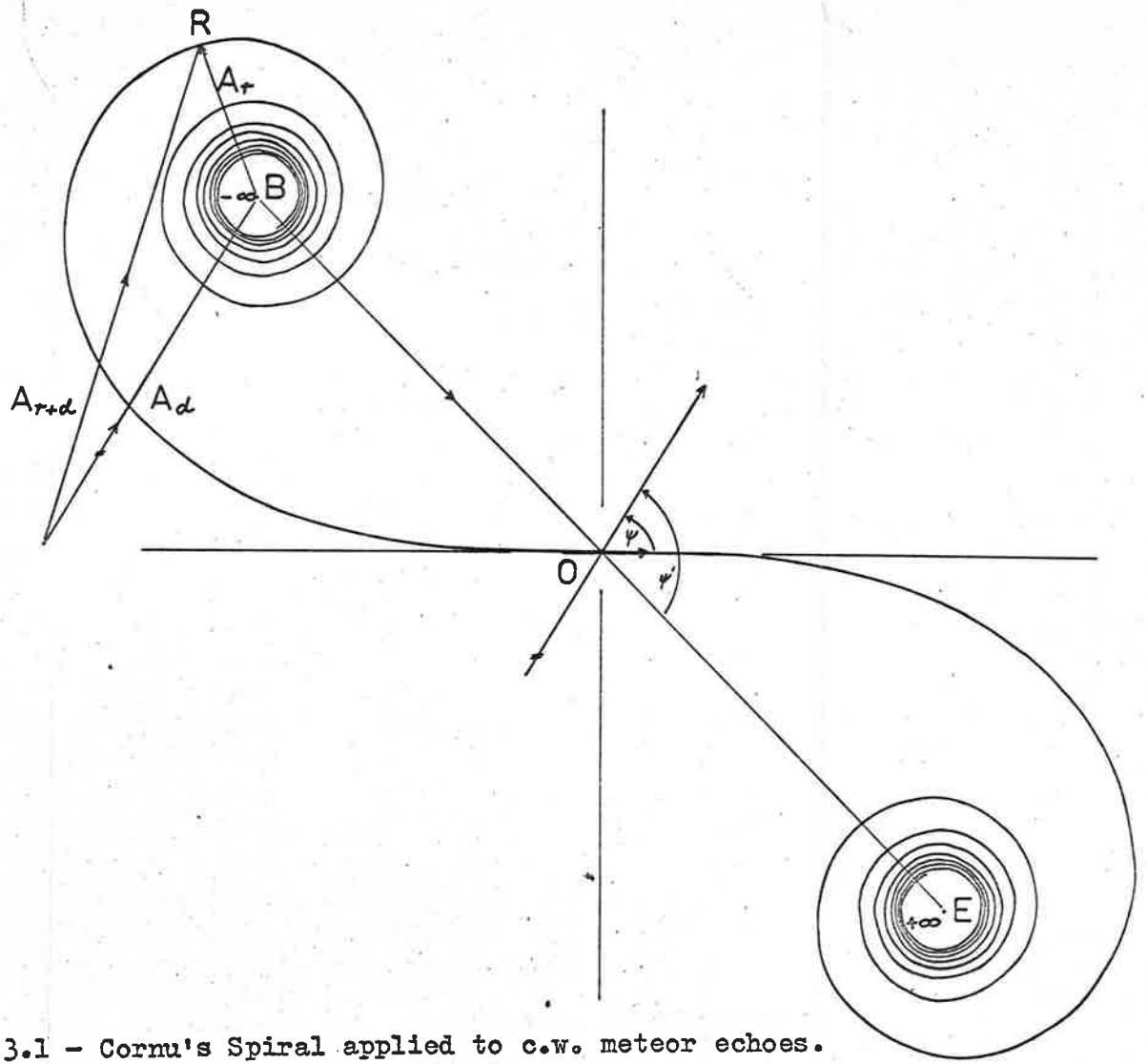

Figure 3.1 – Cornu's Spiral applied to c.w. meteor echoes.

$$A_r = F_r(C+iS)$$

which is not the function for the reflected wave from a meteor trail. This has led to some confusion in the past (Mainstone 1959)† and has not been made clear in McKinley's book (1961). Figure 1 shows a plot of

$$A_r = F_r(C-iS)$$

with the axes shifted in the conventional manner to the point $(+\frac{1}{2}, -\frac{1}{2})$. The term $e^{i\phi}$ in equation 3.5 is the RF time dependent function.

The amplitude of the groundwave is given by

$$A_d = F_d e^{i(\omega t - 2\pi D/\lambda)} \qquad \ldots (6)$$

where D is the transmitter-receiver spacing.

Define $\psi = 2\pi(2R_o - D)/\lambda + \beta$ $\qquad \ldots (7)$

from (3), have

$$\psi + \phi = \omega t - 2\pi D/\lambda$$

hence

$$A_d = F_d e^{i(\phi+\psi)} \quad \ldots \quad (8)$$

and the resultant amplitude of groundwave plus skywave is given by

$$A_{r+d} = F_r(C-iS)e^{i\phi}+F_d e^{i(\phi+\psi)}$$

which expands to

$$A_{r+d} = F_r(C\cos\phi+S\sin\phi)+F_d\cos(\phi+\psi)+i(F_r(C\sin\phi-S\cos\phi)+F_d\sin(\phi+\psi)) \quad \ldots \quad (9)$$

Using $I_{r+d} = A_{r+d}.A^*_{r+d}$ we have

$$I_{r+d}= F_r^2(C\cos\phi+S\sin\phi)^2+F_d^2\cos^2(\phi+\psi)+2F_rF_d(C\cos\phi+S\sin\phi)\cos(\phi+\psi)$$
$$+F_r^2(C\sin\phi-S\cos\phi)^2+2F_rF_d(C\sin\phi-S\cos\phi)\sin(\phi+\psi)+F_d^2\sin^2(\phi+\psi)$$

which reduces to

$$F_r^2(C^2+S^2)+F_d^2+2F_rF_d(C\cos\psi-S\sin\psi) \quad \ldots \quad (10)$$

The rapid oscillation of I_{r+d} before and after the

specular reflection point s = 0 constitutes the diffraction pattern commonly known as a 'whistle'. Further analysis of this diffraction waveform is given in Chapter 5. When referred to in the context of time, the specular reflection point is often called the 't_o' point.

3.2 Principles of Method.

At 27 Mc/s the reflection from a meteor trail is specular i.e. the reflected radiation from the trail can be considered as coming from a section such that the path length between the transmitter and receiver is a minimum. If several spaced receivers are used each receiver will have its corresponding specular reflection point for a particular trail. This is illustrated in Figure 3.2. Suppose the meteor velocity is v km/sec, and the time of arrival of the meteor at each specular reflection point for the receivers R_o, R_1 and R_2 is t_o, t_1 and t_2 sec. respectively. The spacing between the reflection points on the trail will be given by

$$s_1 = v(t_1 - t_o)$$

$$s_2 = v(t_2 - t_o)$$

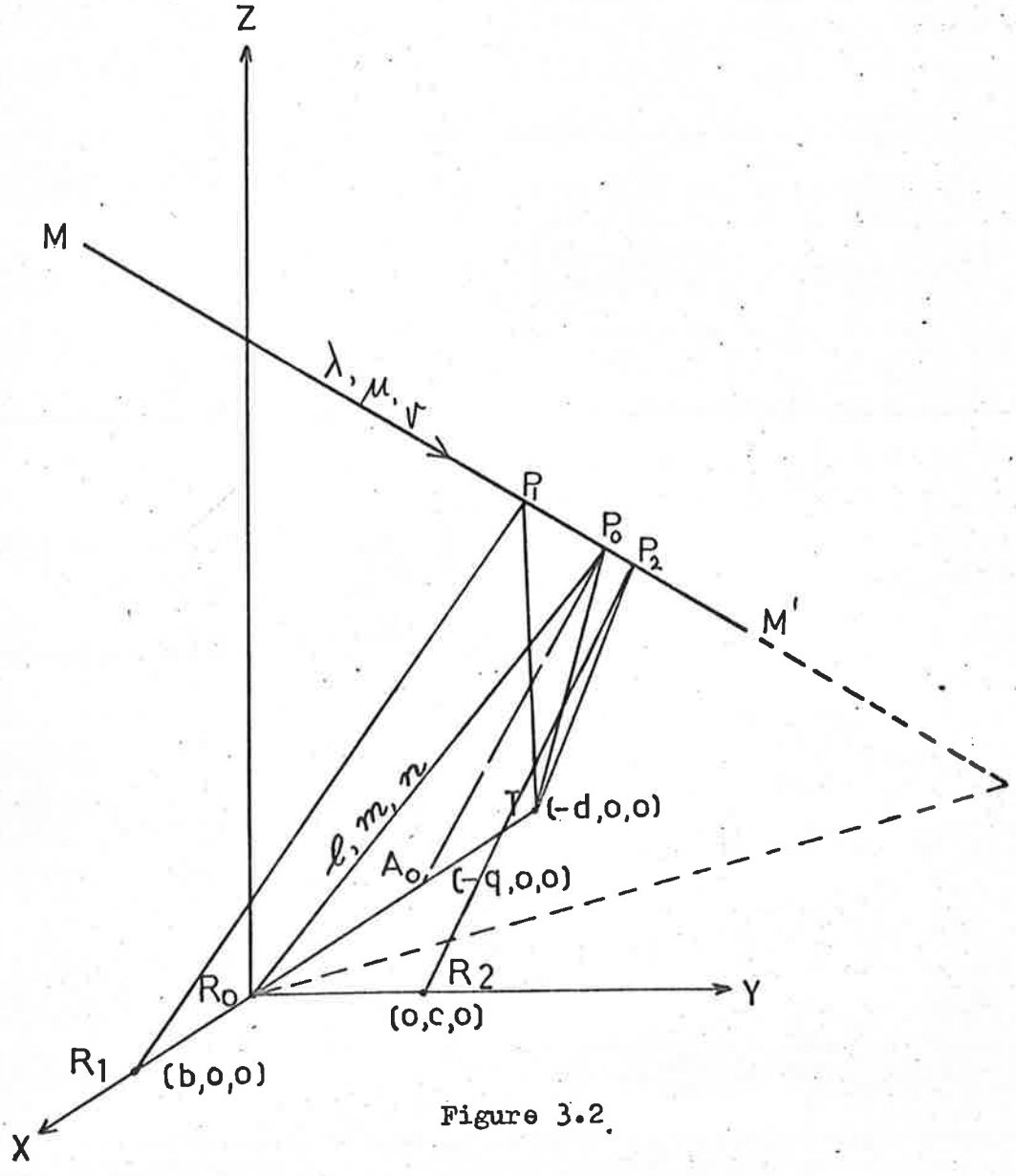

Figure 3.2.

where s_1 is the distance P_0P_1 etc. The basic parameters measured are velocity and the two time differences. These time differences are a function of the ground geometry and the direction cosines of the trail. By measuring the time differences and applying the solution given in Section 3.3 to the spaced station problem one can determine the trail direction cosines. Knowing the velocity of the meteor one can then determine the elements of the orbit in which the meteor was travelling before it encountered the earth. The ground geometry of the Adelaide system is shown in Figure 3.

As the trail is formed a diffraction pattern is observed at each receiver prior to the meteor reaching the geometrical specular reflection point. A less easily distinguished pattern is also observed after this point, but usually this is obscured by the body doppler. The latter is a low frequency beat of large amplitude, observed at each receiver, between the reflected skywave and the direct groundwave. It is caused by the trail drifting with the atmosphere and indeed the phenomenon is used at Adelaide to study upper atmospher winds. The method has

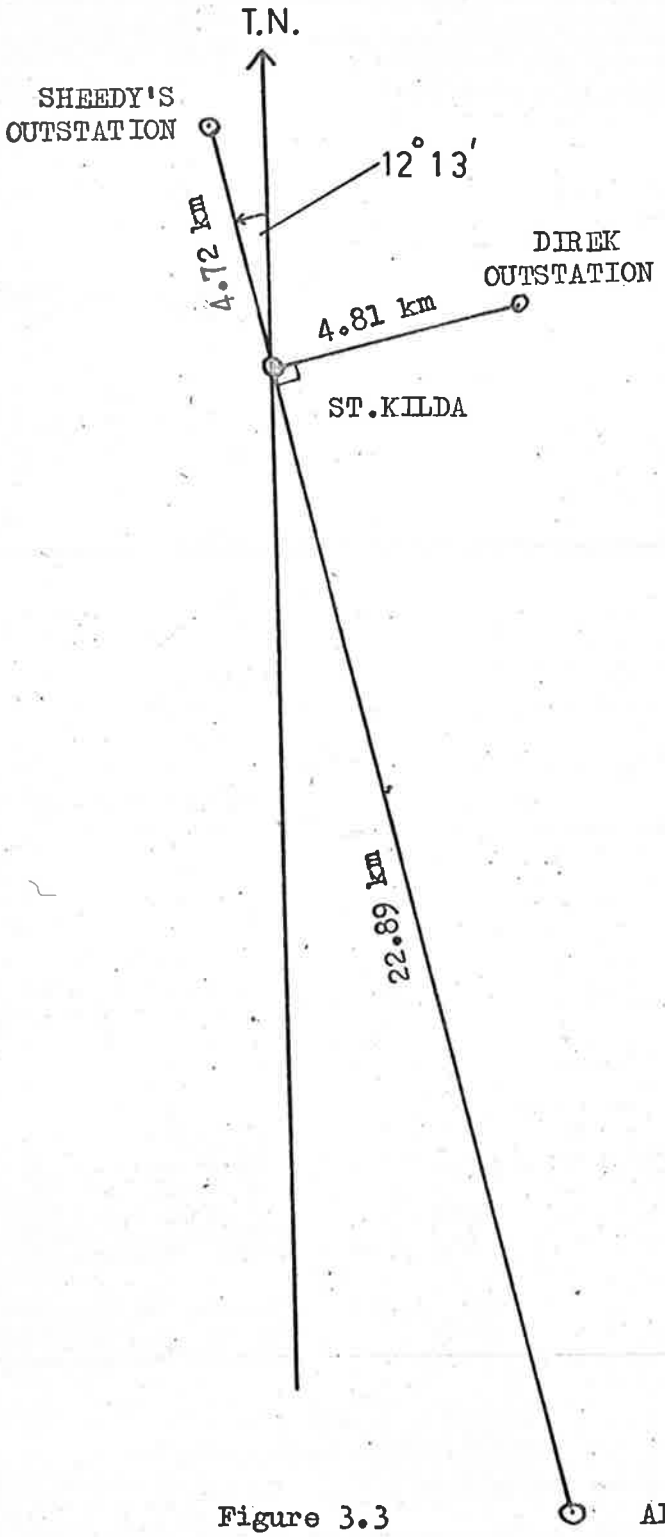
T.N.
SHEEDY'S
OUTSTATION
12° 13'
4.72 km
DIREK
OUTSTATION
4.81 km
ST.KILDA
22.89 km
ADELAIDE

Figure 3.3

been described in detail by Robertson, Liddy and Elford (1953) and Huxley (1957). A comparison of the relative phases of the body doppler waveforms from various spaced antennas at the main station provides enough information to determine the specular reflection point direction. A radar range is necessary to fix the point in space and to determine the absolute velocity of the meteor, as the observed diffraction pattern only determines a quantity dx/dt, which is related to the velocity ds/dt by equation 3b. On differentiating (3b) with respect to time, we obtain

$$\frac{ds}{dt} = \sqrt{\frac{r_o \lambda}{4}} \cdot \frac{dx}{dt}$$

The direction cosines of the main station reflection point are used in the determination of the trail direction cosines from the observed separation of the t_o points at the various receiving stations.

3.3 The Spaced Station Problem.

Consider Figure 2. A meteor trail MM' is

illuminated by a transmitter at T, the reflected skywave being received at R_o, R_1 and R_2; let the corresponding specular reflection points on the trail be P_o, P_1 and P_2 respectively. From Fermat's Law the path length TP_oR_o is a minimum. It follows that the bisector of the angle TP_oR_o is perpendicular to the trail MM'. Suppose this bisector meets TR_o at A_o, and similarly the bisector of TP_1R_1 meets TR_1 at A_1. Assign the coordinates (-d,0,0) to T, (b,0,0) to R_1, (0,c,0) to R_2 and (-q,0,0) to A_o. Let the direction cosines of R_oP_o be ℓ,m,n; those of the trail be λ,μ,ν.

Let ϵ_1 be the distance measured along the trail from P_o to P_1 and ϵ_2 the distance from P_o to P_2 (positive in the direction of travel of the meteor). The parametric equation of the trail is

$$\left.\begin{aligned} x &= \ell r_o + \lambda\epsilon \\ y &= mr_o + \mu\epsilon \\ z &= nr_o + \nu\epsilon \end{aligned}\right\} \quad \ldots (11)$$

where r_o is the length R_oP_o

The spaced station problem is to find suitable equations for λ, μ, ν using ϵ_1 and ϵ_2 as basic data.

As $r_o/TR_o \longrightarrow \infty$, A_o tends to the bisector of TR_o, A_1 of TR_1 etc. In the limiting case the coordinates of A_o are $(-d/2,0,0)$; of A_1, $(-(d-b)/2,0,0)$. If the ground spacing is small enough it can be easily shown that

$$\left.\begin{aligned} \lambda &= \frac{\epsilon_1}{b/2} \\ \mu &= \frac{\epsilon_2}{c/2} \end{aligned}\right\} \qquad \ldots (12)$$

This is true for three spaced radar stations, and is sufficiently accurate for the method of Davies and Gill (1960), where the transmitter is coincident with one receiver. However, for the Adelaide survey, where TR_o is 23 km, the approximation leads to errors of more than a few percent.

An exact solution is derived in Appendix 2.1. λ is given as the root of a cubic, the coefficients of which are not merely functions of ϵ_1 and the ground geometry, but also depend on ℓ,m,n. There is also a quadratic in μ, the coefficients of which involve λ. Using a high speed digital computor, there is no reason why these exact

solutions should not be applied using the equations developed in Appendix 2.1. However, at the time this problem was first discussed there were no computors available in Adelaide, and it was planned to use the exact solutions to develop maps of the errors involved in using the approximate equations (12).

An alternate approach was then suggested by J.R.G. Morris, of Armstrong-Whitworth Aircraft Ltd., which promised to be more easily applicable with limited computing facilities. He suggested an expansion of the solution in a power series of $1/R_o$ to the required degree of accuracy. By considering the spheroids of contact of the meteor trails under the condition of specular reflection he was able to develop such a solution. This method was finally adopted and is given in detail in Appendix 2.2. To the second order in $1/R_o$, with the following notation:

$$TR_o = 2d_o$$

$$R_oR_1 = 2d_1$$

$$R_oR_2 = 2c$$

$$TP_i + P_iR_i = 2\rho_i \qquad i = 0,1,2$$

λ_o and μ_o are the zeroth order approximations that correspond to the system of three spaced radar stations, and are given by

$$\lambda_o = \epsilon_1/d_1$$

$$\mu_o = \epsilon_2/c$$

$$\lambda = \lambda_o(1-(2d_o+d_1)\ell/r_o+(d_1^2+d_1d_o-d_o^2)(1-2\ell^2)/r_o^2+(2d_o+d_1)^2 \cdot\ell^2/r_o^2)-\lambda_o^3(d_o+d_1)^2/r_o^2 \quad \ldots (13)$$

$$\mu = \mu_o(1-(\ell d_o+mc)/r_o-(d_o^2(1-2\ell^2)-c^2(1-2m^2)+(\ell d_o+mc)^2)/r_o^2) -\lambda d_o(m-(\ell d_o m+c(1-m^2))/r_o)/r_o \quad \ldots (14)$$

$$r_o = \rho_o(1-\ell d_o/\rho_o-d_o^2(1-\ell^2)/\rho_o^2 \quad \ldots (15)$$

$$\nu = -(1-\lambda^2-\mu^2)^{1/2} \quad \ldots (16a)$$

and also,

$$\nu' = -(\mu m+\lambda(\ell+d_o/r_o)(1-d_o^2/r_o^2))/n \quad \ldots (16b)$$

ϵ_1 and ϵ_2 are measured from the observed time differences and ℓ, m and ρ_o are measured independently from the doppler waveforms and the radar range respectively. By this means we have available one redundant measurement. It is convenient to rearrange (16b) to

$$n' = (\mu m + \lambda \ell')/\nu \qquad \ldots (17)$$

where $\ell' = (\ell + d_o/r_o)(1 - d_o^2/r_o^2)$

and treat this value of n' as the redundant value. It is not an accurate method of evaluating n, as under certain conditions discussed in Section 3.4, small errors in ϵ_1, ϵ_2 can cause large errors in n'. However, it does give us a means of assessing the accuracy of the data, and in fact (17) is used to modify the data into better all-round consistency.

3.4 The Height of the Reflection Point.

using $\nu = (1 - \lambda^2 - \mu^2)^{\frac{1}{2}}$

for convenience ν is taken as positive and is the cosine of the observed radiant zenith angle. The condition that both heights are equal demands that n = n', hence from (17)

$$\lambda^2(\ell'^2 + n^2) + 2\lambda\mu(\ell' m) + \mu^2(m^2 + n^2) - n^2 = 0$$

which is a conic of the form

$$A\lambda^2 + 2H\lambda\mu + B\mu^2 + C = 0$$

$\Sigma = AB - H^2 = n^2(1 - \ell^2 + \ell'^2)$ is always > 0

$\Delta = ABC - CH^2$ reduces to

$$n^2((\ell' m)^2 - (\ell'^2 + n^2)(m^2 + n^2)) = -n^2\Sigma,$$

hence always < 0

Thus the locus of the observed point is always a real ellipse in the λ,μ plane. As $C = -n^2 = \Delta/\Sigma$, the centre is always $\lambda = \mu = 0$. It can be easily shown that if either ℓ' or $m = 0$, the two axes of the ellipse are $\lambda = \mu = 0$. It has been shown that for the two heights to be identical, the point λ,μ must lie on an ellipse whose parameters are functions of ℓ, m. In practice the observed values of λ,μ will not exactly satisfy the above, and the point λ,μ will lie a little off the ellipse, say at P on Figure 4. $n = (1 - \ell^2 - m^2)^{\frac{1}{2}}$ is a more accurate measurement of the true reflection point zenith

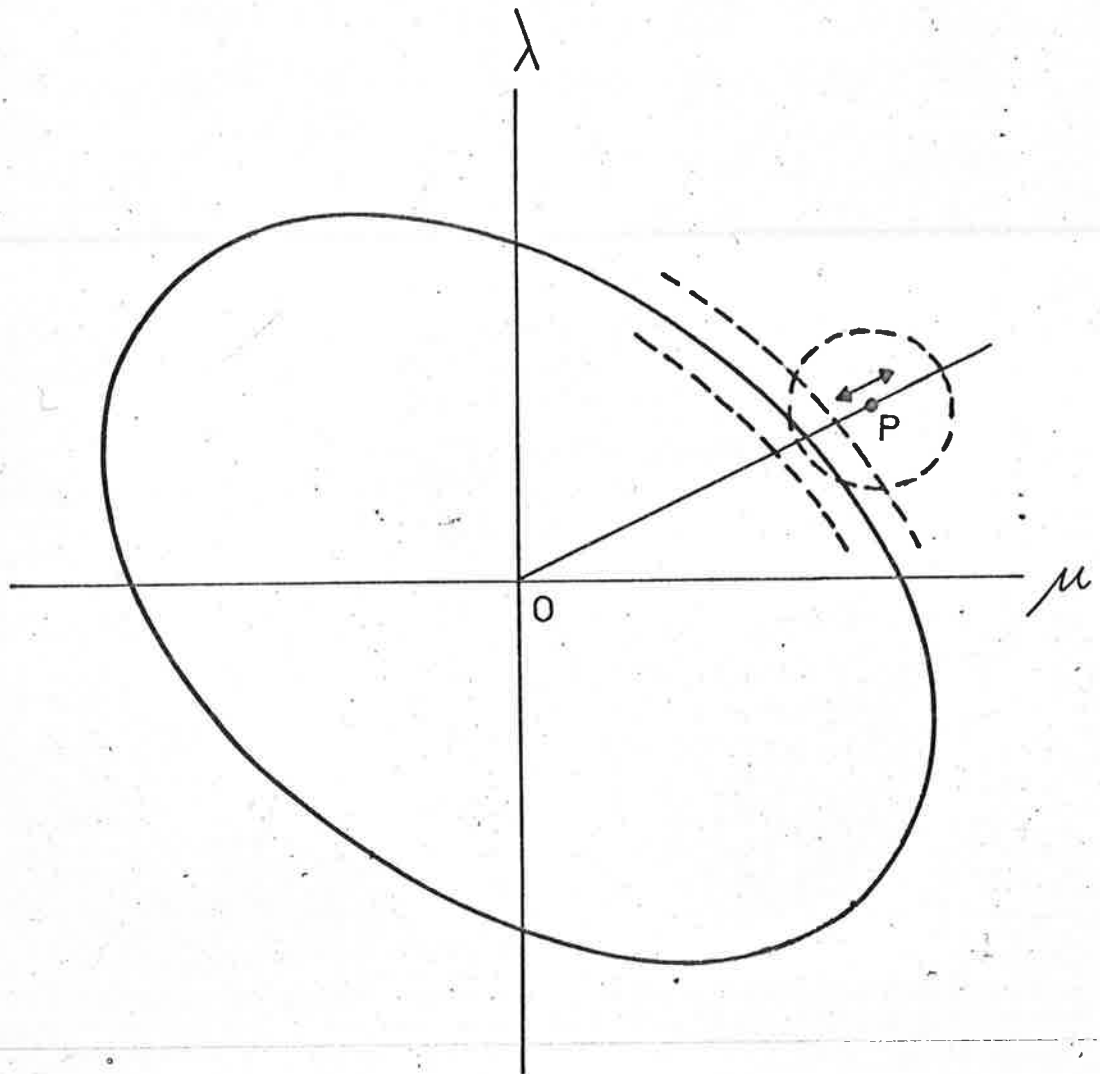

Figure 3.4

angle than the redundant value n'. Particularly if ν is small, a small variation in the magnitude of λ or μ can severely effect the value of n'. The simplest way to reconcile an observed point O with the theoretical ellipse is to move P towards or away from the centre along the line OP. The question is how much movement is allowed in any particular observation? The ellipse will have a certain error zone defined by the errors in ℓ,m. Similarly, P will have a zone of error defined by the errors in λ,μ. Ideally the point P should be moved to the centre of overlap of the two zones. A simple attempt at this is made in the reduction program. If the reflection point is high in the sky, both ℓ and m will be small. Hence the value of n can be expected to be accurate. This echo would result from a radiant near the horizon, with ν small. Small errors in λ,μ will greatly effect ν and the value of n' from (7) will be inaccurate. Thus the error zone of the ellipse will be narrow and that of the point P large. Accordingly, the point P is moved to bring the value of n' almost coincident with n. If the radiant is high in the sky the situation tends to be

reversed. It is not completely so, because fundamentally the measurement of n is more direct and accurate than the application of (17) to find n'. In the latter case P is moved a restricted distance towards the ellipse. By altering the time differences P is moved parallel to $\lambda = 0$ and $\mu = 0$. Ideally the path of P should be perpendicular to the ellipse, but a sufficient approximation to this is the line from the centre, OP. Adjustment of P along OP can be made by increasing or decreasing the meteor velocity by a few percent. λ and μ are thus adjusted in proportion to their absolute value, as

$$\epsilon_1 = v(t_1 - t_o)$$

$$\lambda_o = \epsilon_1/d_1$$

similarly for μ_o.

In an attempt to satisfy the conditions discussed in the previous paragraph, the velocity is altered to bring the two heights to within (16-12.n) km of each other. This function was found empirically and has proved

satisfactory in practice.

In computing the survey, the further restriction was added that no velocity was altered by more than 10%, the mean absolute alteration was 2% for each month. Furthermore, if the observed velocity was computed from an echo with a large number of usable Fresnel diffraction cycles, and thus could be expected to be accurate, the allowable velocity adjustment was correspondingly decreased. In practice, if a total number of m diffraction cycles were used to compute the velocity for the three traces, the allowable adjustment was (10-2m/7)%. This would be about 6% for an average echo.

Another feature of this optimization of the data is that it provides a very sensitive measure of the overall accuracy of the velocity reduction technique. Any tendency for the velocities to be too high will result in n' being too large and consequently the optimization will show a tendency to always decrease the velocity. Over thirteen months the following mean values were obtained for the percentage optimization of velocity: +1, +1, +0, -0, +0, -0, -0, -0, -1, -0, -0, -0, -0%. The values

obtained for the mean height differences were: +1, +0, -0, -0, -0, -0, -0, -0, -1, -1, -0, -0, -0 km. The predominant negative sign indicates that n' > n and the velocities were generally higher than reality, but the difference was certainly less than 1%. This seems an excellent independent check on the velocity reduction program.

---

* The notation used in these formulae is such that multiplication and division take precedence over addition and subtraction.

† His thesis ' Radio Measurements of Meteor Velocities ' is in error on this point.

CHAPTER 4

EQUIPMENT

4.1 General.

The orbit survey system consists of a c.w. and a radar transmitter on 27 Mc/s at Adelaide, a main receiving station at St. Kilda, about 23 km north of Adelaide, and two outstations, one 5 km north, the other 5 km east of St. Kilda. The main receiving station at St. Kilda has a spaced aerial array to determine the direction cosines of the reflection point and a radar receiving system to determine the range of each echo. This is the equipment necessary to measure the winds in the meteor region, and operates on a routine basis for about one week each month.

The main station has a F.M. link receiver for each outstation. The output from each is recorded along with that from one of the main station 27 Mc/s receivers. All recording is done photographically on 35 mm film.

The three outputs are also delayed 1.3 sec on a multi-channel tape delay unit before going to the orbit-display unit. To save film each echo triggers a sequence unit which actuates the three display units and their cameras. The tape delay unit is inserted in order to observe the initial build-up of each of the three station echoes, which takes place before the doppler waveform at the main station can trigger the displays. The C.W. reduction is performed on the diffraction pattern prior to the t_o point, unlike the radar system, where the reduction is done on the pattern following the t_o point. The C.W. doppler beat usually obscures the latter whistle.

Each outstation 27 Mc/s receiver output is transferred via F.M. VHF link back to St. Kilda, where all three station signals are recorded in the following way:

The wind equipment records the radar range and the five doppler beat outputs, with a frequency response from DC to 50 c/s, for the purpose of defining the position and drift of the main station t_o point in space.

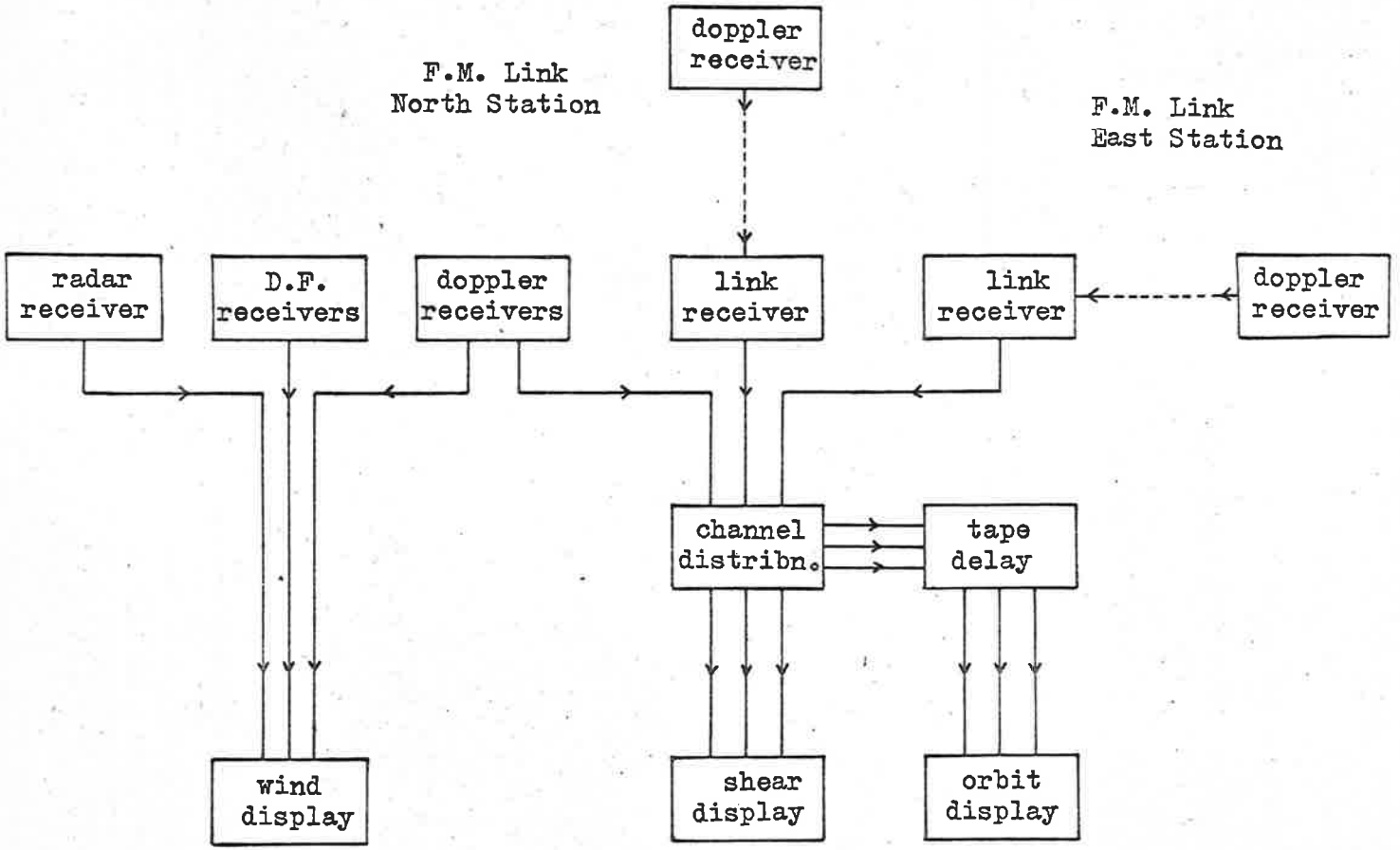

Figure 4.1 St KILDA RECEIVING STATION

The turbulence display records the doppler beat waveform from one of the main station receivers and each outstation with a frequency response similar to that of the wind equipment.

The orbit display, with a higher film speed of 1.8 in/sec, records the turbulence information for a limited time after the display is triggered, and also, by virtue of the tape delay unit, the build up pattern of each echo for about 300 msec prior to the time of the main station t_o point. Thus allowance is made for the maximum of about 100 msec time difference between station echoes. Each echo is recorded for approximately 600 msec. The resolution is such that measurements can be made to less than 0.5 msec. Thus the bandwidth of the outstation signal, DC to 600 c/s, can be fully utilised. The block diagram of the equipment is shown in Figure 1.

4.2 Transmitters and aerials.

The C.W. transmitter at Adelaide feeds about 300 watts into a three-element Yagi suspended along and near the roof of the Physics department. The Yagi is directed to the zenith and aligned along 117° T.N. The transmitter is modulated by a sharp 90° phase shift at a rate of 50 c/s. This produces pulses or 'phase spikes' at this rate on the doppler beat waveform. The length of each phase spike corresponds to the difference in time between the direct ground wave and the reflected skywave. The phase spikes trace out a doppler beat shifted 90° either leading or lagging the main trace depending on whether the trail is advancing or receding. Thus the sense of the wind drift can be determined immediately. The radar transmitter feeds 10 kW peak pulse power on 27 Mc/s at a p.r.f. of 100 c/s into a similar antenna end on to the C.W. antenna.

The layout of the receiving antennas at St. Kilda is shown in Figure 2. These are all $\lambda/2$ dipoles $\lambda/4$ above ground and aligned along 77° T.N. This alignment is necessitated by the wind direction finding system which requires that the antennas be perpendicular to the wavefront from Adelaide.

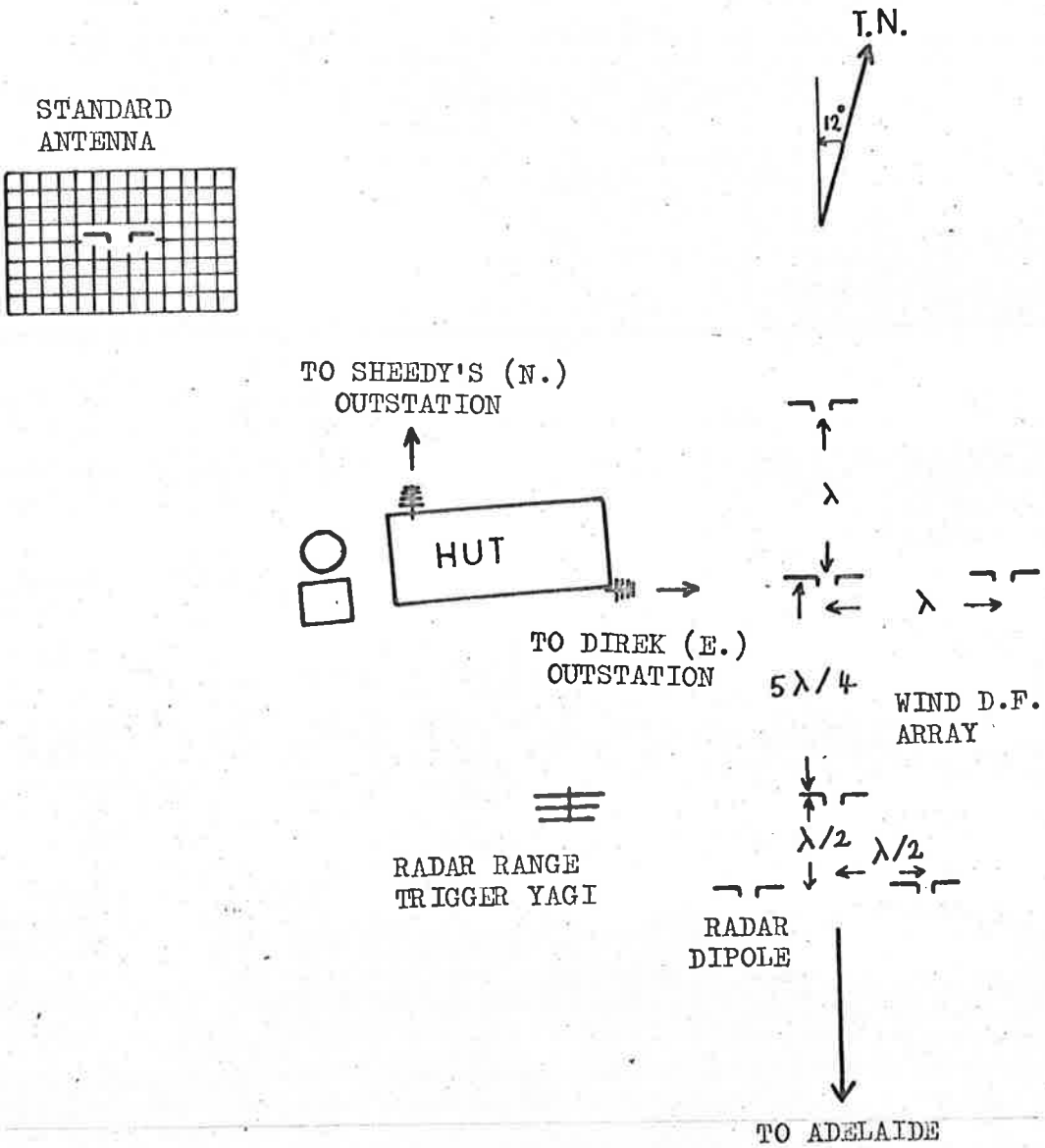

Figure 4.2 - Antenna layout at St Kilda.

4.3 The Outstations.

A block diagram of the equipment is shown in Figure 4. The installation is given in detail in Figure 3, as it was novel and highly successful in protecting the equipment from weather and vandals. Cooling air was drawn in through the aerial post by the blower in the bottom of the box; exhaust was through gaps underneath the lid. For minor repairs the outstation could be raised by pulley on the permanent gantry, or for more major work easily pushed into a station wagon by one man.

The detector level from the 27 Mc/s receiver was superimposed as AM modulation on a carrier of 2 kc/s for the northern outstation, 5 kc/s for the eastern station. These two carriers provided F.M. for the 167 Mc/s link to St. Kilda. The link frequency was slightly shifted for one outstation to avoid interaction between links, however the directional Yagi antennas at right angles to each other effectively prevented any such interaction.

4.4 St. Kilda - Tape Delay.

For the orbit survey section, the main station receiver output was put on a carrier of 3.5 kc/s and all three channels fed into the multi-channel tape delay record amplifier. Here the channels were mixed and suitably amplified before going to a common record head. During amplification the modulation depth was artificially increased for reasons explained later. The playback signal was amplified and then separated into its constituent channels by means of three multi-section band-pass filters. The 3 db points of each filter section were as follows:
1.4 to 2.6 kc/s, 2.9 to 4.1 kc/s and 4.4 to 5.6 kc/s. Despite the band proximity, the filters were sharp enough to keep intermodulation below 1%. The bandwidth of 1.2 kc/s for each channel was enough to pass the fastest whistle and also the phase spikes used in determining the sense of the doppler beat. Each channel was then detected by a bridge diode network and finally passed into a 0 to 600 c/s demodulator to remove the various carrier frequencies. Thus the

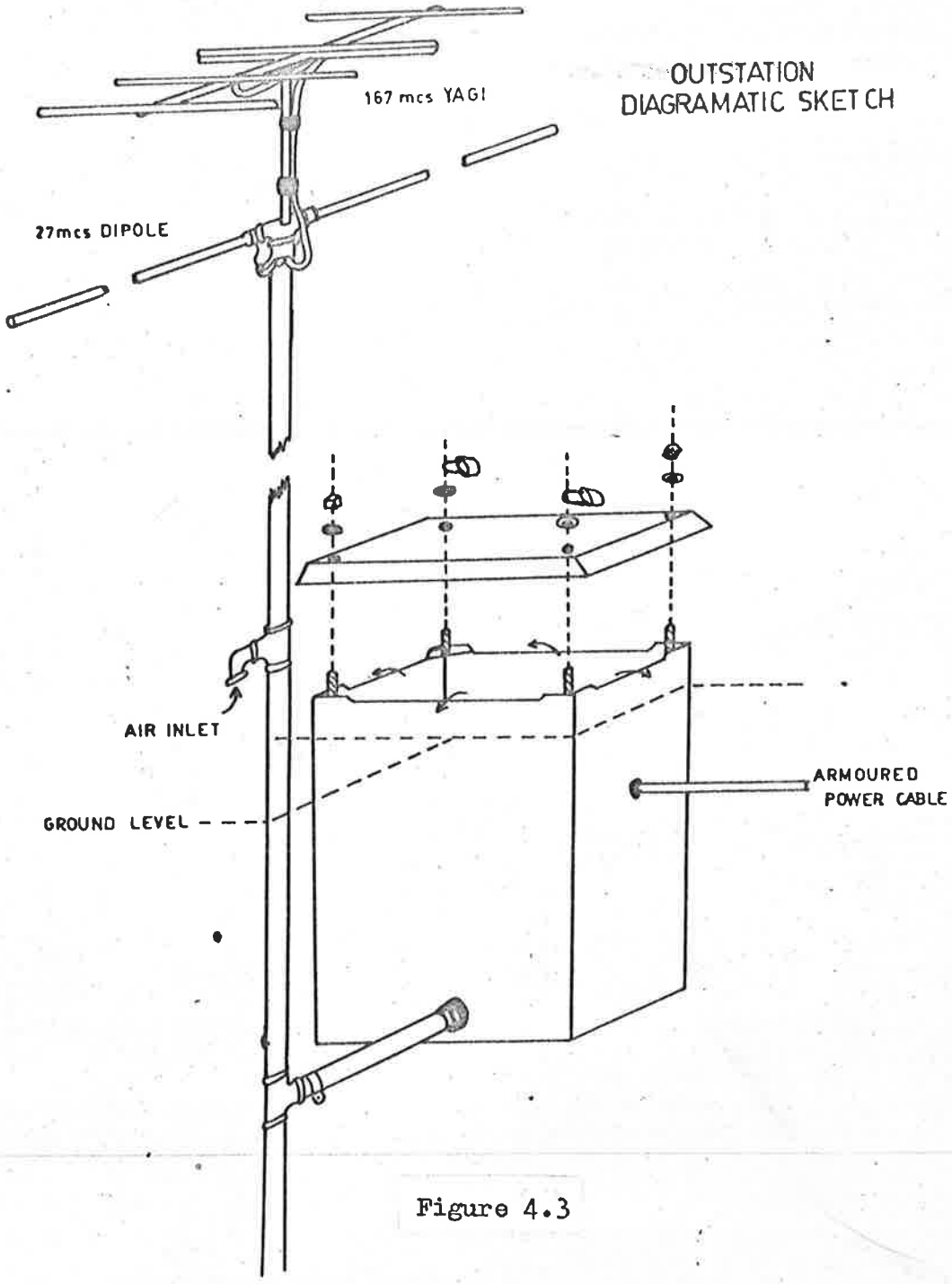
OUTSTATION
DIAGRAMATIC SKETCH
167 mcs YAGI
27mcs DIPOLE
AIR INLET
GROUND LEVEL
ARMOURED
POWER CABLE

Figure 4.3

three delayed 27 Mc/s receiver outputs were available for suitable amplification before going on to the Y plates of the display C.R.O. tubes. The DC receiver detector level was maintained throughout.

The following points may be of interest. The tape unit had to operate 24 hrs/day unattended and a unit was available which, while far from ideal, was modified to do this job. A 7 in reel of 1/4 in tape (1800 ft of long play) was used with aluminium foil sensors at each end of the tape. These operated an automatic reversal network which reversed the functions of record/playback at the respective heads. The complex switching for this operation necessitated the use of miniature REX transformers to keep the record and playback leads at low impedance (1 KΩ). It would have been far preferable to employ fast rewind and keep the tape recording in the one direction. For the fainter whistles one needed to see less than 5% modulation and at this level it was necessary to be very careful about tape flow, otherwise level fluctuations would distort and even obscure the whistle waveform. Providing for both directions of travel only aggravated this problem. The level fluctuations seemed to be caused largely by edge effects, consequently the use of $\frac{1}{2}$ inch tape would decrease this trouble. It would also enable multi-track tape heads to be used and possibly allow all channels to employ the same best carrier frequency. It would also eliminate the filter networks necessary for channel mixing.

The tape speed employed was $7\frac{1}{2}$ ins/sec and could have profitably been raised to 15 ins/sec to keep to fluctuations of the 5 kc/s carrier below 5%. Tape response to the 2 kc/s carrier was much better and the tape noise for this channel was correspondingly lower. A modulation increasing network was employed on the 3.5 kc/s and 5 kc/s channels to raise the effective modulation level of the whistle waveforms. This network caused third harmonic distortion of the carrier, but providing the increase was kept below 2X this distortion produced no noticable effect. The network was frequency conscious and did not act on the low frequency doppler beat. The circuits for this unit and for the record/playback emplifiers are given in Appendix 3.

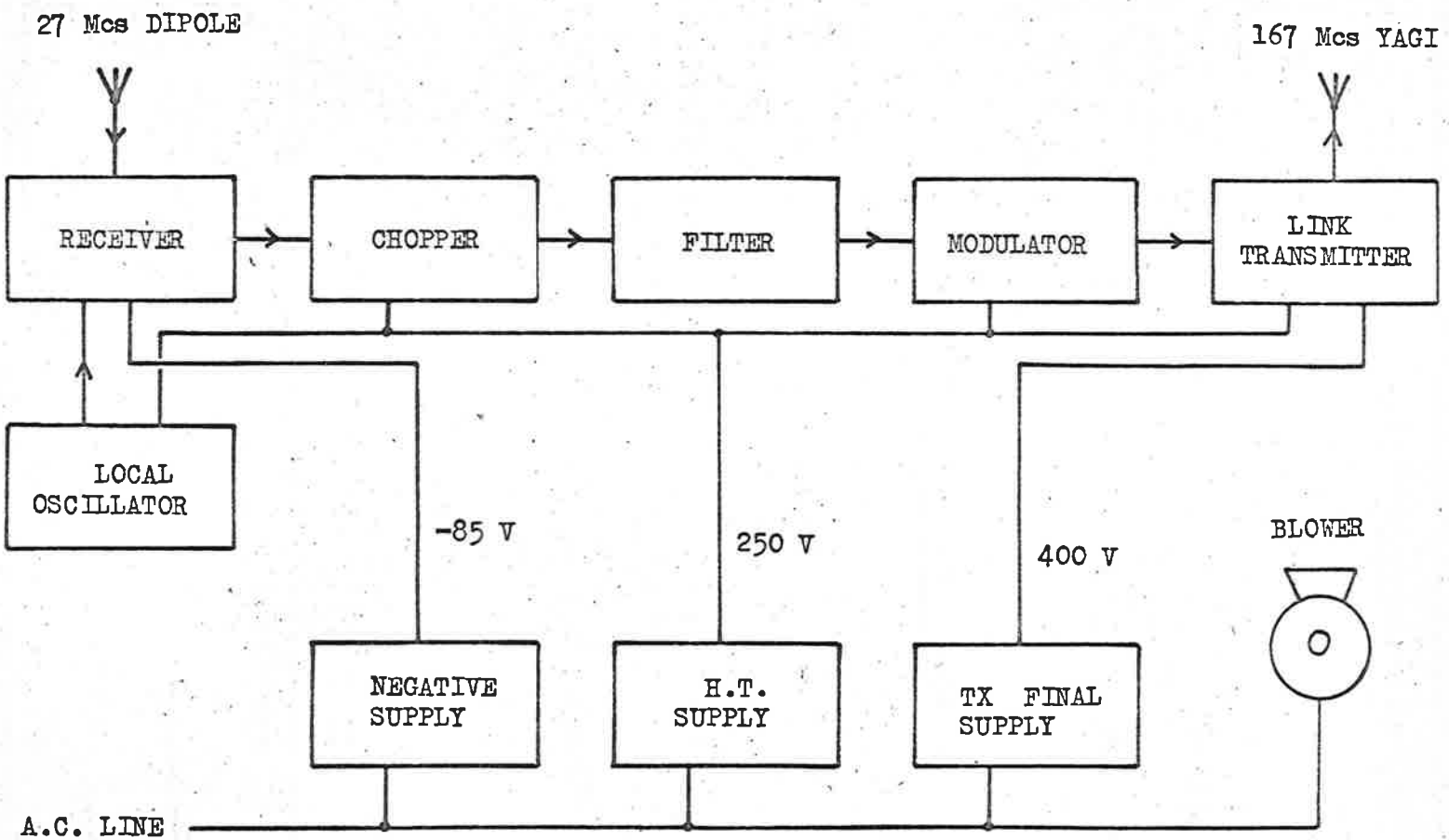

Figure 4.4 OUTSTATION

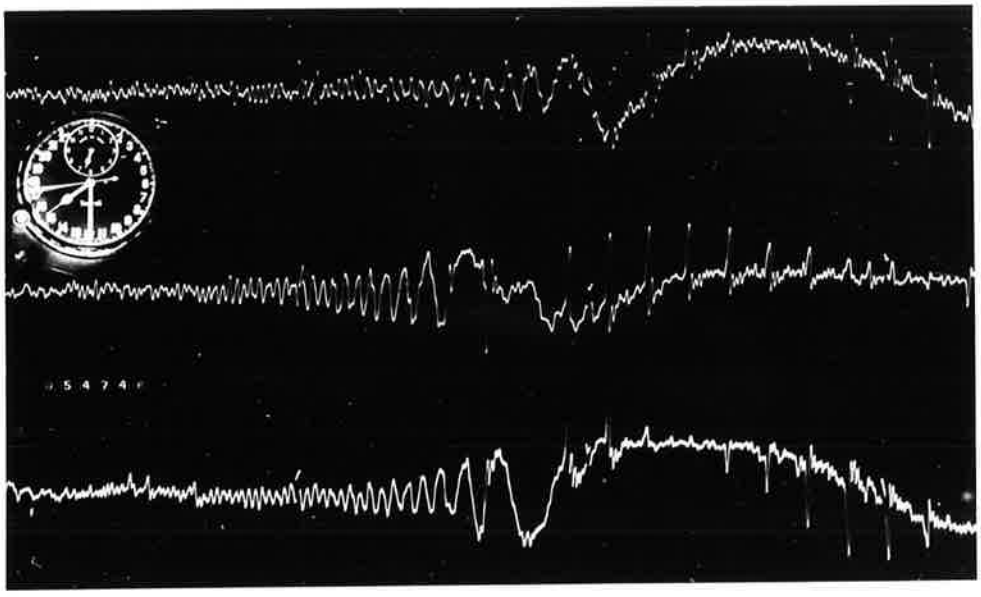

ORBIT

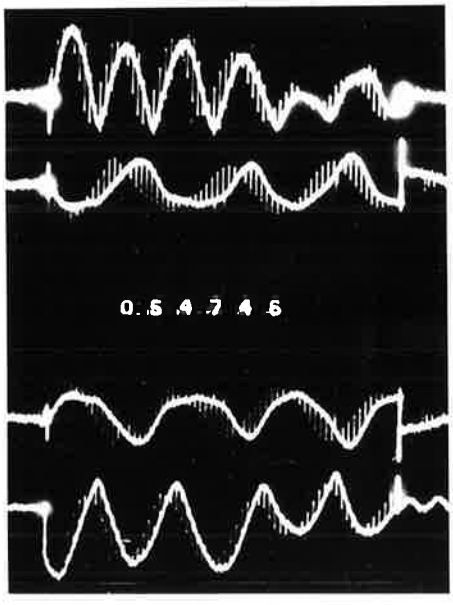

SHEAR

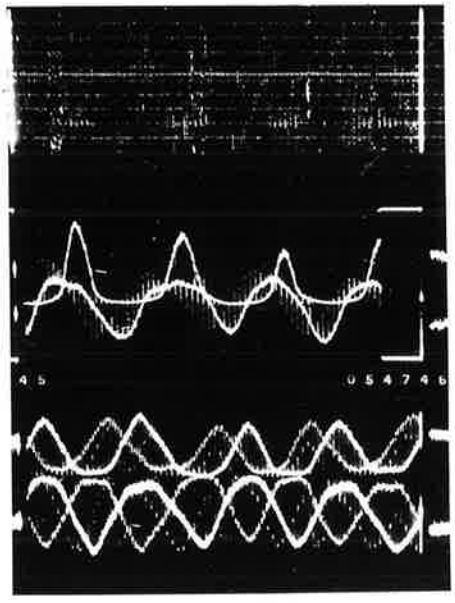

WIND

Fig 4.5

In order to assume excatly the same delay on each channel the signals were mixed and fed into a common full track head. Thus problems of head alignment did not effect the accuracy of the time separations. The gap between the playback and record head was about 10 in, giving a signal delay of 1.3 sec. The signal was continuously erased, recorded and played back, the playback signals going to the display unit. Only on receipt of a trigger from the wind equipment would these delayed waveforms be recorded on film.

4.5 St. Kilda - Photographic Display.

A complete record from all three displays is shown in Figure 5. The diffraction traces are good, but by no means outstanding. In spite of the low transmitter power one or two exceptional echoes showed diffraction patterns well past fifty Fresnel zones. Figure 6 shows both a very good echo and a poor echo which nevertheless could still be adequately reduced.*

The design of the orbit display sequence unit was based on a variable delay photographic timer (Radio, Television and Hobbies 1956). On receipt of a 24 V pulse from the wind equipment the sequence unit set in motion the following sequence of events:

(i) During the first 700 msec approximately, the clock light came on, the counter actuated and the electronic flash was triggered to record the echo number.

(ii) From 700 - 1300 msec after the initial trigger the clock was turned off, the camera clutch closed and the C.R.O. tubes brightened. At the end of this sequence the equipment then resumed its quiescent state ready for the next echo.

With careful adjustment of the first delay, a camera run of 600 msec was sufficient to ensure that all the significant information in the three signals was fully recorded. This allowed for up to 100 msec time displacement between the traces.

To ensure accurate trace timing, a time marker unit inserted 1 msec pulses at intervals of 100 msec on the Y plate of each C.R.O. tube. All time measurements were taken independently for each trace

ORBIT EQUIPMENT

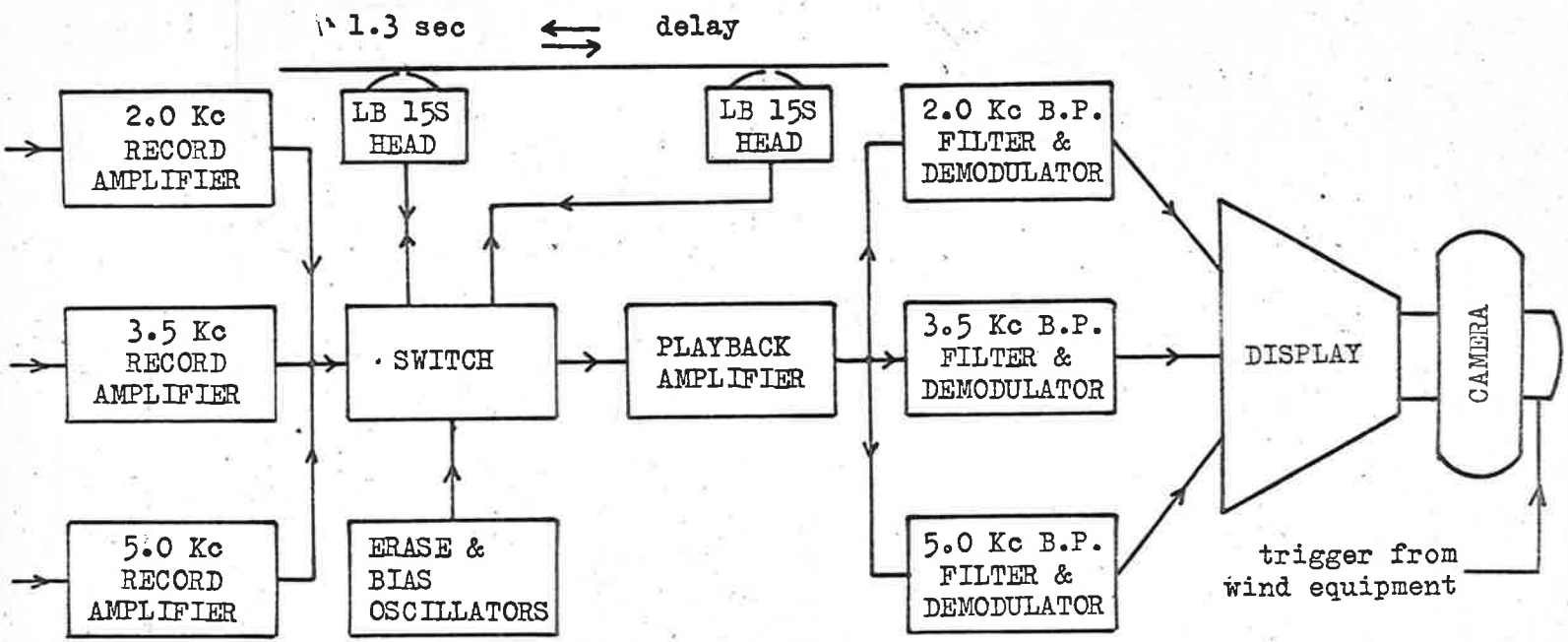

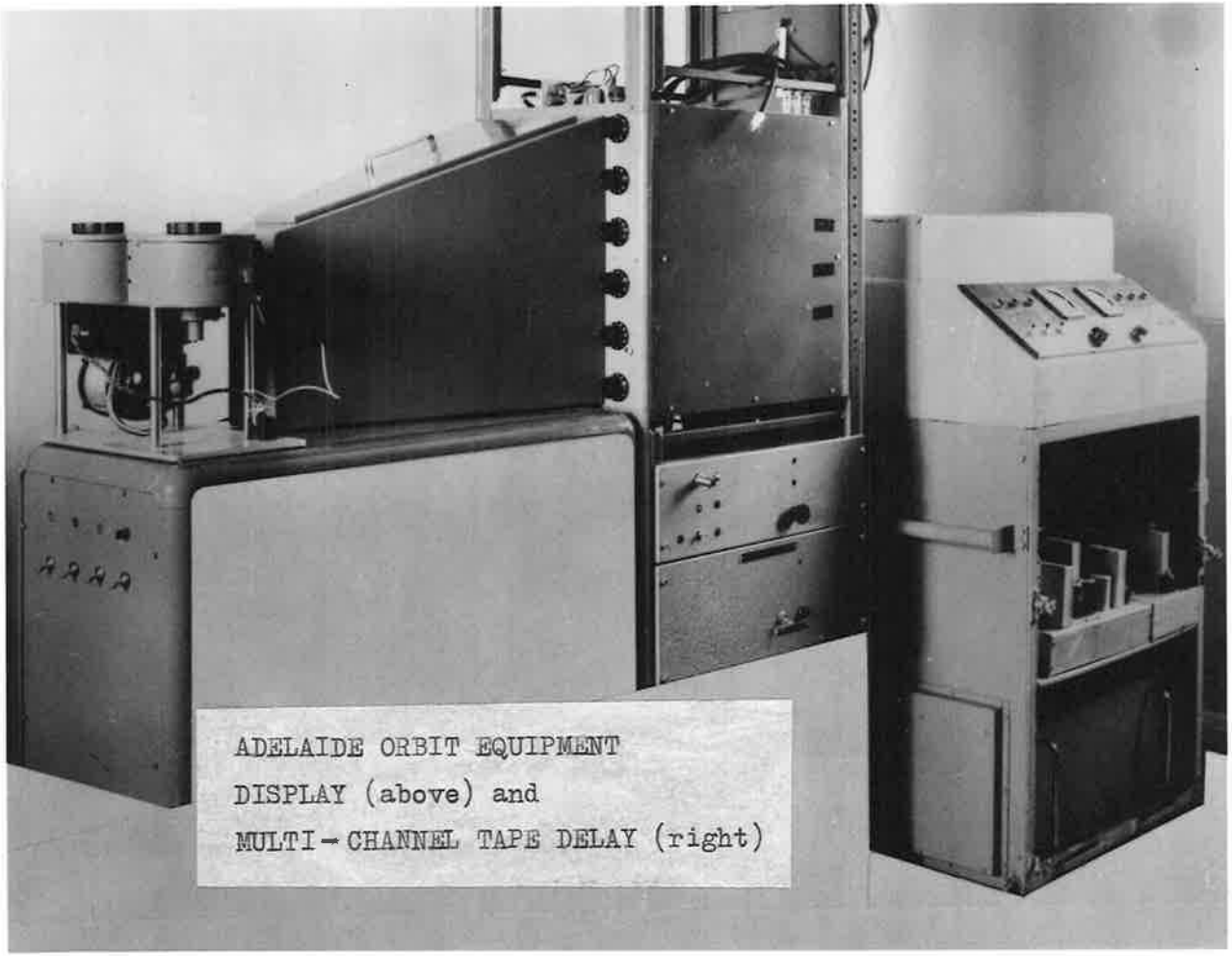

ADELAIDE ORBIT EQUIPMENT
DISPLAY (above) and
MULTI-CHANNEL TAPE DELAY (right)

plate 4

relative to its time marker. Thus it did not matter if any of the traces were misaligned in the X direction with respect to the others. It was only necessary to ensure that the Y direction for each trace was vertical.

The Y shift amplifiers for each trace were of simple design (Appendix 3), the frequency response being attenuated below 300 c/s to about 1/3 of the 300 c/s value at DC. This was to selectively increase the normal whistle to doppler amplitude ratio and to avoid the doppler beat signal overloading the amplifiers.

The time base depended on constant film speed. The camera motor was run continuously and a magnetic clutch was operated to run the film through. Tests with a signal generator indicated no measurable acceleration of the film after the C.R.O. tubes were brightened and no jerking of the film during recording. The absolute speed of the camera was determined by the frequency of the mains supply. The calibration of the film speed is described in Chapter 5.

The electronic counter flash unit was of novel design. In order to correlate the records from each of the three displays each echo was given a number. The wind and turbulence displays had no dead time corresponding to the 700 msec delay in the orbit equipment. Thus, unless the sequence units were to be further complicated, the counters in these displays had to be photographed whilst the film was in motion. A 1 msec pulse of light from an electronic flash tube was 'piped' to the counter figures from behind the display face by internal reflection along a carefully curved piece of perspex. The flash tube was operated well below its rated energy output and the unit was extremely reliable. Each of the three tubes has to date flashed over 300,000 times without replacement. The counters too were reliable; during the survey they rarely got out of step.

In the orbit display an eight-day clock was illuminated for each echo by a 3 W globe during the initial 700 msec delay. The time of each echo was thus available to within a few seconds; however for the echo reduction it was sufficient to read to the nearest minute. Careful placing of the light source to avoid specular

reflection on to the camera lens ensured high quality photographic recording without the necessity of removing the glass from the clock face.†

4.6 Operating levels.

The 27 Mc/s receivers had a noise figure of 2 db and the sites for all three stations were in open farmland and were electrically quiet. The height of the C.W. transmitter antenna was adjusted to give a ground wave signal of 6 μV at the input to the receivers. At this operating point the signal level of each receiver output was about 26 db above noise. The low transmitter power (250 W) was responsible for the poor signal/noise ratio of many of the echoes used in the survey. The tape 'noise' discussed earlier in this Chapter contributed significantly only to the 5 kc/s channel (trace 3), and even this is not apparent from the records (Figures 4.5 and 4.6). The records published by McKinley (1951) show very little noise. He used a transmitter of 1.5 kW output on 30.02 Mc/s. This factor alone would account for a signal/noise ratio $\sqrt{6}$ better than that of the Adelaide survey. However, he does not state the level of the ground wave at his receiving station. For a given transmitter power it is this level that determines the magnitude range of the meteors observed. This survey was limited to meteors producing trails of maximum line density greater than 3.10^{11} electrons/cm.

---

*The data for this echo is given in Appendix 5.2 (Echo No. 36958).

†Unfortunately the clock was over-exposed for several of the echoes shown in Figure 6.

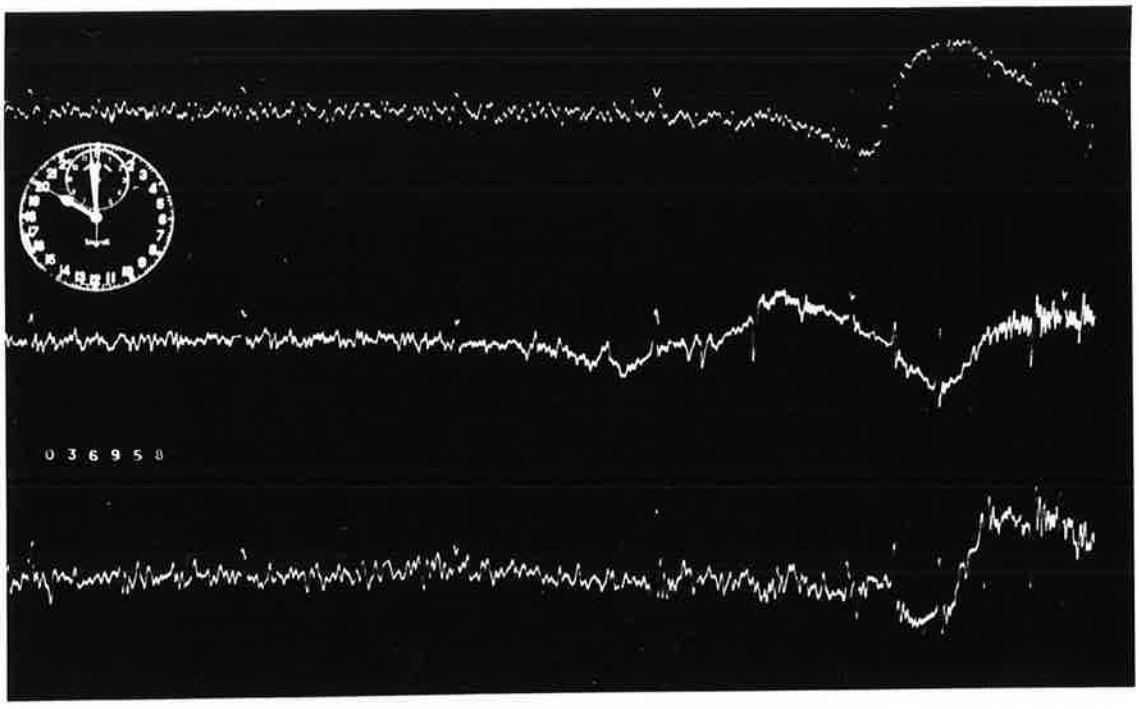

a

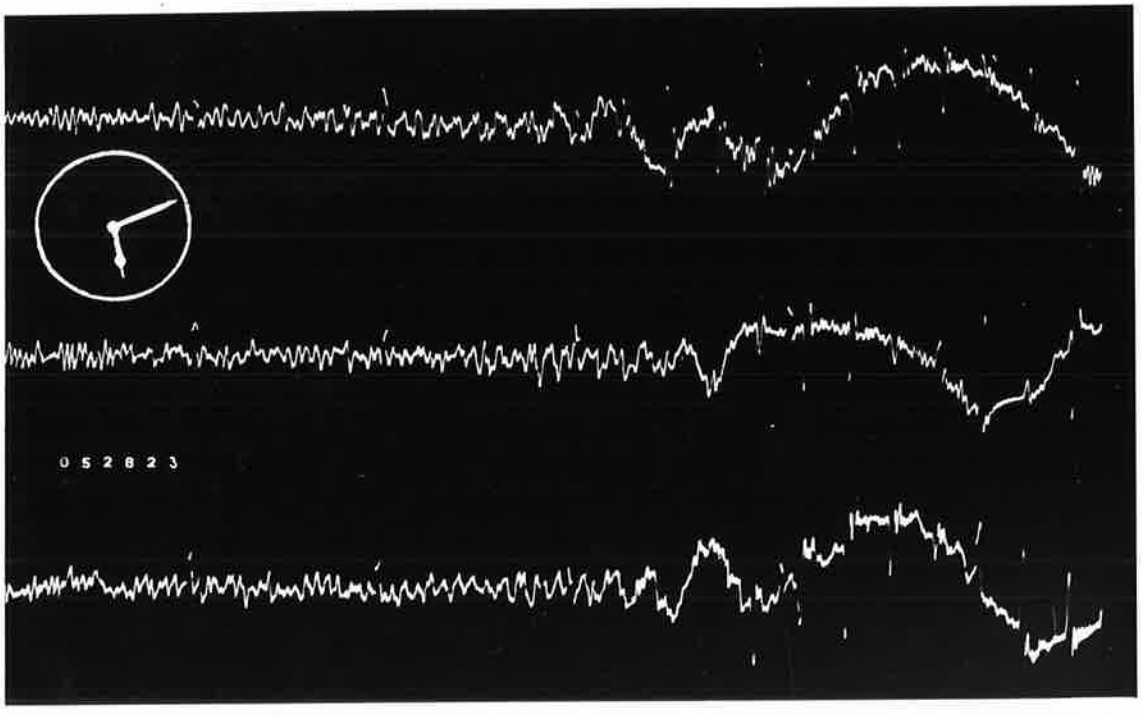

figure 4·6

b

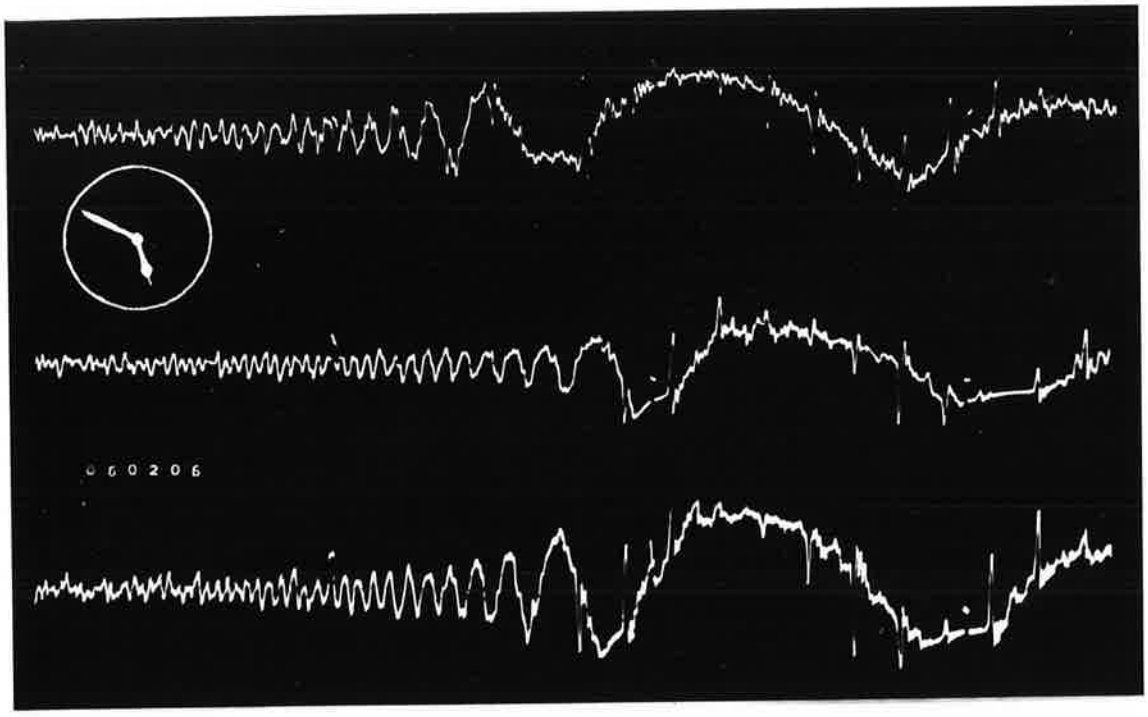

c

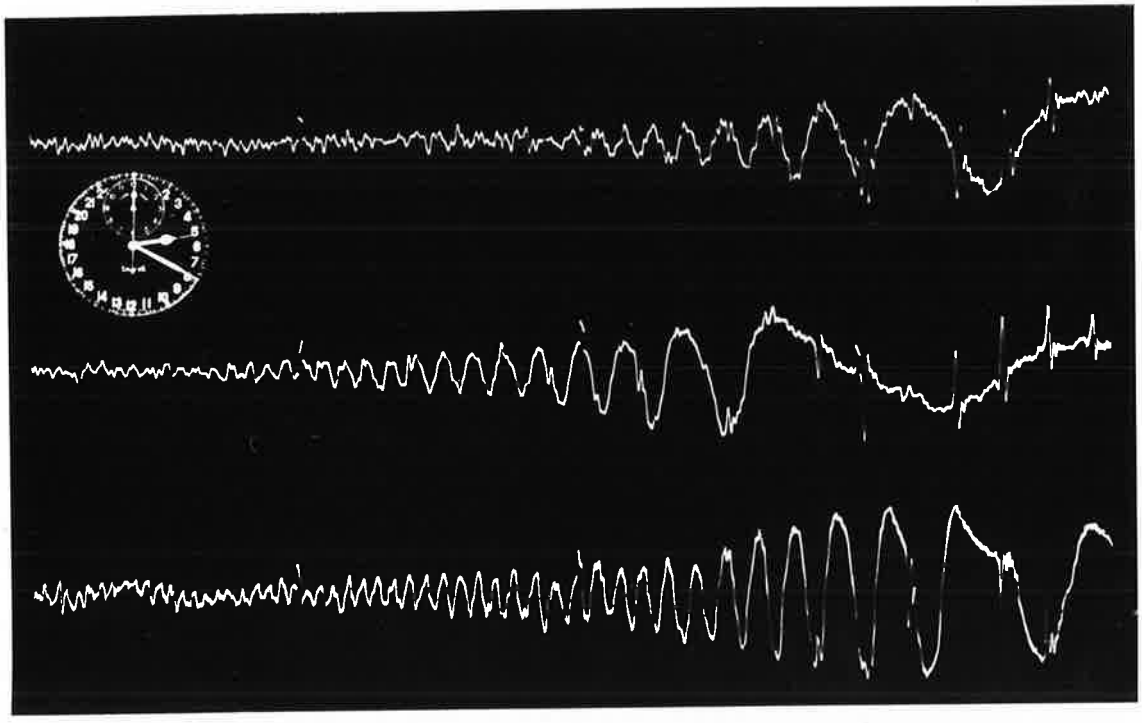

d

CHAPTER 5

REDUCTION OF DATA

5.1 Theory of Reduction.

In Chapter 3.1 we have shown that the amplitude of the groundwave plus skywave is given by

$$A_{r+d} = F_r(C-iS)e^{i\phi} + F_d e^{i(\phi+\psi)} \quad \ldots (1)$$

$$\text{where } \psi = 2\pi(2R_o - D)/\lambda + \beta$$

Consider the physical significance of the angle ψ. It is the phase of the ground wave vector GW relative to the phase of the element of skywave RW reflected from the t_o point. Differentiating equation 3.7 gives

$$\frac{d\psi}{dt} = \frac{4\pi}{\lambda} \frac{dR_o}{dt}$$

By definition $\frac{d\psi}{dt}$ is thus positive for a receding echo. Imagine both vectors rotating anticlockwise at R.F. corresponding to ω in equation 3.3a. If the trail recedes, the rotation of RW is slowed down while GW continues at the normal rate. The variation of ψ with time gives rise to the doppler beat. In this instance GW moves slowly ahead of RW and ψ increases with time.

A more useful picture is to consider the phase of RW as zero, the groundwave vector GW rotating slowly in an anticlockwise direction as illustrated in Figure 1a. In drawing Cornu's spiral as a representation of the amplitude of the reflected wave A_r (Figure 3.1), one has implied that the vector RW is in fact stationary in time.

BE is the resultant skywave vector when the trail has completely formed and it sometimes is more convenient to measure the phase angle ψ' of the ground wave relative to this vector.

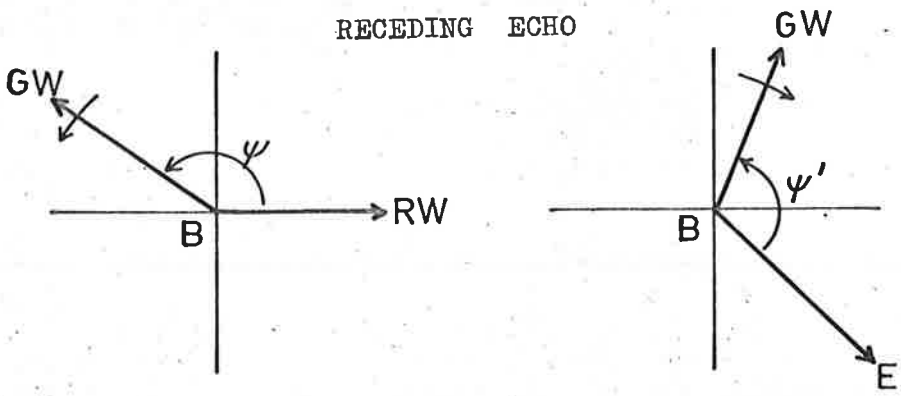

(a) Figure 5.1 (b)

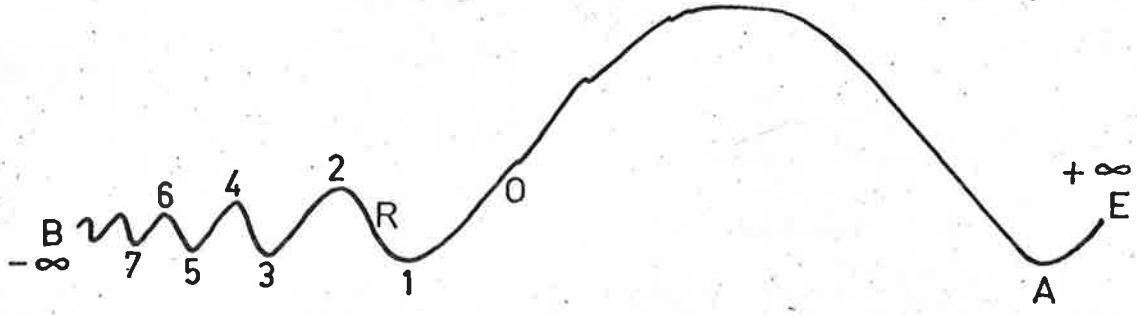

Figure 5.2

$$\psi' = \psi + \pi/4$$

To analyse the pre-t_o diffraction waveform it is also convenient to move backwards in time, hence another picture for a receding trail is that shown in Figure 1b. The direction of rotation of GW has been reversed, but ψ (and ψ') are still measured in the correct sense, from RW (and BE) to GW.

Consider a typical record of the form illustrated in Figure 2. It can be related to Figure 3.1 as follows: O is the t_o point, B approximates the $-\infty$ point, and E the $+\infty$ point. The post-t_o whistle has been largely obliterated by the larger doppler beat waveform caused by the variation of ψ' with time. The point A is a doppler minimum, hence

$$\psi' = \pi^c$$
$$\text{and } \psi = 3\pi/4^c$$

and at any point t sec before A

$$\psi(t) = 3\pi/4 \pm \frac{A}{R}\Big] 2\pi ft \qquad \ldots (2)$$

where A refers to an advancing echo, use positive sign;
R " " " receding " " negative "
f is the doppler frequency.

Of particular interest is the value of ψ at the t_o point, ψ_o say. This is the value of ψ used in (1), and it is this value that determines the appearance of the echo in the vicinity of the t_o point. McKinley (1951) has plotted the echo waveforms for varying ψ_o, assuming the doppler frequency is zero. These are shown in Figure 3 for ground and skywaves of equal amplitude. A fast doppler can considerably distort these waveforms, but in practice they are an excellent guide in estimating the position of the t_o point.

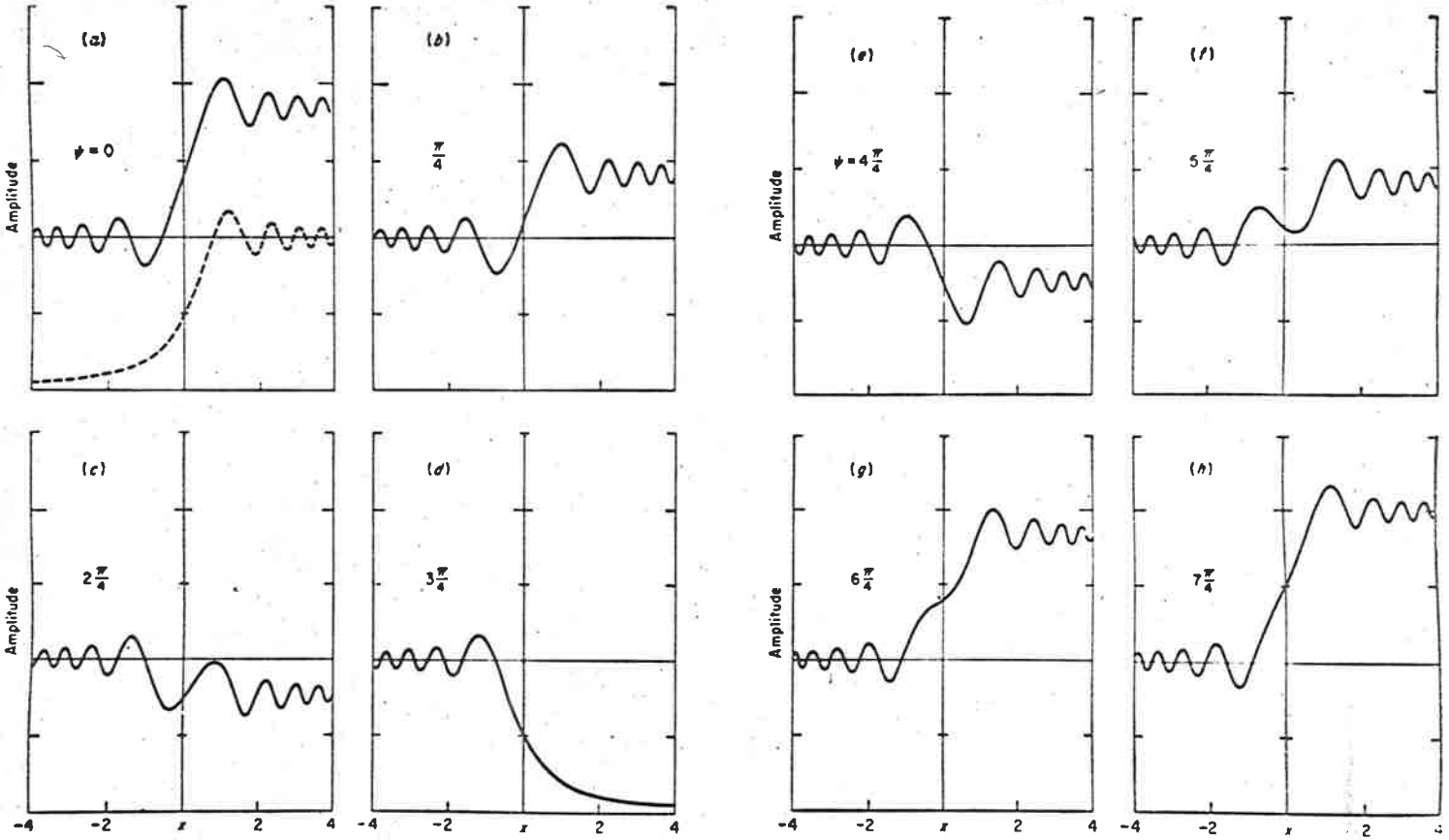

Theoretical amplitude-time curves of meteor echoes based on the diffraction theory. Receiver output voltage is plotted against the argument x of the Fresnel integrals, which is directly proportional to time. The dashed curve in graph (a) is for the noncoherent radar case. The solid curves are computed for the cw or coherent-pulse radar case, for selected values of ψ, and for equal strengths of the reference voltage and the final meteor-echo voltage.

Figure 5.3 - Diffraction waveforms for varying ψ_o. - by courtesy of D.W.R. McKinley -

As the diffraction waveform is formed, a maximum occurs whenever the rapidly oscillating skywave vector BR (Figure 3.1) is in the same direction as the more slowly moving groundwave vector. A minimum occurs when they are π^c out of phase. The rate at which the point R moves along the spiral is a linear function of the velocity of the meteor. To determine the velocity it is necessary to determine the one to one correspondence between points such as R on the echo waveform (Figure 2) and on the theoretical spiral (Figure 3.1). In practice, only the maxima and minima are used since in the presence of noise these points are the most clearly and easily defined. With the notation of equation 3.3b the position of R on Cornu's spiral is defined by the value of x, x being negative prior to the t_o point, O. To determine the x value of a diffraction maximum or minimum it is necessary only to know the number of maxima and minima prior to the t_o point and the value of the phase angle ψ over the spiral.

In the absence of wind the GW vector is stationary relative to the axes in Figure 4 and the diffraction maxima occur successively at x_1, x_2, x_3 etc. For a receding wind the GW vector rotates clockwise as one moves backwards in time, and the successive maxima would be shifted to x_1', x_2', x_3' etc. The variation of x with ψ has been determined graphically and from tables. The set of x values for the first ten minima is tabulated against ψ in Appendix 4. It does not follow, however, that the nth maximum is on the nth loop of Cornu's spiral, as a rapidly receding echo could 'wind in' the x value to the extent of the nth maximum being on the n + 1th loop.

5.2 Reduction Procedure.

McKinley (1951) and Mainstone (1960) determined the velocity of each echo by measuring the time interval between two chosen maxima or minima. McKinley, for ease of reduction, chose the 4th and 9th cycles; Mainstone reduced the majority of 65 echoes on the time interval between the 2nd and 5th maxima. With the advent of digital computing there is obviously a large waste of information

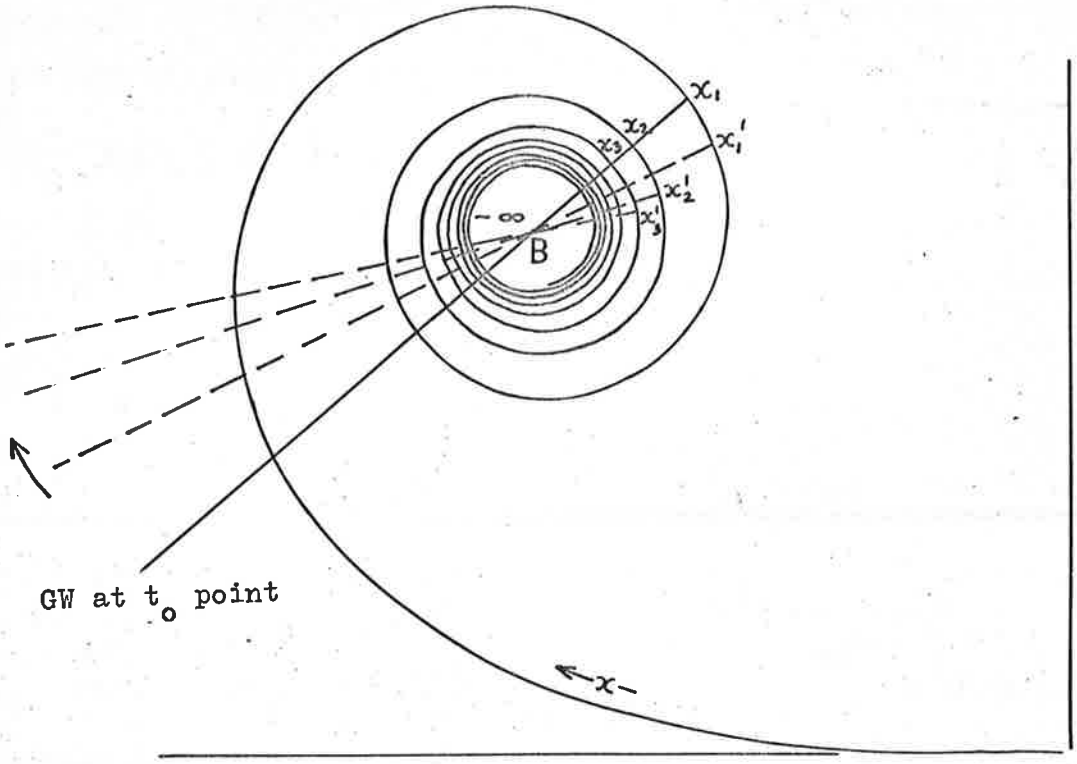

Figure 5.4 - The effect of a receding wind on successive diffraction maxima and minima.

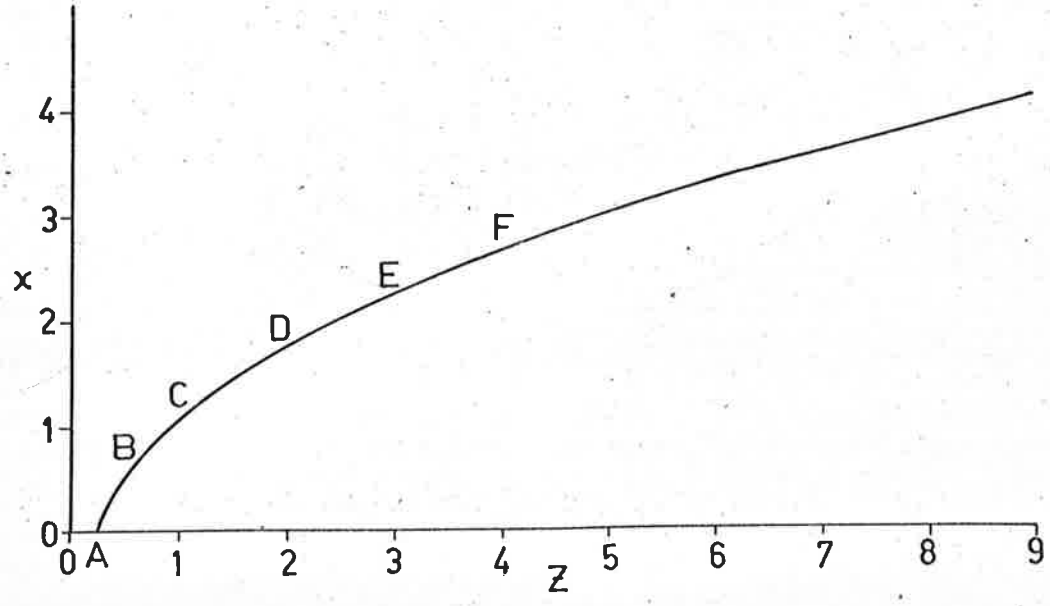

Figure 5.5 - A plot of x(Z)

in only choosing two points on the waveform, with a consequent reduction in accuracy. Knowing the one to one correspondence between the observed waveform and the theoretical spiral a more accurate procedure can be developed.

Assign to each diffraction maximum and minimum prior to the t_o point an 'item number', $J > 0$ say, commencing from the t_o point and working backwards in time. For convenience, divide the values of ψ by π, i.e. $360^o \equiv 2$. Now, unless a very fast doppler distorts a borderline waveform, it can be seen from Figure 3 that for

$$0.75 \leqslant \psi_o < 1.5$$

the first item will be a maximum.

For $$1.5 \leqslant \psi_o < 2.75$$

the first item will be a minimum.

We can define a function Z such that

$$Z(J) = 3 - \frac{1}{2}\Big] + J - P(J) \qquad \ldots (3)$$

where the value 1 is chosen if the first item is a minimum, the value 2 if a maximum; J is the item number, P(J) is the phase angle ψ appropriate to the time T(J) of the Jth item.

$$P(J) = \psi_o \begin{matrix} + \\ - \end{matrix} \begin{matrix} A \\ R \end{matrix}\Big] \cdot |u| \cdot T(J)/2.8 \qquad \ldots (4)$$

Equation 4 is derived from 5.2 and the constants have been given numerical values. u is the wind drift velocity in metres/sec and is related to the doppler frequency f by

$$u = f. \lambda/2$$

Where λ is the R.F. wavelength. The value of ψ_o is estimated both from the appearance of the echo and from the nearest doppler maximum or minimum (applying equation 5.2). It should be noted that although the starting point T = 0 is usually in the vicinity of the t_o point, it does not have to be; ψ_o in this context represents the phase angle at the arbitrary axis T = 0.

Equation 4 represents an extrapolation of a constant rate of rotation of the GW vector back into the diffraction pattern. For a high wind shear, $d\psi/dt$ would not be constant and P(J) could be seriously in error. The points along the trail appropriate to the various Fresnel zones are several km removed from the t_o point. An attempt could be made to allow for this by an addition of a $T^2(J)$ term in (4), but from the observed values of shear it appears for the majority of meteors to be a second order correction. There are other factors of this order that have been ignored (e.g. non-uniformity of ionisation and the variation of the phase change on reflection β with electron density), therefore the inclusion of the shear term alone would appear to be of doubtful value.

By expressing the phase in the form of Z we have defined an angle which is a monotonic increasing function as one moves back in time from the t_o point. x is thus a continuous function of Z. For convenience we are considering both x and T positive prior to the T = 0 axis. A plot of x against Z is shown in Figure 5. This curve can be approximated by a succession of straight lines AB, BC, CD etc., and the function x = x(Z) is fed into the computor in this form. The plot of x against T should be a straight line for a meteor of constant velocity and the computor makes a least mean squares fit of x against T to all the items of information. It calculates the slope V (also referred to as x/T) and the intercept T_o of the best fit straight line

$$x = V(T - T_o)$$

where V $\propto$ velocity of meteor.

T_o is the time difference between the true t_o point and the selected T = 0 axis. This is illustrated in Figure 6.

From Figure 5 and equations 3 and 4, it can be seen that the x value for the first item is very strongly dependent on ψ_o. This is also illustrated in Figure 3 by the variation of the position of say the first minimum prior to the t_o point with varying ψ_o. The value of ψ_o is optimized by the computor within certain variable limits. If ψ_o is in error the best fit curve to the values of x against T is no longer a straight line. It is a curve which asymptotically approaches a straight line as $x \rightarrow \infty$. The curve shown in Figure 6 is typical of an error of 0.5 (90^o) in ψ_o. It is thus reasonable to expect that the r.m.s. deviation of all the points from the best fit straight line to be a minimum for the correct value of ψ_o.

A program was devised that varied ψ_o in 20 steps each of 0.05 (9^o), either side of the estimated value. The r.m.s. deviation was computed for each step and the minimum value was found. The value of ψ_o appropriate to this minimum r.m.s. deviation was accepted as the true value and the corresponding slope V of the straight line taken as a measure of the velocity of the trace concerned. There was one major drawback. If this method of optimizing ψ_o were valid, then the mean discrepancy between the velocities computed for each of the three traces should be a minimum over a large enough number of echoes. It was not. This last test was taken as the ultimate measure of any reduction procedure.

Consider the factors contributing to the r.m.s. deviation:

(i) film reading errors,
(ii) error in ψ_o,
(iii) distortion of the theoretical waveform by non-uniformity of the trail, shear etc.

The contribution of (i) can be estimated, but no attempt has been made to determine the separate contribution of (iii).

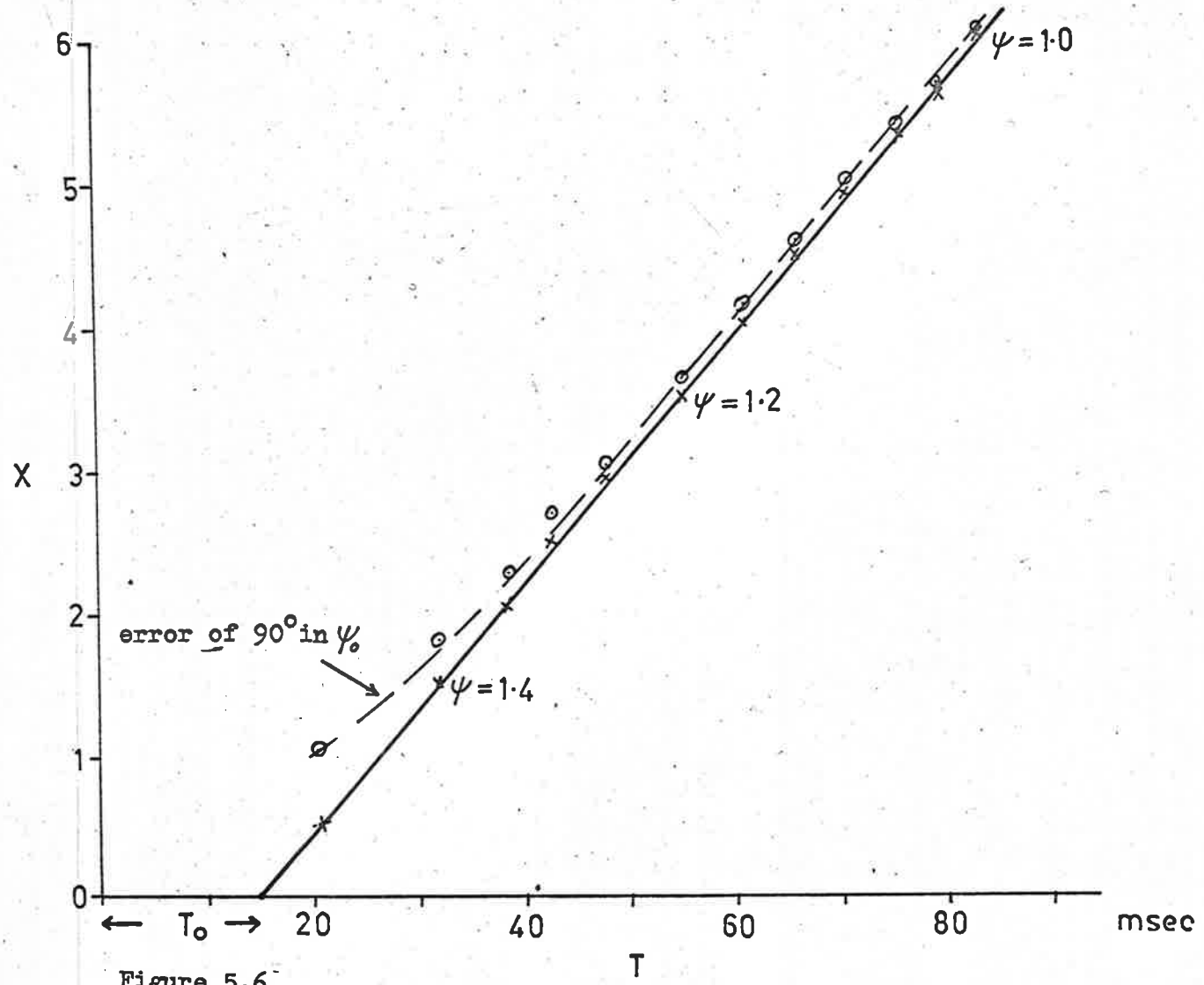

Figure 5.6

Define the function $\mathcal{E}$,

$$\mathcal{E} = p_1.(1.0 - p_2(N-4)/14).(p_3 + p_4/V) \quad \ldots (5)$$

where N is the number of items; P_i, i = 1, 4 are variable parameters. The quantity $\mathcal{E}$ is an estimate of the r.m.s. deviation that one could expect for a best fit straight line of slope V to N points. The values of P_i were estimated in the following manner: A reasonable guess was made on the basis of data already reduced graphically, and a new optimization process was developed. A straight line is fitted to the data as before. If the calculated r.m.s. deviation $< \mathcal{E}$, the estimated value for ψ_o is accepted. If not, the sense of the error in ψ_o is determined from the first item (whether the first point lies above or below the fitted straight line), and ψ_o is varied by 0.05 (9^o) as before. A new line is fitted and the r.m.s. deviation calculated. This is repeated until the r.m.s. deviation $< \mathcal{E}$, with a set limit of 20 steps as before. If the expected fit is not forthcoming in this range of ψ_o, the best of the 20 sets is chosen, i.e. the set with the minimum r.m.s. deviation, and the corresponding shift in ψ_o is noted. This process is repeated for each of the three traces. If any of the traces do not optimize with respect to ψ_o within the limit of 20 steps, the value 0 is assigned to a variable 'jump'. This enables the statistics of the number of traces that successfully optimize to be printed out against N and V (the variables in equation 5) by the computor at the end of a month's run.

Working with 136 echoes from December 1960 the parameters P_i were varied and the optimization statistics studied. The value of p_1 was decreased from 1·2 to 0.6 msec and p_2, p_3 and p_4 were adjusted so that the percentage of traces that optimized successfully was nearly independent of N and V. A slight increase in the percentage with both increasing N and increasing V was regarded as satisfactory. These results are shown in Table 1. Decreasing p_1 to 0.6 however, had caused the mean discrepancy between the

TABLE 1

Adjustment of parameters p_i

The data for 12/60 was run for six sets of p_i:

	p_1	p_2	p_3	p_4
(1)	1.2	0.3	0.3	0.5
(2)	0.6	0.3	0.3	0.5
(3)	0.6	0.0	0.7	0.3
(4)	0.9	0.05	0.65	0.35
(5)	1.2	0.05	0.65	0.35
(6)	9.9	0.05	0.65	0.35

These six sets of p_i resulted in the following optimization statistics:

Percentage of traces that optimized successfully as a function of slope x/T.

x/T	·30	·50	·70	·90	1·10	1·30	Mean x/T	Mean trace discrepancy
(1)	100	97	99	100	97	100 %	66.6	6.3 %
(2)	83	65	59	47	51	23	69.0	7.3
(3)	84	80	88	93	95	100	68.0	6.8
(4)	100	97	98	100	97	100	66.7	6.4
(5)	100	99	100	100	100	100	66.5	6.4
(6)	100	100	100	100	100	100	66.1	6.8

Percentage of traces that optimized successfully as a function of the number of items ($\frac{1}{2}$ Fresnel cycles).

I	4	6	8	10	12	14	16	18
(1)	100	98	99	99	100	95	100	97 %
(2)	88	78	68	49	45	49	44	30
(3)	88	83	80	84	88	90	90	96
(4)	100	98	97	96	100	95	100	96
(5)	100	98	98	100	100	100	100	100
(6)	100	100	100	100	100	100	100	100

velocities computed for each of the three traces to rise slightly to 6.8%. Keeping p_2, p_3 and p_4 constant, p_1 was then steadily increased to 1.2 msec. At this point the mean velocity discrepancy between traces had dropped to 6.4%. If p_1 were put equal to 9·9 msec, so that no optimization of ψ_o was undertaken, the velocity discrepancy rose again to 6.8%. The effect is small but significant. At p_1 = 0.6 the mean value of V (over 408 traces) was 68.0. At p_1 = 1.2, V = 66.5 and at p_1 = 9·9, V = 66.1. Between the two extremes of optimization the mean velocity had shifted 1.9%. The sharp rise between p_1 = 0·9 and p_1 = 0.6 should be noted. The value p_1 = 1.2 caused ψ_o to be left unchanged for the majority of traces, but was sufficient to effectively correct or throw out echoes for which a gross error had been made in estimating ψ_o. The set (5) was chosen for the values p_i. *

Because of the shift in mean velocity for varying p_1, the second optimization process (that of reconciling the two values for the height of the reflection point) was of great value. This process is very sensitive to mean velocity and was used as a check on the first optimization. The ultimate accuracy of the velocity reduction can be seen to depend strongly on the correct estimation of the phase angle ψ_o.

5.3 Film Reading.

The echoes used in this survey were read on a Telereader. This film reading system provides automatic readout facilities on to punched paper tape. The readout accuracy was more than sufficient, about 10 units/msec of echo waveform. The Telereader output was calibrated in terms of the interval between the phase spikes on the doppler records. These are locked to the mains supply such that five are approximately equivalent to 100 msec. If enough measurements are taken over varying times of the day the mean can be taken as 100 msec exactly. This was done for each month during the survey, in order to detect any changes in camera motor speed. There was one change during April after the camera motor was rewound and a 2% slowing down in December 1961 for some as yet

unaccountable reason.

Simultaneous time markers of approximately 1 msec duration were placed on each trace at intervals of about 100 msec. A set of corresponding markers served to locate the T = 0 zero line for each of the three traces. The method of film reading was as follows:

(i) The orbit films were scanned and a note taken of all the echoes that looked promising.

(ii) The wind film was read for these echoes. About 20% of the echoes with suitable diffraction waveforms were also suitable for wind analysis. This was usually due to the doppler at the main station being insufficient to uniquely determine the direction cosines of the reflection point. The orbit calculations can proceed without this information, but some accuracy is lost. This survey was limited to those echoes with complete doppler information.

(iii) The turbulence film was read for this reduced list of echoes. The doppler drift for each trace, the type of echo (persistent or short duration) and any other information pertaining to turbulence was noted. These first three stages of film reading were carried out on manually operated film readers, the information being read off scales and noted by hand.

(iv) The echoes from (iii) were then analysed in detail on the Telereader in the following manner.

(a) A suitable set of time markers were chosen.

(b) From the doppler the phase angle ψ_o was estimated at some point near the apparent t_o point. It was here that some experience was required, as a fast doppler could significantly alter the appearance of an echo in the vicinity of the t_o point. The first maximum or minimum was occasionally completely suppressed. A direct estimate of ψ_o from the nearest doppler (equation 2) had often to be

reconciled with a different estimate from the appearance of the echo (Figure 3). The estimate of ψ_o was used in the computor to indicate whether the first item was a maximum or minimum (equation 3) and this too had to be borne in mind.

(c) The times of the successive maxima and minima were automatically punched on paper tape as the cross hair was moved from item to item. The time of the time marker was read out as the last item. Steps (b) and (c) were repeated for the second and third traces.

(d) The echo clock time was written down. In step (b) the values of ψ_o were also noted manually.

Stage (ii) was read by a member of the computing staff (M.H.C.), stage (iii) by a colleague (R.G.R.). The author read stages (i) and (iv). The months of December 1960 and July 1961* were read twice at widely spaced intervals of time on different film readers in order to estimate the film reading errors. This is discussed in Chapter 10. Film reading is usually the limiting factor in deciding the number of echoes to be used in a survey of this kind. It is interesting to note that even using the automatic read-out facilities of a Telereader, the author could only read about 100 echoes/day.

---

* The Telereader data was of much higher standard than the data from the manual film reader. The latter data was used in the estimation of the parameters p_i in Section 5.2. The set (4) in Table 1 was chosen to run the survey data from the Telereader. The mean trace discrepancy was 5.3% (c.f. 6.4%) for December 1960

CHAPTER 6

GEOCENTRIC CORRECTIONS

6.1 Retardation in the Earth's Atmosphere.

One difficulty often encountered in the measurement of meteor orbits is that of allowing for the retardation suffered in the earth's atmosphere. This survey is more fortunately placed in this respect than that of Davies and Gill (1960), in that the position of the reflection point in space is known as well as the direction cosines of the trail. Thus with the aid of the A.R.D.C. model atmosphere (1959) all the atmospheric parameters at the reflection point are available. To take full advantage of this the following theoretical expression for retardation was developed from the fundamental equations given by Herlofson (1948). The main limitation is that one must assume a solid spherical particle and a surface area to mass ratio, G. In practice, many meteors fragment. While this cannot be allowed for on an individual basis, the effect is to raise the mean value of G. One could hope to estimate this by deceleration measurements.

Unfortunately the outstation spacing used in this survey is too small to measure the deceleration of individual meteors. The best that can be done is to estimate a mean value of G over the mass range, used in the survey. The relationship between G and ΔV, the velocity difference between two points on the trail, can be used in two ways.

(i) By measuring ΔV an experimental determination of G can be made.

(ii) With a known or assumed value of G a mean value of retardation can be calculated for each meteor as a function of observed reflection point height, meteor velocity and radiant zenith angle. This calculation is made for every echo used in this survey.

Section 6.1)

From Herlofson

$$4\pi r^2 \rho_m \ell \, dr = \tfrac{1}{2}\pi r^2 \rho_a v^2 \sec\chi dz \qquad \ldots \quad (1)$$

and

$$4/3\pi r^3 \rho_m dv = \pi r^2 \rho_a v \sec\chi \, dz \qquad \ldots \quad (2)$$

where r is the radius of the meteor,

ρ_m " density of air,

ρ_a " density of the atmosphere,

ℓ " latent heat of evaporization of the meteor

" corrected for heat transfer,

v " meteor velocity,

χ " radiant zenith angle,

z " height.

(1) and (2) give

$$dr/r = v\,dv/6\ell$$

This is integrated from outside the earth's atmosphere to the reflection point

$$\int_{r_\infty}^{r} \frac{dr}{r} = \int_{v_\infty}^{v} \frac{v\,dv}{6\ell}$$

where $r_\infty > r$, $v_\infty > v$; the subscript ∞ refers to the state before the meteor is subjected to change by the atmosphere. That is

$$\ell n\, r/r_\infty = v^2/12\ell - v_\infty^2/12\ell$$

Write $\xi = v^2/12\ell$,

$$r/r_\infty = \exp(\xi - \xi_\infty) \quad \ldots (3)$$

Assume hydrostatic equilibrium

i.e. $dp = -g\rho_a dz$

Substitution into (2), using (3), gives

$$\exp \xi . dv/v = -3\sec\chi . \exp \xi_\infty . dp/4g\rho_m r_\infty \quad \ldots (4)$$

Now $dv/v = d\xi/2\xi$,

hence from (4), integrating from infinity to the reflection point where the pressure is P

$$\int_{\xi_\infty}^{\xi} \frac{\exp t}{t} . dt = -\frac{3\sec\chi . \exp \xi_\infty . P}{2g\rho_m r_\infty} \quad \ldots (5a)$$

where t is any variable

Approximate $\int_{\xi_\infty}^{\xi} \frac{\exp t}{t} . dt$

by $\frac{\exp(\xi_\infty + \Delta\xi/2)}{\xi_\infty + \Delta\xi/2} \cdot \Delta\xi \quad \ldots (5b)$

where $\Delta\xi = \xi - \xi_\infty < 0$.

This approximation is valid for all reasonable decelerations. For convenience, write $\Delta\xi = \xi_\infty - \xi > 0$ and from (5) we have

$$\Delta\xi \exp(-\Delta\xi/2) = K\rho\sec\chi\,(\xi + \Delta\xi/2) \quad \ldots (6)$$

where $K = 3/(2g\rho_m r_\infty)$

This is equivalent to

$$\Delta v(E \exp(-v\Delta v/12\ell) - 1) \doteq v \quad \ldots (7)$$

where $E = 2/K\rho\sec\chi$, a dimensionless number ~ 30 for most meteors in the mass range considered here.

Now Jacchia (1949) has given a value of 3.10^{11} ergs/gm for ℓ, so for the fastest possible meteor, v = 72 km/sec, and a retardation Δv of 2 km/sec

$$v\Delta v/12\ell = 0.5 \text{ approx.}$$

i.e. $$0.6 \leq \exp(-v\Delta v/12\ell) \leq 1.0$$

Equation (7) can thus be solved by the method of successive approximations as follows:

Put $$\Delta v(E-1) = v \quad \ldots (8)$$

resubstitute in (7) to obtain

$$\Delta v(E\exp Q - 1) = v \quad \ldots (9)$$

where $Q = -v^2/12\ell(E-1)$, also a dimensionless number. From the definition of E and K we have

$$E = (4g/\rho \sec \chi).(\rho_m r_\infty/3) \quad \ldots (10)$$

Write $G = 3/\rho_m r_\infty$, the ratio of surface area/mass for a solid spherical body.

From (10)

$$E = 40 \cos \chi/G.p \quad \ldots (11)$$

where p is the atmospheric pressure in kg/metre^2.

If V is the velocity in km/sec, and we use Jacchias' value for ℓ,

$$Q = -V^2/(360(E-1))$$

For most meteors, $0.8 \leq \exp Q \leq 1.0$

and $$\Delta V = V/(E \exp Q - 1) \quad \ldots (12)$$

Equation (12) can be applied to each meteor if an initial value of G is assumed. It takes into account the measured values of height, radiant zenith angle and velocity.

6.2 Measurement of Surface area / Mass ratio.

From the last section it can be seen that if one could measure α, V, ΔV and p for each meteor, G as a function of α could be determined. From evaporation theory there is

enough information to determine α_{max}, the maximum electron line density, and thus G could be determined as a function of meteor mass.

From equations (8) and (11) it can easily be shown that to a first approximation

$$G = 40.\frac{\Delta V}{V} / \frac{dp}{dz} .\Delta s \qquad \ldots (13)$$

where Δv is the velocity difference over a distance Δs along the trail, taken in the direction of motion.
There are two such observations for each echo, these were weighted by Δs and the mean taken. For a preliminary survey the echoes were treated on a monthly basis, only echoes which satisfied the various quality tests (see Chapter 9) were chosen. The values for G obtained from December 1960 to December 1961 were:
+246, +411, +843, -455, +210, -400, -402, -60, -278, -13, -18, +98 and +124.
The negative sign indicates a mean acceleration rather than a deceleration!

The results for the value of G show that the random errors encountered in the reduction of each of the three traces were considerably greater than velocity differences due to deceleration alone. This is not unexpected in view of the

small outstation spacing and the results indicate the need for larger samples. The mean value for the absolute velocity difference between the main station and each outstation trace averaged about $4\frac{1}{2}\%$. With a better statistical treatment it should be possible to set an upper limit to G for the mass range of the meteors observed in this survey. Kaiser (1953) has given a value of $G = 50\ cm^2/gm$ for radio meteors. This value was used in equation (11) to compute the retardation for each meteor. The results indicate that this value is an upper limit for the meteors observed in this survey. The distribution of numbers of meteors with calculated retardation is given in Chapter 10.

6.3 The Movement of the Specular Reflection Point due to Wind.

In Figure 1 MM' is the path of a meteor, velocity V and P is the geometric t_o point relative to the transmitter and receiver at O. Let the trail be receding under the action of a uniform wind whose line of site component in the direction OP is u metres/sec. For simplicity we shall consider the radar case where the transmitter and receivers are coincident rather than the spaced C.W. technique.

If there were no wind the observed t_o point would occur at P such that OP is perpendicular to MM'. If a steady wind is blowing the ionised trail will lie along PW at the instant the meteor reaches P. PW makes an angle θ to the meteor path such that $\theta = u/V$ and consequently the

condition for specular reflection will not be satisfied until the meteor reaches P' where OP' is perpendicular to P'W'. The delay of the t_o point is approximately Ru/V metres, or

$$Ru/V^2 \text{ sec} \qquad \ldots (14)$$

If the line of sight wind velocity is not constant along the trail, i.e. a shear is present, θ will vary with height and at any instant the trail will be curved. However, to a first approximation this will not effect the calculated delay of the t_o point, as the measured value of u is the wind drift component at the observed t_o point, and the angle the trail makes with the meteor path at that point is still $\theta = u/V$.

To obtain radiants one does not want the direction cosines of the trail P'W' but rather those of the meteor path MM'. From what follows it can be seen that a wind shear will cause an error in the theoretical time difference between two successive specular reflection points. Suppose the measured times of the observed t_o points at two stations are t_1', t_2' and the geometric times appropriate to the path MM' are t_1, t_2.

$$\Delta t' = t_2' - t_1'$$

$$\Delta t = t_2 - t_1$$

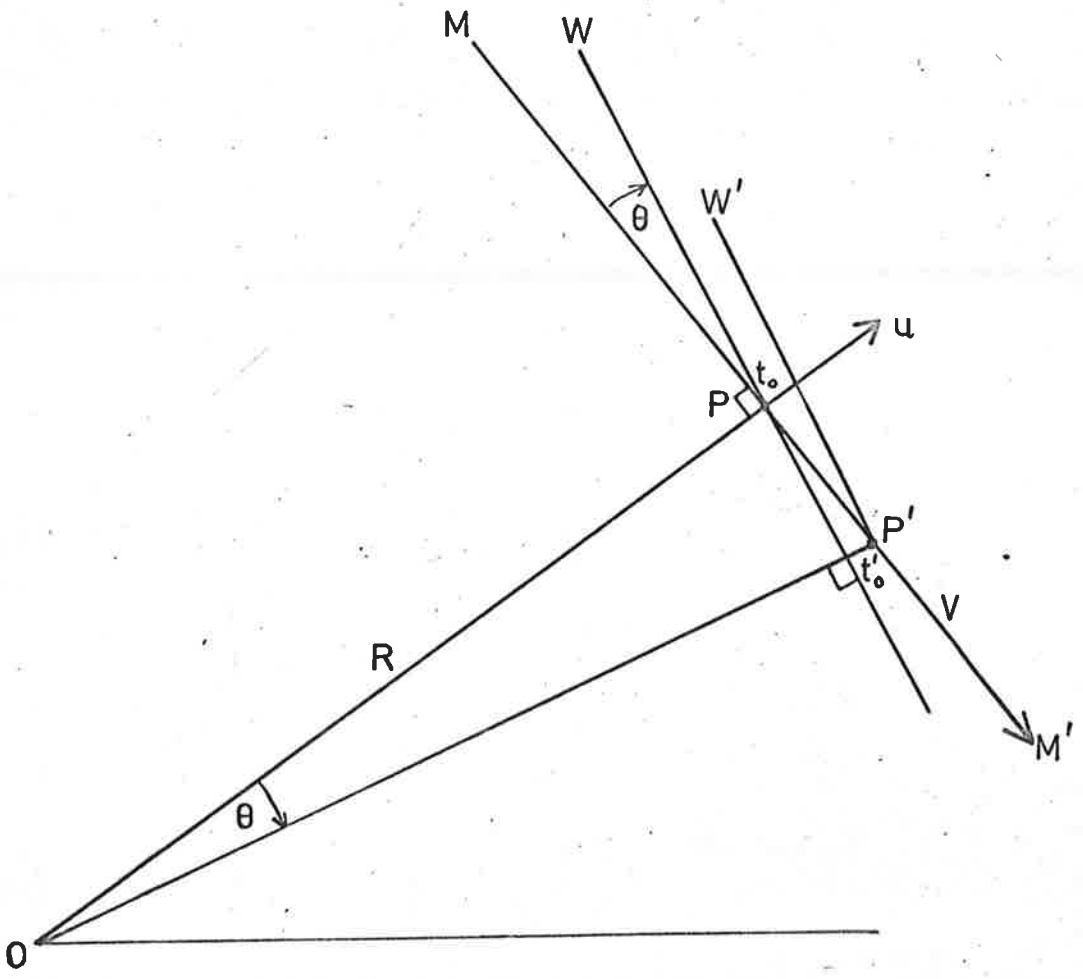

Figure 6.1

Hence, neglecting terms of second order

$$\Delta t' = t_2 + Ru_2/V^2 - (t_1 + Ru_1/V^2)$$

$$\text{i.e. } \Delta t' = \Delta t + R(u_2 - u_1)/V^2 \qquad \ldots (15)$$

Substituting the distance along the trail, $s = Vt$, this expression can be reduced to

$$\Delta t = \Delta t'(1 - \delta/2)$$

where $$\delta = \frac{2R}{V} \cdot \frac{u_2 - u_1}{s_2 - s_1} = \frac{2R}{V} \cdot \frac{du}{ds} \qquad \ldots (16)$$

This formula has also been derived by Kaiser (1955). If one tries to apply equation (16) in practice, small errors in the measurement of s can lead to large and incorrect values of δ and hence Δt. With the additional information available to this survey, that of measuring u at each reflection point, it is obviously more accurate to calculate the delay or advancement of the t_o point separately at each reflection point. Errors in the measurement of u can only lead to second order errors in Δt if an equation of the form of (15) is applied. The resultant correction is independent of the spacing Δs, and in fact, one does not need to calculate a value for the shear $\frac{du}{ds}$ at all.

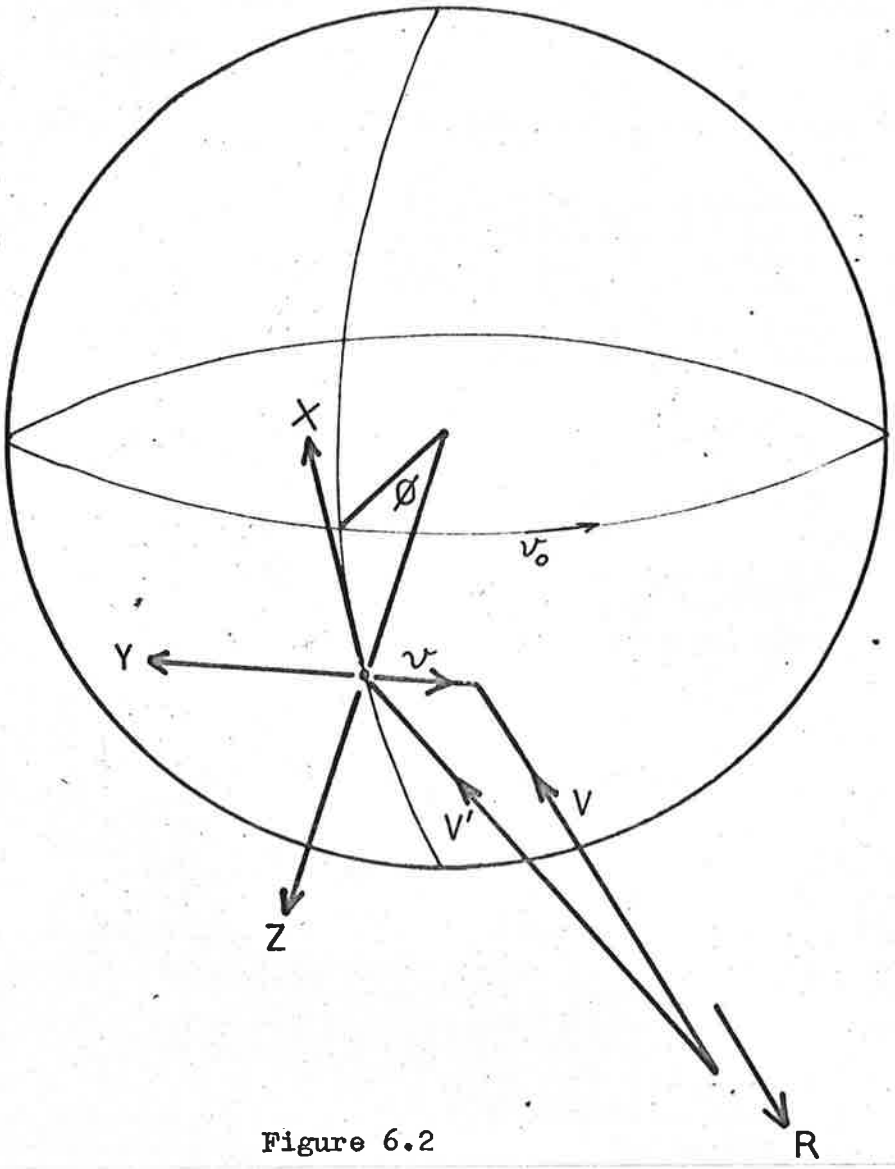

Figure 6.2

6.4 Correction of the Radiant for Diurnal Motion.

Porter (1949) has given formulae for the correction of the radiant position due to the diurnal motion of the observer. These are

$$\Delta\alpha = - 26.58 \cos\phi.\cosh.\sec \delta/V$$

$$\Delta\delta = -26.58 \cos\phi.\sinh.\sin \delta/V$$

such that $\alpha_{true} = \alpha_{obs} + \Delta\alpha$

and similarly $\delta_{true} = \delta_{obs} + \Delta\delta$

where ϕ is the latitude of the observer, h the local hour angle, δ the observed declination of the radiant and V is the velocity of the meteor.

An alternate approach which is more applicable to the method used in this survey of determining radiants is to correct the observed direction cosines of the trail before calculating α, δ. Consider a meteor true radiant R, true velocity $\underline{V}$, observed velocity $\underline{V}'$ as shown in Figure 2. Suppose the motion of the observer is $\underline{v}$, with respect to reference axes X, Y, Z.

$$\underline{V}' = \underline{V} - \underline{v} \qquad \ldots (17)$$

Also

$$\underline{V}' = V' \begin{vmatrix} \lambda' \\ \mu' \\ \nu' \end{vmatrix} \qquad \ldots (18)$$

where λ', μ', ν' are the observed direction cosines of the trail; λ, μ, ν the true values.

Now, $$\underline{v} = \begin{vmatrix} 0 \\ v^2 \\ 0 \end{vmatrix} = \begin{vmatrix} 0 \\ -|v_o \cos\phi| \\ 0 \end{vmatrix}$$

$$= \begin{vmatrix} 0 \\ -0.381 \\ 0 \end{vmatrix} \text{ km/sec for Adelaide}$$

Also,

$$V = (v_1^2 + v_2^2 + v_3^2)^{\frac{1}{2}}$$

$$= (V_1'^2 + (V_2' + v_2)^2 + V_3'^2)^{\frac{1}{2}}$$

Which is equivalent to

$$V = (V'^2 + 2v_2V_2')^{\frac{1}{2}} \qquad \ldots (19)$$

since $v_2^2 << V^2$

This can be further reduced to

$$V = V' + v_2 \cdot V_2'/V'$$

$$= V' + v_2 \cdot \mu'$$

$$= V' - 0.381\ \mu' \text{ for Adelaide} \qquad \ldots (20)$$

From 18

$$\lambda = V_1/V = V_1'/V = V_1'/V' \cdot V'/V$$

$$= \frac{V'}{V} \cdot \lambda' \qquad \ldots(21a)$$

similarly $$\nu = \frac{V'}{V} \cdot \nu' \qquad \ldots(21b)$$

But $$\mu = \frac{V_2}{V} = (V_2' + v_2)/V$$

$$= V'/V \cdot (V_2' + v_2)/V'$$

which reduces to

$$\frac{V'}{V} \left| \mu' - \frac{| r_o \cos\phi |}{V'} \right|$$

$$= \frac{V'}{V} \left| \mu' - \frac{0.381}{V'} \right| \qquad \ldots (22)$$

In practice one first calculates V from (20) and then applies (21) and (22) to obtain the true direction cosines from the observed values. This approach has the advantage of correcting the magnitude of the velocity of the meteor, as well as the direction of the radiant.

CHAPTER 7

ANTENNA POLAR DIAGRAMS

7.1 Method of Determination of Antenna Gain.

If a transmitter radiates P watts, wavelength λ, from an antenna gain $G_t(\theta,\phi)$, the power collected at a range of R metres by a receiving antenna, gain $G_r(\theta,\phi)$, is given by

$$\omega = PG_rG_t\lambda^2/(4\pi R)^2 \quad \ldots (1)$$

where θ and ϕ are the zenith and azimuth angles respectively. For a given transmitter power the product of the two antenna gains can be written

$$G_r(\theta,\phi).G_t(\theta,\phi) \propto (R.V)^2 \quad \ldots (2)$$

where V is the input voltage to the receiver. If the polar diagram i.e. the plot of G against θ,ϕ, is known for one antenna, an experimental determination of $(R.V)^2$ will provide the radiation pattern of the unknown antenna. This is the basis of the method used at Adelaide to determine the radiation pattern of the transmitting antenna.

A 'standard' $\lambda/2$ dipole $\lambda/4$ above ground was carefully erected over an earth mesh. The analysis assumes that this antenna radiates according to the theoretical pattern. The latter was calculated by the method outlined in the M.I.T. book 'Principles of Radar' (1953). This provides the gain figures along and perpendicular to the antenna axis. The complete map of θ,ϕ must be interpolated from the axial values, the interpolation being based on the generally accepted radiation pattern of such a dipole. An aircraft was used to compare the polar diagrams of the standard antenna and the antenna under test in the following way.

The aircraft was flown on a spiral flight pattern either simultaneously over both antennas, if they were at the same site,

or in turn if they were separated. Spiral flight paths were chosen in order that the aircraft always presented the same attitude to each antenna for a given θ,ϕ. The polar diagram for the antenna under test could then be determined in terms of the polar diagram of the standard antenna by comparing the signals received at each antenna when the aircraft was in the same relative position with respect to each antenna (the coordinates θ,ϕ were always referred to the axis of the antenna under consideration). The standard antenna, assumed gain G_s, is first used to provide a plot of the effective radiation of the transmitting antenna located in the aircraft. The flight path is illustrated in Figure 1.

An Auster aircraft was fitted with a 27 Mc/s transmitter feeding about 2 W into a ferrite crossed dipole antenna built into the fusilage. The Auster was chosen for both economy and for the fact that it is fabric covered. While the aircraft flew a spiral pattern of twelve or more laps from 2000 ft to 9000 ft (radius ~ 3/4 mile), the ground crew recorded its position with two balloon tracking theodolites. For the first flight the two available receiving channels were fed from the standard antenna and one of the main station receiving dipoles, gains G_s and G_r respectively. Recording was done on a four channel pen recorder, the third channel being used for markers indicating the time of an optical bearing, the fourth for 1 sec time markers. A sample record is shown in Figure 2. An observer in the aircraft (the author) noted the altitude as a function of time and advised the pilot on the progress along the set flight path. The latter information was relayed by VHF from the ground.

Optical bearings were taken approximately every ten seconds or less and the time of the observation was recorded automatically by the observer pressing a button and so producing a mark on channel 3 of the pen recorder. The bearing itself was spoken into a telephone worn by the observer and recorded on a tape recorder. The recording system had to be able to identify the observed bearing of the aircraft with the output from the receivers, together with the height records taken in the aircraft.

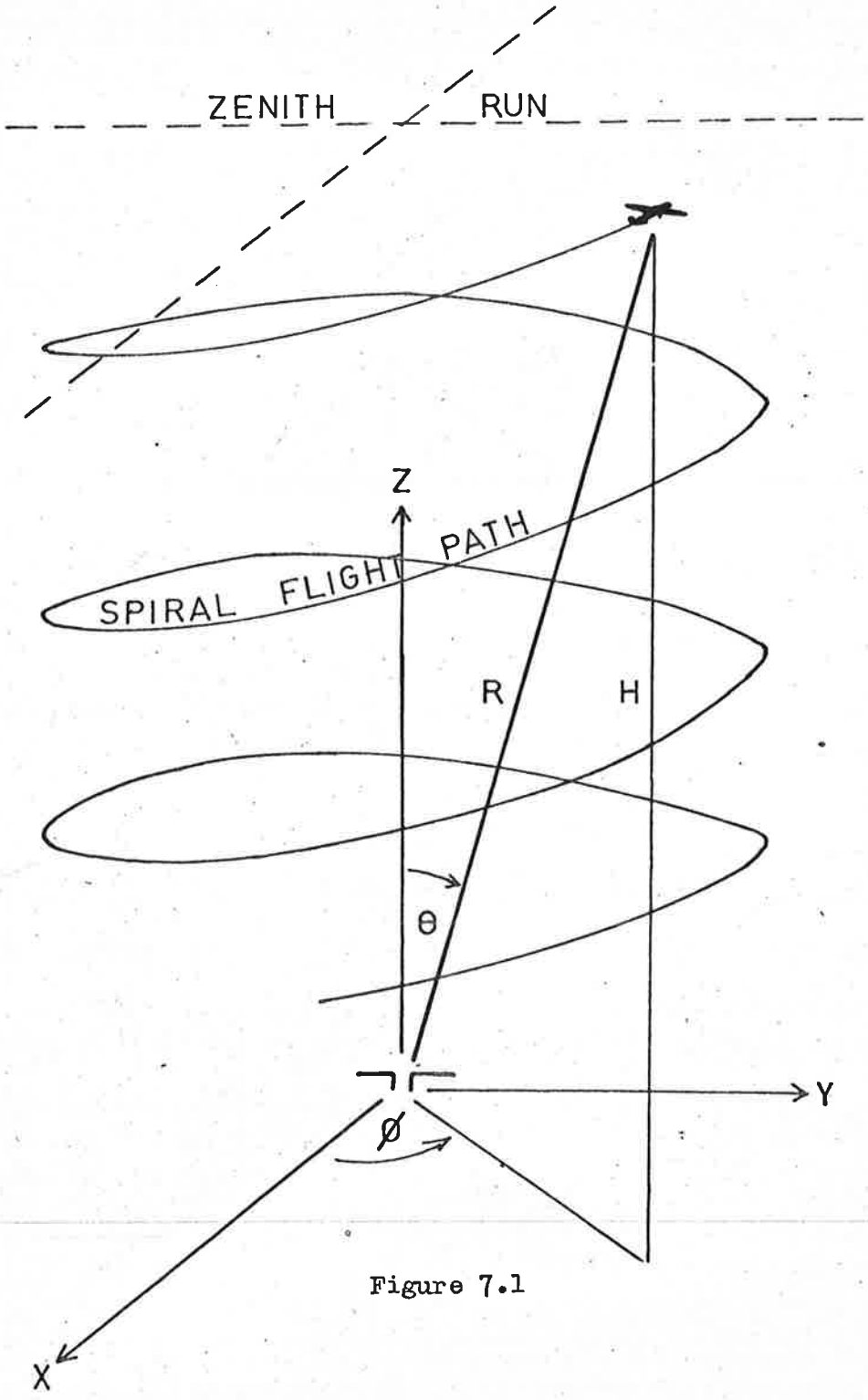

Figure 7.1

Figure 3 indicates the manner in which all the observations were coordinated. Times were spoken into the telephone link every minute or so and recorded, along with the theodolite bearings, on both tape recorders. The VHF two-way link conversation with the aircraft was recorded on only one tape recorder to avoid over-riding any theodolite bearings. Attenuators were placed between the antennas and the inputs of both receivers and were adjusted manually between 0 - 30 db to keep a satisfactory level of output on the pen recorder; the level of attenuation was noted on the pen recorder chart as the flight progressed.

Theodolite observations were taken about every ten seconds on the position of the aircraft. Knowing the flight pattern one could interpolate between these observations to find the bearing for any time. The chart was 'sampled' every four seconds to determine the input to each receiver. For a flight of one hour there were thus about 900 observations of $(VR)^2$. These observations were finally divided or 'boxed' into 5° x 10° divisions of zenith and azimuth angles. For the complete hemisphere there were thus 648 boxes, but those at elevations lower than 20° and higher than 80° did not receive any values from the spiral runs.

By choosing a spiral flight path the azimuthal variations in the aircraft antenna pattern were not involved in the plot of $(VR)^2$. G_p is defined as the plot of $(VR)^2/G_s$; it should be noted that $G_p(\theta,\phi)$ is not the polar diagram of the aircraft antenna, but a plot of the effective radiation of the aircraft antenna referred to an origin at the receiving antenna under consideration.

The variation of G_p with azimuth for a spiral flight pattern is a measure of the polarization factor between the aircraft and ground antennas. The variation of G_p with zenith angle is a combination of polarization and the true radiation pattern of the aircraft. The plot of G_p can thus only be used for similar spiral flight paths and an unknown antenna with linear polarization.

In addition to the spiral pattern, a run over the zenith was made on a constant bearing each time along and perpendicular to the aerial axis. These zenith runs result in an entirely different set

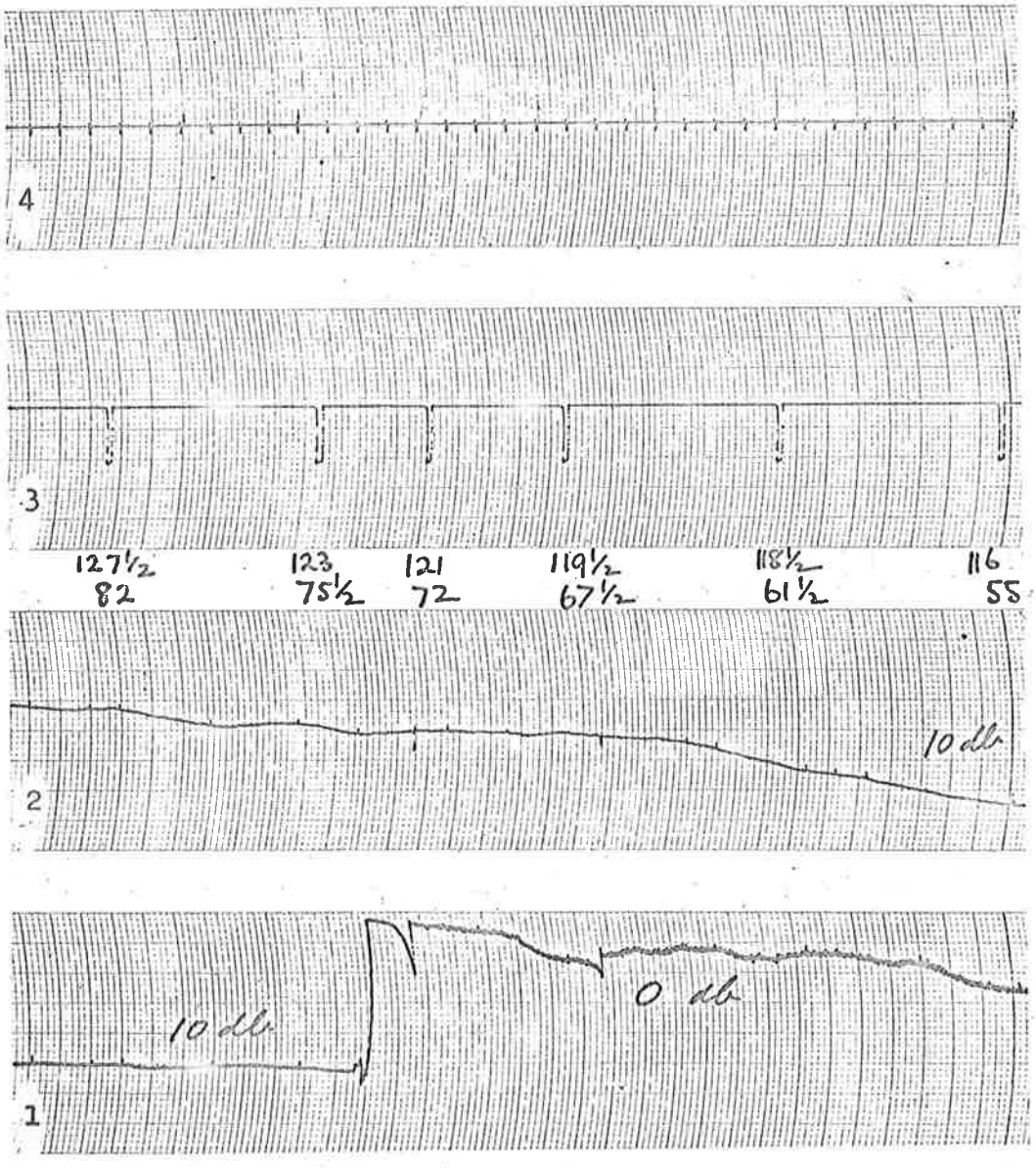

Figure 7.2 Sample chart record.

of values for G_p, as the aircraft is presenting a varying attitude to the ground station. These zenith runs indicated that the polarization of the aircraft antenna was effectively along the fusilage. Zenith runs have the advantage that the polarization factor is constant on a given aircraft heading, but have the disadvantage that the plot of G_p will now include the variation of the aircraft antenna's radiation with azimuth. Of the two, it was thought that polarization should produce a smoother and more easily recognised variation. The spiral pattern also had the advantage of covering the θ,ϕ map more uniformly in a given time.

7.2 Program 163.1

The preparation of the maps of $(VR)^2$ proceeded as follows:

(i) The two receiver output values were sampled every 4 sec and the time read for each sample.

(ii) The time for each theodolite observation was read from the pen recorder, the actual observation having been transcribed from the tape recording.

(iii) The time for each observation of the height of the aircraft was read from the observer's log.

These three sets of data were fed into the I.B.M. 7090 computor with program 163.1 (see Appendix 5). The height for each theodolite observation was computed by linear interpolation from the data (iii). The height, bearing and hence range relative to each antenna for each sample value of receiver output was computed by suitable interpolation from the data (ii). The method of interpolation varied to suit either a zenith run or spiral flight pattern. The output for each ground antenna was of the form:

191536 28 317 569

where 19.15.36 is the G.M.T. of the sample in hours, minutes and seconds; 28 and 317 are the zenith and azimuth angles of the aircraft relative to the particular ground antenna under consideration; 569 is a normalised value of $(VR)^2$.

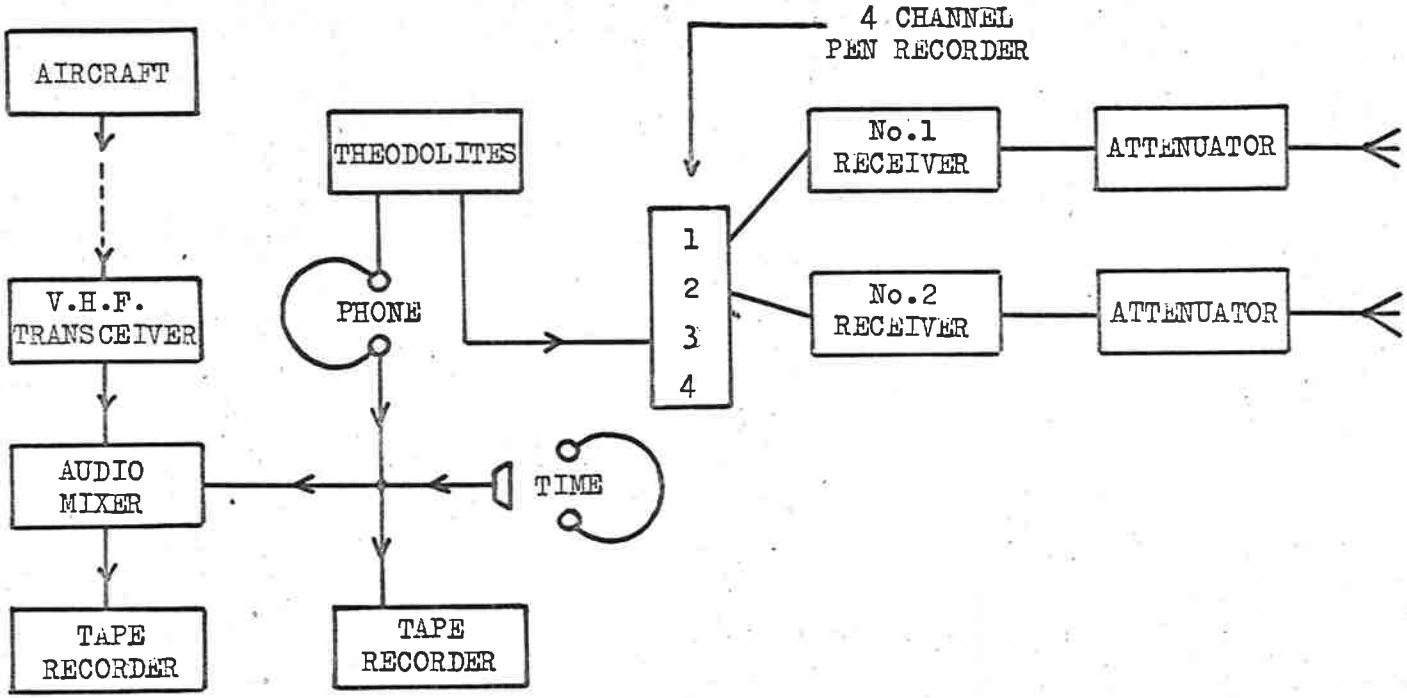
AIRCRAFT
V.H.F.
TRANSCEIVER
AUDIO
MIXER
TAPE
RECORDER
THEODOLITES
PHONE
TAPE
RECORDER
TIME
4 CHANNEL
PEN RECORDER
1
2
3
4
No.1
RECEIVER
No.2
RECEIVER
ATTENUATOR
ATTENUATOR

Figure 7.3

The first flight over St. Kilda receiving station during a fine afternoon was somewhat abortive owing to excessive turbulence. Henceforth flights were made in smooth conditions at 5 a.m. However the data was sufficient to show that the response of the standard dipole over a ground mesh was similar to that of the dipole used in the survey. This was both expected and reassuring, and in the distribution program 167.1 the theoretical figures for the standard dipole have been used for the receiving antenna.

The second flight was made over Adelaide to plot the patterns of both the C.W. and radar antennas. The VHF radio broke down in the aircraft, but this did not seriously effect the flight. The spiral flight data extended from 20° to 70° elevation and covered all azimuths. The data was meagre at both extremes of elevation, the varying bank of the aircraft making the observations unreliable above 70°.

The third flight was over St. Kilda again, with the standard antenna on one channel and an imitation of the supported dipole used in the Mawson survey on the other. The latter observations were made to test the suspected loop characteristics of the Mawson antenna discussed in Chapter 2.

7.3 Programme 163.2

One method of defining the gain of an antenna is as follows: Define $f^2(\theta,\phi)$ as the normalised plot of the relative power gain of the antenna such that

$$f^2(\theta,\phi)_{max} = 1$$

$$\text{i.e.} \qquad G(\theta,\phi) = G_{max} \cdot f^2(\theta,\phi) \qquad \ldots \quad (3)$$

Define Ω as the integral of the function $f^2(\theta,\phi)$ over the surface of the unit sphere

$$\Omega = \int_{\phi=0}^{2\pi} \int_{\theta=0}^{\pi} f^2(\theta,\phi) \sin\theta \, d\theta \, d\phi \qquad \ldots \quad (4)$$

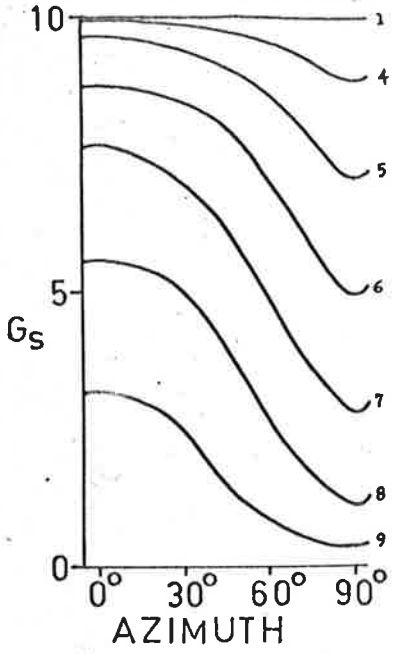

Legend for figures 4a,6a,6b,7 and 8:

Curve 1 – $0^\circ < Z < 05^\circ$
2 – $05^\circ < Z < 10^\circ$
3 – $10^\circ < Z < 15^\circ$
4 – $15^\circ < Z < 20^\circ$
5 – $20^\circ < Z < 30^\circ$
6 – $30^\circ < Z < 40^\circ$
7 – $40^\circ < Z < 50^\circ$
8 – $50^\circ < Z < 60^\circ$
9 – $60^\circ < Z < 70^\circ$

Figure 7.4a

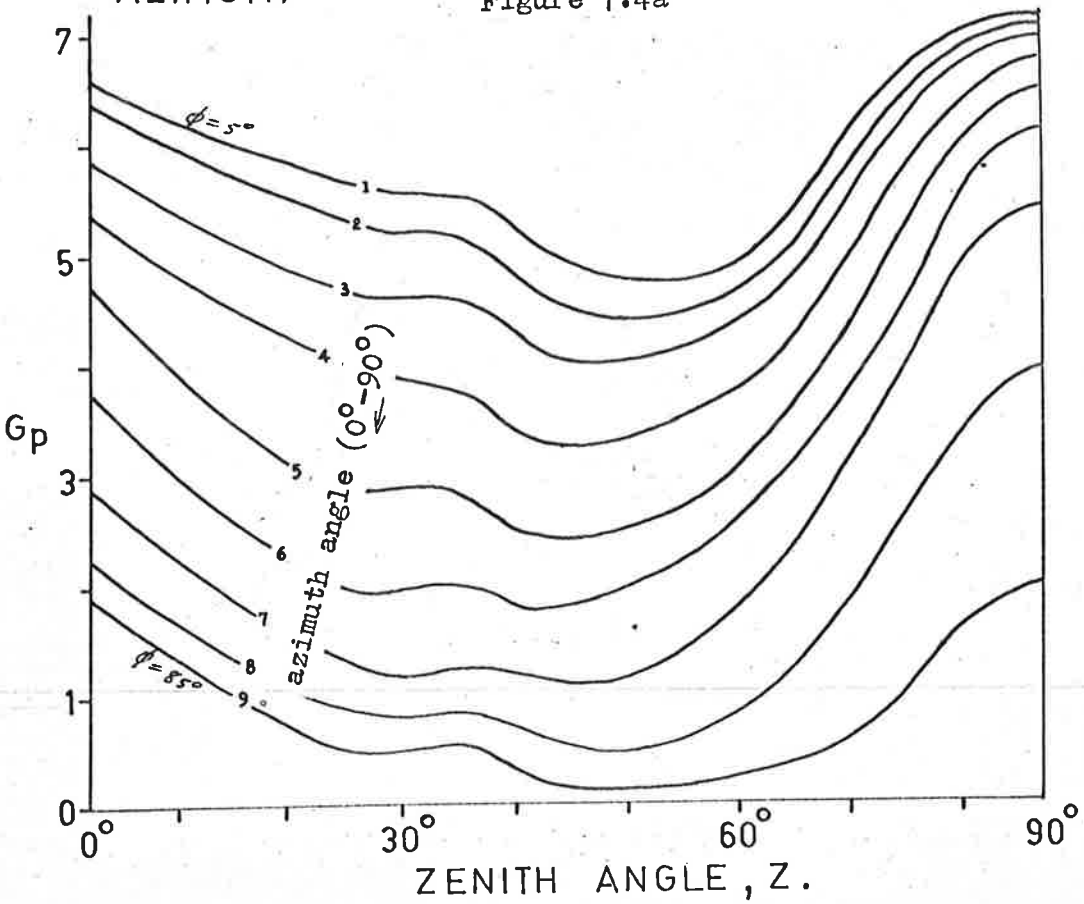

Figure 7.4b

$$f^2(\theta,\phi) = 1 \text{ for all } \theta,\phi.$$

Hence $$\Omega = 4\pi$$

The gain, G, of any antenna system over an isotropic radiator is defined by

$$G = 4\pi/\Omega \qquad \ldots (5)$$

After plotting the output of 163.1 for the product of the gains of the standard and aircraft antennas, $G_s \times G_p$, the data were smoothed by combining the four quadrants in azimuth. This is possible because the theoretical figures for the standard antenna are symmetrical and the azimuth variation of the aircraft should only be that due to polarization, also symmetrical with respect to the standard antenna axis.

Program 163.2 accepts the plot of any set of $G_1 \times G_2$, divides by G_2 and normalises the resultant plot of G_1 to a plot of $f_1^2(\theta,\phi)$. All gain functions used in this thesis are power gains over an isotropic radiator. This set of G_1 is summed to compute the gain G of the system, which is then printed out.

For the first stage, the plot of $G_p \times G_s$ and the theoretical set of G_s are used as $G_1 \times G_2$ and G_2 respectively. The output is the set of G_p values. Remembering the physical significance of G_p, the computed gain is meaning-less; the set of G_p is merely a partial plot of the effective radiation of the aircraft antenna relative to some antenna axis on the ground.

7.4 Results of the Antenna Calibrations.

The smoothed plot of G_p is shown in Figure 4*b*. It can be seen that the effective radiation decreases with azimuth to a minimum value at $\phi = 90^\circ$. In this context azimuth has been defined as ϕ in Figure 1. This is consistent with the zenith run data which

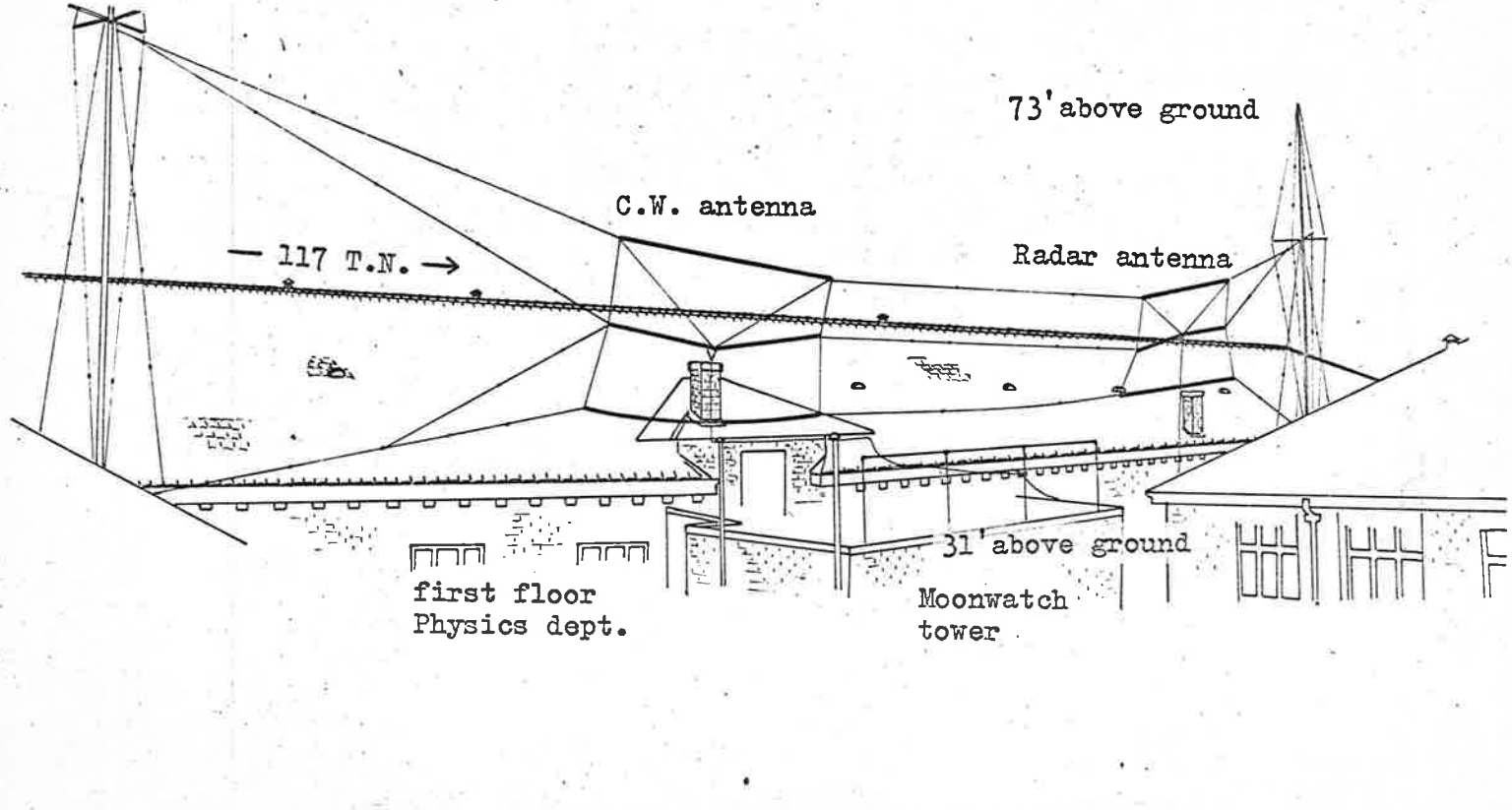

Figure 7.5 The setting of the transmitting aerials.

indicated that the aircraft antenna polarization lay along the fusilage. The plot from the Adelaide flight over the C.W. transmitter, together with this set of G_p values, was run through program 163.2. The smoothed plot of G_{cw} is shown in Figure 6a The pattern deserves comment. The null at $\phi = 90^\circ$ is not unexpected, that azimuth being end on to the antenna; however there is no corresponding null at $\phi = 270^\circ$. The size of the peak at 250° is doubtful. The pronounced minimum in the set of G_{cw} at $\phi = 90^\circ$ indicates that the increase in radiation at $\phi = 250^\circ$ is real, as any error in G_p will have a symmetrical effect on G_{cw}. The size of the peak is very dependent on the magnitude of G_p in the vicinity of $\phi = 90^\circ$. If the theoretical figures for the radiation of the standard dipole in the end-on direction were too large, the calculated values of G_{cw} would be proportionately too large in the vicinity of $\phi = 90^\circ$ and 270°. The effect of this would not be so obvious on the deep minimum at 90° as on an increase slightly offset at 250°. Figure 5 shows the physical setting of the transmitting antennas. There is a slight tilt to the C.W. antenna in such a way as to increase the radiation at high elevation at $\phi = 270^\circ$. It is possible, but not probable, that interaction with the radar antenna, also at $\phi = 270^\circ$, could distort the radiation pattern. It would be most unusual, however, for the distortion to be so evident at high elevation.

The only available means of independently confirming or disproving the polar diagram of Figure 6a is to compare the azimuthal variation of the product $G_r \times G_{cw}$ (where G_r is the theoretical gain of the dipole used for the control receiver at St. Kilda) with the observed plot of echo reflection points. There are facilities in program 166.2 (Chapter 9.3) for the output of such a combined antenna map. A mean height of the reflection points is assumed and allowance is made for the orientation and spacing of the antennas. The observed reflection point plot is dependent on the distribution of sporadic radiants, but the symmetry of this distribution can be utilised. The fact that the plot of the observed reflection points shown in Figure 7 is nearly

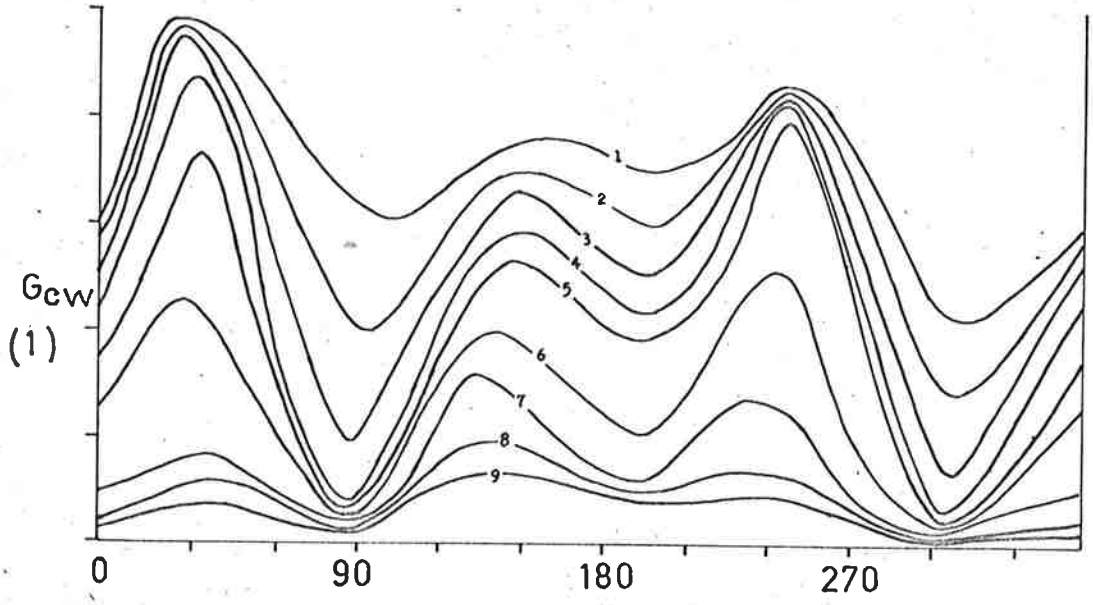
Gcw
(1)
1
2
3
4
5
6
7
8
9
0
90
180
270

(a)

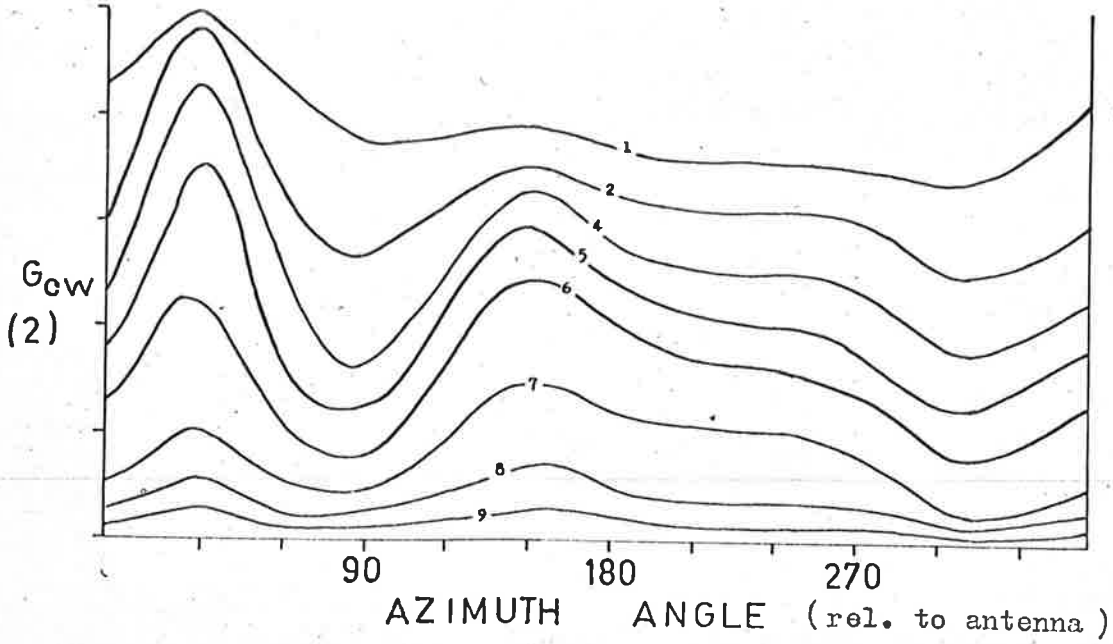
Gcw
(2)
1
2
4
5
6
7
8
9
90
180
270
AZIMUTH ANGLE (rel. to antenna)

Figure 7.6 (b)

symmetrical about the N-S axis indicates that the product $G_r \times G_{cw}$ is also symmetrical. The polar diagram shown in Figure 6a does not give rise to a symmetrical $G_r \times G_{cw}$ plot. The azimuthal distribution for zenith angle $z = 35^\circ - 40^\circ$ is shown as a dotted line in Figure 8. The peak at $\phi = 200^\circ - 210^\circ$ (rel. T.N.) results from the peak at $\phi = 250^\circ$ (rel. antenna axis) in the transmitting antenna polar diagram given in Figure 6a. The transmitting antenna polar diagram was therefore modified to that shown in Figure 6b. The peak at 250° has been drastically reduced, but the positions of the maxima and minima have not been altered. In view of the observed rate of reflection points in the east-west direction the depth of the minima at 90° and 310° (rel. antenna axis) have been reduced. Figure 8 gives the $G_r \times G_{cw}$ plot for this modified transmitter polar diagram. If anything, the C.W. antenna radiation peak at 250° appears to have been reduced too much, but the error is not significant. In general this plot of $G_r \times G_{cw}$ agrees quite well with the observed plot of reflection points shown in Figure 7. There are no significant reflection points of zenith angle greater than 65°, and those between 60° and 65° all lie in the region of azimuth $140^\circ - 230^\circ$. This is consistent with the combined antenna plot.

As a project in itself the results of the antenna calibration were a little disappointing. The fundamental difficulties were the anisotropic nature of the radiation from the aircraft, and the necessity to assume the radiation pattern of the standard antenna. If these could be overcome the method should be capable of revealing reasonably fine structure in the polar diagrams of antennas in situ. For the requirements of the meteor survey the results were quite adequate. The calculated gain of the elementary Yagi used for the C.W. transmitter was 12.6. In comparison with the figure 5.16 used for the $\lambda/2$ dipole $\lambda/4$ above ground, this is smaller than the figure usually accepted for such a Yagi. However, the zenith runs showed no indication of a minor lobe that would be associated with an antenna of higher gain, and the distribution of reflection points indicates a broad beam, low-gain antenna.

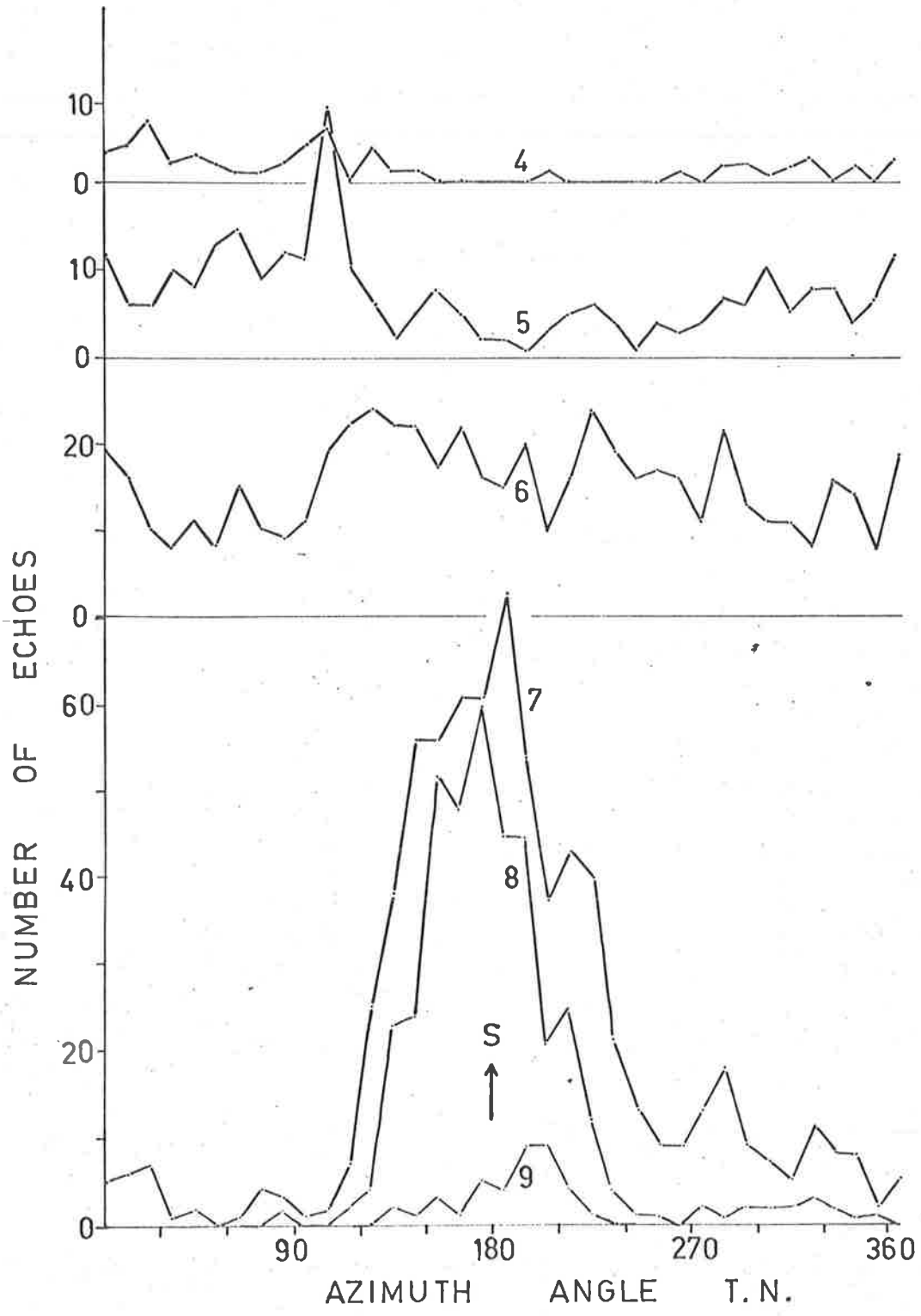
10
0
4
10
0
5
20
0
6
0
60
40
20
0
7
8
S
9
NUMBER OF ECHOES
90
180
270
360
AZIMUTH ANGLE T. N.

Figure 7.7

The diurnal variation in echo rate associated with any given radiant is remarkably independent of the details of the polar diagrams of the antennas used for transmitting and receiving, providing they are of the same general type looking towards the zenith. The Kaiser rate function, discussed fully in Chapter 9, has been calculated for the polar diagram presented in Figure 6b and also for the case using a theoretical dipole as a transmitting antenna. There is no significant difference in the two theoretical rate variations for say, the δ-Aquarid shower; both fit the observed rate equally well. This implies that the details of the antenna polar diagrams will have no significant effect on the observed distributions of geocentric radiants and orbital elements.

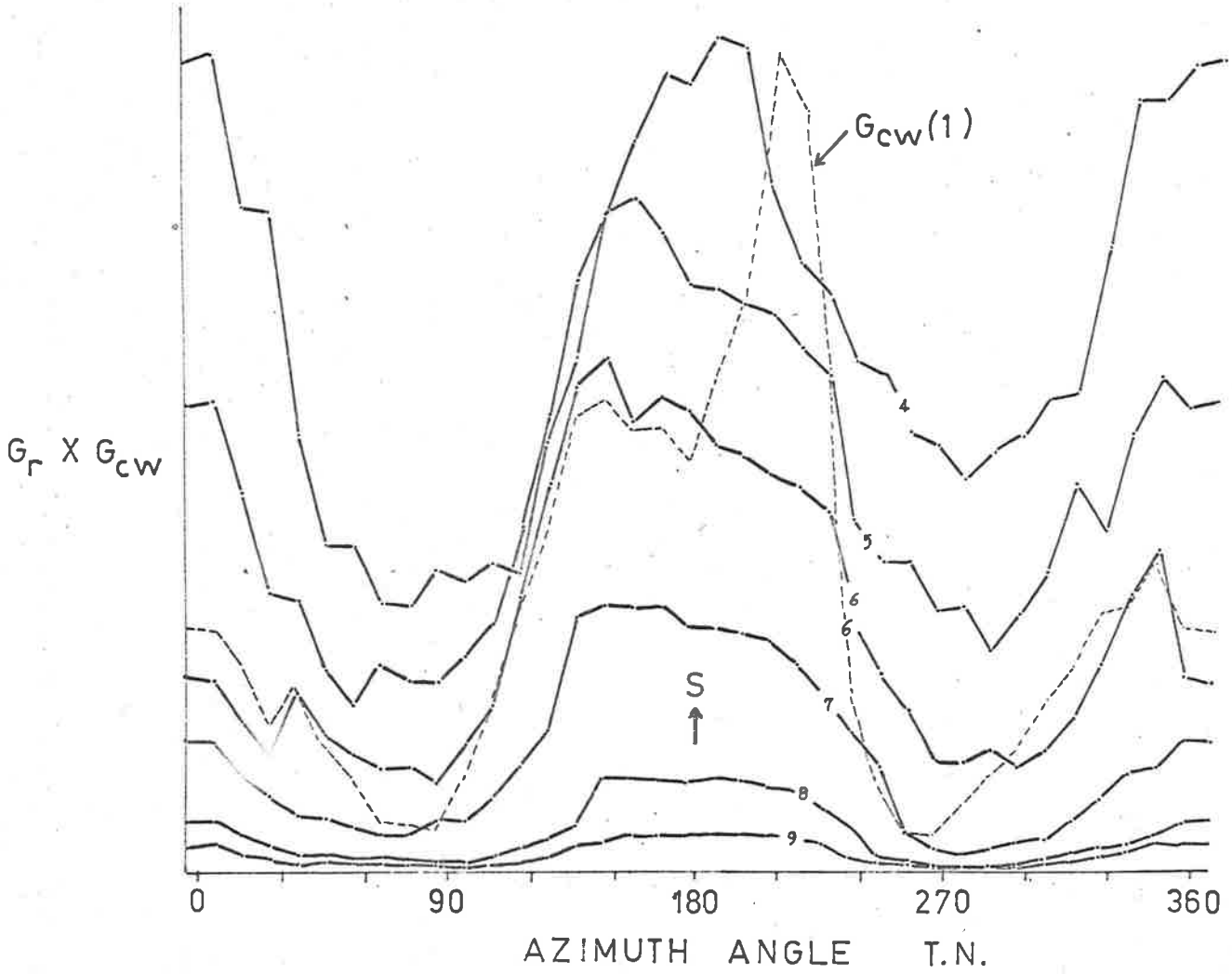

Figure 7.8

CHAPTER 8

OBSERVATIONAL SELECTION FACTORS

In this chapter we discuss the various factors that determine whether or not a meteor is detected. From the probability of detection we can calculate weighting factors to apply to each echo to compensate for the selection imposed by the method of observation. The basic assumption is made that the probability of detection of a meteor is proportional to the receiver voltage output.

8.1 The Dependence of Electron Density on Velocity.

The electron density of the trail depends on the mass and velocity of the meteor and the zenith angle of the radiant in a manner described by the equation (Weiss 1958)

$$\alpha_{max} = 12(\beta_o v_{max}^{\eta}/\mu H)\, m_\infty \cdot F(\eta)^2 \cdot (1+2F(\eta)^{-3}) \cos\chi \quad \ldots \quad (1)$$

$$\text{where } F(\eta) = 1 + 3(2+\eta)\, \ell/v_\infty^2 \quad \ldots \quad (2)$$

and $\beta = \beta_o v_{max}^{\eta}$ is the probability that an evaporated meteor atom will produce a free electron. m, r, ρ_m are the mass, radius and density of the meteor respectively; μ is

the mass of an individual meteor atom; ℓ is the latent heat of evaporization of a meteor atom, corrected for the efficiency of heat transfer; H is the atmosphere scale height and χ is the zenith angle of the radiant. The subscript ∞ refers to the initial state of the meteor.

If we assume Jacchias' value of 3.10^{11} ergs/gm for ℓ and some value $0 < \eta < 5$ for η, we can allow for all the variables in (1) except m_∞. At a later stage it is hoped to calculate this for each echo, as the survey provided for amplitude measurements on every echo. However, observations made during the last ten years indicate that the number-mass distribution of sporadic meteors varies as m^{-2} and therefore it seems reasonable to suppose that the mass range of the majority of the meteors observed in this survey will not be large. Furthermore, the errors arising from assuming a constant value for m_∞ in 8.1 will not distort the observed distributions. Thus for this survey we assume

$$\alpha_{max} \propto v_{max}^{\eta} \cdot F(\eta)^2 \cdot (1+2F(\eta)^{-3}) \cdot \cos\chi \qquad \ldots \quad (3)$$

From Lovell (1954), the power ω at the receiver is given by

$$\omega = \frac{\alpha^2 P G_r G_t \lambda^3}{32\pi^2 R^3} (e^2/mc^2)^2 \qquad \ldots \quad (4a)$$

for Lovell-Clegg scattering, and

$$\omega = \frac{\alpha^{\frac{1}{2}} P G_r G_t \lambda^3}{54\pi^3 R^3} (e^2/mc^2)^{\frac{1}{2}} \quad \ldots (4b)$$

for persistent scattering. The notation is the same as that given in Appendix 1.

These expressions become equal at $\alpha = 1{\cdot}17.10^{12}$ electrons/cm and are assumed to hold exactly for lower and higher electron densities respectively, although physically the change from one kind of scattering to the other is neither rapid nor well marked. The change from one to the other must be considered when calculating the power at the receiver for an echo of different parameters.

The procedure adopted in allowing for the observed value of v_∞ is to normalise the observed value of α in the following manner. Given the range and direction of the echo a value α_{obs} is calculated from equations 4, assuming the power at the receiver to be the minimum recordable value, $\bar{\omega}$. In practice, the observed power at the receiver will be larger than $\bar{\omega}$, but until amplitude measurements become available, this approximation is acceptable in view of the mass distribution. The value α_{obs} is then normalised by equation 3. to an equivalent meteor of velocity 40 km/sec. The value ω_N, the receiver power corresponding to the normalised value of α_{obs}, is calculated from (4), care being taken to change from one function to the other if the value $1{\cdot}17.10^{12}$ is crossed

while normalising α_{obs}.

The weight attached to the observed echo is thus given by

$$W_1(\alpha, v_\infty) = (\omega_N/\bar{\omega})^{\frac{1}{2}} \quad \ldots (5)$$

Thus allowance has been made for observational selection due to the dependence of α_{max} on velocity.

The value of η in (1) and (3) is in some doubt, estimated values ranging from 0 to 5. Distributions have been computed for $\eta = 0$, 2 and 4.

8.2 Velocity Selection.

The echoes used in this survey are those for which there is a usable diffraction waveform on all three traces and sufficient doppler on the wind records to determine the direction cosines of the reflection point (at least $1\frac{1}{2}$ cycles is necessary). The faster and hence higher echoes diffuse more rapidly and so tend to have insufficient doppler for inclusion in this survey. This effect must be considered as a selection factor.

It is also necessary to have an indication of radar range to determine the absolute velocity from the slope x/t. However, no significant proportion of the echoes are lost due to insufficient radar.

The observed echoes can be divided into four groups:

(i) an indication of x/t on at least one trace.

(ii) as above, with an observed range to give true velocity.

(iii) as above, with a diffraction pattern on all three traces.

(iv) as above, with sufficient doppler to locate the specular reflection point in space.

To compare the velocity distributions of groups (i) and (ii) it is necessary to show that the distribution of x/t is equivalent to that of the true velocity. This is in effect saying that the range should be independent of velocity. There is only a slight dependence owing to the tendency of faster meteors to evaporate at greater heights, but it is sufficiently small to be able to directly

compare x/t distributions for the two groups and so draw conclusions regarding any velocity selection imposed by the radar range requirement.

It is not expected that the additional requirement of group (iii) over group (ii) should impose any selection. The requirements of group (iv) may certainly do so; an example has already been mentioned. Considerable analysis is necessary to reliably determine the selection factors discussed above, and no attempt has been made in this survey to include them. Preliminary enquiries have indicated that the effects are not severe.

8.3 Fragmentation.

Davies and Gill (1960) state: "If a meteor disintegrates in the atmosphere into ionizing fragments, the smaller pieces are retarded more than the larger ones and a train of particles is formed. If the length of this train becomes comparable with, or exceeds, those of the early Fresnel zones of the trail, a diffraction pattern is unlikely to be seen. It can be shown that, if the individual fragments of the meteor themselves obey Herlofson's equations, the length of the train of particles is likely to be proportional to $(v^2 \cos \chi)^{-1}$." On this basis one could apply a weighting factor

$$W_{frag} = 1 + \text{const.}/v^2 \cos \chi \qquad \ldots \quad (6)$$

but in the absence of information about the constant in (6), this factor has not been included in this survey.

In view of the lack of a definite value for η in equation 1, the author believes that there is little value in devoting a lot of time to the various factors discussed above. Should an accurate value of η be available, however, the data will be analysed more fully to obtain information about these factors.

8.4 The Kaiser Rate Function.

Whether or not a particular meteor from a given radiant is

detected depends on the position of the reflection point in the echo plane (see Figure 2.1). For a meteor of given parameters (radiant, velocity etc.), the power at the receiver $\propto G_r.G_t/R^3$, regardless of the type of scattering. However, the exact whereabouts of a meteor encountering the earth from a given radiant is a matter of chance. This applies to all radiants. If each echo were weighted on the basis of the position of the reflection point e.g. $W \propto (R^3/G_r.G_t)^{\frac{1}{2}}$, one would have the anomaly of applying different weights to meteors having identical parameters. The weight applied to each echo should be a measure of the inverse probability that an echo of those parameters will be detected. For any given radiant it is therefore necessary to integrate the probability of detection over the whole of the available portion of the echo plane. For this purpose we shall use the Kaiser Rate Function.

With reference to equation 2.2 one can define a function $f(\chi,A)$ as the relative rate to be expected from a radiant of zenith angle χ, azimuth angle A. Assuming the mass distribution parameter s = 2 for sporadic meteors, we have

$$f(\chi,A) = \frac{h \cos\chi}{\sin^2\chi} \int_{\theta=-\pi/2}^{\pi/2} \frac{d\theta}{\propto(\theta)\cos^2\theta} \qquad \ldots (7)$$

where the notation is the same as that in equation 2.2. This is merely an extension of that equation to allow for the variation of the antenna gain with azimuth.

To obtain the map of $f(\chi,A)$ over all the sky, (7) is integrated numerically for all χ, A. By choosing an interval of 5^o for θ, each integral can be replaced by a summation of 36 values of the integrand. Dividing the map into 5^o x 10^o intervals of χ, A respectively, the complete solution of (7) involves 648 summations. The labour was prohibitive when the Mawson survey was

undertaken by hand and the familiar Kaiser equation, which is independent of azimuth, was adopted. With the availability of the I.B.M. 7090 computor, however, this limitation does not exist and the extension of the Kaiser rate function to allow for azimuth was a relatively straightforward matter.

A mean echo height of 93 km is assumed and a map of the product of $G_r \times G_t$ is computed, allowing for the orientation of each antenna and using the subroutine DIFFER to allow for the spacing. Using equations 4, a map of limiting α values is prepared as a function of the reflection point zenith and azimuth angles relative to the receiving station at St. Kilda. The map of $f(\chi,A)$ is then computed according to equation 7. The print out of this map is normalised to a maximum value of 1000. The integration has also been performed for the Mawson equipment, assuming both antennas behaved as theoretical $\lambda/2$ dipoles $\lambda/4$ above ground. The result of this integration shows that the limited function $f(\chi)$ found in Chapter 2.5 is a sufficient approximation for that study.

The probability that a meteor, from a radiant whose direction is given by χ,A, will be detected is proportional to $f(\chi,A)$. An echo from a radiant, direction χ,A, is therefore weighted by $W_2(\chi,A)$

$$\text{where} \quad W_2(\chi,A) = 1.0/f(\chi,A) \qquad \ldots \quad (8)$$

This weighting factor allows for the antenna polar diagrams and includes the dependence of ionization on radiant zenith angle (the factor $\cos\chi$ in equation 1).

As $f(\chi,A)$ is derived from a summation over a considerable portion of the sky, it is not sensitive to any minor variations in antenna polar diagrams.

8.5 Astronomical Selection.

A weighting factor, inversely proportional to the probability of collision of a particle with the earth, has been

given by Wipple (1954)

$$W_{astro} = \frac{\pi V_g \sin i}{R^2 V_\infty^2}\left(2 - \frac{1}{a} - p\right) \quad \ldots (9)$$

where V_g is the geocentric velocity, V_∞ is the relative velocity of the particle at the top of the earth's atmosphere, R is the radius of the Earth and $p = q(1 + e)$, where q is the perihelion distance, e the eccentricity, a the semi-major axis and i is the inclination of the particles' orbit.

Program 167.2, listed in Appendix 5.3, computes the distributions deemed necessary for all the observed and calculated quantities. Subroutine JUDITH weights each echo according to the factors discussed in this Chapter.

CHAPTER 9

REDUCTION PROGRAMS

These programs are written in the I.B.M. Fortran language for the I.B.M. 709/7090 data processing system. No attempt is made to present a translation of the programs into normal mathematics, and the legend of variable names in Appendix 5 is mainly limited to data input and output. This section describes the principles and steps observed in reducing the data.

9.1 No. 165.2 - Combined Orbit Program.

The program is divided into a main section and several subroutines. The latter perform the actual mathematical reduction of the data, the former ties the subroutines together and executes the 'chores' of reading and storing the data. Let us first discuss the main section of the program.

Page 256 defines the allocation of storage, the size of the matrices and reads in the constant data used later in the various subroutines. Most of the next page is devoted to zeroing the running sums used in computing the mean values of groups of up to 300 echoes. Normally these are rezeroed at the start of each month's data.

The data was handled in the following way. Each echo needed five punched cards. The first, the 'header' card, provided the number of the echo, the wind drift at the three reflection points, the phase angle ψ (see Chapter 5) at the time T = 0 for each trace, the time and date of the echo in zone time, and finally, the type of echo. The last item indicated whether it appeared to be short duration, intermediate or long enduring. The next three cards were punched automatically during the film reading and contained the times of the diffraction maxima and minima used for each trace, together with the relative time of each simultaneous time marker. The fifth card contained the doppler information necessary to compute the direction cosines of the main station specular reflection point, and the range of the echo.

In addition, at the start of each astronomical day, two cards were inserted containing the necessary astronomical information from the Astronomical Ephemeris. The first of these merely served as a 'warning' card. This system was also used in the case of 'vary', the data card giving the scale factors of the film reader for each trace. The survey data was first submitted in card form, an interim program checked the order of the cards, computed the direction cosines of the reflection point and wrote the complete set of data on magnetic tape. This procedure paid dividends in avoiding hold-ups when actually computing, which was done from this tape rather than from cards.

To continue with the main section of the program. Having read in a set of data for an echo the reduction of the film reader data is performed in subroutine 'HELEN' in the manner described in Chapter 5. The individual subroutines are described in more detail later in this chapter. The geocentric information relevant to the radiant and reflection point is computed by subroutine 'GLENYS'. The essential output from this stage is geocentric velocity and radiant position. The third main subroutine, EILEEN, calculates the orbital elements of the meteor by the method described by Porter (1949). Should the echo fail to meet the requirements of a closed orbit meteor at any stage, the cause of failure and relevant information is immediately printed out. Hyperbolic meteors are treated this way, pending future re-analysis. If the echo passes as a closed orbit meteor, all the output information necessary for any future analysis is stored.

Following storage (page 259), the echo is tested in various ways to determine its quality. The first of these tests decides whether the velocity differences between the three traces are within normal tolerances. These tolerances are functions of the number of Fresnel cycles used in the echo reduction. The echo is also checked to determine whether the value 0 or 1 was assigned to the quality JUMP for each trace. If the former is the case, the number of phase optimization steps (Chapter 5) taken must be less than 19. The third test checks that the two values for reflection point

height (Chapter 3) agree to within 20 km, and that the number of optimization steps (i.e. percentage change in echo velocity) taken to bring the two heights together has not reached the allowable limit. This limit is determined by the number of Fresnel cycles used in the echo reduction, and cannot be exceeded, even if the two values of reflection point height differ greatly. The last test checks that the retardation correction is less than 7.0 km/sec.

If the echo fails any of these tests it has a value of 0 assigned to the quantity NQ, and is not classed as 'OK'. However, it is still stored and is available for distribution calculations, if required. If it passes all tests the echo is classed as OK and makes its contribution to the sums for various mean values, e.g. deceleration. In the normal course of events control then transfers back to statement 130 (page 258) to read in another echo.

If the echo is the last of a month's data, the mean values are computed and printed out, and the stored information is written up on an output magnetic tape. Facilities are also provided to print out all the information relating to each echo at this stage; but usually this final listing is made separately from the output tape at some later date.

Let us now consider the subroutines in detail.

(i) Subroutine HELEN.

The listing appears after that of the main program in Appendix 5. In the manner described in Chapter 5, this subprogram computes the least mean square fit to the data for each of the three diffraction traces. It counts the number of items of information and assigns the last item under the name of 'simul'. This is the relative time of the simultaneous time marker. From the value of the phase angle ψ_o it decides whether the first item corresponds to a maximum or minimum and then computes the value of ψ (P(J) in the program) for each item. Using the theoretical curve it assigns the appropriate theoretical x value (see Figure 5:7) to each item and then computes the slope and intercept of the best fit straight line. For the purpose of this fit the error is assumed to be due to the observed value of time. The mean deviation of all the

points from the straight line is also calculated and this value is tested to see if it lies within the tolerances specified for an echo of the calculated slope and number of items (see Chapter 5). If it does, the slope and intercept are accepted; if not, the phase angle ψ_o is varied in steps of 9^o (to a maximum of 180^o) until the deviation is acceptable. If the deviation is still not acceptable, the best set of data in the range is chosen, and the value 0 assigned to the variable 'jump'. This enables a check to be made at the end of each month's computation that the mean deviation requirements are acting evenly on all classes of echoes.

This procedure is repeated for each trace and the final slope used in determining the velocity of the echo is the mean of that of each trace weighted according to the number of items used in its determination. The three intercepts used in determining the time differences are calculated from the best fit of a line of slope equal to the mean fitted to the three sets of data. The effective decelerations, i.e. the percentage differences between the slopes of traces 1 and 2 and traces 3 and 2 are also calculated.

(ii) Subroutine GLENYS.

The input to this program is basically the three time differences and the mean slope, x/t. Also needed are the main station reflection point direction cosines, the radar range from the wind equipment and the sidereal time from the Astronomical Ephemeris. The local mean solar time if first calculated for the echo. The 'wind' direction cosines are converted to N.S. axes and the reflection point zenith and azimuth angles computed. The observed echo velocity is obtained from the x/t slope and the radar range. After allowing for t_o point movement due to the observed winds, the time delays between the two sets of stations are calculated and hence the direction cosines of the meteor path are determined. In the manner described in Chapter 3 these direction cosines are optimized to satisfy the height of the main station reflection point, calculated from the wind data.

The observed radiant azimuth is referred to True North, and the deceleration due to the earth's atmosphere is calculated using the pressure data from the A.R.D.C. 1959 model atmosphere. The velocity vector, i.e. velocity and radiant position, is corrected for the diurnal motion of the observer (Chapter 6.3) and also for zenith attraction (Porter 1949). The zenith and azimuth angles of this corrected radiant are then transformed to declination and right ascension.

(iii) Subroutine EILEEN.

From the data obtained from the previous subroutine this programme closely follows the method given by Porter (1949) for determining the orbital elements. The six elements computed are a, e, i, ω, Ω and ν, i.e. semi-major-axis, eccentricity, inclination, argument of perihelion, longitude of ascending node and true anomaly respectively. Also calculated are the perihelion distance, aphelion distance, period, longitude of perihelion, and for both the true and apparent radiant in heliocentric coordinates, the longitude and latitude and elongation from the apex. The longitude is also referred to the apex in order to combine the results over the year. If the orbit is either parabolic or hyperbolic the data is not stored; the appropriate elements are immediately printed out for future re-analysis.

(iv) Minor Subprograms used in 165 are:

AZ - This function returns an azimuth angle when given two direction numbers.

TCHEK - A subroutine which positions and checks the output tape before updating it with new data.

9.2 Antenna Gain and Associated Programs, 163.1 and 163.2

These have been described in Chapter 7. However the method of handling the data in 163.1 can be mentioned again. The continuous chart record is sampled every few seconds even though observations of the aircraft are only made at less frequent intervals. Thus the number of points obtained for the map of $(VR)^2$ is a

maximum and not limited by the number of optical observations.

Subroutine DIFFER is also associated with other programs. Any observation or bearing in spherical cylindrical coordinates is taken as input, together with the cartesian coordinates of another origin. The subroutine returns the coordinates of the observation to the calling program relative to the new origin. Using a spaced station technique for this survey, this subroutine has many applications.

Appendix 5.2 contains a brief legend to these two programs.

9.3 The Kaiser Rate Function and Associated Programs.

Program 166.2

The principle of this program has been described in Chapter 8.3. The input is comprised of the following:

(i) The variation in gain of both the receiving and transmitting antennas as a function of coordinates relative to each respective antenna. These gains do not need to be normalised in any way.

(ii) The orientation with respect to True North and spacing of the two sets of axes used in (i).

(iii) The mean echo height, transmitter and limiting receiver power, and R.F. wavelength.

The output can be part or whole of the following:

(i) The normalised maps of the $f^2(\theta,\phi)$ (see Chapter 7.3) values for each antenna relative to T.N., and their computed gains over an isotropic radiator. The latter computation is performed by subroutine NORMAL, which is basically the same as program 163.2.

(ii) The combined antenna gain map $G_r \times G_t$ as a function of zenith and azimuth angle relative to the receiver (and T.N.). Allowance is made for antenna orientation and spacing. A mean echo height is assumed.

(iii) A map of limiting α values.

(iv) A map of the Kaiser Rate Function. This is usually punched out for direct insertion into the associated program 166.3,

Section 9.3)
and for use in the distribution subroutine JUDITH.

Program 166.3. The Diurnal Rate Variation of any Radiant.

Input to this program is comprised of the coordinates (R.A. and Dec.) of any radiant, the sidereal time for the days over which the shower has been observed, or is expected, and the Kaiser Rate Function map from program 166.2.

The zenith and azimuth angle of the radiant is computed for each of the 24 hourly intervals for each day listed, and the appropriate value of the Kaiser Rate Function selected, printed out and stored. When the list of days is completed, the mean value for each hourly interval is computed and printed out. These values are a measure of the theoretical diurnal variation in rate for the given radiant over the listed period for the Adelaide equipment.

Included in the input data is a normalization figure, and the diurnal rate variation is normalized to a total of that many echoes over the day. The program is extremely useful in predicting the times of maximum response to any particular shower. The theoretical and observed diurnal variation in rate is given in Chapter 10 for the δ-Aquarid shower.

A simple variation of this program is to compute the equipment response as a function of radiant declination. This is also shown in Chapter 10.

9.4 Distribution Program.

This program reads the output tape from program 165.2 and prints the various geocentric and heliocentric distributions. The printout is divided into six groups.

(i) Seasonal maps of the echo rate as a function of ecliptic latitude and longitude (relative to the Apex of the Earth's Way).

(ii) The ecliptic longitude distribution for all bands of latitude; the ecliptic longitude distribution for all months, and the ecliptic longitude distribution for all

seasons. In all cases the ecliptic longitude is measured relative to the apex.

(iii) The distributions with semi-major axis, eccentricity and inclination.

(iv) The distributions with individual orbital elements.

(v) Monthly maps of the echo rate as a function of declination and right ascension. These maps are very useful in identifying possible showers. Any significant grouping, however, has to be further examined for the velocities of the contributing echoes.

(vi) Maps of the radiant and reflection point distribution as a function of zenith and azimuth angles, and the distributions with individual geocentric quantities.

The printout of each group is controlled separately. The uncorrected distributions were printed for all six groups. Only groups (ii), (iii), (iv) and (vi) were required for the distributions corrected for observational selection, and groups (iii) and (iv) for the distributions corrected for both observational and astronomical selection.

The corrections for observational and astronomical selection were made by the subroutine JUDITH in the nammer described in Chapter 8.

Subroutine JUDITH.

This subroutine weights each echo for observational and astronomical selection. There are five weighting factors. W(1) corrects for the velocity of the meteor, W(2) for the radiant direction. W(3) is not used. W(4) is available to correct for the probability of fragmentation, but has not been used to date. W(5) corrects for astronomical selection, and of course is not applied when correcting for observational selection only. Each weighting factor is normalised to an approximate mean value of 1.0, and the combined product multiplied by 5.0. The combined weight is necessarily an integer and is not allowed to exceed 25. In this manner the weight can vary by a factor not exceeding 5 from

the mean, unless it is equal to 0.

In correcting for observational, and observational and astronomical, selection the distributions were calculated for three values of η (Chapter 8.1), equal to 0, 2 and 4. The uncorrected distributions were also printed for OK echoes only.

9.5 Program Checking.

Every program has been checked for correct operation. In the case of the main reduction program 165.2 it is not practicable to manually work through the complete program with a given set of input data in the same manner as the computor. The three main subroutines were developed independently over a year, and as each change or addition was made it was checked on a desk calculator. When any two sections were combined care was taken to check for any interaction. Thus the complete program has been checked in sections on a desk calculator and all the sections checked for mutual interaction.

The antenna gain programs were easily checked with a desk calculator, but the Kaiser Rate Function program 166.2 took more time in view of the numerical integration. One cell of the function $F(X,A)$ was calculated and the agreement (within 3%) was deemed sufficient.

For the Distribution program 167.2 the main thing to be checked is the possibility of a calculated subscript being outside the dimensioned range of the variable. If this occurs the contribution of the echo will be made incorrectly to some cell of another variable. This will become obvious by the sum of the distribution in question being less than the correct value. Three echoes have been lost from the heliocentric velocity distribution in this way, but the error is not significant. The weighting factors applied by subroutine JUDITH have been checked for several echoes on a desk calculator.

CHAPTER 10

RESULTS OF THE ADELAIDE SURVEY

10.1 Accuracy of Results.

The accuracy of the system is fundamentally governed by the accuracy with which the experimental diffraction waveforms can be interpreted and reduced to the straight line $x = V(T - T_o)$ (Chapter 5.2). A measure of the accuracy with which this has been done is given by the plot in Figure 1. This shows the distribution of velocity separation between the traces (DEC 1 and DEC 2), plotted against the minimum number of items ($\frac{1}{2}$ Fresnel cycles) used in the reduction of the three traces, for 134 echoes in December 1960. The data was read on a manual film reader and is inferior to that of the main survey. The straight line $D = 25 - I(min)$ is the allowable limit for an echo to be classed as OK (see Chapter 9.1).

To assess the accuracy of the film reading, and to some extent the reduction procedures, the echoes for July were read twice. The re-reading included the wind information. For the first reading the orbit data was not read on the Telereader, but on the manual and less accurate reader with temporary scales. The unit of time was .1 msec compared to the 1/15 msec unit of the Telereader. This loss of accuracy is reflected in the mean values for the r.m.s. deviation from the best fit straight line (Chapter 5.2), 0.8, 0.7 and 0.7 msec for the first reading, and 0.6, 0.6 and 0.6 msec respectively for the Telereader data. The most suitable value for p_1 was about 1.2 for the first reading (the values of p_i discussed in Chapter 5.2 are based on this data), but the survey echoes read from the Telereader were computed with $p_1 = 0.9$. Even so, this value could have profitably been smaller, as the vast majority of echoes did not have the phase angle ψ_o optimized at all.

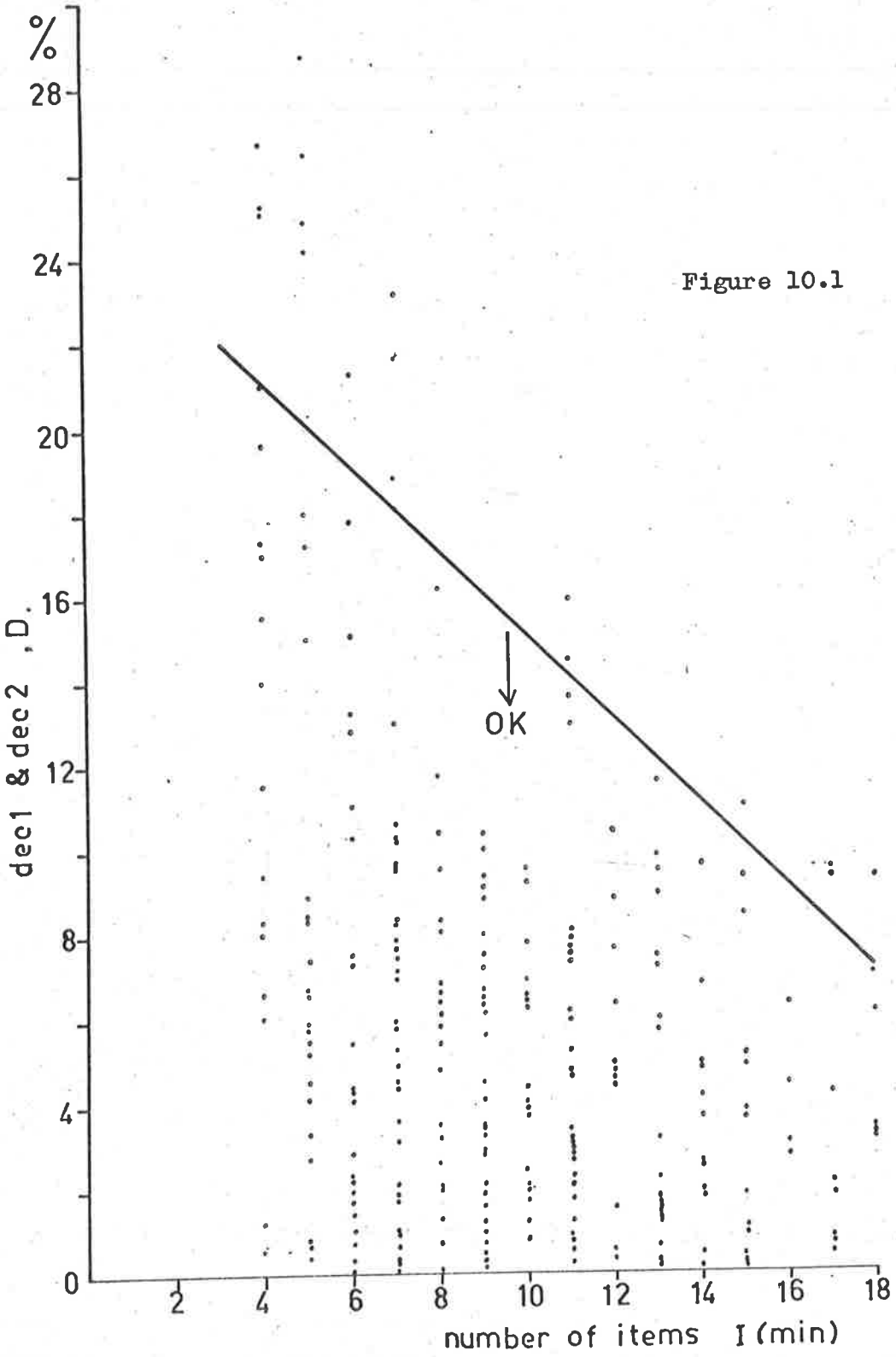
%
28
24
20
16
12
8
4
0
dec1 & dec2 , D.
OK
2
4
6
8
10
12
14
16
18
number of items I (min)

Figure 10.1

Figure 10.2

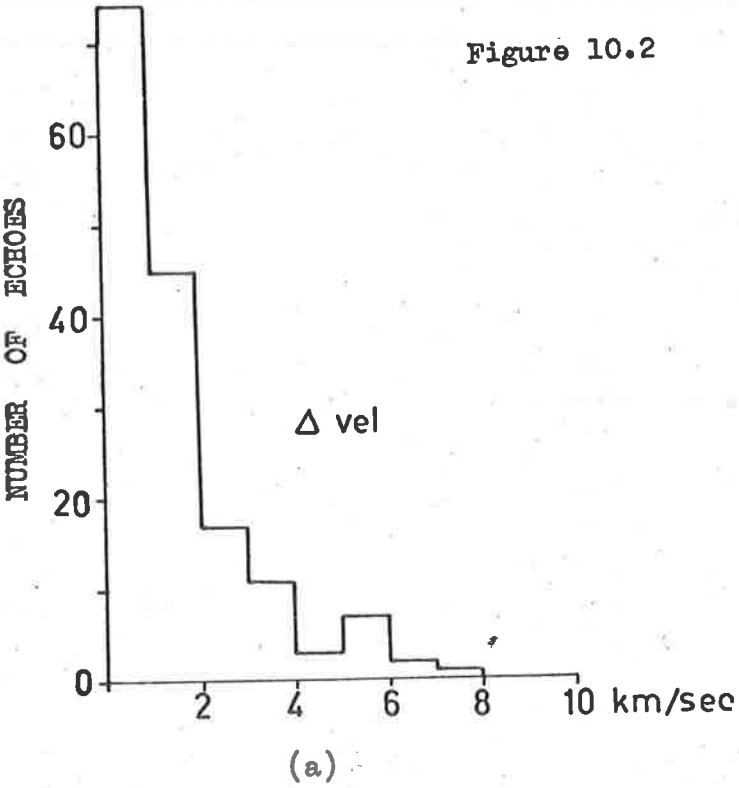

(a)

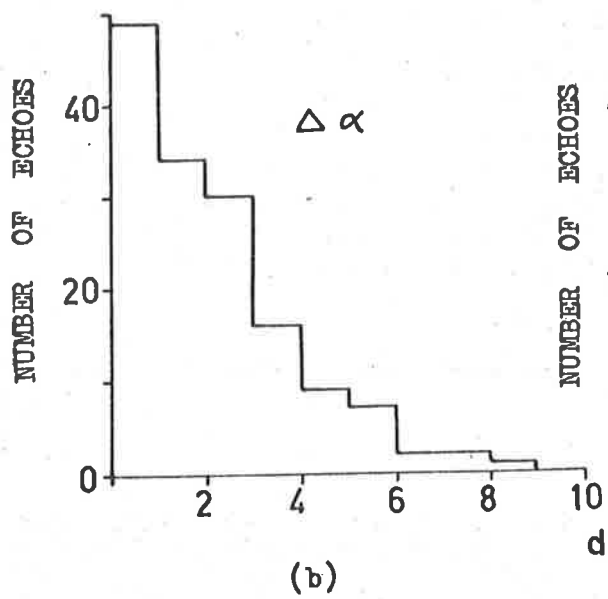

(b)

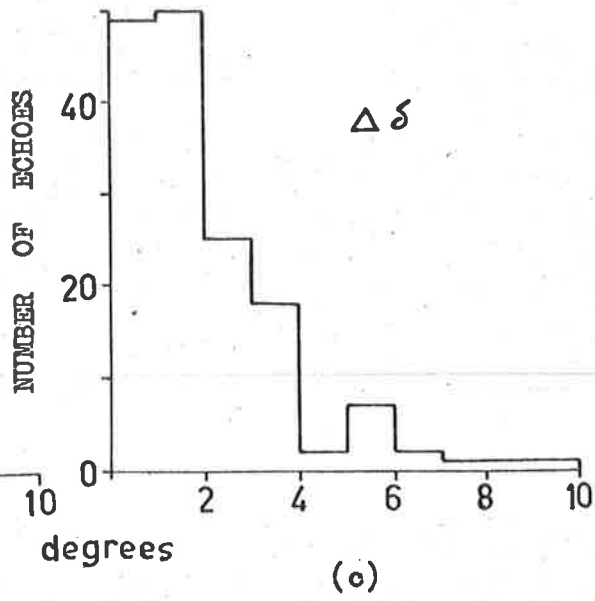

(c)

The first set of data was computed with three separate programs which were later reorganized into the three subroutines, HELEN, GLENYS and EILEEN, given in Appendix 5.1. The results thus provide a check on some aspects of the programming. Some differences certainly result from rounding-off errors, but these are small compared to the differences resulting from the film reading. It should be noted that with the present system of film reading the T = 0 axis is chosen quite arbitrarily (Chapter 5.2) and no two sets of data for the one echo will be the same. It is not always necessary to include the first 'item', if ψ_o is chosen appropriately and consequently two sets of input data cannot normally be compared in any useful manner.

There were 161 echoes in common from a total of 192 echoes available for comparison from the second reading. Hyperbolic orbits were excluded from the second print-out; these echoes are discussed in Section 10.2. There were 7 echoes from the 161 compared that were obviously in error (difference in right ascension $> 10^{\circ}$); the distributions for the differences in right ascension, declination and observed velocity for the remaining 154 echoes are shown in Figure 2. The values of the r.m.s. deviations from zero indicate the accuracy to be expected for each quantity as Ra. $\pm 2.7^{\circ}$, dec. $\pm 2.2^{\circ}$ and vel. $\pm$ 2.1 km/sec.

These values are upper limits to the expected errors in the survey data as the first reading was very much inferior to the second. The latter was done not only with the better film-reader, but also with improved techniques with less chance of error, and greater experience in interpreting waveforms. The errors are similar to those expected by Davies and Gill (1960) for the results of their survey.

The values for the orbital elements, e, i, ω and 1/a, were compared for 73 echoes, but the results are not as straightforward as those for the radiant vector. A diagram showing the significance of the six elements is given in Figure 4. The size of the meteoric orbit is defined by a, its shape by e, the orientation of its plane in space by i and Ω, and the direction

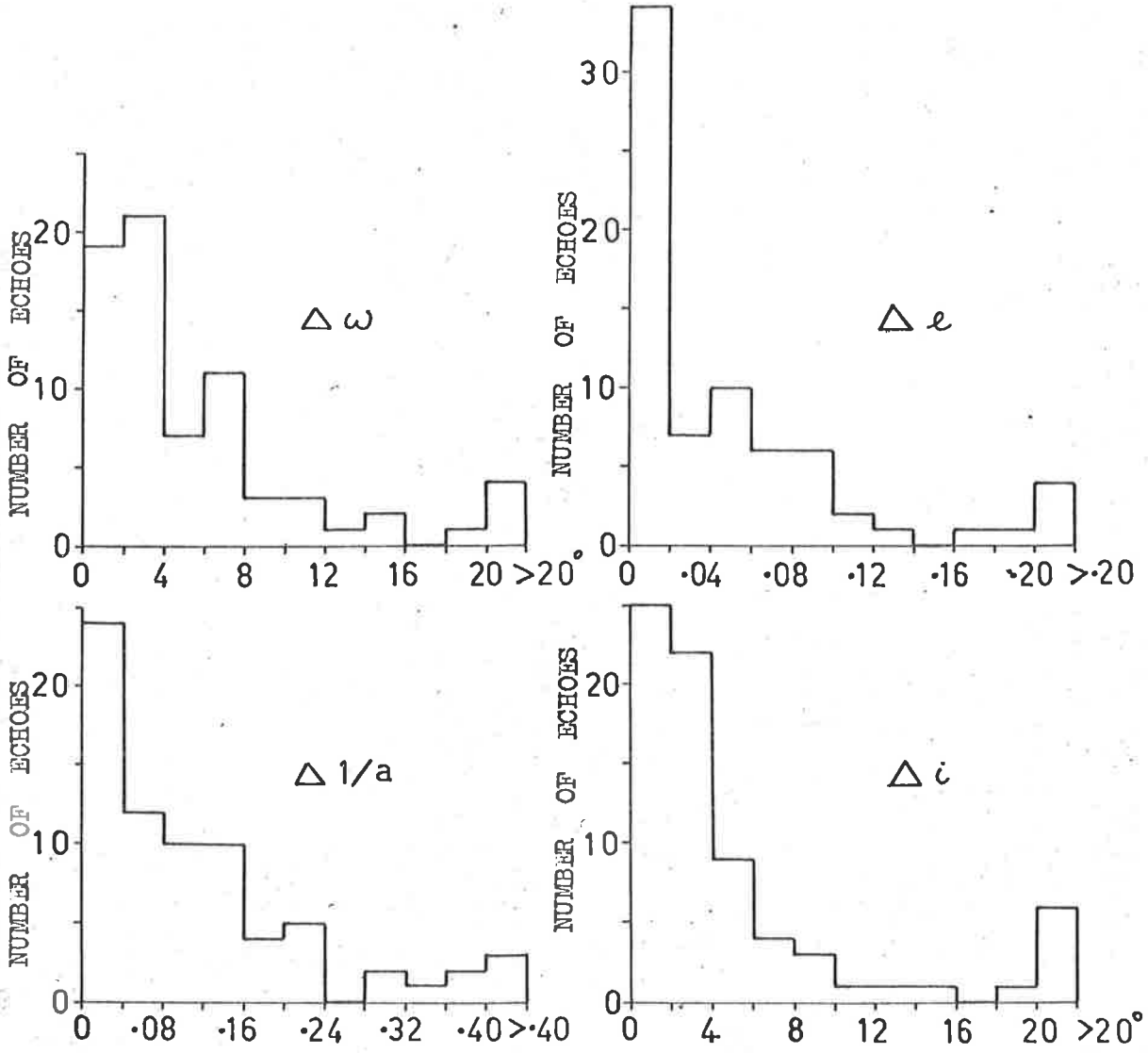
NUMBER OF ECHOES
Δ ω
0 4 8 12 16 20 >20°
NUMBER OF ECHOES
Δ e
0 ·04 ·08 ·12 ·16 ·20 >·20
NUMBER OF ECHOES
Δ 1/a
0 ·08 ·16 ·24 ·32 ·40 >·40
NUMBER OF ECHOES
Δ i
0 4 8 12 16 20 >20°

Figure 10.3

of the major axis in that plane by ω. The position of the meteor in the orbit is given by the true anomaly ν. Except for a change of 180° as the radiant moves across the ecliptic, Ω is dependent only on the day of observation, hence a comparison of the four elements a, e, i and ω is sufficient. The quantity 1/a is more convenient to consider as $a \rightarrow \infty$ as $e \rightarrow 1.0$. The relationship between errors in the radiant vector and the resultant errors in the orbital elements is not simple. For example, for $e > 0.95$, the value of i becomes unreliable, while ω is inaccurate for orbits of small e. The distributions for the differences between the 73 echoes are given in Figure 3. With these limitations in mind the comparison indicates average errors of the following order: $e \pm 0.05$, $i \pm 4^{\circ}$, $\omega \pm 6^{\circ}$ and $1/a \pm 0.12$. These results are very similar to those estimated by Davies and Gill.

In order to assess the effect of variations of input data on the radiant vector and orbital elements, a set of data was programmed with a steady variation in one item of data for each echo ('item' is not used in the special context of Chapter 5.2). The results of this are listed in Table 1, the last row for each echo indicates the probable order of error in the input data for an average echo. Table 2 lists the output data for four Geminid meteors with a variation in the value of the mean surface area/mass ratio, G. The results are consistent with a value of between 5 and 50 cm^2/gm. The low height of the reflection point (85 km) of echo number 55799 causes the retardation correction to be much larger than for the other echoes. Whether this height is in error or this particular meteor is more massive than the others has not yet been determined.

10.2 Hyperbolic Orbits.

From the survey of 2072 echoes 224 were initially rejected as having parabolic ($1.0 \leqslant e < 1.02$) or hyperbolic ($e \geqslant 1.02$) orbits. These were recomputed with the retardation factor G = 5 instead of 50, and the velocity optimization limited to 1%. Only 68 echoes still had hyperbolic orbits, showing that these two

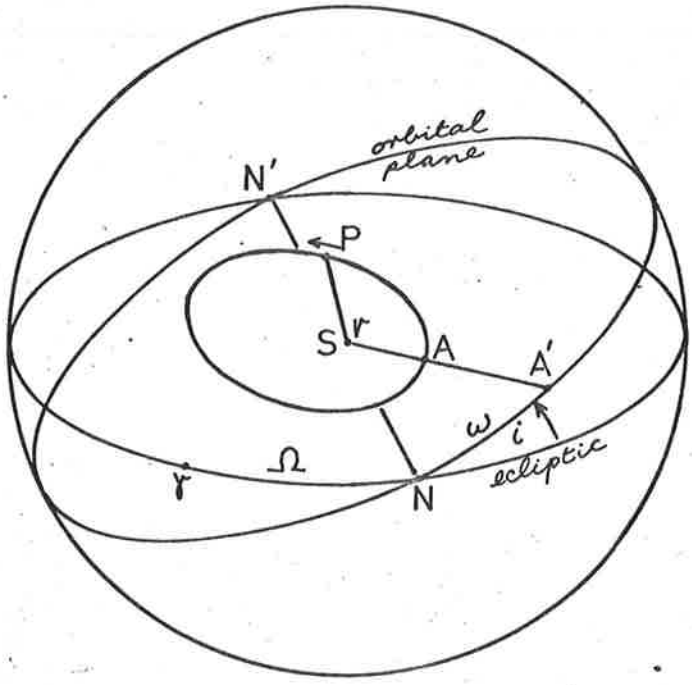

Figure 10.4 ORBITAL ELEMENTS

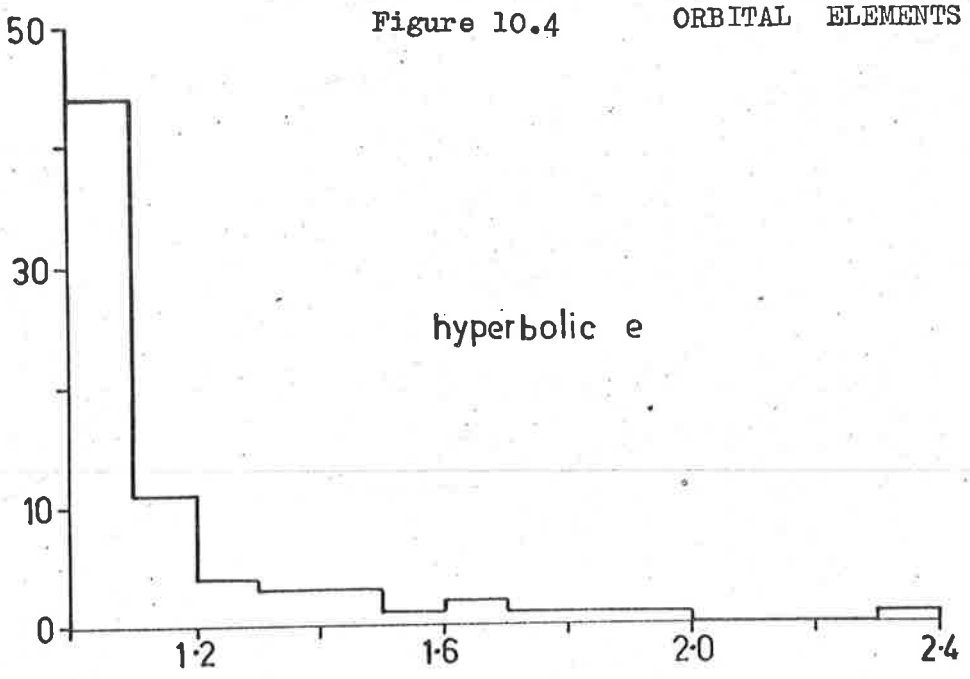

Figure 10.5

TABLE 1

VARIATION RUN

Echo	Variation		Ra.	Dec.	Vge.	e	i	ω	1/a
		2.10	153.0	+15.6	31.5	.889	9	333	1.044
00409	$\psi(3)$	2.30	154.5	17.7	32.3	.897	16	334	1.030
		2.50	155.3	18.0	32.4	.898	18	334	1.047
		±0.2	±1.1°	±1.2°	±0.5	±.004	±5°	±½°	±.009
		0.80	189.2	-75.4	39.5	.676	68	321	.362
01457	$\psi(1)$	1.00	185.1	-74.8	39.8	.679	68	324	.353
		1.20	181.4	-74.0	40.2	.683	69	327	.344
		±0.2	±3.9°	±0.7°	±0.4	±.004	±½°	±3°	±.009
		-20	188.0	+4.9	59.3	.667	161	294	.776
00623	WIND 3	-30	187.4	5.2	59.8	.689	161	292	.723
		-40	187.0	5.0	59.5	.693	162	294	.738
		±10 m/sec	±0.5°	±0.1°	±0.2	±.013	±½°	±1°	±.019
		1400	301.9	+4.3	24.0	.889	16	110	.163
02659	SIML 2	1500	306.9	7.2	22.3	.908	15	119	.124
		±½ msec	±0.5°	±0.3°	±0.2	±.002	±.1°	±1°	±.004
		+.46	147.3	-57.0	42.0	.757	72	22	.256
02892	ℓ	+.54	140.3	-58.0	40.8	.849	68	21	.159
		±0.02	±1.7°	±0.3°	±0.7°	±.023	±1°	±¼°	±.024

TABLE 2

4 GEMINIDS VARYING G .

Echo	WH	G	drag	Vge.	e	i	ω	1/a	
52318	95	05	0.1	33.9	.893	19	324	.746	
		50	0.6	34.4	.900	20	324	.721	
		100	1.3	35.1	.909	20	324	.687	
		250	4.1	38.1	.940	24	326	.537	
		500	-	-	1.011	41	330	0	Hyperbolic
52345	91	05	0.1	30.9	.859	16	325	.904	
		50	1.2	32.0	.874	16	325	.862	
		100	2.7	33.6	.895	18	326	.797	
		250	11.9	43.2	.981	29	331	.281	
		500	-	-	21.90	10	295	0	Hyperbolic
55799	85	05	0.3	30.4	.839	14	317	.781	
		50	5.4	35.7	.916	17	318	.526	
		100	-	-	1.059	41	325	0	Hyperbolic
		250	-	-	-	-	-	-	
		500	-	-	-	-	-	-	
55991	96	05	0.0	32.0	.880	13	327	.889	
		50	0.4	32.4	.885	13	327	.874	
		100	0.9	32.9	.892	14	328	.856	
		250	2.5	34.6	.913	15	329	.782	
		500	7.1	39.4	.958	19	332	.548	

corrections had been the cause of the non-ellipticity of the majority of the 224 echoes. This does not mean that the correction for retardation was too large or that the optimization was invalid on the average. It has already been noted that 50 cm/gm appears to be near the upper limit for G, the ratio of surface area/mass, for the meteors considered in this survey. For the more massive meteors G will be less than 50 cm/gm and the application of this value to all the meteors would certainly be expected to cause some anomalous and incorrect values for retardation. The correction is also sensitive to the measured height of the reflection point, and should the wind data be inaccurate for some meteors the computed correction could be greatly in error. Incorrect wind data will also cause an error in the velocity through the optimization process, but it is quite evident from the computed reflection point heights that the wind heights are generally the more accurate. Thus optimization (Chapter 3.4) on this basis must improve the accuracy of the data on the whole, even though it may adversely effect a few particular echoes.

The spread in eccentricity for the accepted echoes of the Geminid shower is $\pm$ 0.03, and the comparisons discussed in Section 10.1 have indicated a mean error of $\pm$ 0.05 to be an upper limit for the survey. However a significant proportion of echoes will have errors of up to $\pm$ 0.1 so that the 44 echoes with $1.0 < e < 1.1$ is not unexpected. The distribution of e for the 68 hyperbolic echoes is shown in Figure 5. There are 24 echoes left with $e > 1.1$.

Consideration of the four hyperbolic echoes in July is interesting, as the data for this month has been read and computed twice. The values for eccentricity, e_1 and e_2 respectively, are compared below:

echo no.	e_1	e_2
84314	0.903	1.201
84847	-	1.184
87008	1.024	1.038
88383	0.987	1.083

Echo number 84847 was not read the first time. Of the three left, only one (87008) was computed as hyperbolic on both occasions, and even then, the value of e is not very much greater than 1.0. To provide a full answer to the question of the significance of the 68 hyperbolic orbits it will be necessary to reread and recompute the data as was done for the month of July. It seems probable, however, that not many echoes will remain as definitely hyperbolic. Those that do have not necessarily originated from outside the solar system, but may have suffered perturbations during their last orbit before encountering the earth.

10.3 Distributions.

The distributions of number of echoes against the various geocentric and heliocentric quantities are given in the following pages. These distributions were computed by program 167.2, which is listed in Appendix 5 and is discussed in Chapter 9.4. The distributions are shown for the observed results and where applicable, they are also shown for the results corrected for observational selection ($\eta = 0,4$) and observational and astronomical ($\eta = 0,4$) selection. These corrections for selection have been discussed in detail in Chapter 8. The word 'observed' signifies 'uncorrected' rather than distinguishing between measured and calculated data (viz. retardation, Figure 12).

To facilitate comparison the distributions are presented in a similar manner to those given by Davies and Gill (1960). As they point out, however, the distributions vary with the magnitude of the meteors used in the survey, and the results for the Adelaide survey are based on more massive meteors than those

detected by Davies and Gill. Only meteors which were large enough to provide a trail of line density greater than 3.10^{11} electrons/cm could be included in this survey. Davies and Gill estimate that the range of meteors included in their survey produced trails of line density between 5.10^{10} and 2.10^{11} electrons/cm.

Showers have not been excluded from the distributions. It has been noted by several observers that showers become less significant as the mass range includes fainter meteors. Davies and Gill concluded that significant groupings contributed less than 2% to the total number of echoes used in their survey. However, it is quite evident from the discussion on showers in Chapter 11 that significant groups of echoes contribute a much greater proportion of the 2004 echoes used in these distributions. Thus the results given here are for a total survey and cannot be assumed to hold for the 'sporadic' content only. The question of division between sporadic meteors and shower meteors is discussed in Chapter 11.

The number of meteors is given as the ordinate in Figures 6-25. The curves have been normalised to within 5% to 2000 meteors. The scale is not given for the corrected distributions, but in all cases it is linear from zero. The distributions corrected for selection are given for two values of η, $\eta = 0$ and $\eta = 4$ (see Chapter 8.1).

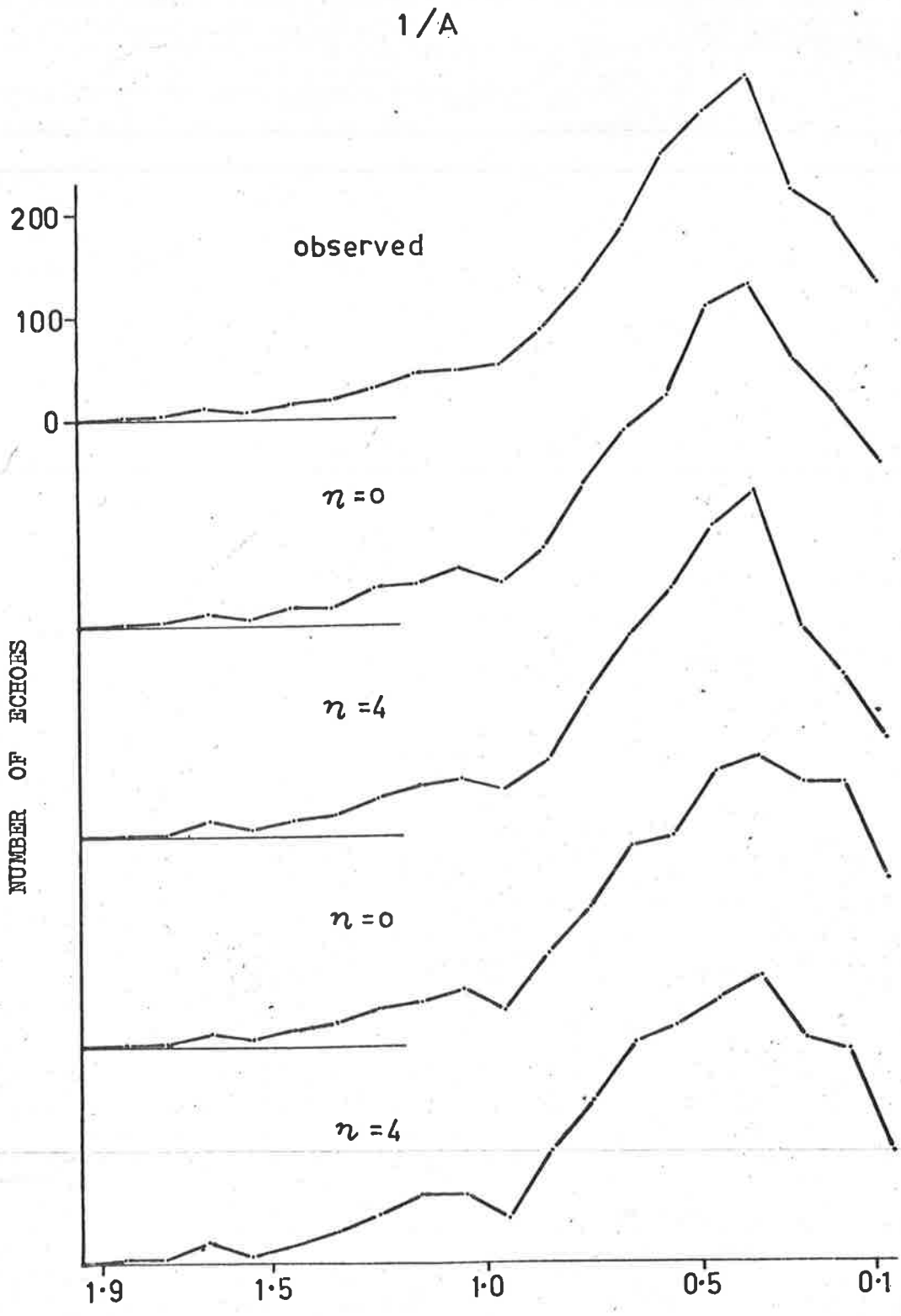
1/A
200
100
0
observed
(a)
n =0
(b)
n =4
(c)
n =0
(d)
n =4
(e)
NUMBER OF ECHOES
1·9
1·5
1·0
0·5
0·1
RECIP.SEMI-MAJOR AXIS

Figure 10.6

Figures 6-10 inclusive show five distributions in the following manner:

(a) - observed results;

(b) and (c) - results corrected for observational selection;

(d) and (e) - results corrected for observational and astronomical selection.

The distribution with 1/a, the reciprocal of the semi-major axis, is shown for the observed results in Figure 6a. The peak occurs at 0.4 (period 4 years) and is little effected by the corrections for observational and astronomical selection. There are significantly less meteors in the range $1.0 < 1/a < 1.5$ than in the distributions of Davies and Gill (1960). This is consistent with a mass range between that of the photographic meteors observed by Whipple (1954) and the much fainter meteors observed by Davies and Gill.

Figure 7 shows the distribution with eccentricity, e, Figure 8 the distribution with inclination, i, for all the meteors detected in the survey. Both show the same general features as those of Davies and Gill, however the increase between 50° and 70° in the distribution with inclination is less pronounced in the Adelaide results.

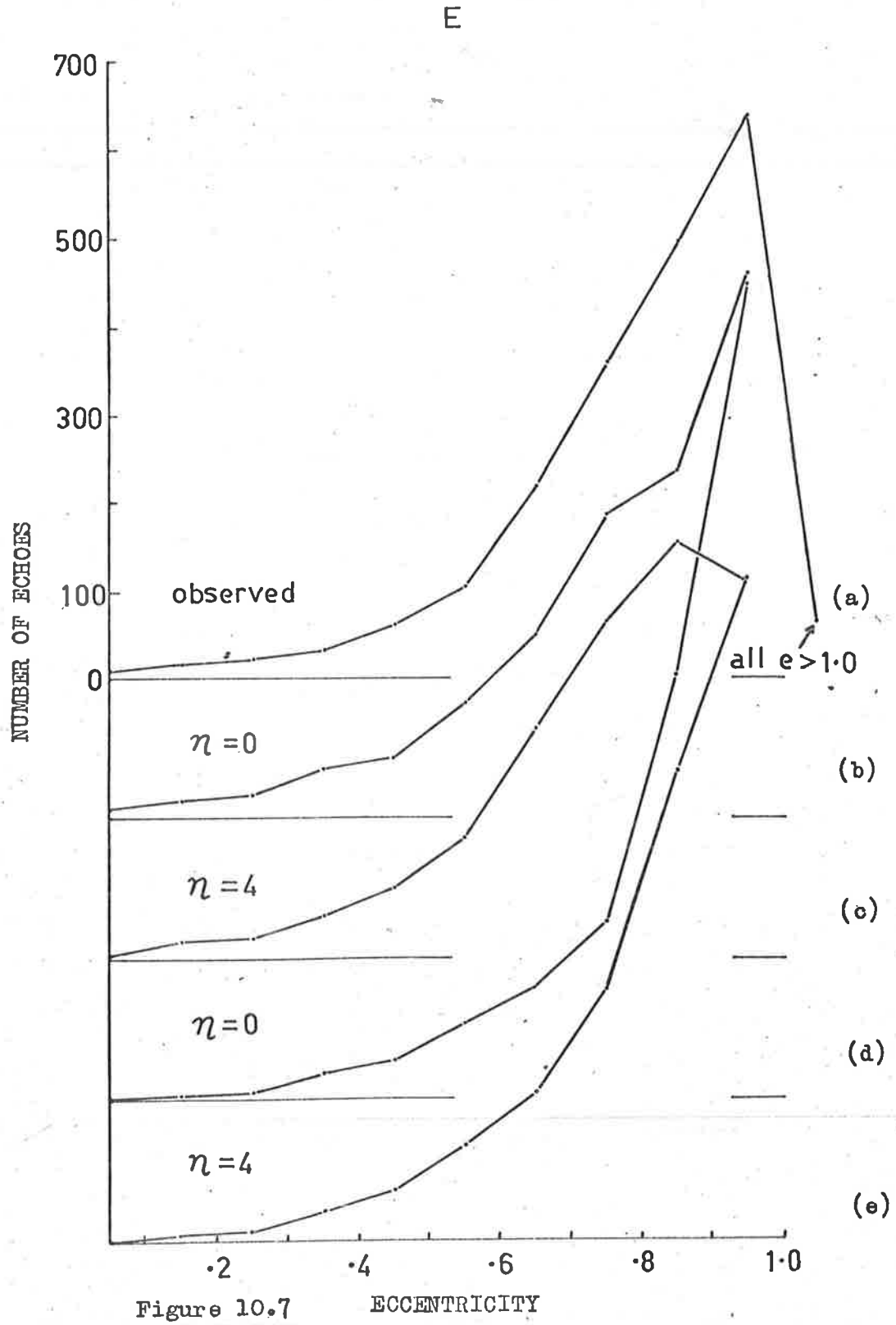
E
700
500
300
100
0
NUMBER OF ECHOES
observed
(a)
all e>1·0
η=0
(b)
η=4
(c)
η=0
(d)
η=4
(e)
·2
·4
·6
·8
1·0
ECCENTRICITY

Figure 10.7

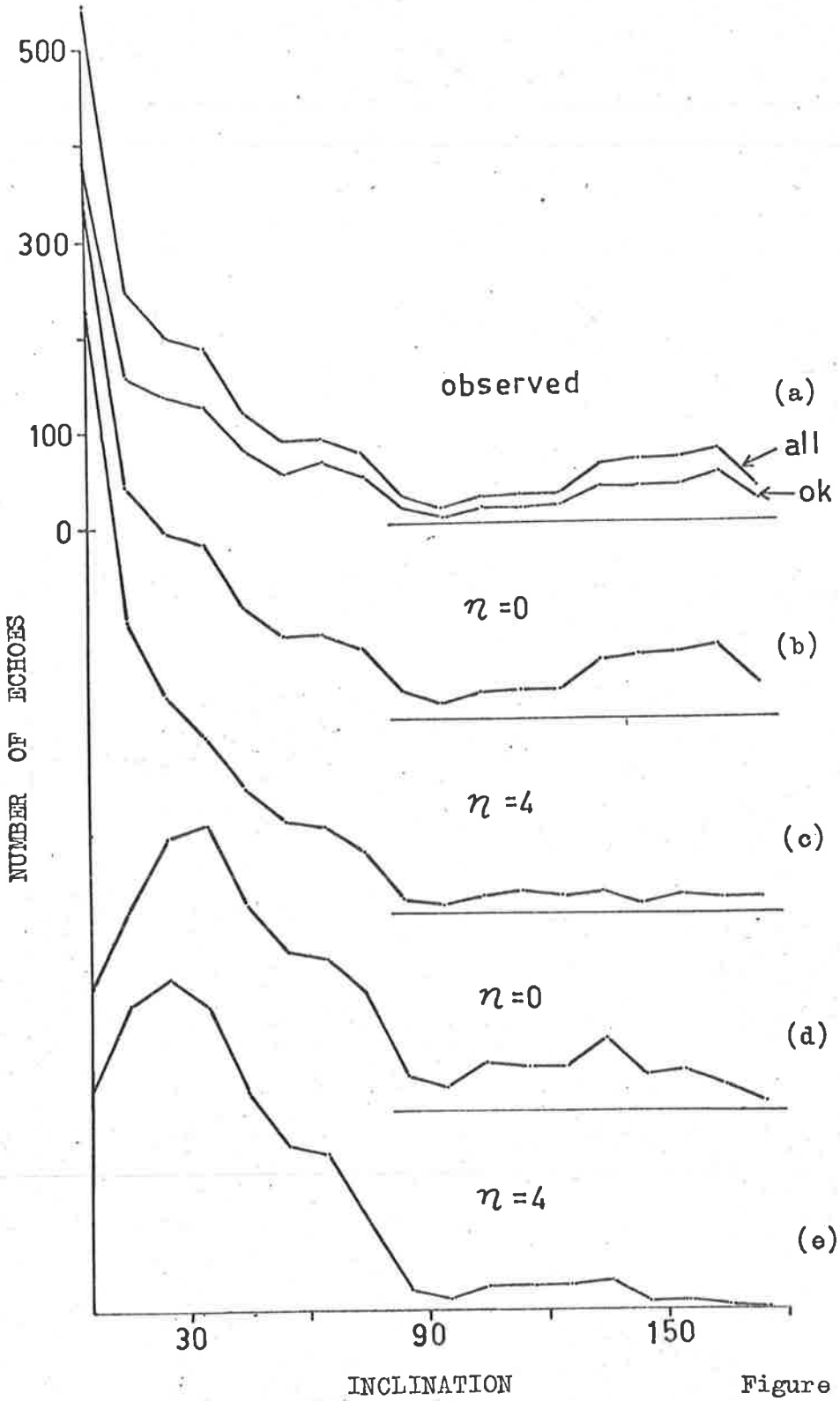
500
300
100
0
NUMBER OF ECHOES
observed
(a)
all
ok
η =0
(b)
η =4
(c)
η =0
(d)
η =4
(e)
30
90
150
INCLINATION

Figure 10.8

Figure 9 shows the distribution with inclination, classified according to semi-major axis and eccentricity in a similar manner to that of Davies and Gill. The corrections for selection are shown for two values of η. The inclination is given in degrees as the abscissae, the number of meteors is shown by the ordinate of each curve in the following manner:

curve 1, $e < 1.0$

curve 2, $e < 0.75$

curve 3, $e < 0.5$

The same general features are exhibited by both surveys, however, as has previously been noted, the peak in the Adelaide survey occurs for $2 < a < 4$ compared to the range $a < 1.3$ for the Jodrell Bank survey. There is also a much greater proportion of long period ($a > 4$) orbits in the Adelaide data.

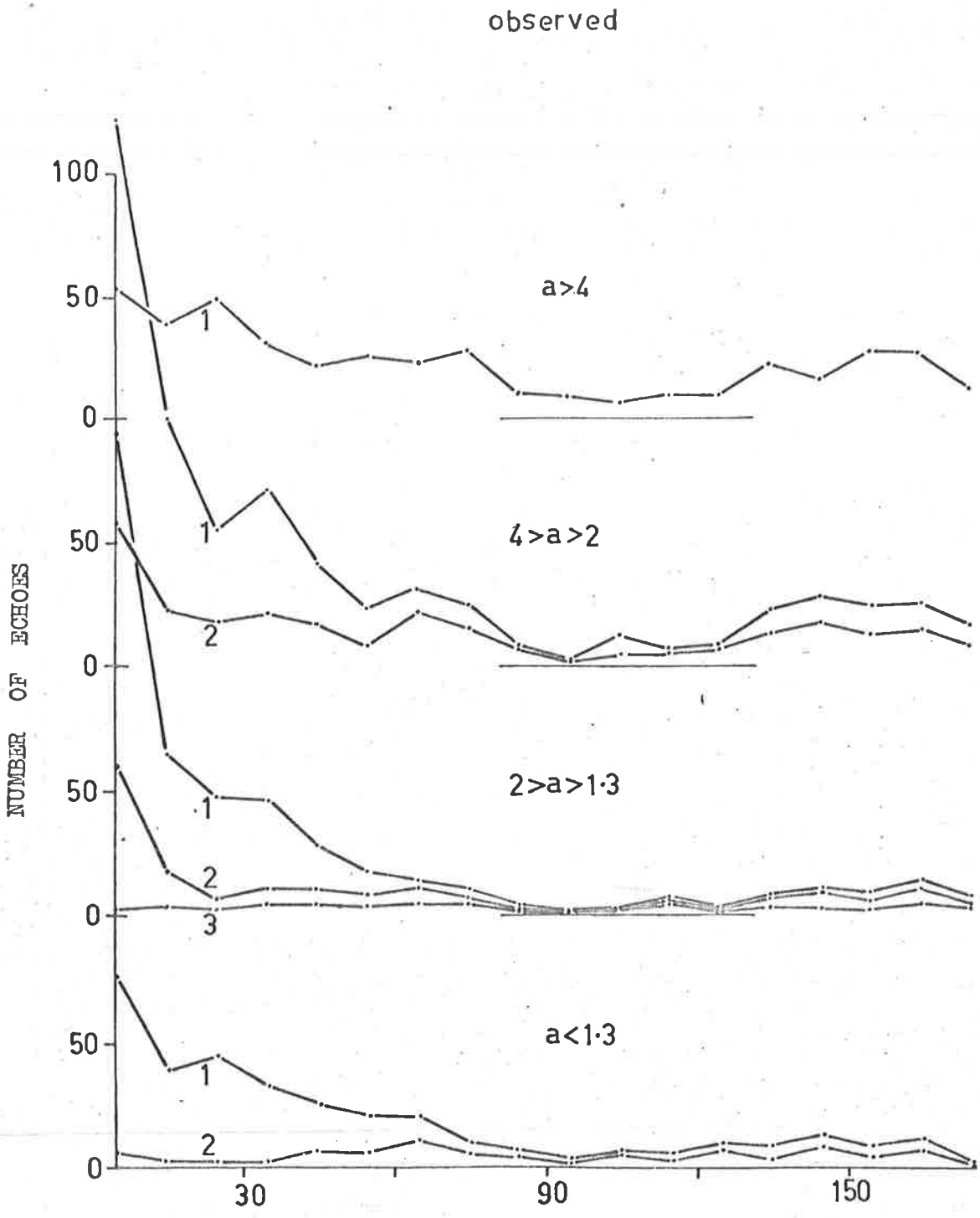
observed
100
50
0
a>4
1
1
50
4>a>2
2
0
50
2>a>1·3
1
2
3
0
50
a<1·3
1
2
0
30
90
150
NUMBER OF ECHOES
INCLINATION

Figure 10.9a

DISTRIB. CORR. FOR OBS. SEL.

$\eta = o$

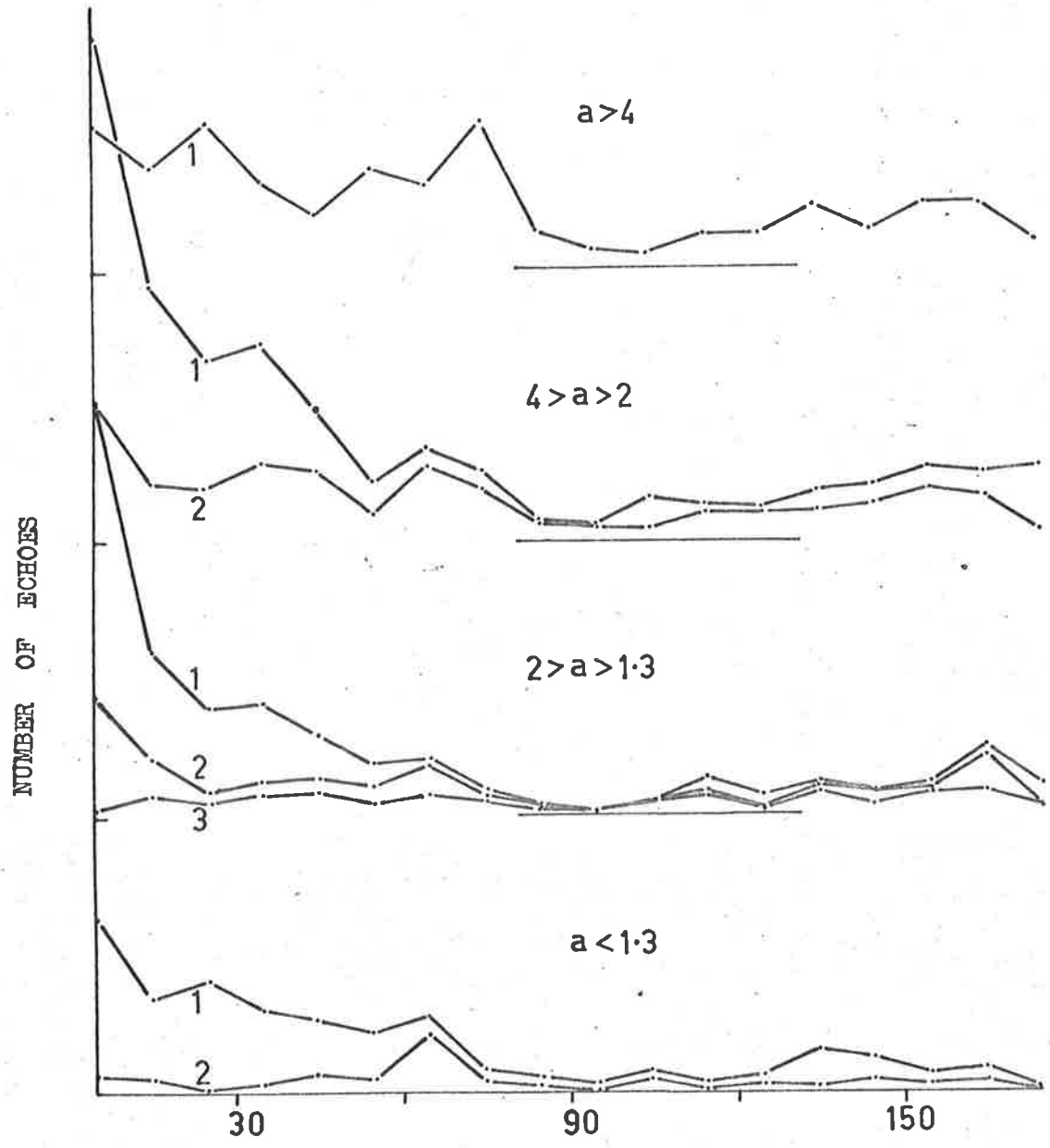

Figure 10.9b

DISTRIB. CORR. FOR OBS. SEL.
$\eta = 4$

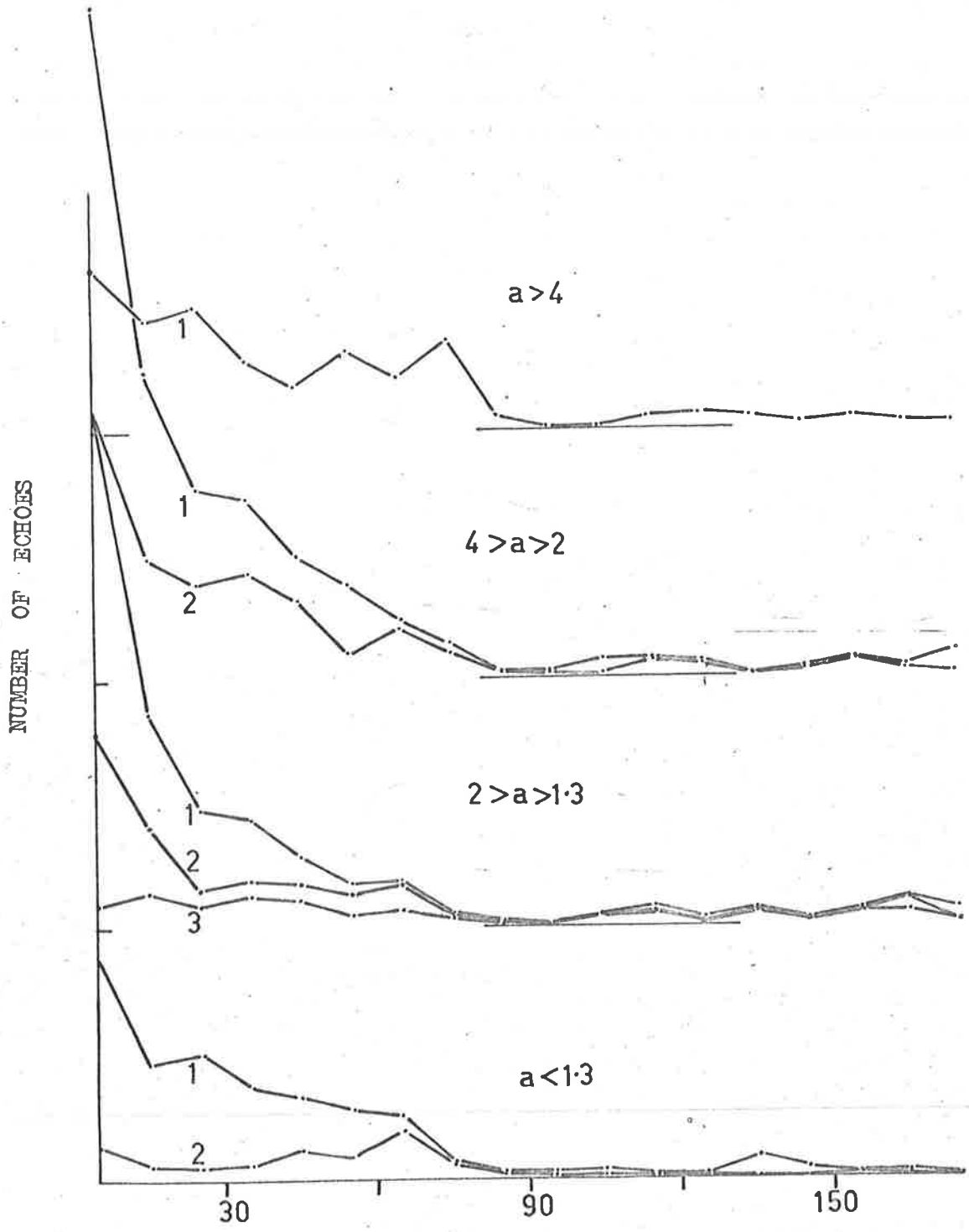

Figure 10.9c

$\eta = 0$

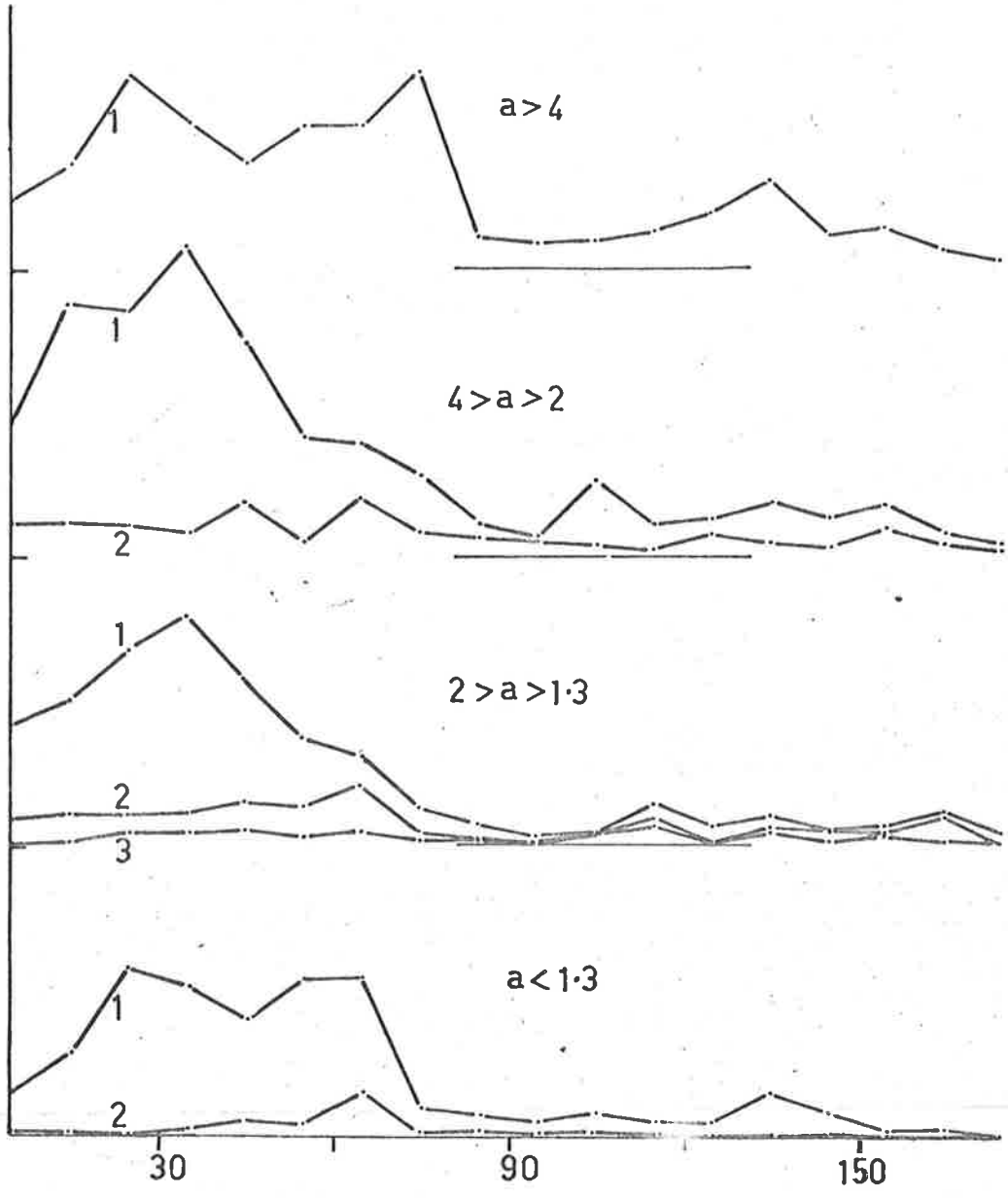

Figure 10.9d

$n = 4$

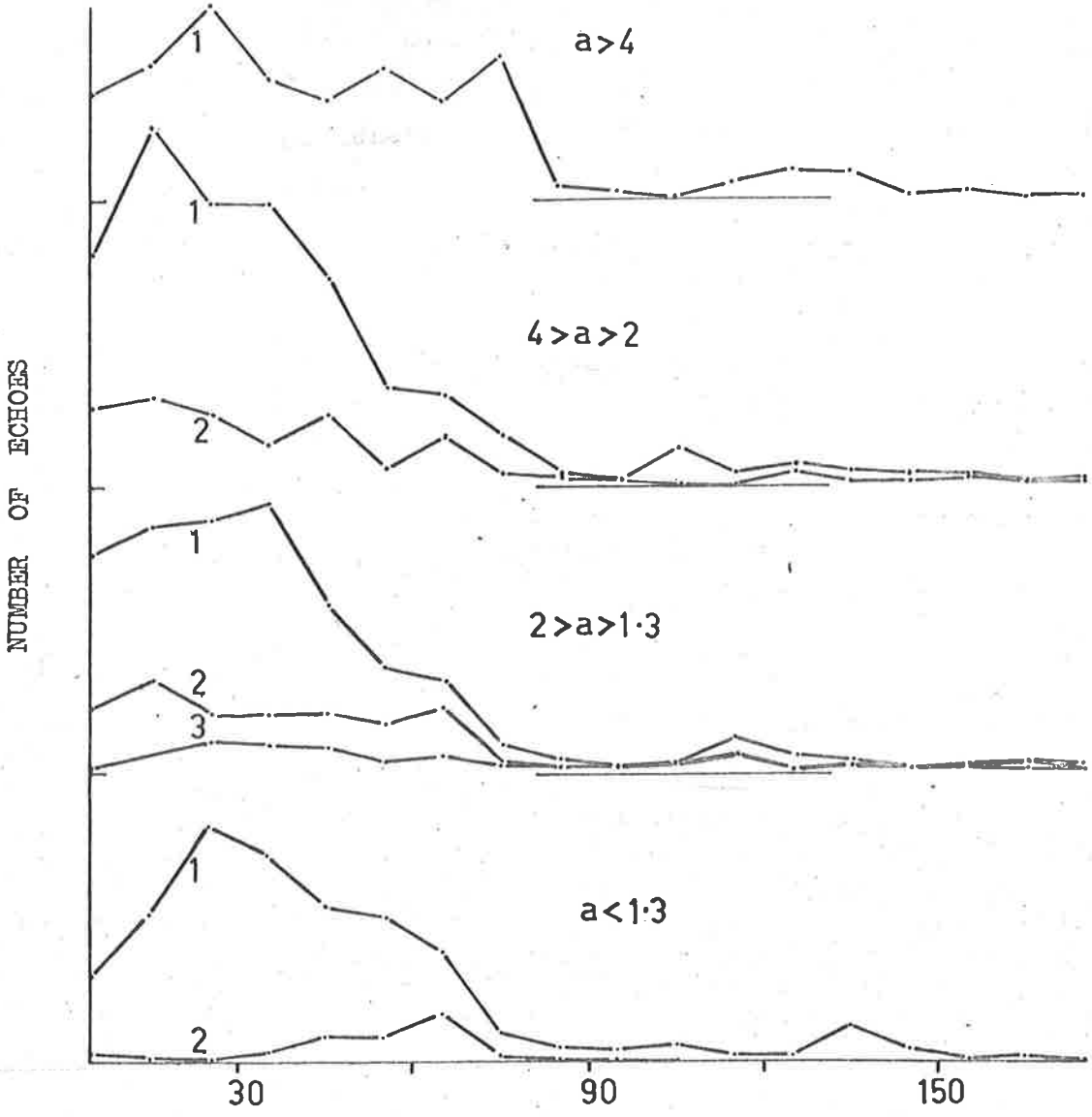

Figure 10.9e

Figure 10 shows the distributions with heliocentric velocity. In Figure 11a, the observed distribution with geocentric velocity is given for all the echoes and for the OK echoes only. There is no significant difference between the two distributions. The distribution for all echoes is shown corrected for observational selection in Figures 11b and 11c.

A comparison of Figure 11a with the distribution given by Mainstone (1960) shows the same general peak at 30 km/sec, but Mainstone's results do not show the smaller peak between 50 and 70 km/sec. However, in view of the fact that the latter's distribution is based on only 65 echoes* the comparison cannot be made in any detail. A comparison with the results of McKinley (1951) is more useful. The subsidiary peak (50–70 km/sec) is even more pronounced in his distributions than in those given here. The results of Davies and Gill agree quite closely with Figure 15 in this respect, although their main peak (30 km/sec) is a little sharper.

Figure 12 shows the observed distribution for the calculated correction for retardation in the earth's atmosphere. This correction has been applied to each echo to obtain the value of true geocentric velocity, the distribution of which is shown in Figure 11.

The observed distribution with ecliptic longitude is given for four groups of ecliptic latitude, β, in Figure 13a. The latter is subdivided in the following way:

curve 1, $+10^{\circ} < \beta < +90^{\circ}$;
curve 2, $-10^{\circ} < \beta < +10^{\circ}$;
curve 3, $-30^{\circ} < \beta < -10^{\circ}$;
curve 4, $-90^{\circ} < \beta < -30^{\circ}$;

The longitude, λ_a, is given with respect to that of the apex. Figures 13b and 13c show the same distribution corrected for observational selection.

---

* The velocity for each echo in Mainstone's results is incorrect by an average of 16%, the correction for wind drift having been applied in the wrong sense.

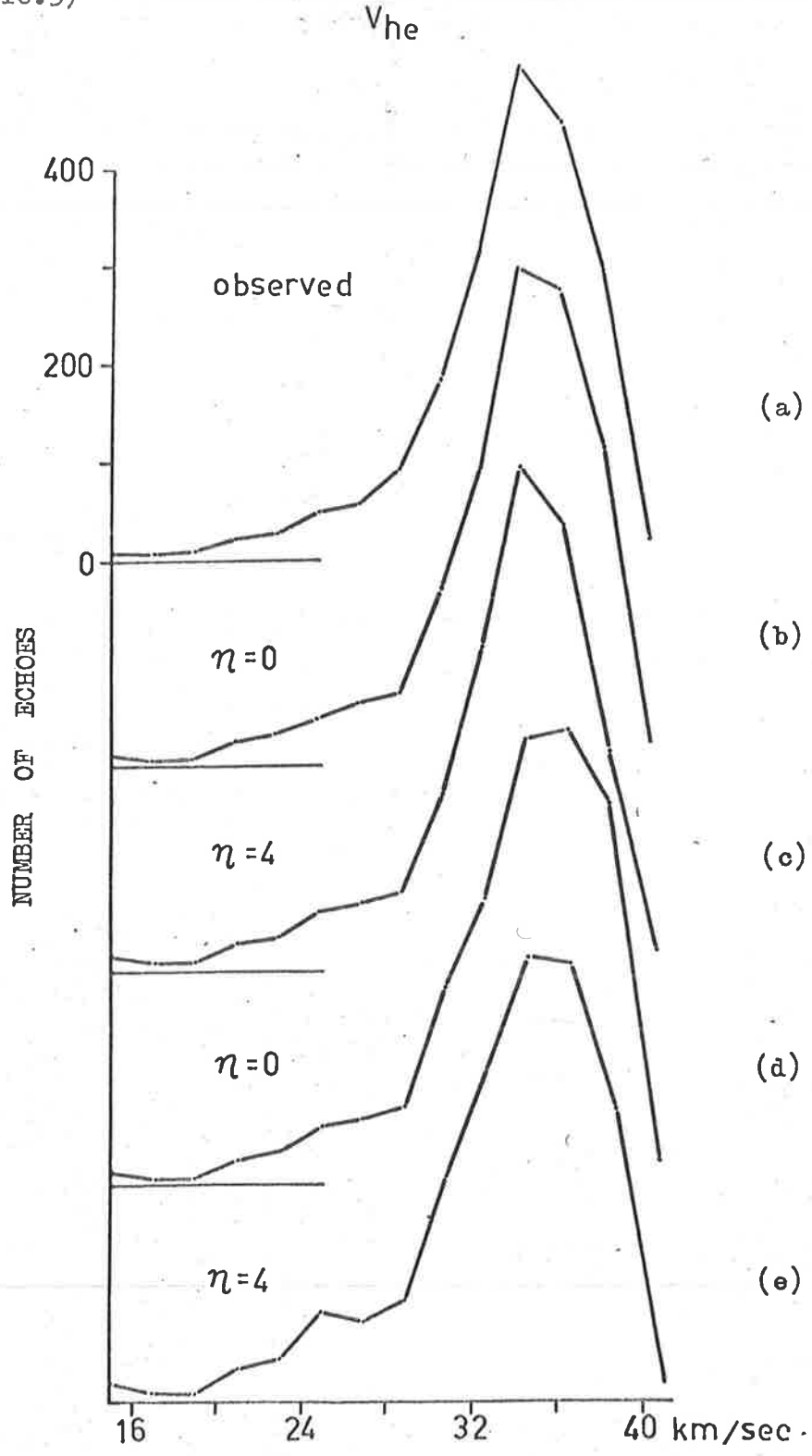
V_{he}
400
200
0
observed
(a)
$\eta = 0$
(b)
$\eta = 4$
(c)
$\eta = 0$
(d)
$\eta = 4$
(e)
NUMBER OF ECHOES
16
24
32
40 km/sec

Figure 10.10

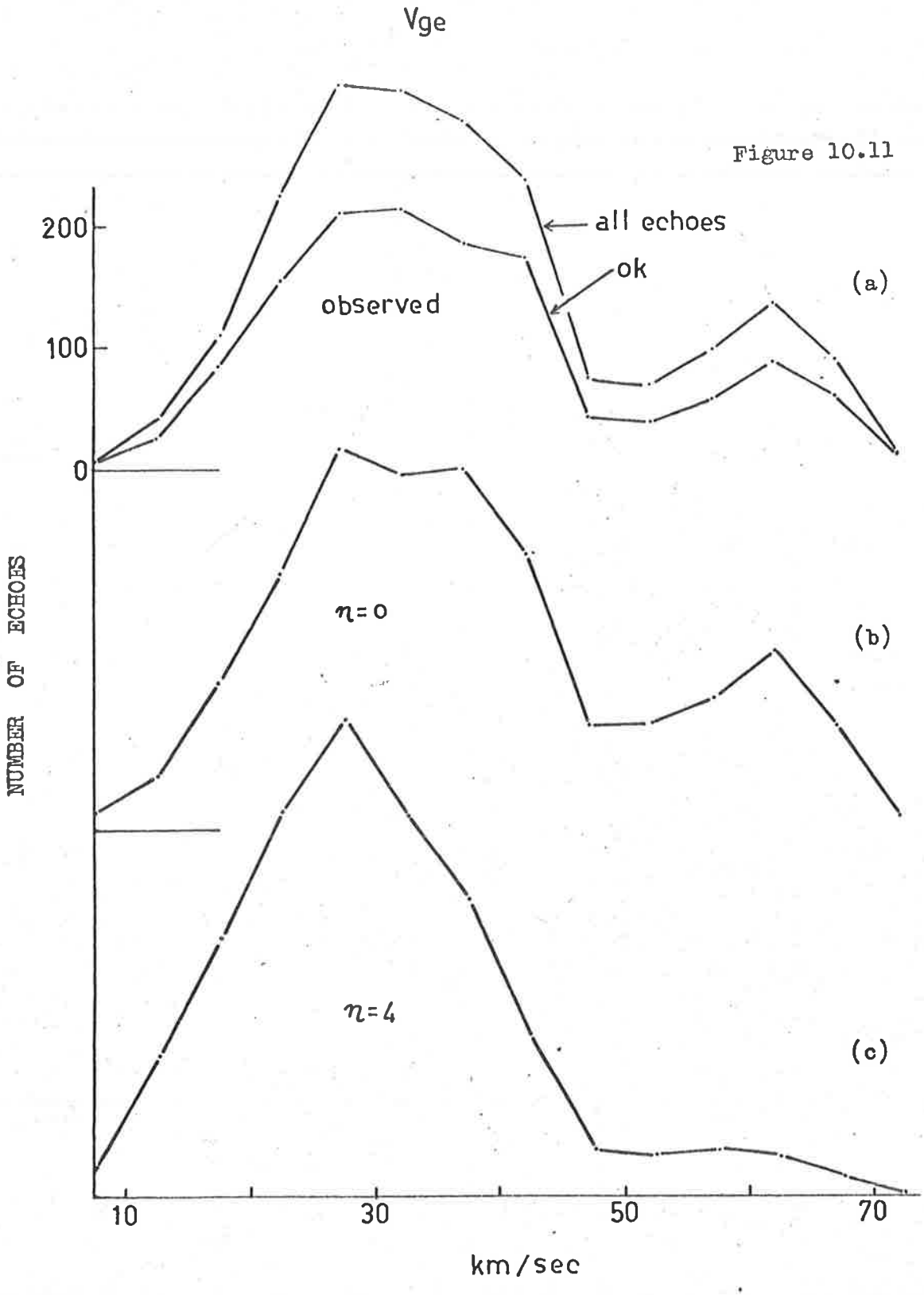
Vge
all echoes
ok
observed
(a)
200
100
0
NUMBER OF ECHOES
η=0
(b)
η=4
(c)
10
30
50
70
km/sec

Figure 10.11

observed retardardation

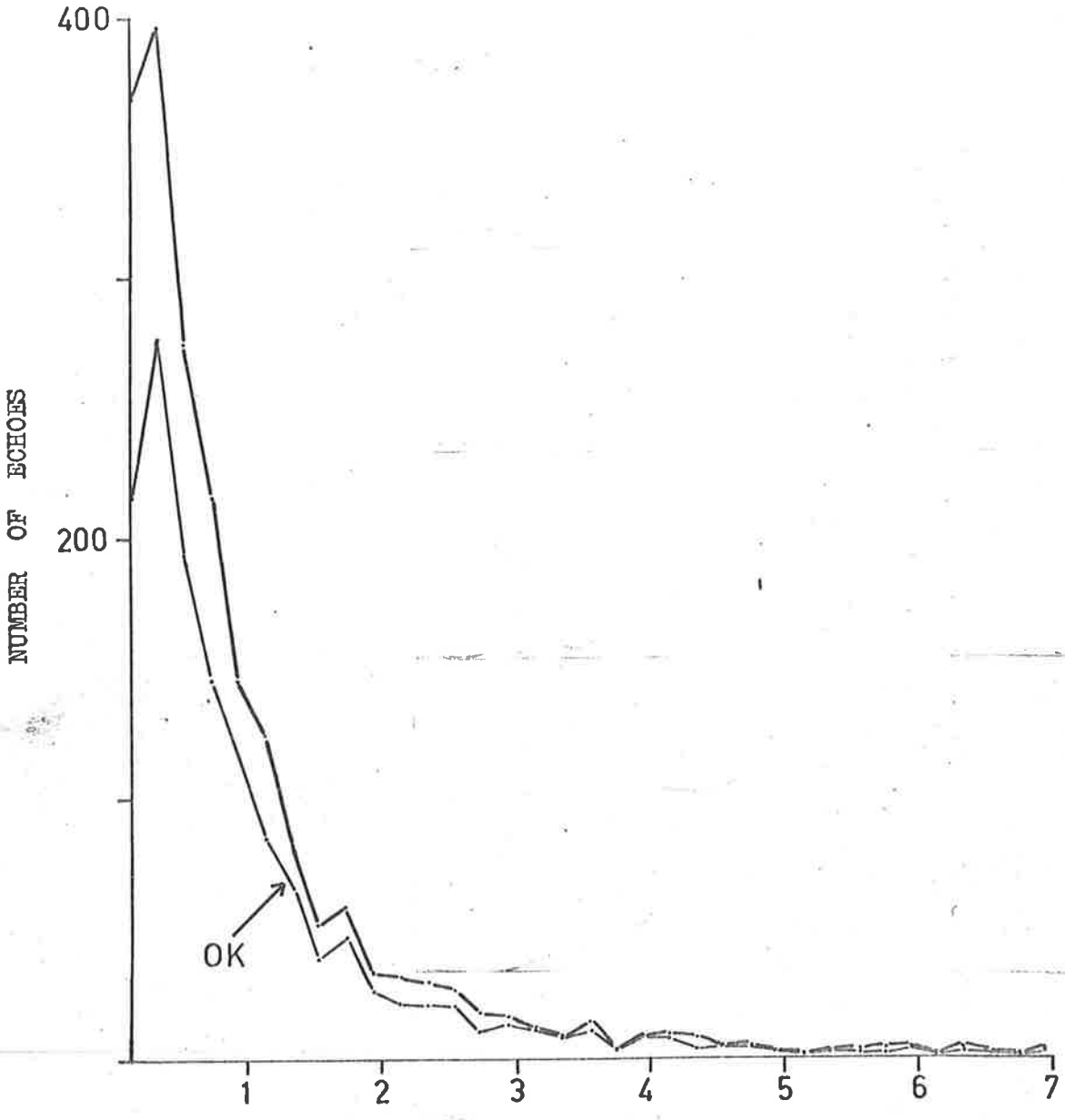

Figure 10.12

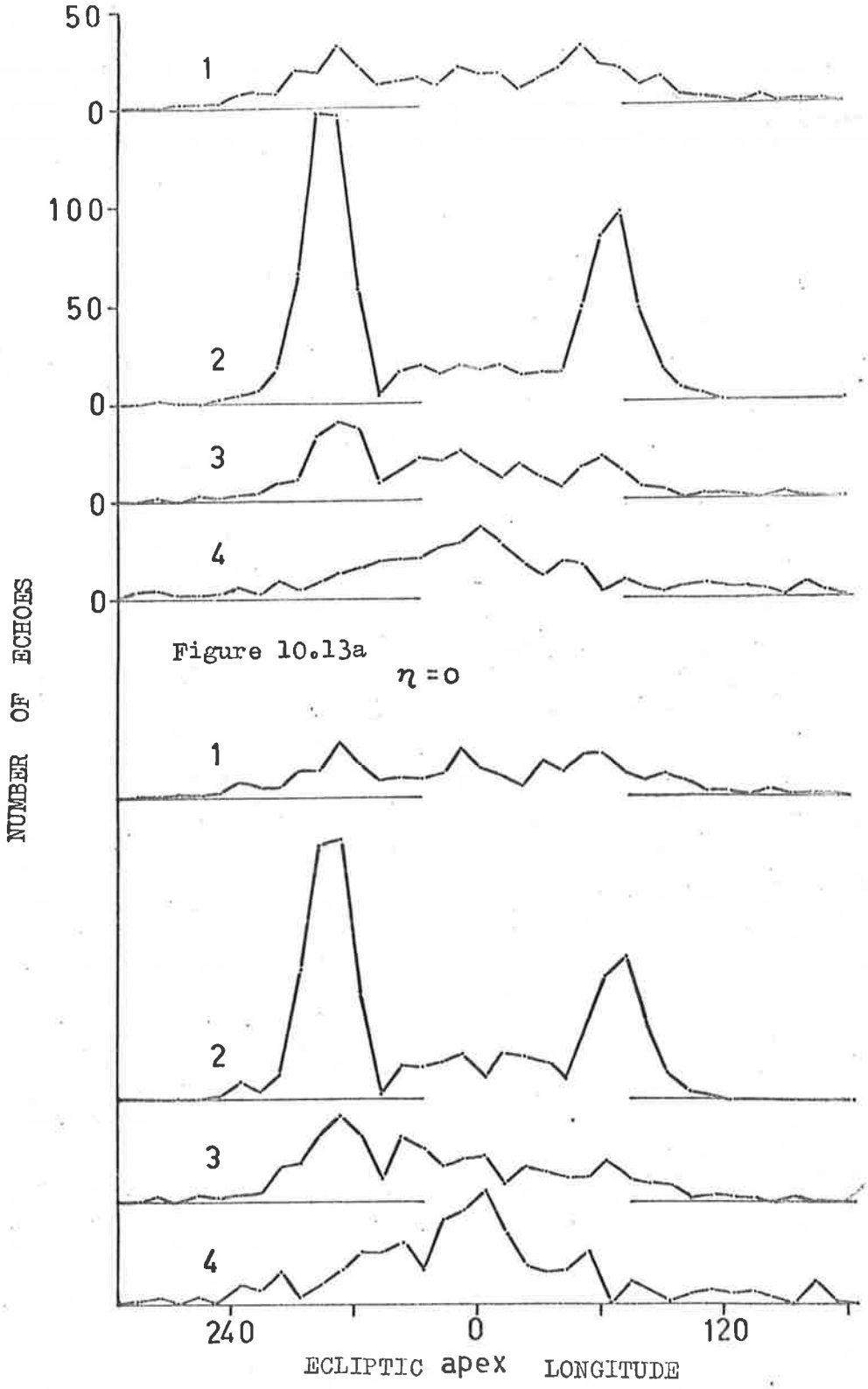

Figure 10.13a

$\eta = 0$

Figure 10.13b

$n = 4$

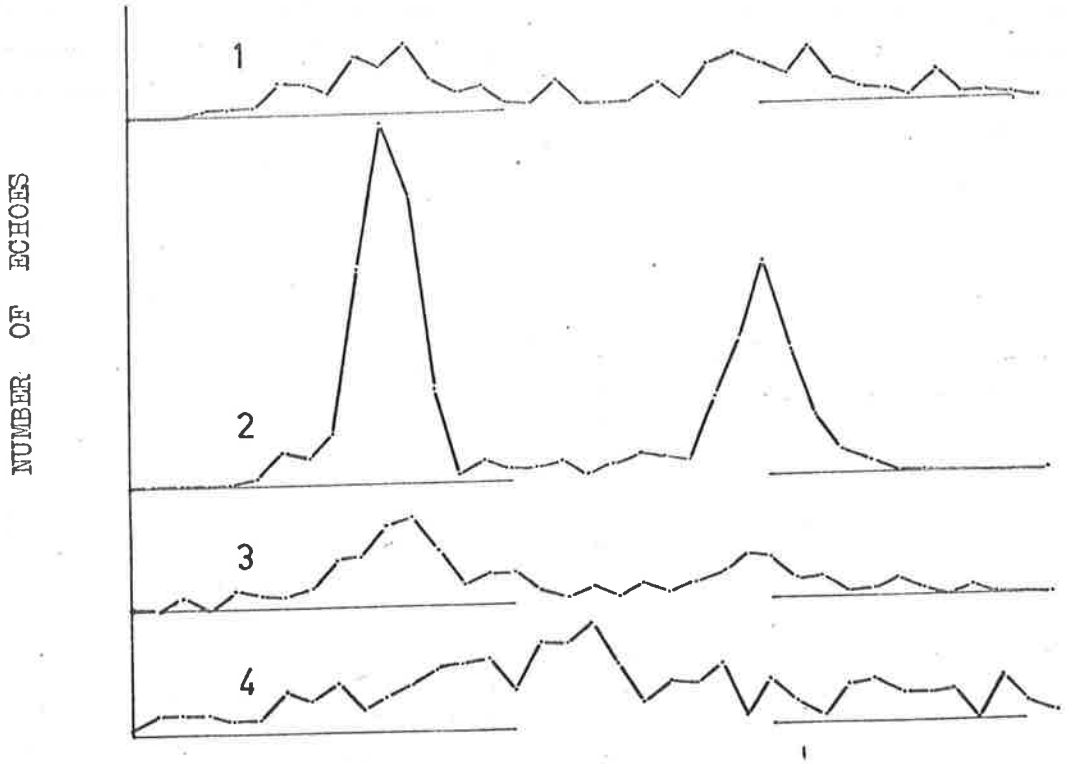

Figure 10.13c

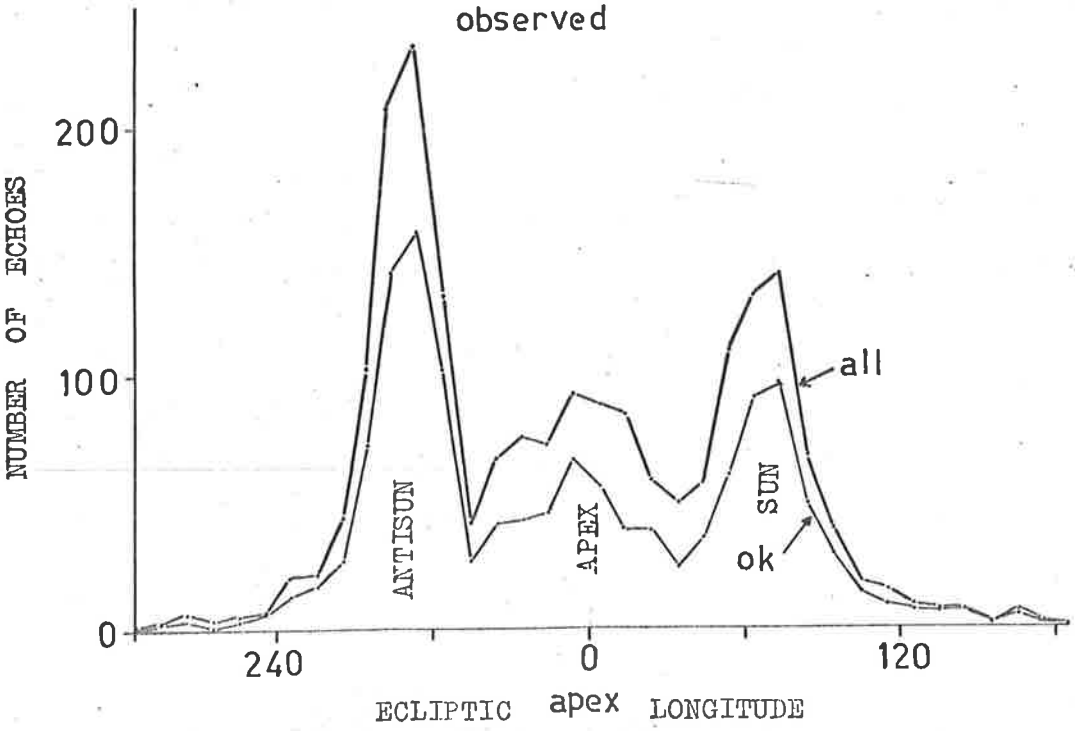

Figure 10.14

It is evident that the sun and anti-sun concentrations at 70° and 290° respectively are much more concentrated near the ecliptic, whereas at high latitudes the broader apex component makes the largest contribution. There is a pronounced asymmetry between the sun and antisun components that is analysed more fully later in this section. A study of the Jodrell Bank results shows a similar asymmetry, but it is not so well marked*.

Figure 14 shows the observed distribution with ecliptic longitude combined for all bands of latitude. Once again, there is no difference between the distribution taken for all the echoes and that taken for the best (OK) echoes only. This figure broadly justified the elementary distributions taken as a model for the Mawson survey (Chapter 2). The asymmetry would explain some of the discrepancies between the theoretical and observed rates.

---

* To aid comparison, the author would like to point out that the appropriate figure (Figure 5) of the paper referred to appears to be incorrectly labelled along the abscissa.

The observed distribution with ecliptic longitude, λ_a, is given for each month in Figure 15a. The distributions are shown corrected for observational selection in Figures 15b and 15c. The most noteworthy feature is the prominence of the anti-sun component from July to October. To further analyse this component, the observed distribution with inclination is shown in Figure 16 for the 459 echoes for those four months for which $265^\circ < \lambda_a < 315^\circ$. The distribution has been classified in a and e in the same manner as Figure 9. It is evident that the same general features are exhibited by the anti-sun group for these four months as by the total for the year taken over all λ_a. There is, however, a complete lack of orbits of inclination greater than 90°.

The list of showers and minor groupings in Chapter 11 shows that many showers contribute to the anti-sun component during these four months. During July and August the δ-Aquarid shower and other radiants in Aquarius contribute to this group. So too do the extremely active radiants in Pisces and Cetus during September and in Aries during October. There are many minor groupings during these months that also contribute. If showers are responsible for this anti-sun peak one would expect it to be less prominent among fainter meteors, and the results of Davies and Gill show that this is in fact the case.

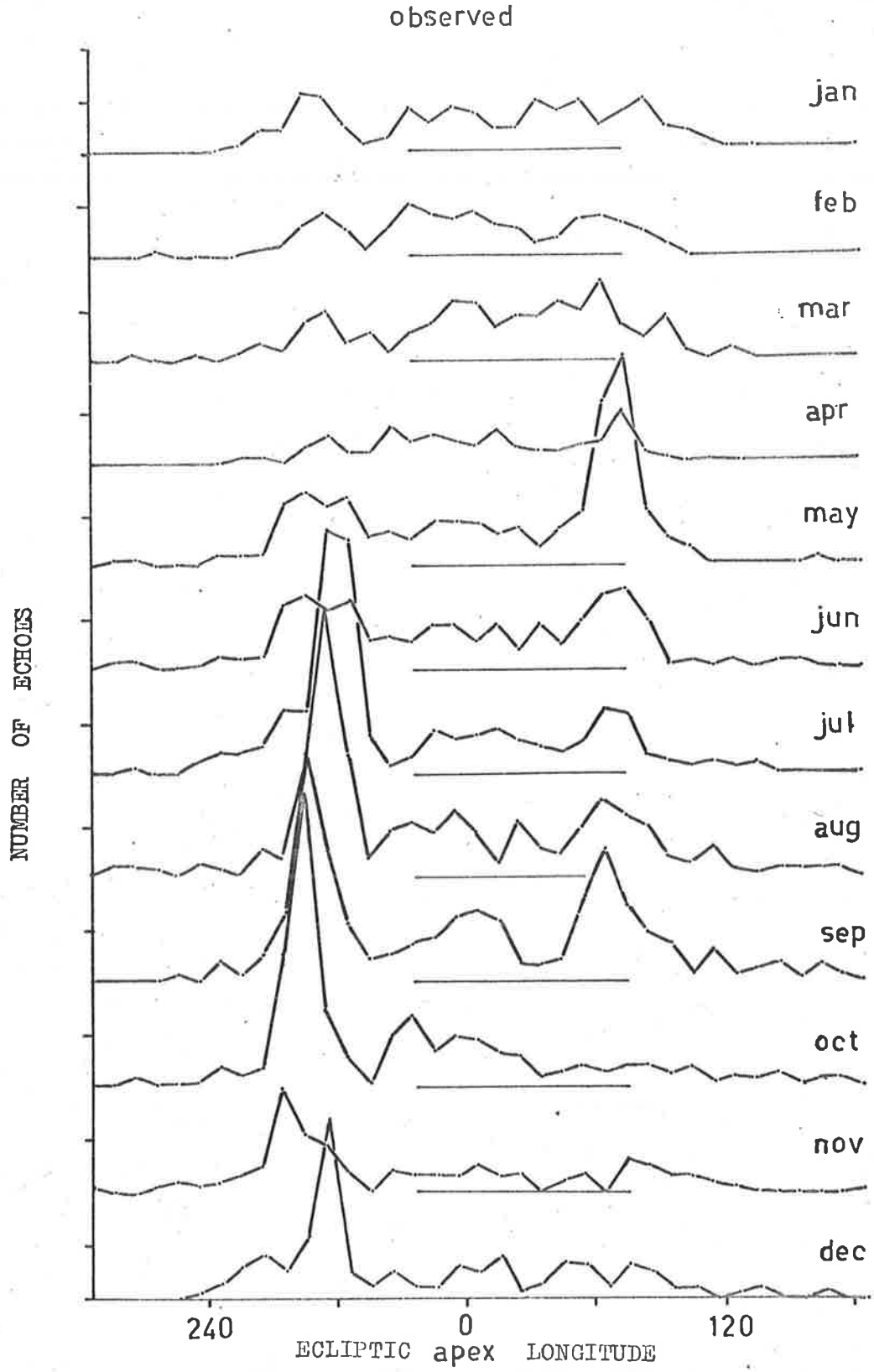

Figure 10.15a

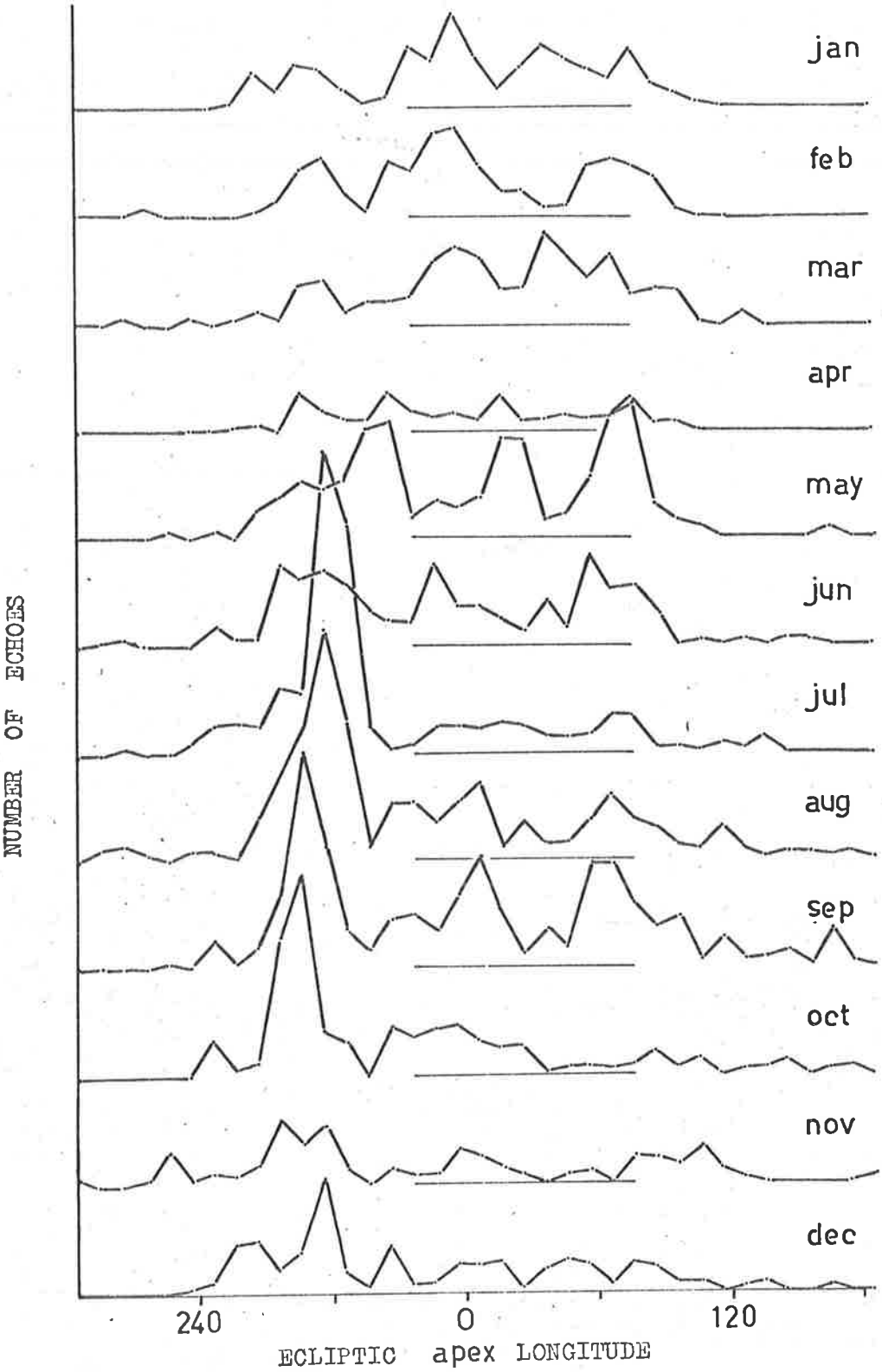

Figure 10.15b

$\eta = 4$

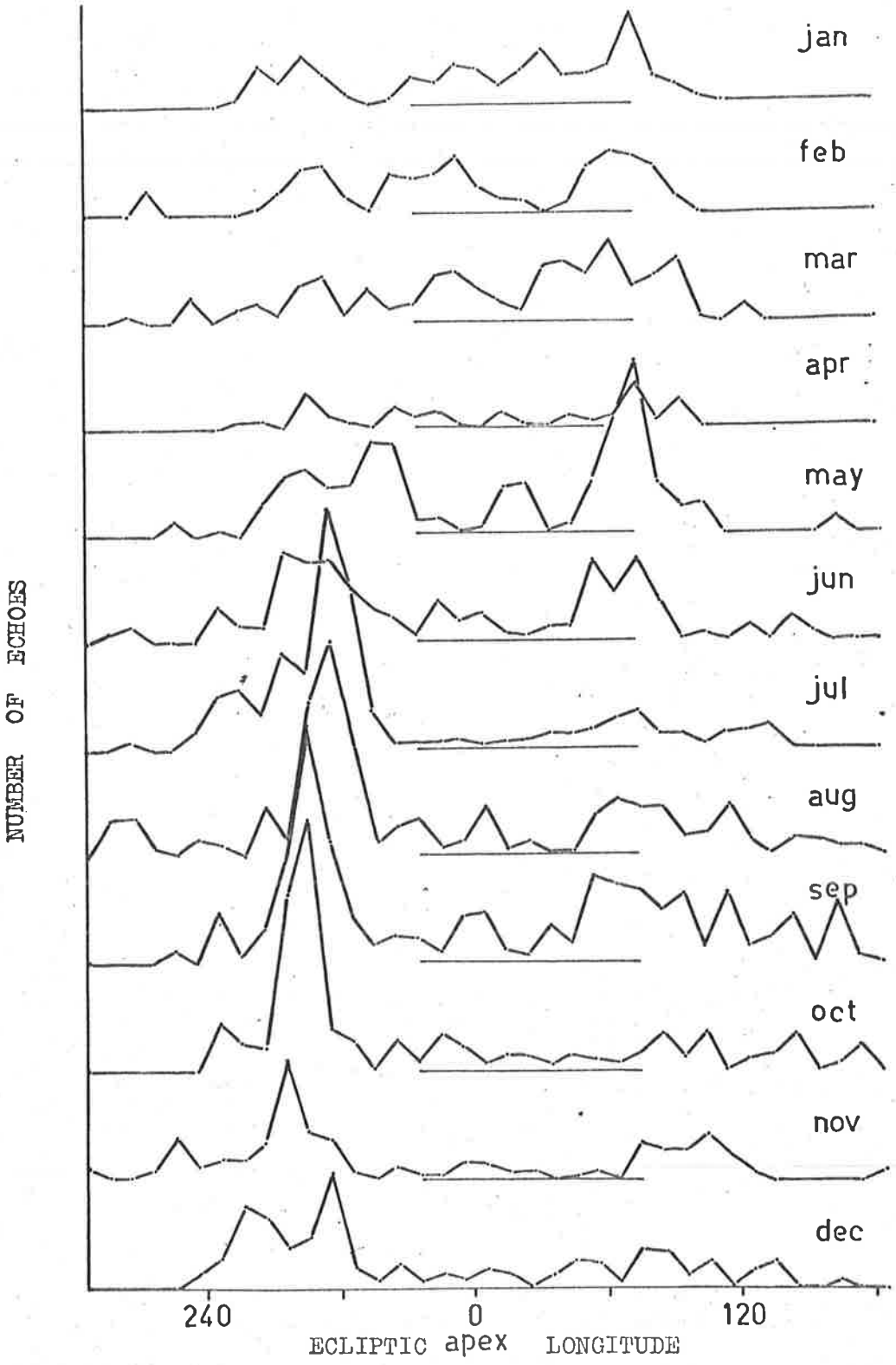

Figure 10.15c

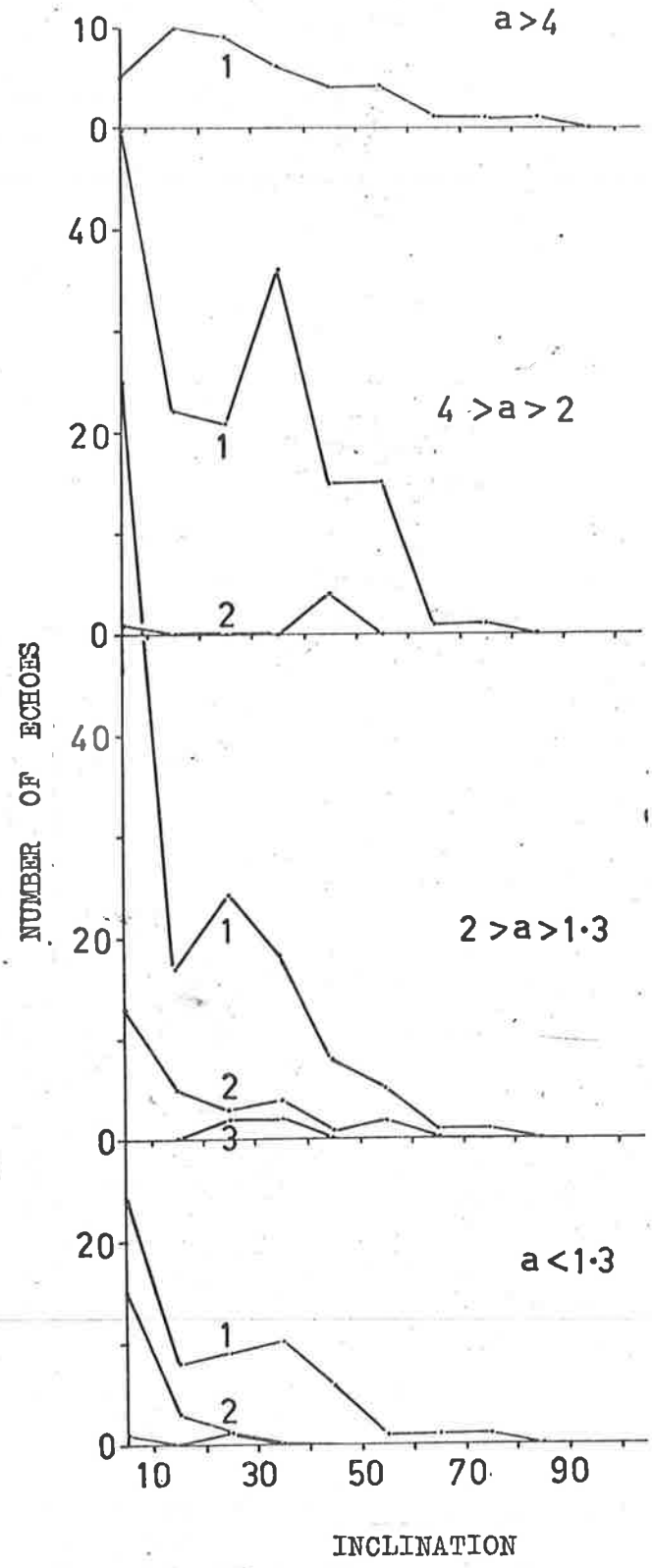

Figure 10.16

Figure 17a shows the observed distribution with ecliptic longitude (λ_a, relative to the apex of the Earth's Way) for each of the seasons. The months have been divided in the following way:

1. Autumn - February, March, April;
2. Winter - May, June, July;
3. Spring - August, September, October;
4. Summer - November, December, January.

The distributions are shown corrected for observational selection in Figures 17b and 17c. The prominent anti-sun peak shows most clearly during the southern Spring. Correction for observational selection also shows the peak up more clearly during the Winter months.

observed

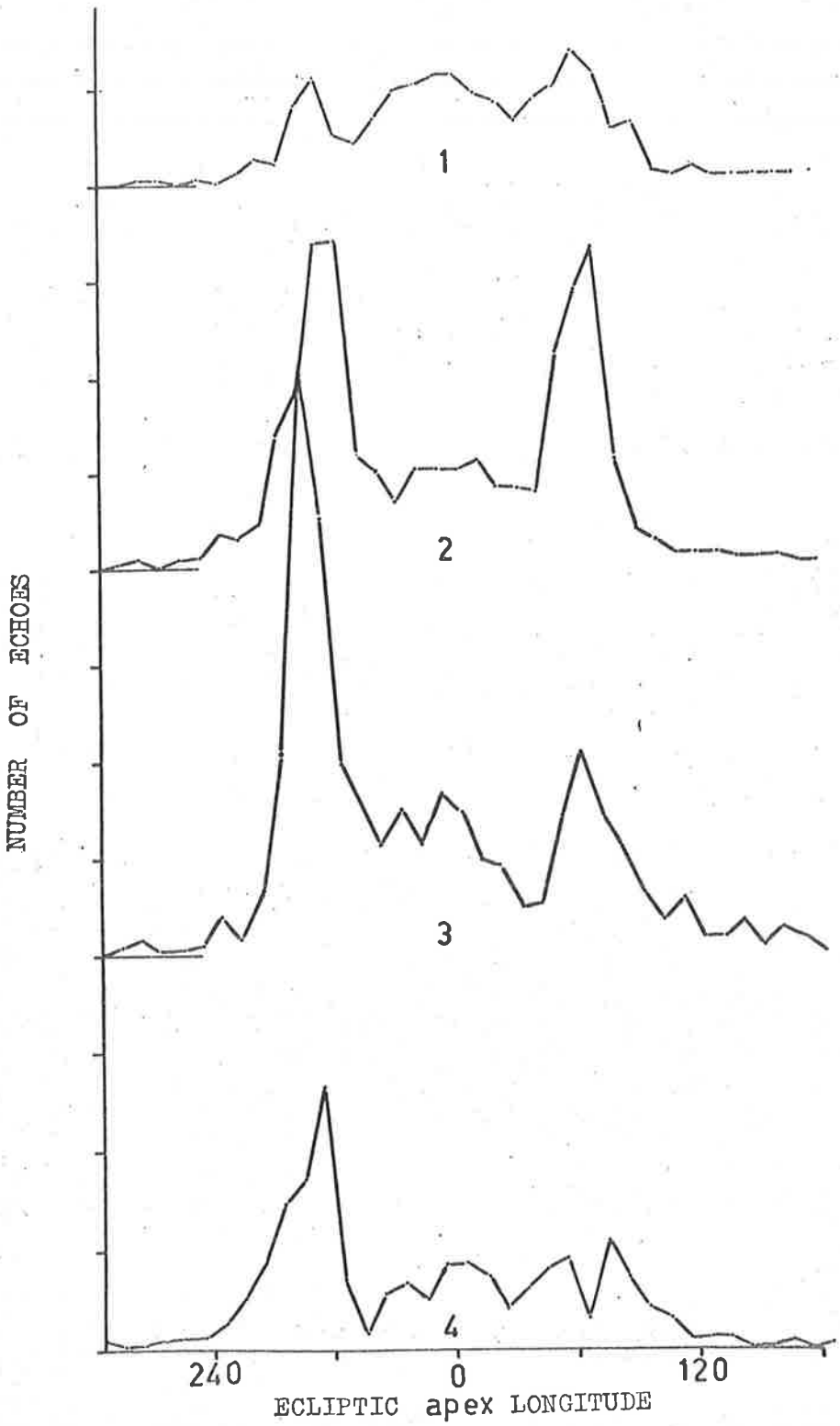

Figure 10.17a

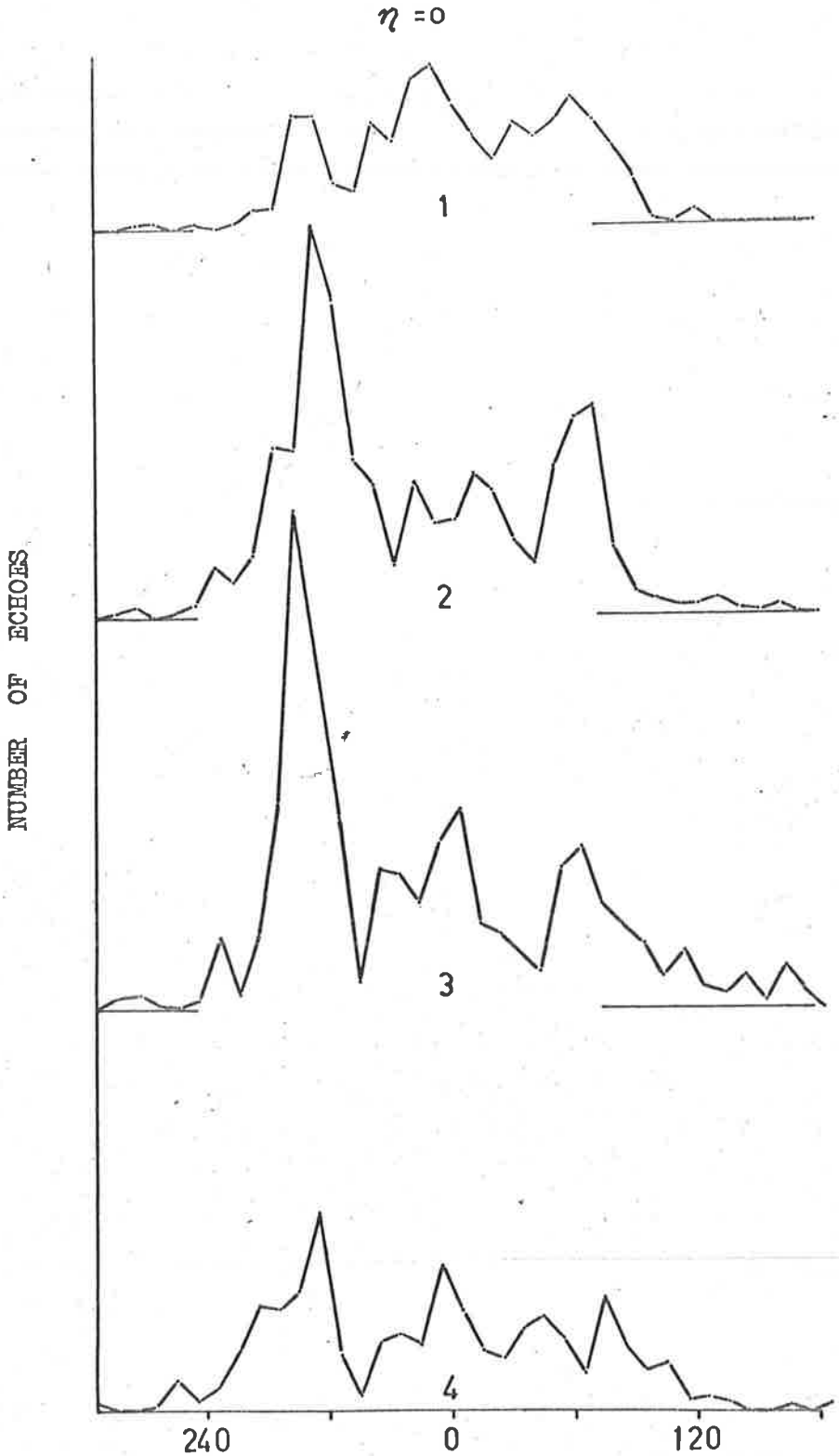

Figure 10.17b

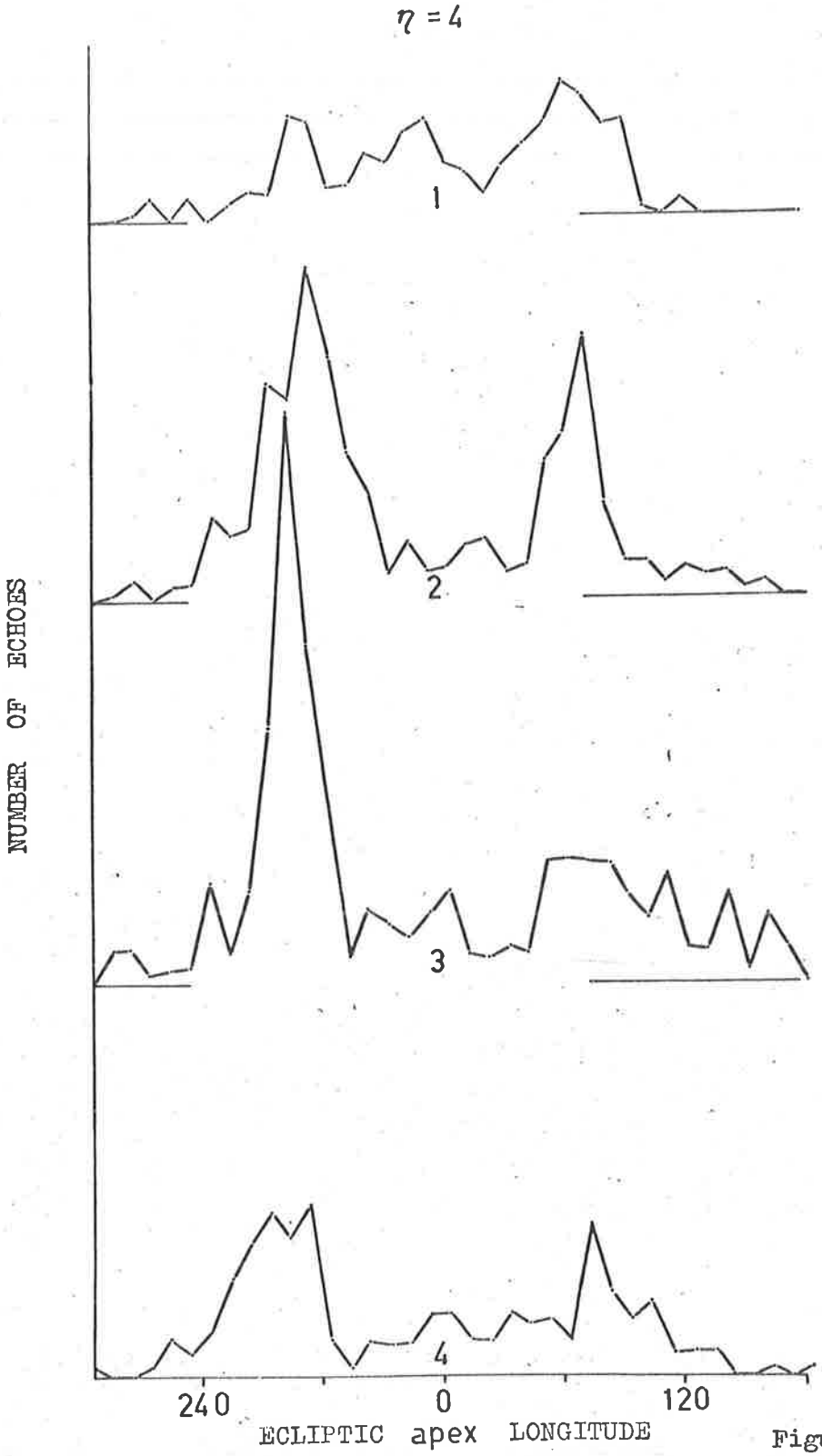

Figure 10.17c

Figure 18a shows the observed distribution with ecliptic latitude, β, for the whole survey. The distributions are corrected for observational selection in Figures 18b and 18c. The similarity of the three distributions and the general symmetry about the ecliptic is not unexpected of a broad beam antenna system at latitude 35°S. The subsiduary peak at $\beta = -10^{\circ}$ appears to consist of fast meteors (it is less prominent in Figure 18c, where $\eta = 4$). This peak is in evidence in the Jodrell Bank results.

Davies and Gill state that north of latitude 30° the weighted number of radiants/unit area is sensibly constant. Figure 18d shows the weighted ($\eta = 0$) number of radiants/unit area for the Adelaide survey, and south of latitude 30° the density rises to a definite peak at -60° to -70°. Whether this is a true difference between the results from the Northern and Southern Hemisphere will have to be confirmed. The accuracy of the curve depends on the accuracy with which the equipment response is known as a function of radiant declination. The fact that Figure 23b shows a steadily increasing function with increasing (negative) declination south of 35°S tends to substantiate the reality of the peak in Figure 18d, as the latter curve has effectively been corrected by this function when weighting for observational selection. The rise in the curve of Figure 23b from -35° to -90° would have to be less than reality to induce a false rise in the distribution of radiant density in that region. Certainly there is nothing in Figure 23b to cause a peak at ecliptic latitude -70°.

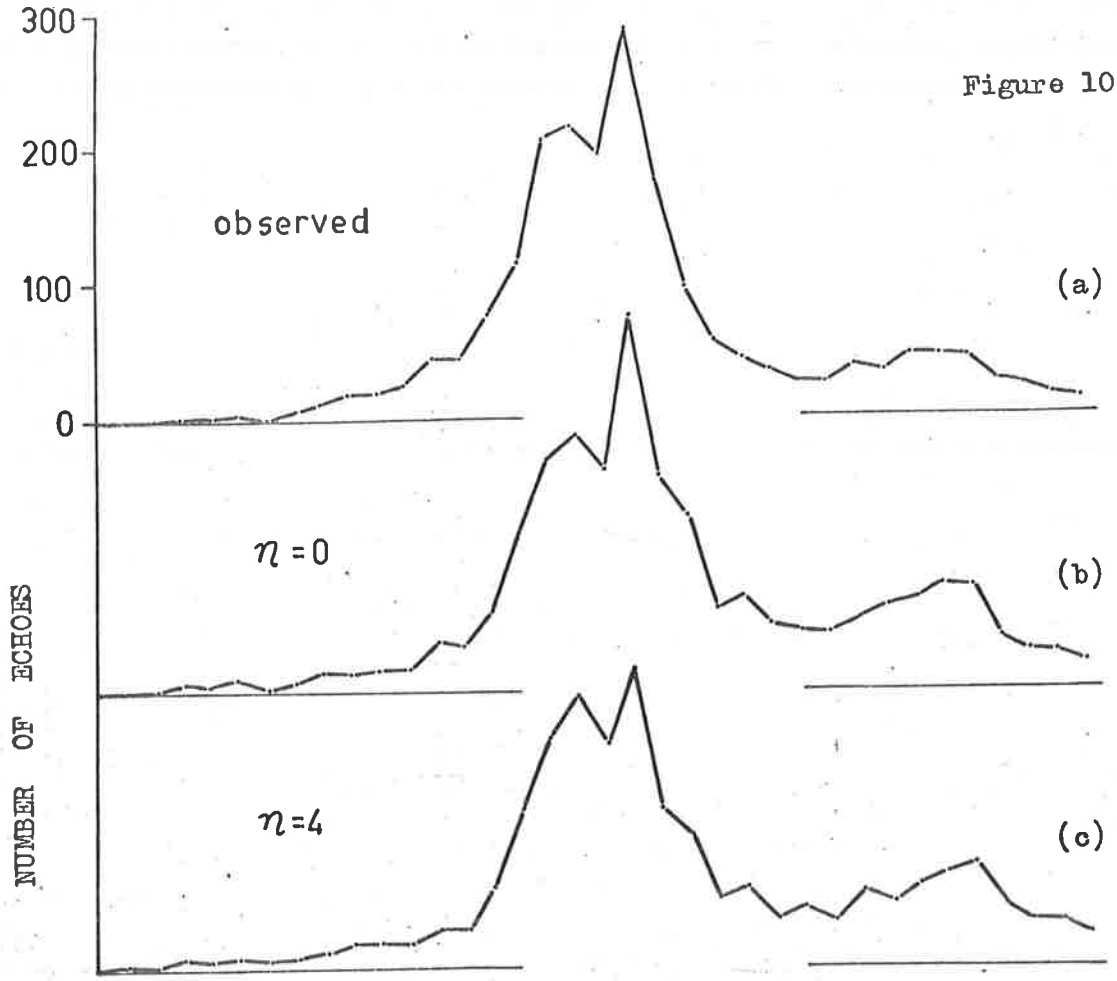

Figure 10.18

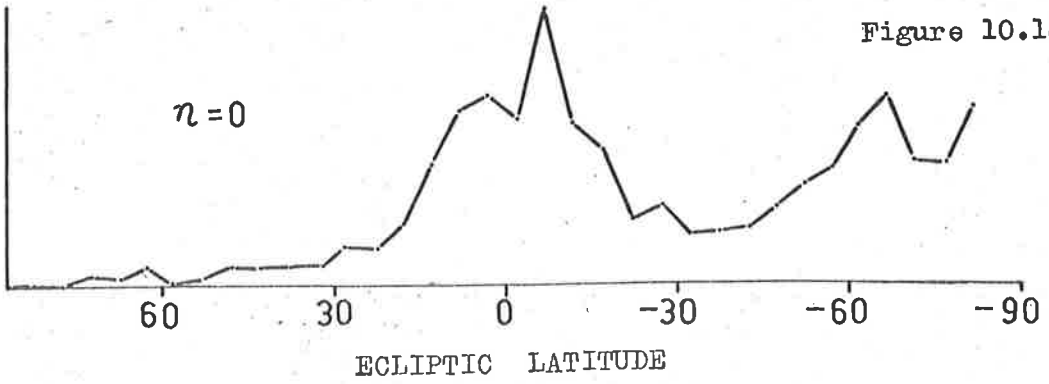

Figure 10.18d

AEL

Figure 10.19

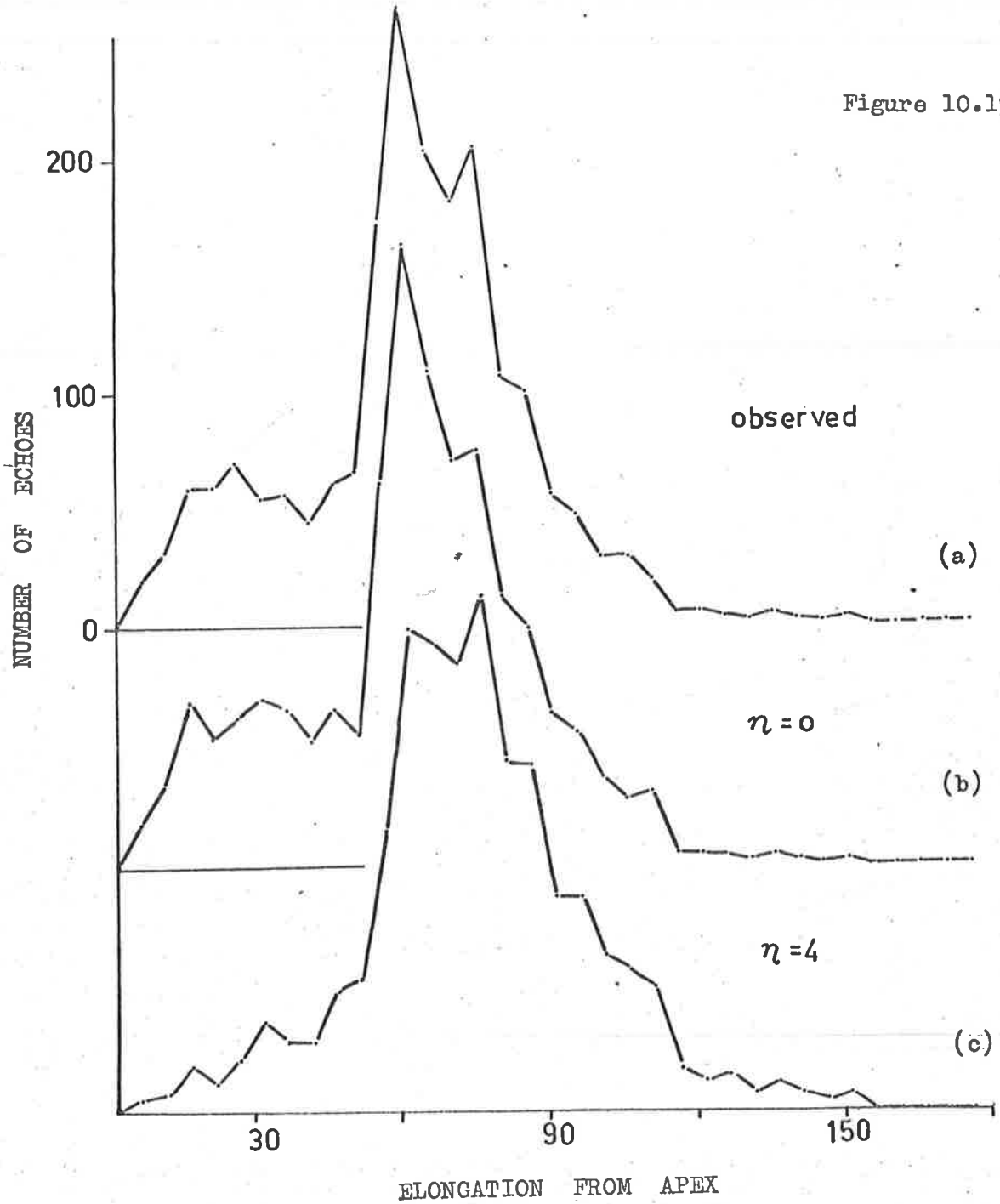

TEL

Figure 10.20

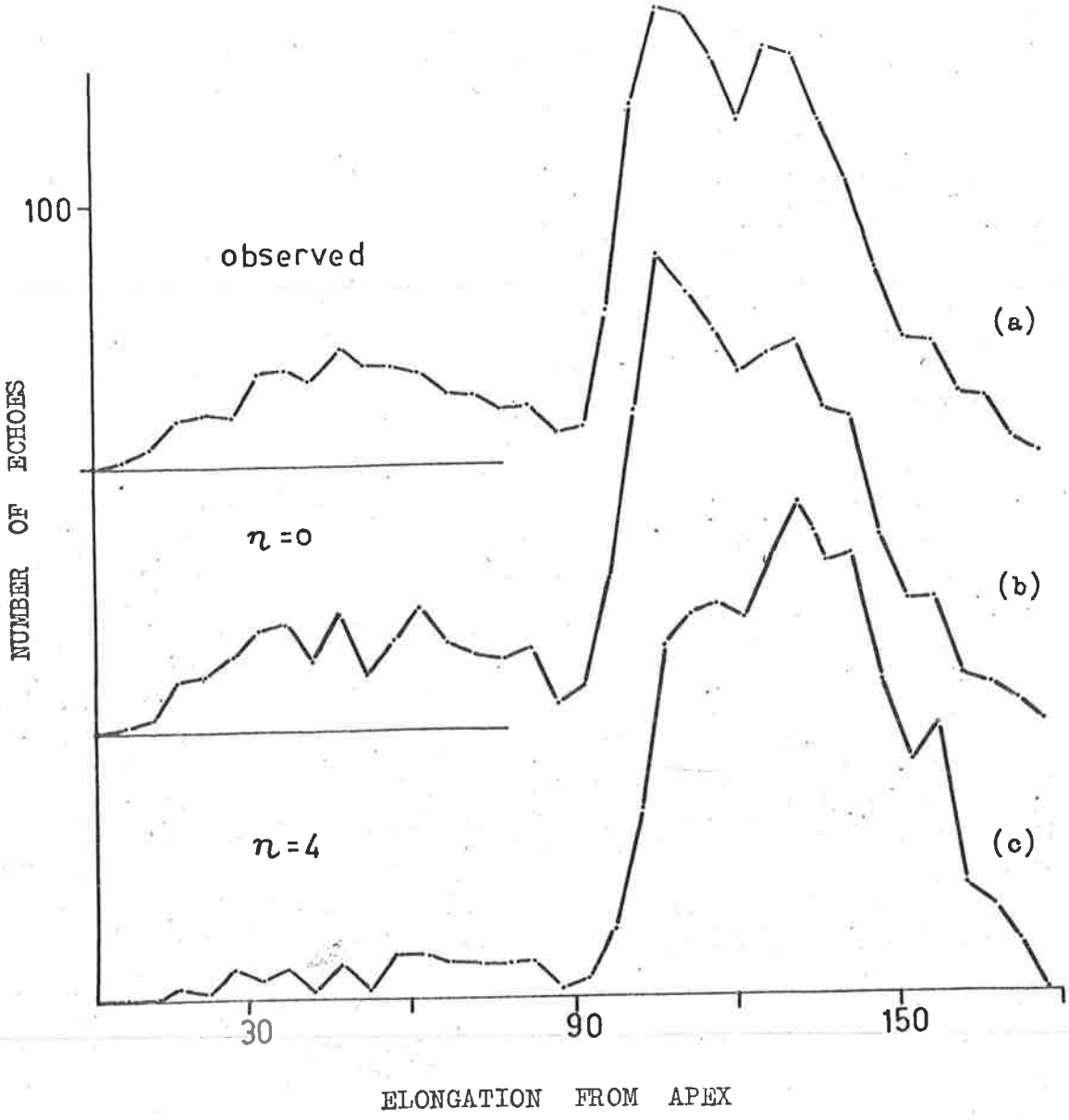

Figure 19a shows the observed distribution with apparent elongation from the apex of the Earth's Way. The distribution has been corrected for observational selection in Figures 19b and 19c. Figure 20 shows the true elongation in the same manner as Figure 19. Figure 20 strikingly illustrates the preponderance of direct over retrograde orbits.

Of particular interest to the Mawson results is Figure 22, which shows the radiant density, corrected for observational selection ($\eta = 0$), as a function of apparent elongation. This figure can be compared with Figure 2 in Appendix 1, which gives the curves for the apex, sun and antisun components assumed for the derivation of the theoretical rates at Mawson. The measured distribution in Figure 22 shows quite clearly the sun and antisun component (60°-80°) rising from the broad apex source. It must be noted, however, that we have found the sun and antisun components far from equal, an assumption made in Chapter 2. This may explain why it was necessary to assume a peak density ratio of 4.5 for the sun and antisun sources compared to the apex source, while Hawkins and Prentice (1957) found a density ratio of 1.5 for the antisun to apex source. Figure 22 indicates that the peak density of the average of the sun and antisun sources is in fact about 1.5 times that of the apex source, but the asymmetry shown in Figure 10.14 indicates that the density ratio for the antisun to apex source would be somewhat greater.

Figure 10.21

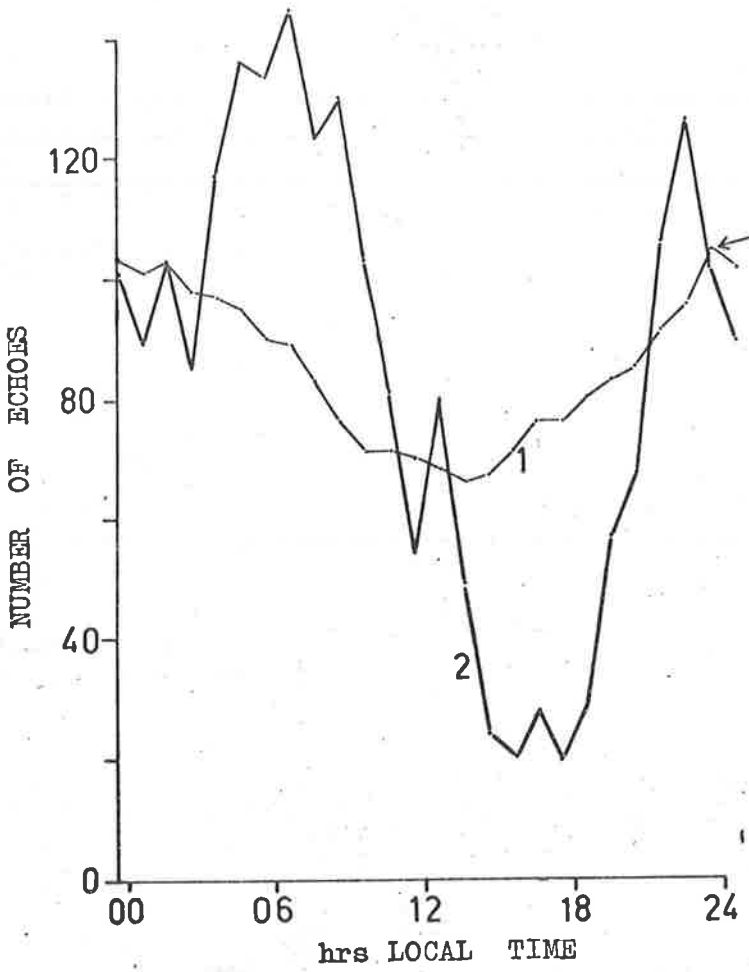

Figure 10.22

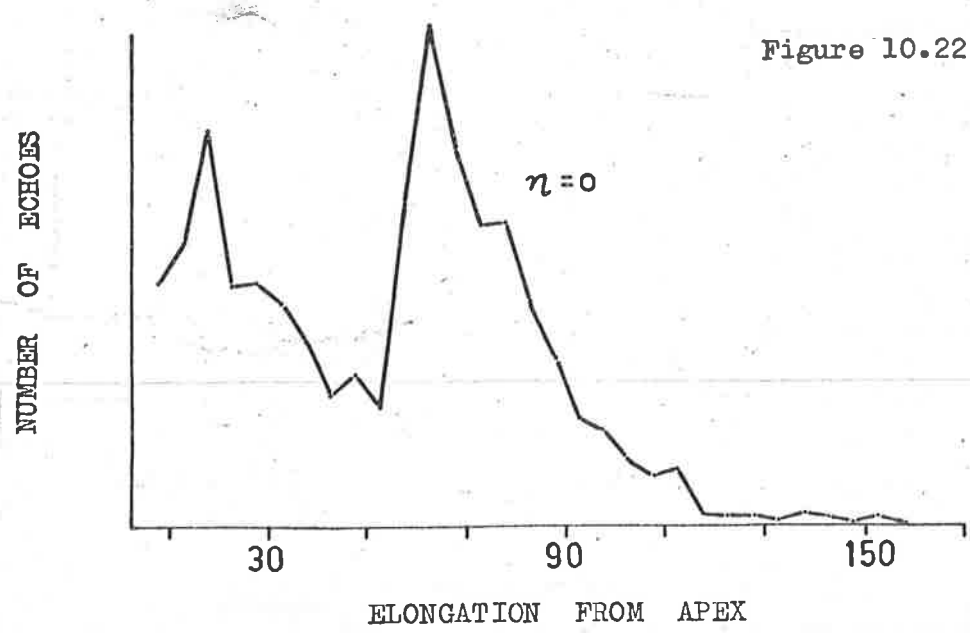

Figure 21, curve 1, shows the diurnal variation in the number of hours recording during the year. The curve has been normalised to the same area as curve 2, which illustrates the diurnal rate variation of the number of echoes suitable for reduction. The ordinate shows the number of echoes in any hourly interval.

Curve 1 shows that of the 1671 hours recording during 1961, the greater proportion was done during the night. However, the diurnal variation is not sufficient to seriously effect the results. The observed echo rate variation can be explained quite satisfactorily in conjunction with the observed distribution with ecliptic longitude (Figure 14). At 06 hr. the broad apex source is at upper transit, while the sharper sun and antisun sources are above the eastern and western horizons respectively. In these positions they will contribute strongly to the echo rate, as the effect of a concentrated source high in the sky is nullified by the poor response of the antennas to reflection points near the horizon. For a short period at about 17-19 hr. local time there are no source centres above the horizon, and this is in fact where the minimum in rate occurs. The peak at about 23 hr. occurs when only the antisun source is in the sky, approximately midway to upper culmination. On reaching upper culmination, at about 01 hr. the rate drops as expected, due to the equipment response falling off with the increased elevation of the source, then rises again as that source sinks and the apex source rises in the sky.

Figure 23a shows the theoretical diurnal rate variation for the S.δ-Aquarid shower for two aerial combinations:

(1) A $\lambda/2$ receiving dipole $\lambda/4$ above ground, and a similar dipole at Adelaide;

(2) A $\lambda/2$ receiving dipole $\lambda/4$ above ground, and a transmitting antenna at Adelaide with a polar diagram as shown in Figure 7.6b.

The observed rate is compared. There may be a significant asymmetry about transit, but this will have to be confirmed on another shower. Certainly the theoretical program 166.3 correctly predicts the onset and cessation of echo detection. It is obvious from curves (1) and (2) that the observed rate variation will be nearly independent of the fine details of the transmitting antenna polar diagram.

Figure 23b shows the theoretical variation in rate as a function of radiant declination, assuming the equipment is recording for 24 hrs/day. It is based on the following parameters for Adelaide:

λ = 11.2 metres

TX power = 250 W

Limiting ω = 5.10^{-13} W

Mass Distrib. s = -2

and the polar diagrams shown in Figures 7.4a and 7.6b.

Figure 10.23

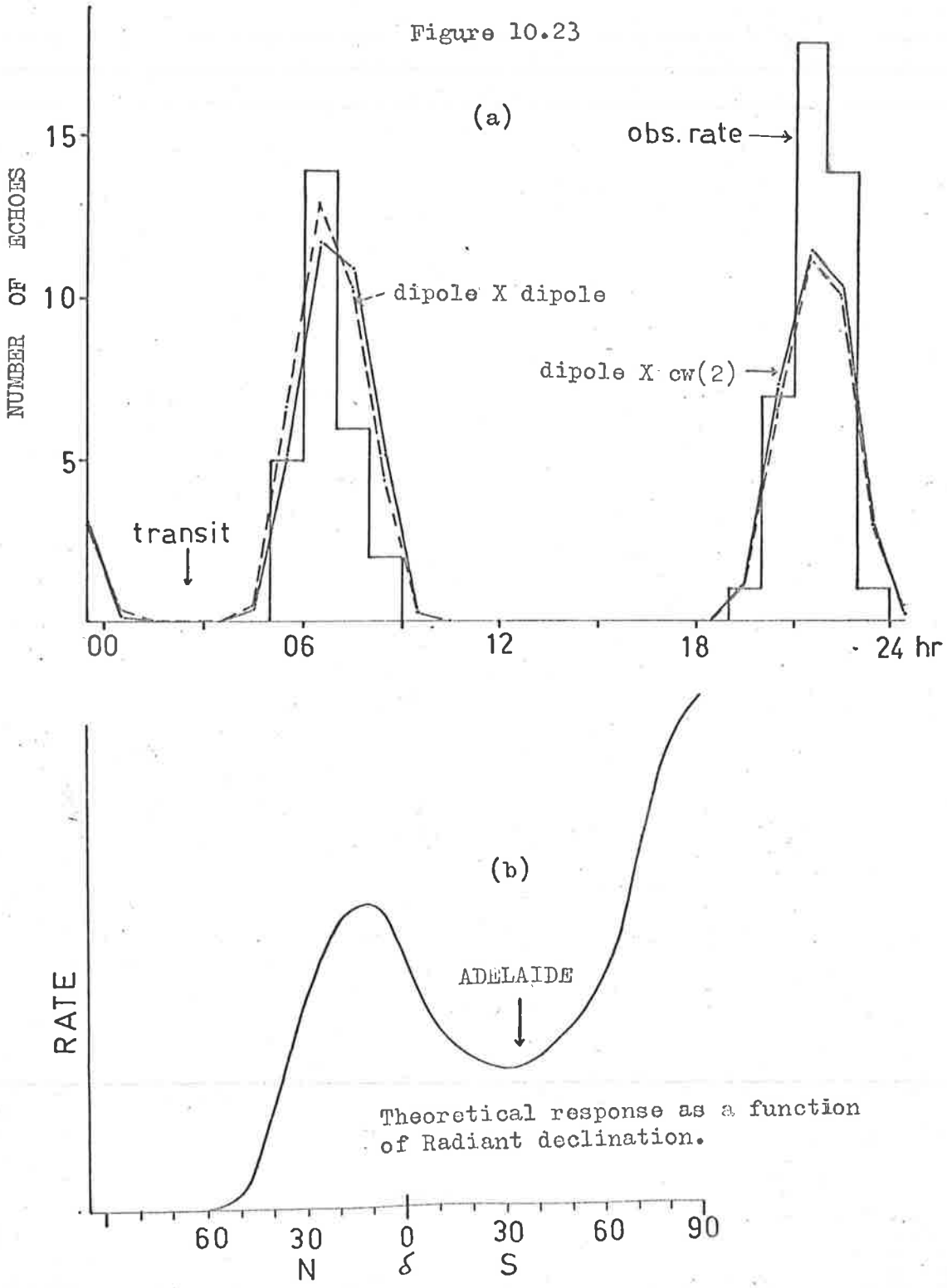

Theoretical response as a function of Radiant declination.

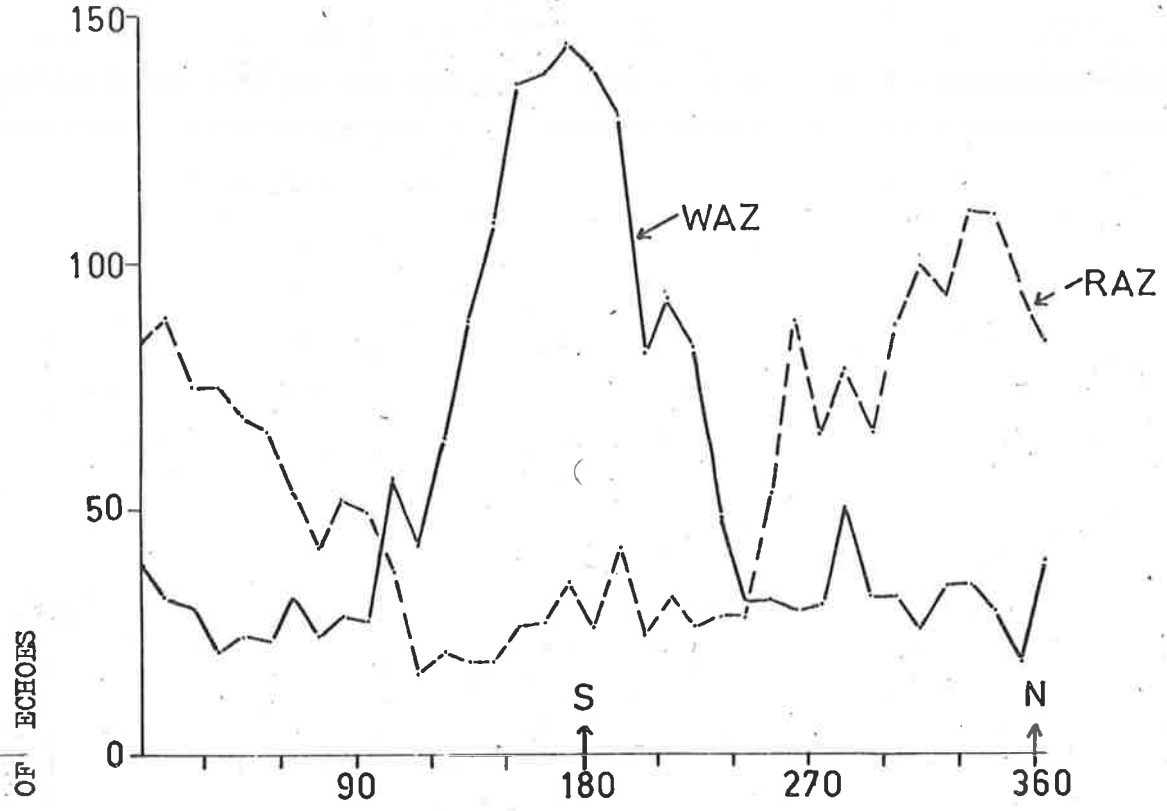

Figure 10.24a

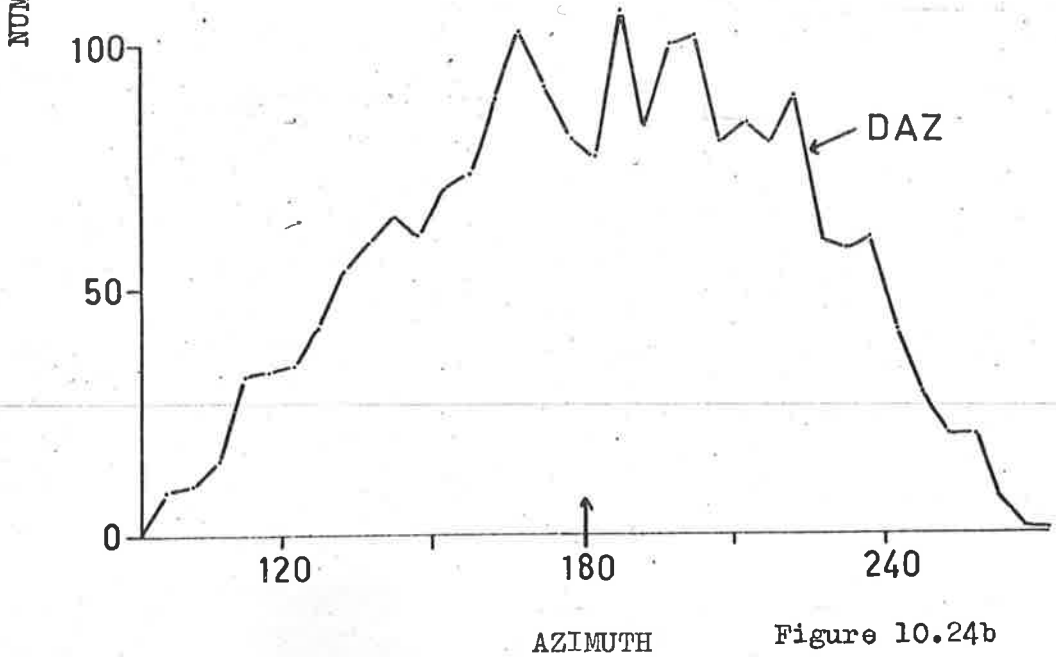

Figure 10.24b

The observed distribution of echoes with the azimuth of the radiant (RAZ) and azimuth of the reflection point (WAZ) is shown in Figure 24a. The distribution of the difference between the two (DAZ = WAZ - RAZ) azimuths is given in Figure 24b. The figures are consistent with the basic assumptions about specular reflection discussed in Chapter 2.2.

Finally, the distribution of echoes with the height of the reflection point is given in Figure 25. The mean height is between 90 and 95 km, which is slightly higher than the mean of the earlier Adelaide data shown in Figure 2.6a.

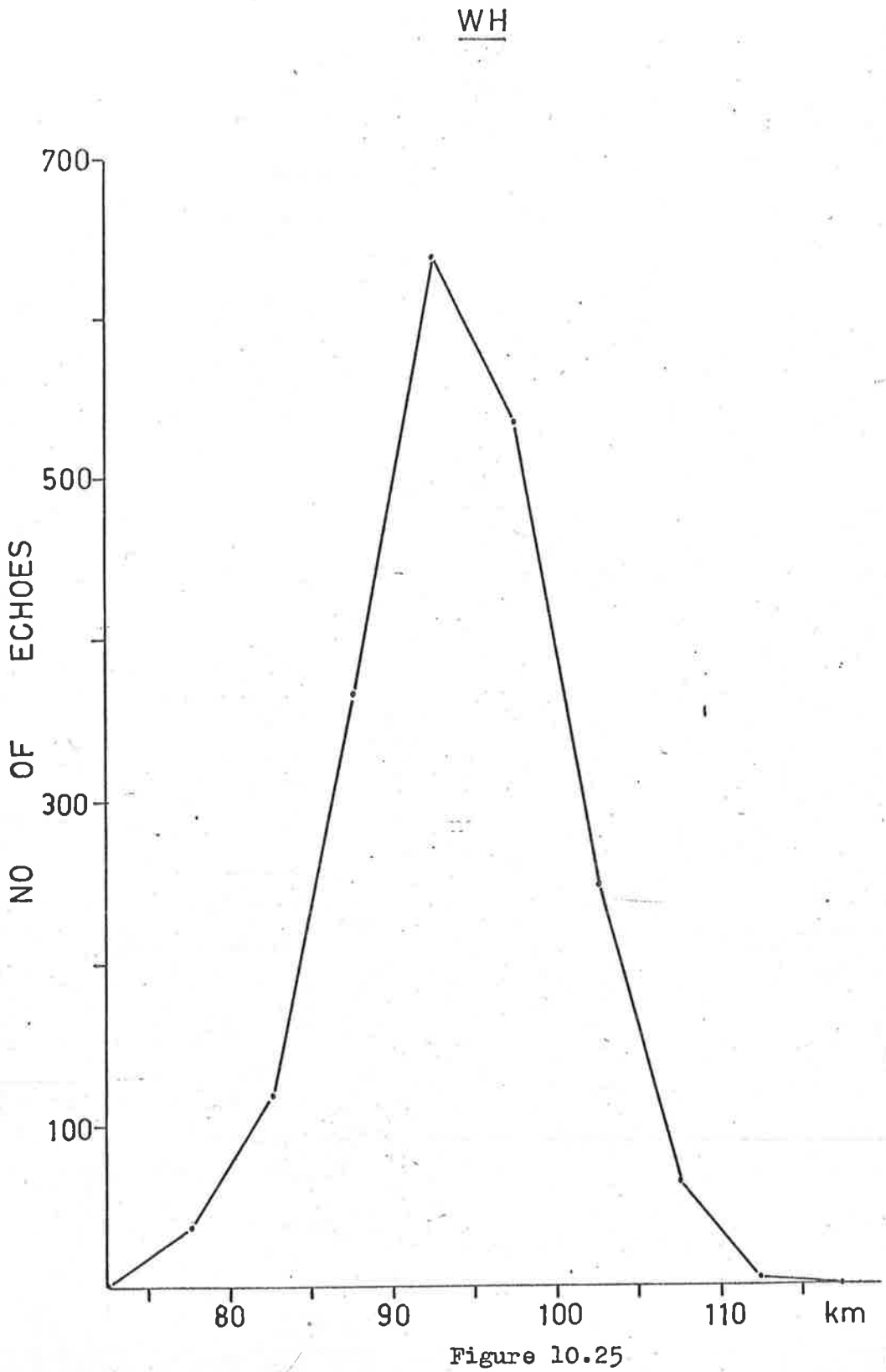

Figure 10.25

CHAPTER 11

SHOWERS

11.1 Sorting Methods.

A preliminary attempt has been made to sort out the shower meteors. In Appendix 5, pages 422 to 427, the radiant maps of right ascension versus declination show many areas of concentration indicating the presence of a shower. The orbit data for all the echoes contributing to these areas of concentration were punched on to cards, and the cards were then sorted on an I.B.M. Sorting Machine. Each area for each month was sorted independently, except for July and August, where the data were combined for the period 23rd July to 5th August. The items sorted were e, i, ω (or Π) and 1/a. The echoes were sub-grouped whenever there was a tendency for any minor group to lie outside the probable range of error of the main group. The allowable range for each element was based on the data of Chapter 10.1. Sometimes (e.g. Southern Taurids) it was not sensible to arbitrarily divide a group which showed no obvious signs of dividing. On the other hand, there were very few radiant groups that did not show some signs of subdividing. This resulted in many pairs of echoes parting from the main group. These have been included in the list in Section 11.2, although the author makes no claims about the significance of such minor groups. The way in which the radiant groups appear to subdivide into minor streams is a consequence of sorting on the orbital elements, rather than only considering the radiant data. It would not be possible, for example, to sort out the complex activity in Aries and Taurus in June without the orbit data.

11.2 Sorting Methods (cont.); List of Grouped Data.

The data has been arranged in the following manner. The sub-groups for each area of radiant concentration are listed in order of longitude of perihelion, Π. The echoes are listed

chronologically within each sub-group. Each sub-group is given a number (top left, under the title, which shows month and radiant area) which is placed alongside the appropriate echo plotted in right ascension, declination coordinates in Figures 1-31. These figures, which give the radiant position and spread for the various sub-groups, are shown following the list of the grouped orbit data. Thus Figure 2 shows the radiant position for the four sub-groups in Cancer, Sextans and Leo in January, the details of which are on page 187.

To aid comparison with previous results the geocentric data for all the sub-groups containing at least three echoes is given in Table 2. The table is arranged in the following manner:

column 1 - the name of the constellation containing the mean radiant;
column 2 - the sub-group number corresponding to that used in Figures 1-31;
column 3 - the mid-date of the period over which the sub-group echoes were detected;
column 4 - (bracketed), the number of days over which the sub-group echoes were detected;
column 5 - number of meteors detected;
column 6 - mean right ascension, corresponding approximately to the mid-date;
column 7 - mean declination;
column 8 - mean observed velocity (not corrected for zenith attraction, retardation, etc.);
column 9 - the name, if any, by which the sub-group has been known to past workers.

Table 1 shows the periods for which the orbit equipment was run during 1961. These figures greatly influence those in columns 3 and 4; in fact the bracketed figure cannot be taken as anything but a lower limit to the duration of the shower. For example, in

TABLE 1

TIMES OF OBSERVATION 1961

JAN 16 to 22	106 hr		
FEB 14 to 22	80 hr		
MAR 10 to 17	141 hr		
APR 12 to 14	39 hr	}	70 hr
APR 28 to 30	31 hr	}	
MAY 18 to 31	178 hr		
JUN 12 to 19	126 hr		
JUL 11 to 15	36 hr	}	169 hr
JUL 22 to 28	129 hr	}	
AUG 01 to 05	81 hr	}	198 hr
AUG 16 to 24	121 hr	}	
SEP 21 to 29	166 hr		
OCT 20 to 31	164 hr		
NOV 15 to 24	128 hr		
DEC 04 to 14	143 hr		

April, the equipment was run for two separated periods, and all the groups detected during this month are in evidence during both periods.

The three mean radiant vector quantities, right ascension, declination and velocity, are only approximate for each sub-group, having been chosen by eye from a data list. It is possible that the figures will be slightly different when the means are calculated correctly. In spite of this, however, the coordinates for the well known showers agree quite well with previous data. Table 3 compares the Adelaide data with that listed by McKinley (1961), and Whipple and Hawkins (1959). There is no sign of any consistent difference in the radiant data which would indicate some consistent error in the Adelaide reduction. There is a slight tendency for the Adelaide

TABLE 2

LIST OF STREAM RADIANTS

Constellation		Time of activity	Number detected		R.A.	Dec.	Vel.	Name
Carina	1.1	19/1	(3)	3	156	-65	40	
Cancer	2.1	20/1	(3)	3	131	+15	31	
Musca	3.1	20/2	(4)	3	195	-74	46	
Virgo	4.1	17/2	(3)	3	177	+06	46	
Virgo	4.2	15/2	(4)	3	178	+02	40	
Capricornus	.1	17/2	(6)	5	307	-17	33	
Aquarius	5.2	18/2	(7)	3	317	-11	33	
Virgo	6.1	15/3	(5)	7	186	-04	31	Virginids
Virgo	6.2	12/3	(5)	3	196	-04	31	Virginids
Aquarius	7.1	14/3	(5)	4	331	-14	38	
Aquarius	7.2	12/3	(2)	4	329	-08	29	
Pegasus	7.3	13/3	(3)	3	326	+03	39	
Aquarius	8.1	14/3	(4)	3	343	-08	29	
Pegasus	8.2	14/3	(6)	7	352	+10	24	
Pisces	9.2	21/4	(17)	3	012	+07	27	
Pisces	9.3	21/4	(18)	4	011	+11	29	
Pavo	11.1	21/4	(18)	4	271	-73	46	
Pavo	11.2	21/4	(18)	4	286	-71	30	
Pisces	12.1	20/5	(3)	3	351	-03	63	
Aquarius	13.1	22/5	(7)	7	355	-18	33	
Pisces	14.1	27/5	(3)	4	029	+12	38	
Aries	14.3	26/5	(6)	8	038	+19	38	
Aries	14.4	26/5	(6)	5	042	+13	30	
Aries	14.5	26/5	(6)	10	045	+18	31	
Taurus	14.6	27/5	(3)	6	051	+18	28	
Pegasus	15.1	14/6	(2)	3	329	+04	63	
Sagittaurus	.1	16/6	(7)	22	275	-25	30	
Aries	17.1	16/6	(3)	4	042	+23	33	
Aries	17.3	15/6	(5)	3	050	+20	42	Arietids
Aries	17.4	16/6	(3)	3	045	+25	39	Arietids

					α	δ	V	
Aries	17.5	16/6	(3)	9	047	+25	43	
Taurus	17.9	16/6	(2)	4	057	+15	38	
Taurus	17.10	15/6	(3)	3	064	+23	32	Zeta Perseids
Taurus	17.11	15/6	(5)	4	065	+15	31	
Taurus	17.12	15/6	(3)	6	066	+26	28	Zeta Perseids
Taurus	17.13	15/6	(6)	7	075	+23	26	
Dorado	18.1	29/7	(7)	4	090	-68	26	
Gemini	19.2	25/7	(2)	4	095	+20	44	
Gemini	19.3	20/7	(17)	6	104	+18	34	
Gemini	19.4	20/7	(17)	5	110	+20	27	
Pisces	20.4	20/7	(14)	3	020	+06	69	
Aquarius	21.3	17/7	(13)	3	321	-06	39	
Aquarius	21.4	10/8	(27)	10	335	-10	36	S.ι-Aquarids$_1$
Aquarius	21.5	22/7	(20)	7	340	-19	40	
Aquarius	21.6	2/8	(25)	12	339	-16	37	S.ι-Aquarids$_2$
Aquarius	21.7	25/7	(6)	3	342	-13	34	
Aquarius	21.8	28/7	(12)	52	340	-17	42	S.δ-Aquarids
Aquarius	21.9	28/7	(14)	6	344	-18	39	
Pisces	21.10	22/8	(5)	6	355	+07	38	
Pisces*	22.1	26/9	(9)	23	017	+06	31	
Pisces*	22.3	26/9	(8)	19	018	+06	30	
Cetus	22.2	25/9	(6)	5	019	-05	30	
Pisces	22.4	27/9	(8)	9	025	+08	30	
Pisces	22.5	25/9	(8)	5	025	+07	25	
Pisces	22.6	25/9	(8)	3	025	+18	41	
Orion	23.1	27/9	(6)	5	089	+03	64	
Monoceros	23.4	24/9	(4)	4	095	+03	65	
Leo	24.2	27/9	(7)	7	160	+12	45	
Sextans	24.3	27/9	(6)	11	153	00	34	Sextanids
Leo	24.4	27/9	(6)	4	160	+12	36	
Leo	24.6	26/9	(4)	5	163	+11	34	
Leo	24.7	26/9	(4)	4	170	+05	34	
Leo	24.8	25/9	(6)	5	170	00	27	

					α	δ	V	
Aries	25. 1	26/10	(31)	64	044	+11	28	S.Taurids
Taurus	25. 2	29/10	(5)	8	049	+06	32	
Taurus	25. 3	23/10	(8)	3	053	+20	43	
Taurus	25. 4	26/10	(8)	4	060	+21	37	
Hydra	26. 1	25/10	(4)	3	127	+06	69	
Canis Minor	. 2	25/10	(4)	3	116	+02	64	
Canis Minor	. 3	29/10	(2)	3	120	+01	67	
Gemini	26. 4	27/10	(8)	14	101	+14	65	
Hydra	26. 7	30/10	(4)	3	137	+03	63	
Lynx	27. 1	28/10	(4)	3	103	-48	39	
Vela	28. 1	20/11	(8)	7	130	-50	41	
Taurus	29. 1	17/11	(31)	9	063	+14	30	S.Taurids
Taurus	29. 2	18/11	(9)	17	060	+17	25	
Taurus	29. 3	18/11	(7)	3	085	+14	43	
Vela	30. 1	7/12	(6)	4	141	-54	38	Puppids/Velids
Scorpius	31. 3	6/12	(3)	3	248	-25	28	
Monoceros	32. 2	10/12	(9)	6	103	+10	41	Monocerotids
Gemini	32. 3	12/12	(7)	16	110	+31	34	Geminids

* These two groups may belong to the same stream, they were separated during the sorting because the range of 1/a was too large.

velocities to be higher. If this were a real error, the radiant declinations would tend to be north of the true values. In fact, the reverse is the case; the Adelaide declinations tend to be slightly south of those listed by McKinley. The difference, however, is not significant. In Figure 3a the right ascension of the Adelaide data has been approximately corrected to the data given by McKinley by adding 1°/day. The declination has not been altered, although the errors could be as much as $\frac{1}{2}^{\circ}$/day. A program has been written to accurately delineate the Adelaide data, but time does not permit its inclusion in this thesis.

The Southern Delta-Aquarid shower was probably the strongest observed during the survey. 52 echoes were detected in spite of the fact that the equipment was shut down for three days at the peak of the shower. The Southern Taurids were observed in October and November, and although the two groups have been treated independently they belong to the same shower. A total of 73 echoes have been classified as belonging to this stream. Two groups in Pisces, 1 and 3, observed during September, were inadvertently separated due to the range of 1/a, however, they obviously are of the same stream. This stream contributed 42 echoes, which means it is quite a major shower, although the author can find no reference to it in previous work. Altogether 583 echoes have been listed for 69 sub-groups in Table 2. The latter figure excludes pairs, but does include groups of three or more meteors. In the next section it is shown that most of the groups of three and four are real, but some are due to chance association. In the larger groups there are probably some meteors included by chance, but similarly some shower meteors are probably excluded because poor quality data has caused too large an error in their orbital elements. Therefore it seems that about 25% of the meteors observed in this survey can come under the classification of "shower meteors". This is quite a different result to that obtained by Davies and Gill, for they estimated that showers contributed less than 2% to their distributions. If one includes the δ-Aquarid shower (35 echoes), this figure is raised to 3%.

TABLE 3a

Shower	Accepted Radiant data			Adelaide Radiant data			Date
Virginids	190	00	30	191	-04	31	20/3
Arietids	045	+23	39	042	+20	42	7/6
				036	+25	39	
				038	+25	43	
ζ-Perseids	062	+24	29	058	+23	29	9/6
S.δ-Aquarids	339	-17	41	340	-17	42	29/7
S.ι-Aquarids$_2$	338	-15	35	342	-16	37	5/8
S.Taurids	052	+14	29	049	+11	28	1/11
				047	+14	30	
Puppids/Velids*	140	-50	?	140	-54	38	6/12
Geminids	113	+32	35	111	+31	34	13/12

* A.A.Weiss - private communication.

TABLE 3b

A comparison of the radiant and orbital elements of two showers listed by Whipple and Hawkins (1959) with the Adelaide data.

Station	α	δ	V^*	e	i	ω	Ω	π	q	Name
Accepted	338	-14	36	.92	06	128	311	079	.23	S.ι- Aquarids
Adelaide 10/8	335	-10	36	.91	06	130	313	087	.22	
Accepted 14/12	103	+08	44	1.00	35	128	082	209	.19	Monocerotids
Adelaide 10/12	103	+10	41	.96	34	138	077	216	.15	

* The 'Accepted' value is V_g, the velocity before entering the Earth's atmosphere; the value given for the Adelaide data is V_o, the observed velocity. The R.A. for the Adelaide data corresponds to the date in Column 2.

The minimum number of meteors in any of their six showers is 6, but this figure needs to be qualified by the scatter they were prepared to accept in classifying meteors as members of a group. If one considers only the sub-groups in Table 2 for which 6 or more meteors are listed, the contribution of showers to the Adelaide results is still about 20%. This figure would be higher if some of the dubious subgrouping were eliminated. The Jodrell Bank survey extended down to meteors of radio magnitude +8*, whereas the Adelaide results do not include meteors fainter than +6. This certainly accounts for some of the difference in the contribution of showers.

It would appear that the terms 'shower' and 'sporadic' do not have very much meaning for the Adelaide data. If one can detect sub-groups, or minor streams, extending down to pairs of echoes in a general radiant concentration, and one concedes that at least some of these are real, then it is logical to assume that there are many minor streams for which only one meteor is detected. These are generally classified as 'sporadic meteors', but in what sense do they differ from shower meteors? The only difference so far established is in the number detected, which not only depends on the equipment parameters, but also must depend largely on chance. It is shown in the next section that in fact the spatial distribution of shower meteors does exhibit some different features from the background distribution. The significance of this is discussed in Chapter 13.

Sorting on each of the orbital elements in turn looking for groups is a slow process and not an infallible one. Many of the minor sub-groups must be missed, and sometimes some of the larger groups could be split up and later discarded. This must have happened to the group of 6 echoes (Figure 14) encircled in the Constellation of Taurus for May. The mean radiant position is $\alpha = 057^\circ$, $\delta = +24^\circ$ for 28/5/61, and the observed mean velocity is V = 24 km/sec. The spread in velocity is small, $23 < V < 26$, and the echoes were observed over a few days at the end of the

---

* From McKinley (1961): $M_r = 40 - 2.5q$, where q is the number of electrons/metre.

month, so they undoubtedly belong to a minor shower.

There is no doubt that many of the subdivisions are invalid, and that some sub-groups should be combined. However, it is impossible to make decisions of this nature while actually sorting, and the best procedure seemed to keep the sub-groups separated initially, and later to recombine them if the division seemed unjustified. A comparison of the December 1961 results with those obtained in December 1960 is interesting in this respect. These comparisons are shown in Figure 30-32 and the data for the 1960 echoes is listed in Table 4. Figure 30: In 1961 the echoes were divided into four minor groups, group 1 having 4 echoes and being identified with the Puppid/Velid shower. In 1960 the echoes were much more closely grouped, and can all be identified with group 1, with the possible exception of echo number 54714 which could correspond to sub-group 2, 1961. The mean radiant vector (R.A., dec., vel.) is 142°, -51°, 41 km/sec, which agrees well with the 1961 results, except for a slightly higher observed velocity. Figure 31: The results are a little confusing; there is no doubt that the same stream is active again, but the sub-grouping does not correspond very well. Sub-group 1 (1960) does not seem to have a corresponding sub-group for 1961, but sub-group 2 (1960) corresponds roughly to sub-groups 2 and 3 (1961). During 1961, however, these two sub-groups appear to be well divided on the basis of eccentricity and longitude of perihelion.
Figure 32: The Geminid shower corresponds well in both years, the mean radiant vector for 1960 being 111°, 31°, 34 km/sec cf. 110°, 31°, 34 km/sec for 1961. The other echoes in the vicinity during 1960 subdivide quite distinctly, the sub-group 1 corresponds very well to the sub-group of the same number in the 1961 results. So too does the sub-group 2, but sub-group 3 (1960) is not matched in 1961, unless the two echoes concerned (50457 and 52564) are inaccurate Geminids. This last hypothesis is strengthened when one checks on the data for each echo. Both had their velocities increased by optimization (8% and 5% respectively) and both echoes had less than the average number of Fresnel cycles to use in their

Table 4

Table for Figure 30*b*

Number	e	i	ω	Ω	Π	1/a	Designation 1960	Designation 1961
50281	.450	074	350	076	067	.561	1	1
52084	.571	070	345	077	063	.441	1	1
52306	.417	072	350	077	068	.595	1	1
55630	.363	076	347	079	067	.651	1	1
54714	.570	067	000	079	079	.437	2	(2)

Numbers 50281 to 55630 are members of the Puppid/Velid shower.

Table for Figure 31*b*

48362	.817	010	232	075	308	.670	1	1
57310	.867	013	224	080	305	.654	1	1
57319	.837	011	235	080	315	.580	1	1
50203	.899	000	250	076	327	.278	2	?
50991	.929	011	064	257	321	.232	2	?
52011	.904	001	259	077	337	.222	2	?
52833	.943	008	089	258	347	.115	2	?

Table for Figure 32*b*

47720	.924	131	118	075	194	.269	1	1
56174	.910	121	129	080	209	.420	1	1
57712	.851	125	125	081	206	.550	1	1
56088	.961	027	132	080	213	.223	2	2
57580	.993	011	133	080	214	.047	2	2
50457	.947	033	153	076	230	.684	3	?
52564	.941	027	152	078	231	.720	3	?

All the echoes listed on this page were recorded during Dec 1960.

reduction. In addition, both failed to qualify as OK during the quality tests (Chapter 9.1). This indicates that sufficient attention has not been paid to the results of these tests, and it certainly would be a good idea to indicate the quality of each echo in any future classification.

Of the six showers listed by the Jodrell Bank survey, four are in evidence in the Adelaide results. The Daytime Arietids and Delta Aquarids were detected by both, but the Taurids (038°, +20°, 28 km/sec) do not appear in Table 2, although several other radiants in Taurus were quite active. Two of the three previously unknown showers were detected and are listed in Table 2. The author made no attempt to search for these until after this table was compiled, so the confirmation is completely independent. The mean orbital elements are compared in Table 5. Davies and Gill remark on the similarity of the orbit of one meteor detected in March 1955 to Whipple's (1954) Virginid meteors. This stream was recorded (in two radiants) by this survey, and it is of interest to compare the radiant and orbital elements of one echo* in particular (number 28056) with both their results. The agreement is remarkable.

11.3 An Improved Analysis for Association.

A more thorough attempt to classify the minor streams detected during this survey has been made, using an I.B.M. 1620 computor. We shall first consider the necessary conditions that must be satisfied before any two orbits are classified as 'associated'.

Each meteor has five orbital elements, a, e, i, π and Ω. The meaning of these is illustrated in Figure 10.4. Only four of these are independent, as they are derived essentially from only four independent quantities, right ascension, declination, velocity and time. We shall regard the semi-major axis, a, as the

* This echo was a very poor one, only 2, $2\frac{1}{2}$ and 3 Fresnel cycles were observed on the three traces; the trace x/T discrepancies were too large for the echo to pass the quality tests; however the echo height optimization brought the velocity to its correct value.

Table 5

A comparison of the mean orbital elements of four showers listed by Davies and Gill with the Adelaide data.

Station	α	δ	V_{ge}	e	i	ω	Ω	π	q	No.	
Jodrell Bank (1)	340	-05	29	.85	02	050	001	051	.24	6	
Adelaide 14/3	343	-08	29	.82	03	060	355	059	.36	3	
Jodrell Bank (2)	050	+26	41	.97	46	019	089	108	.04	6	
Adelaide 16/6	050	+20	42	.98	18	022	084	106	.04	3	D.Arietids
"	045	+25	39	.96	33	021	085	106	.06	3	
"	047	+25	43	.98	40	020	085	104	.04	9	
Jodrell Bank (3)	339	-19	43	.96	30	150	304	094	.09	35	δ-Aquarids
Adelaide 28/7	340	-17	42	.97	34	153	305	099	.07	52	
Jodrell Bank (6)	048	+22	41	.98	21	324	208	172	.10	8	
Adelaide 23/10	053	+20	43	.98	25	328	209	177	.09	3	

A comparison of the radiant and orbital elements of one Virginid meteor selected from the Adelaide data with one echo from Jodrell Bank and one of four photographic meteors recorded by Whipple at Harvard.

Station	α	δ	V_{he}	e	i	ω	Ω	π	q	Listed number
Jodrell Bank	186	+06	39.4	.87	08	274	001	274	.50	2537
Harvard	190	+03	37.8	.85	06	290	357	287	.38	1934
Adelaide 14/3/61	185	+03	37.6	.84	05	290	353	284	.38	28056*

*See previous footnote

dependent variable. $a = a(e, \Pi)$ is determined by the restriction that the orbit of the meteor must intersect the Earth's orbit. The longitude of the ascending node, Ω, can be ignored if groups of meteors over a short interval of time are being considered. We shall restrict the interval of searching for associated orbits to about ten days. In this way the year's data can be divided into monthly groups.

The expected error (one standard deviation) in any orbit is given approximately by:

$$\begin{aligned} 1/a &\pm 0.08 \\ e &\pm 0.04 \\ i &\pm 4^\circ \\ \Pi &\pm 5^\circ \end{aligned}$$

Accordingly, we can now state that the definition of "association" between any two orbits is that the following conditions are all satisfied:

$$\begin{aligned} \left|\frac{1}{a_1} - \frac{1}{a_2}\right| &\leqslant 0.15 \\ \left|e_1 - e_2\right| &\leqslant 0.07 \\ \left|i_1 - i_2\right| &\leqslant 7\tfrac{1}{2}^\circ \\ \left|\Pi_1 - \Pi_2\right| &\leqslant 7\tfrac{1}{2}^\circ \end{aligned}$$

These limits are qualified by the condition that if $e < 0.3$, the allowable range of $\Delta\Pi$ is increased to $7\frac{1}{2}^\circ - 100.(e-0.3)$. This is due to the observed decrease in the accuracy of Π as $e \to 0$. In the limiting case of a circular orbit, Π is undefined. This qualification can result in an association between two orbits not being mutual, but in practice there are very few cases of this occurring.

The following procedure was then followed:

(1) The data (2101 echoes) was grouped into 14 decks on a monthly basis. Each deck was then treated independently. Each orbit (known as the 'primary orbit') in any one deck was compared one by one with all the orbits (known as the 'secondary orbits') in the deck. For every orbit in the deck that passed the association tests, 1 was added to a quantity known as the 'association count' of the primary orbit. The output of this program consisted of the association count for each orbit in the deck. This must be at least one, as every orbit encountered itself in the deck of secondary orbits. The deck was then re-ordered on the basis of the association count the orbit with the most associations heading the deck.*

(2) The detailed list of groups of associated orbits from a particular deck was then compiled in the following manner: Suppose the first orbit in the re-ordered deck has an association count of 19. This orbit would be held as a primary, and the whole deck tested again for associated orbits. There would be 19 such associations, and as each one is encountered, the orbit reference number is punched out. Each of the 19 orbits is then 'marked' to indicate it has already been chosen as a member of a group. The next unmarked orbit is then chosen as a primary and the above procedure repeated.

By ordering the deck in descending order of association count, we have ensured that the orbit chosen as the primary for the start of a particular group is in fact the central orbit of the group.

Marked orbits were not excluded from <u>contributing</u> to another group, but only from <u>initiating</u> a group. To put it another way, once having contributed to a group, an orbit cannot become the centre of a subsidiary group.

---

* The size of the I.B.M. 1620 store necessitated that the re-ordered deck only contained orbits with an association count of at least 2.

The numbers of groups complied in this manner for each month of observation are listed in Table 6. Besides the normal periods of operation in July and August, there was a separate run during the δ-Aquarid shower in late July and early August. This is listed as the July/August deck, and it contains the largest group of associated orbits recorded during the survey, 42 δ-Aquarid orbits. It is interesting to note that the two groups in Pisces during September (radiants 22.1 and 22.3 in the previous section) were also brought out as separate groups by this procedure. Perhaps the most important question to be answered concerns the statistical significance of these groups. It is obvious that the large groups would not arise purely by chance, but what of the smaller groups containing only a few members? This question is considered in the next section.

11.4 The Statistical Significance of Small Groups.

In order to determine the reality or otherwise of the smaller groups, a random set of data was constructed in the following manner: The number and eccentricity for each orbit was transferred onto a new card. The real data was thoroughly shuffled and the values of i transferred one by one to the ordered deck of new cards. The real data was again shuffled and the values of V transferred. The value of a was then calculated for each of the new orbits to satisfy the condition that each orbit must intersect the Earth's orbit. This 'random data' was then split into 14 decks of size equal to the 14 decks of real data. These decks were then sorted for groups in exactly the same manner as we used for the real data. The results are listed in Table 7. No groups of more than five orbits are obtained for the random data, so it is obvious that all the real groups containing six or more orbits are significant. However the significance of the smaller groups is not immediately apparent. We must consider the probability of group formation before any conclusions about the smaller groups can be reached. To do this, we must review the process of compiling groups of, say, n orbits. As the data deck has been ordered in descending associ-

TABLE 6

	number of orbits	n = 2		n = 3		n = 4		n = 5		n > 5	
		O	E	O	E	O	E	O	E	O	E
Dec '60	115	9	6	4		4		1		1	
Jan	119	5	8	2	5	0		0		1	
Feb	104	7	6	1		0	6	0		0	
Mar	145	15	14	3		0		1		0	
Apr	70	6		2	8	1		0		0	
May	209	8	16	5		2		1		11	
June	188	12	14	8		3		1	NONE	8	NONE
July	36	2		0	10	0	6	0		0	
Jul/Aug	287	13	23	8		5		3		13	
Aug	143	10	10	3	9	3		0		3	
Sep	262	18	2	13		5		2		11	
Oct	189	11	12	5		1		2		7	
Nov	108	5	12	3	6	1	6	1		4	
Dec '61	126	11		3		4		1		2	
TOTAL	2101	132	142	60	39	29	18	13	0	61	0

O - Observed

E - Expected

This table gives the number of groups of n associated orbits (observed) formed for each of the fourteen decks of real data. Alongside each figure is the number of chance groups (expected) expected if the data were random.

ation count, all groups of n+1 or more orbits will already have been compiled. Many of the orbits in the deck will be marked. These are not available to initiate any groups of n. If a large number of orbits are excluded in this manner, the probability of a group of n forming by chance association will be lessened. We shall assume that the probability p(n) of a group of n orbits being formed by chance is proportional to both the total number of orbits in the deck, and to the number of unmarked orbits available for initiating groups of n. Call these numbers N_t and N_i respectively.

Thus,

$$p(n) \propto N_t \cdot N_i \qquad \ldots(1)$$

N_t is constant for any given deck, but N_i will depend on the number of orbits marked by previously compiled groups. Strictly speaking, N_i changes after each group is formed, but it is sufficient to consider it as a function only of n, i.e. constant while all groups of n orbits are being compiled. The approximate value of N_i is given by

$$N_i(n) = N_t - N_m(n) \qquad \ldots (2)$$

where N_m is the number of different orbits already chosen to form the groups containing n+1 or more orbits.

From this theory we should expect the number of chance groups of n orbits r(n) to be a linear function of the product $N_t \cdot N_i(n)$. Naturally, because of the nature of the problem, the scatter will be considerable, but the linear trend of r(n) with $N_t \cdot N_i(n)$ should be clear. The results from the 14 decks of random data are shown in Figure 1 for groups of 4, 3 and 2 orbits. If the number of groups of n orbits is large, the true value of $N_i(n)$ will progressively decrease below the value given by equation (2). We would thus expect the actual curve to fall below the straight line for high values of r(n). This is apparent in the curve for n = 2, where the number of orbits marked throughout the course of compiling pairs is a significant proportion of the total.

The plotted curves of Figure 1 are now used to calculate the expected number of chance groups of n orbits for each of the 14 decks of real data. Only the linear portion of the curve for n = 2

TABLE 7

Deck	N_t	n = 2	3	4	5
1	115	7			
2	119	9	1	1	
3	104	6	1		
4	145	7	2		
5	70	3			
6	209	20	10	2	
7	188	24	2	3	
8	36	2			
9	287	28	9	5	1
10	143	11	3	1	
11	262	26	10	4	2
12	189	18	4	2	
13	108	4	1		
14	126	13	4	1	
TOTAL	2101	178	47	19	3

This table gives the number of groups of n associated orbits formed for each of the fourteen decks of random data. From these figures it is possible to estimate the number of groups expected by chance for the real data.

need be used, as the values for $N_t.N_i(2)$ in the real data never exceed $4 \cdot 1.10^4$. The product $N_t.N_i(n)$ was found for n = 2,3,....5 for all decks of real data. The greatest value for $N_t.N_i(5)$ in the real data is $5 \cdot 3.10^4$, but the lowest value of $N_t.N_i(5)$ in the chance data for which a group of 5 orbits was formed is $6 \cdot 7.10^4$. From this we can conclude that the 13 groups of 5 orbits found in the real data are significant.

The expected number of chance groups is listed for the decks of real data in Table 6. The expected numbers have been combined where necessary to give a value of at least 5, so that a χ^2 test could be applied. It appears that there is a significant excess of real groups of 3 and 4 orbits over the number expected by chance. However the number of chance pairs exceeds the number found in practice. Although it is difficult to justify its application, the χ^2 test was applied to the results for n = 2, 3 and 4. The excess of groups of 3 and 4 orbits was significant at the 5% level; the observed numbers of pairs did not differ significantly from the expected distribution.

It is probable that the calculated number of groups exceeds the true number expected by chance for the following reasons:

(1) The 'random' data used was not truly random - we have shown that the observed data from which the real data was constructed contained a large proportion of real groups. This would increase the probability of chance association over the true value.

(2) The error in the estimate of N_i by equation (2) is such that the calculated number of groups will exceed the true number.

These approximations may account for the excess of the calculated number of pairs expected by chance over the number obtained in practice, and they only strengthen the conclusion that many of the groups of 3 and 4 orbits are real. Further evidence to support the significance of the groups of 3 and 4 orbits is given by an examination of the low inclination streams that intersect the Earth's orbit during the hours of darkness from July to October. This is discussed more fully in the next section.

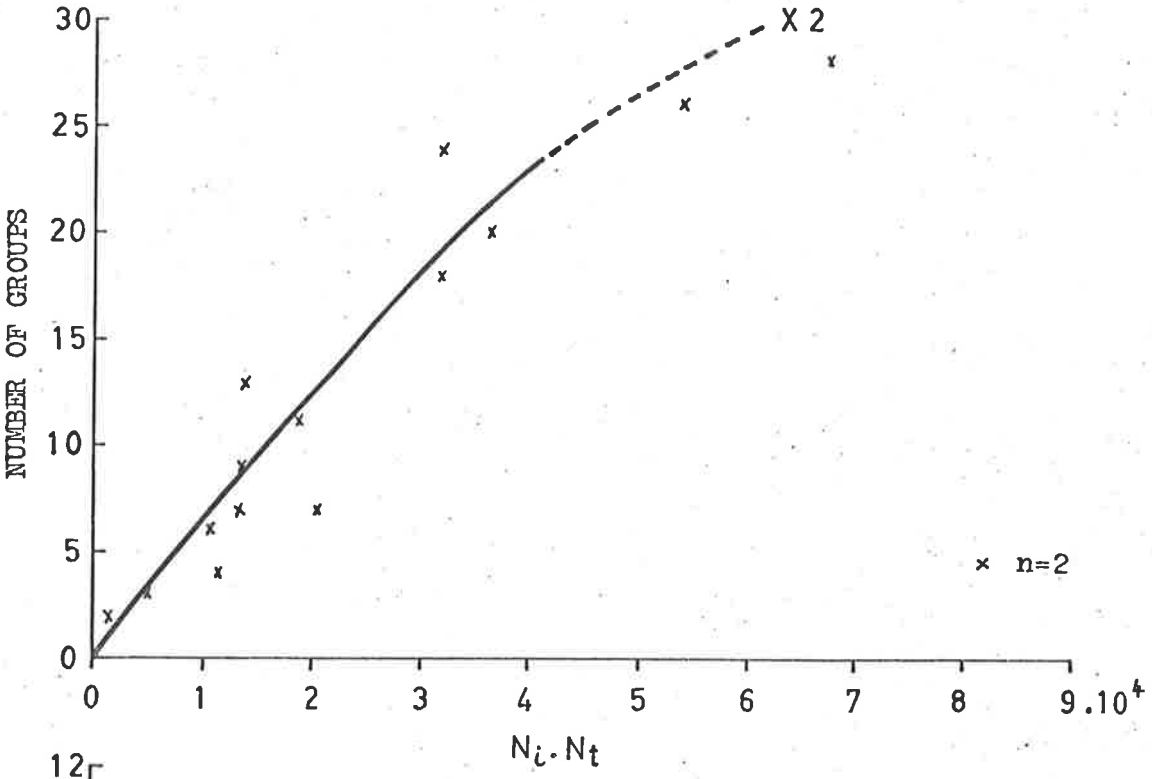
30
25
20
15
10
5
0
NUMBER OF GROUPS
X 2
× n=2
0 1 2 3 4 5 6 7 8 9.10⁴
Ni. Nt

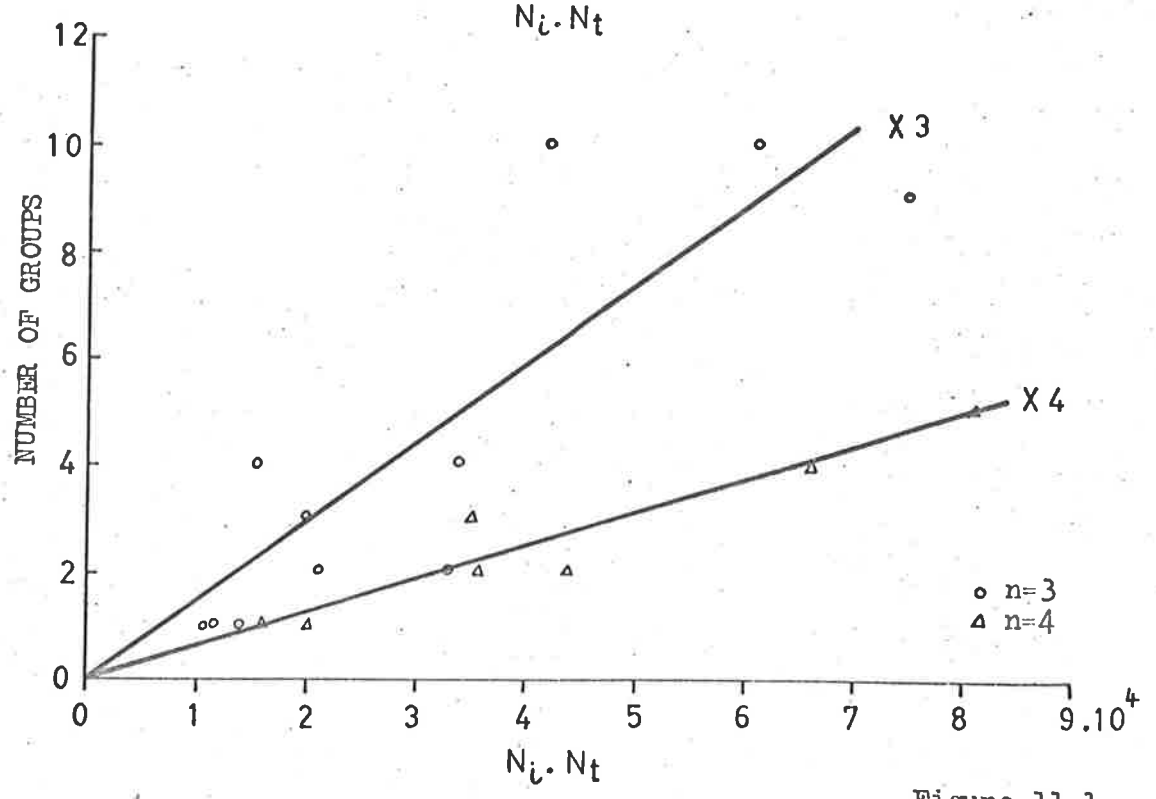
12
10
8
6
4
2
0
NUMBER OF GROUPS
X 3
X 4
o n=3
Δ n=4
0 1 2 3 4 5 6 7 8 9.10⁴
Ni. Nt

Figure 11.1

If the background of sporadic meteors consists of a vast number of unresolved streams we would expect to find an excess of the observed number of pairs of orbits over the number expected by chance. The number of real groups should increase with decreasing n. The fact that this is not observed for n = 2 can either be taken as evidence that the sporadic background originated in some different manner to the shower meteors, or it can be attributed to over-estimation of the number of groups expected by chance. It is difficult to decide between these two possibilities using the Adelaide data along, although evidence given in the next section does indicate that most of the pairs for the period July to October are due to chance association. Accurately reduced photographic data may provide the necessary evidence, for with this data the association limits can be greatly reduced. The number of groups expected by chance would accordingly be much less, and whether or not there is a real excess of pairs should be easier to determine.

11.5 Shower Meteors.

Interesting confirmation of the reality of the groups of 3 and 4 meteors can be obtained from the low-inclination streams which impinge on the Earth during the night-time from July to October. In Section 10.3 the prominent anti-sun component in the distribution with ecliptic longitude was noted for these months. Figure 2a shows the combined distribution for the four months. The anti-sun component at $270^\circ < \lambda_A < 310^\circ$ is nearly three times as large as the Sun component at $50^\circ < \lambda_A < 90^\circ$. In order to analyse the anti-sun component, let us attach to each orbit a number g which has the following meaning.

(1) g = 5 indicates that the orbit contributed to some group containing at least five orbits. These meteors can be regarded as definite shower meteors.

(2) g = 3 indicates that the orbit contributed to some group containing three or four orbits, but not to any larger group.

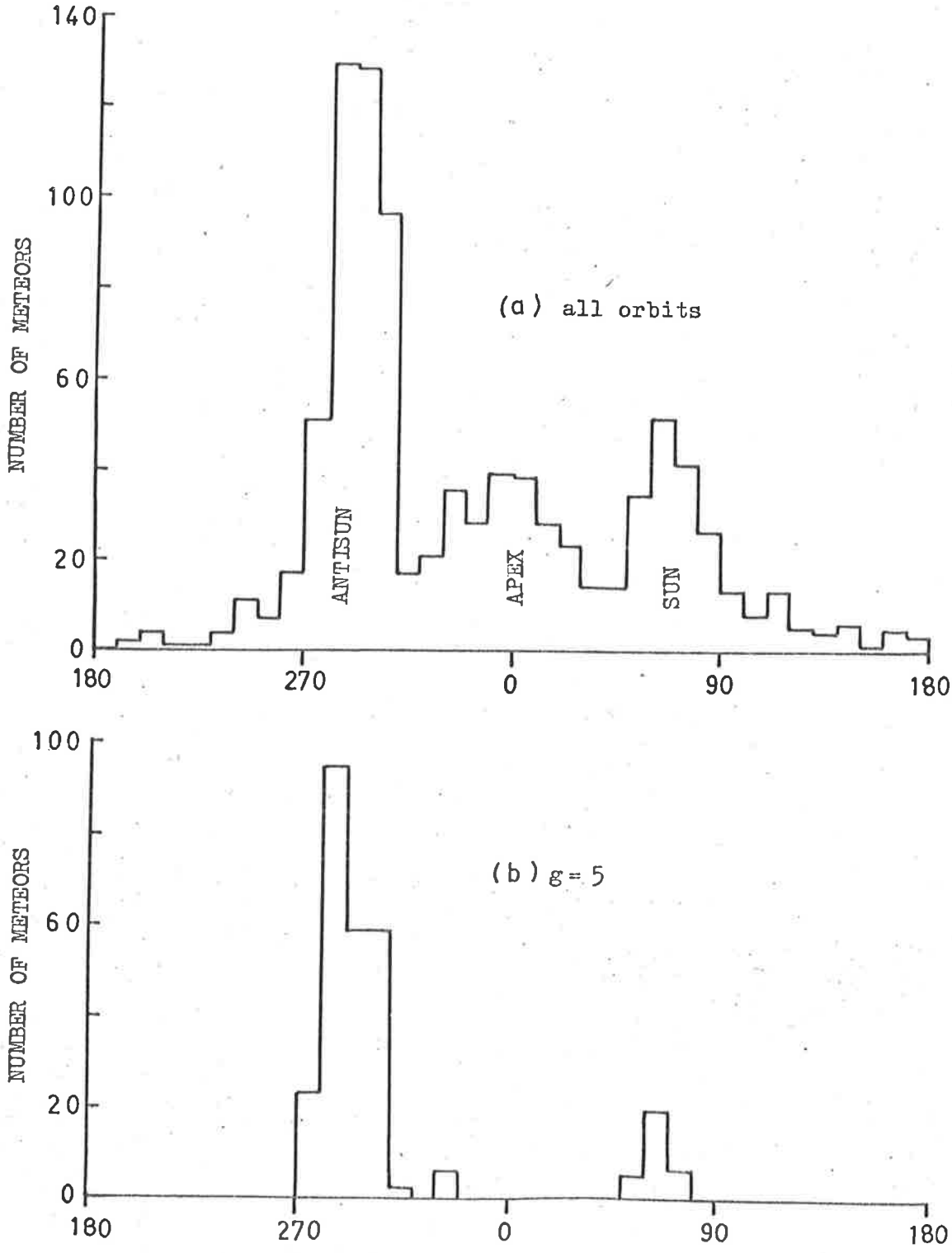
140
100
60
20
0
NUMBER OF METEORS
(a) all orbits
ANTISUN
APEX
SUN
180
270
0
90
180
100
60
20
0
NUMBER OF METEORS
(b) g = 5
180
270
0
90
180
LONGITUDE RELATIVE TO THE APEX

Figure 11.2

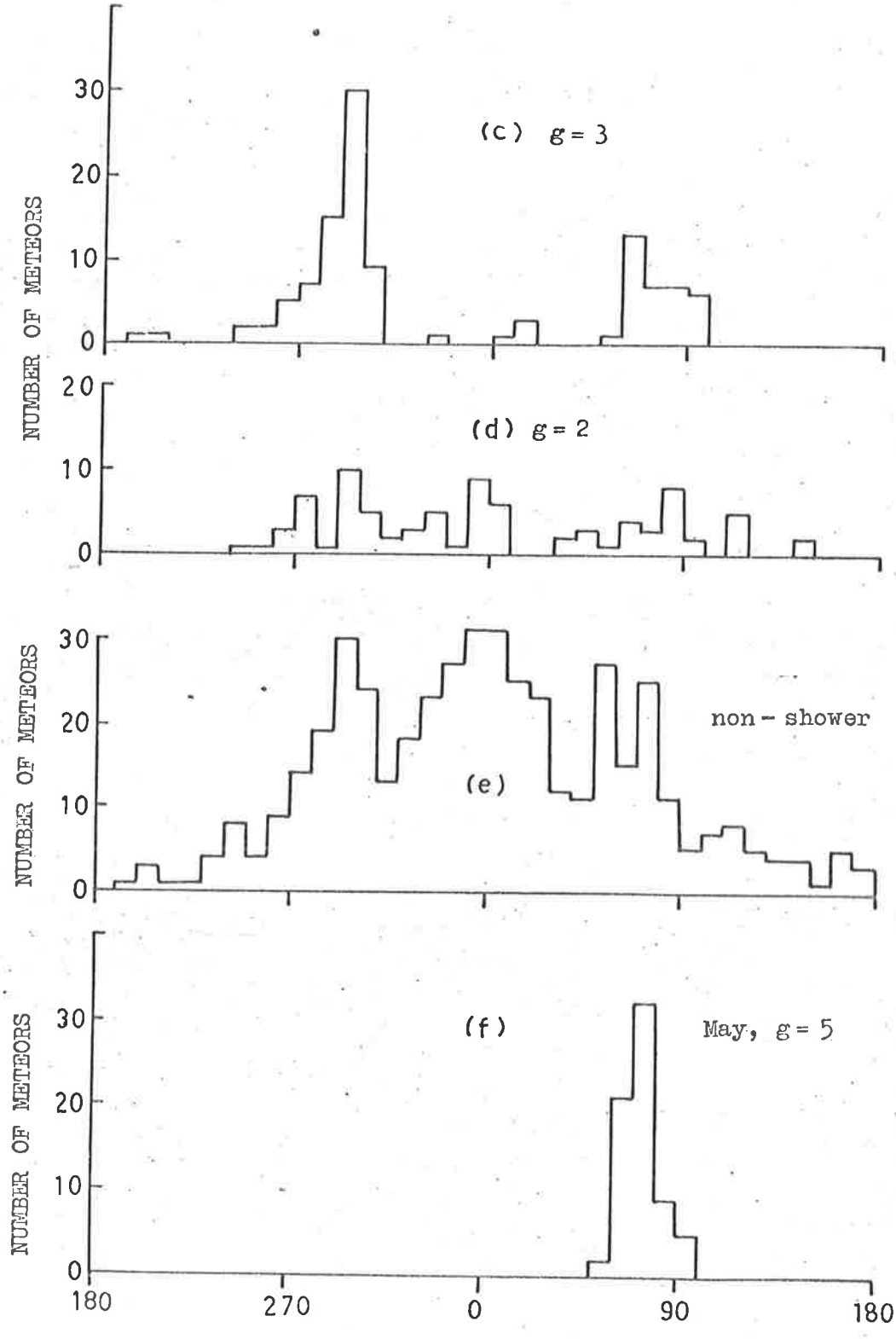

Figure 11.2 LONGITUDE RELATIVE TO THE APEX

(3) $g = 2$ indicates that the orbit contributed to a pair, but not to any larger group.

Figures 2b, 2c and 2d show the distribution with λ_A for these three components of the meteors contributing to the distribution of Figure 2a. Figure 2e shows the distribution of Figure 2a less the three components, i.e. for all meteors not contributing to any group in the four month period. This distribution has no significant asymmetry, showing that the excess anti-Sun component apparent in Figure 2a is almost entirely due to shower meteors. The distribution for these meteors ($g = 5$) is shown in Figure 2b. There are no meteors outside the Sun and anti-Sun components.

The distribution for $g = 3$ given in Figure 2c shows that these meteors are predominently members of showers. Were these groups of three and four meteors due to chance, the distribution for $g = 3$ would be similar to that shown in Figure 2e, with only a slight excess in the region of the anti-Sun. In fact the distribution shows only a few meteors not coming from the direction of the Sun or anti-Sun.

On the other hand, the distribution for those meteors for which $g = 2$ (shown in Figure 2d) does not differ significantly from the parent distribution, i.e. the distribution without the meteors contributing to groups containing three or more orbits. This parent distribution is almost identical to that shown in Figure 2e. Thus we have evidence indicating that most of the pairs of orbits obtained from the analysis of Section 11.3 for these four months are due to chance association.

The conclusion that the prominent anti-Sun component for this period is due to shower meteors raises an interesting point. These streams, providing they are of reasonably low inclination, should be visible after perihelion passage as daytime showers. These meteors would appear to emanate from near the Sun, and a simple calculation shows that they should encounter the Earth during May and June. An inspection of Figure 10.15a shows that there is, in fact, a very prominent Sun component of meteors during May. Further confirmation is given by the distribution with ecliptic

longitude of those meteors in May for which g = 5. This is shown in Figure 2f. Without exception, they all come from near the Sun. The Sun peak in May thus appears to be due to some of the streams that contribute to the anti-Sun peak from July to October. This is considered in more detail in Chapter 12.

11.6 The Spatial Distribution of Shower Orbits.

It is of interest to consider the orbital distributions of the shower meteors alone. If these meteors either have a different origin to the sporadic background or have evolved in some different manner, they will probably show a different distribution in space.

The distribution with reciprocal semi-major axis for those orbits which contribute to groups containing at least five meteors is shown in Figure 3a. The median value is little different from that for all orbits, but there is a distinct lack of short-period orbits. This correspondsto the lack of such orbits in the bright photographic data considered by Whipple (1954). He estimated that his data contained at least 50% of shower meteors.

The distribution with inclination is shown in Figure 3b. High inclination and retrograde orbits are lacking in comparison to the total distribution shown in Figure 10.8. The distribution with eccentricity, given in Figure 3c, shows that there are no shower meteors in orbits with eccentricity less than 0.6. These three distributions indicate that the short-period highly inclined orbits of low eccentricity, which appear to become more prominent with smaller magnitudes (Hawkins, 1962), do not contribute to the total distribution as showers, but rather as meteors in individual and separate orbits.

The fourth distribution for shower meteors, given in Figure 3d, shows the distribution with longitude of perihelion π. Only the meteors with $i < 30^\circ$ or $i > 150^\circ$ have been used, so that this distribution effectively gives the orientation of the line of apsides. The bulk of the shower orbits lie in the range $90^\circ < \pi < 180^\circ$. The intense nighttime showers from July to October and the corresponding daytime showers in May and June contribute most to

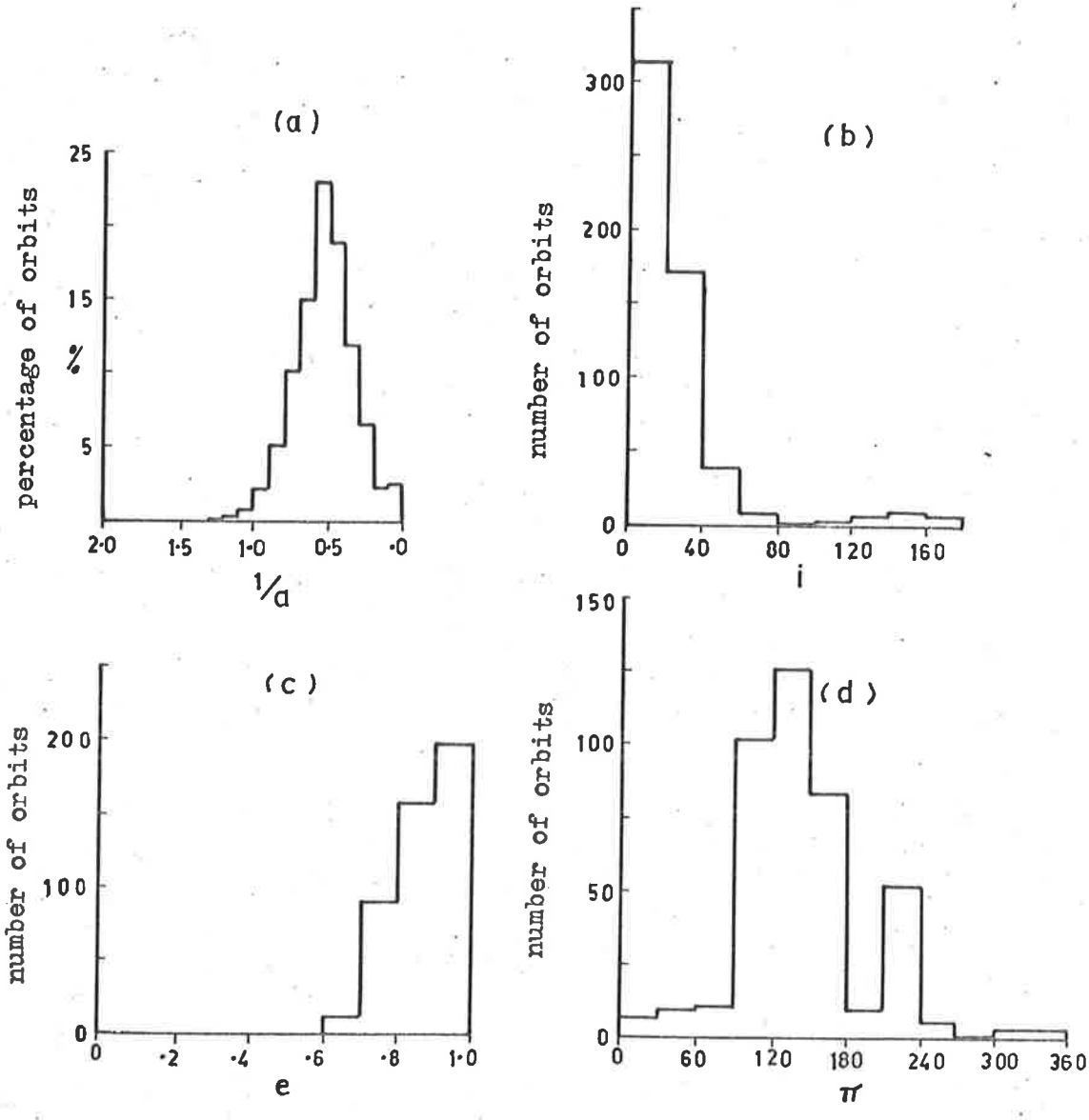

ORBITAL DISTRIBUTIONS FOR SHOWER METEORS

Figure 11.3

this range. The December Geminids make up the major part of the subsidiary peak at $210^\circ < \pi < 240^\circ$. The distribution (not shown) for the six months November to April alone has a slight maximum at $\pi = 180^\circ$, if the Geminids and November Taurids are excluded.

These distributions lead to an important query: there is a great deal of evidence to link the origin of shower meteors with short-period comets, and these comets and asteroids show a pronounced alignment of perihelia with Jupiter. Why, then is there no sign of a maximum in the vicinity of the perihelion of Jupiter (about 13°) in the distributions discussed above? In endeavouring to answer this question, we must ask whether the present observed distribution of perihelia for shower meteors is of real significance, or whether it varies with time according to the particular streams that intersect the Earth's orbit? This is discussed more fully in Chapter 13.

We have shown that the distribution of shower meteors in space is significantly different to the distribution of all meteors. This may indicate that either the origin or the evolution of these meteors is different. In Chapter 13 it is shown that most of the observed differences can be explained by postulating a more recent origin for shower meteors than for the sporadic background.

11.7 A Possible Cometary Association.

Porter (1952) lists 19 approaches of short-period comets within 0.1 a.u. of the Earth's orbit. Ten of these, including 1819 IV (McCrosky and Posen 1959) and 1917 I (Whipple 1954) have produced recognized showers. For 5 of the remaining 9 comets, meteor radiants have been predicted at declinations south of -20°, which is out of the range of the observatories making comprehensive photographic observations of meteors. It is of immediate interest to search the Adelaide data for any minor streams which may be associated with these 5 comets.

The meteor radiant, 31.3 in Scorpius in December corresponds quite well with the predicted radiant for comet Lexell 1770 I. Porter gives the predicted date as December 5, and the three meteors

in group 31.3 were detected on December 5, 6 and 7. The predicted radiant is $\alpha = 256^\circ$, $\delta = -25^\circ$, the mean for the group 31.3 is $\alpha = 248^\circ$, $\delta = -25^\circ$.

The values for ω and Ω do not agree very well. The comet was only sighted once, and some errors may be expected in the values of ω and Ω for the comet in view of the low inclination, but the extent of the differences would probably invalidate the association were it not for one fact. The comet underwent a close encounter with Jupiter in 1779 and moved into a fresh orbit in which the comet has since become unobservable. A similar encounter may well have altered the values of ω and Ω and also decreased the semi-major axis to the value observed for the three meteors of group 31.3. The eccentricity and inclination agree very well. Both sets of orbital elements are listed for comparison in Table 8. The approximate value of Tisserand's criterion T_c is given in the last column.

TABLE 8

	a	e	i	ω	Ω	π	q	T_c
Lexell I	3.16	.786	1.6°	224°	132°	356°	.674	0.50
Scorpids	2.6	.80	2°	264°	74°	338°	.50	0.55

The validity of the association will depend on the results of accurately calculating the secular perturbations suffered by both the comet and the meteors. If the association is genuine, the orbits of both should converge at some time in the past.

CHAPTER 12

METEOR STREAMS OF LOW INCLINATION

In this chapter some of the low-inclination streams are discussed, with particular regard to those that intersect the Earths' orbit twice.

12.1 Conditions Necessary for Double Intersection.

From Figure 1a it can be seen that an observable orbit in the plane of the ecliptic will intersect the Earth's orbit twice. In practice, because of the finite width of a meteor stream, one would also expect streams of low inclination to give rise to two showers throughout the course of a year. The limit of inclination for this to occur will depend on the accentricity of the orbit and the width of the stream in question. Figure 1b illustrates the close approach of a low inclination stream to the Earth's orbit. A necessary condition for the stream to be detectable is that the distance of closest approach, d, must be less than the radial width of the stream. It is shown later that the Southern δ-Aquarid stream of inclination 34°, which gives rise to a night-time shower in July and August, also intersects the Earth's orbit after perihelion passage as a day-time shower in June. The fact that a stream with such a high inclination can be observed twice is due to the high eccentricity of the orbit, 0.97, and the width of the stream, which is at least 0.45 a.u. The majority of the streams which give rise to two showers have inclinations less than 10°.

In 1940 Whipple first put forward the hypothesis that the October-November Taurid stream would encounter the Earth again in June, but as it would be coming from near the sun after perihelion passage, it would be invisible except as a few bright fireballs. His prediction was verified with the discovery of the June day-time streams by the Jodrell Bank radar group in 1947. Since then several day-time showers have been found that have their night-time counterparts later in the year; among these is the Daytime Arietid/δ-Aquarid pair mentioned above.

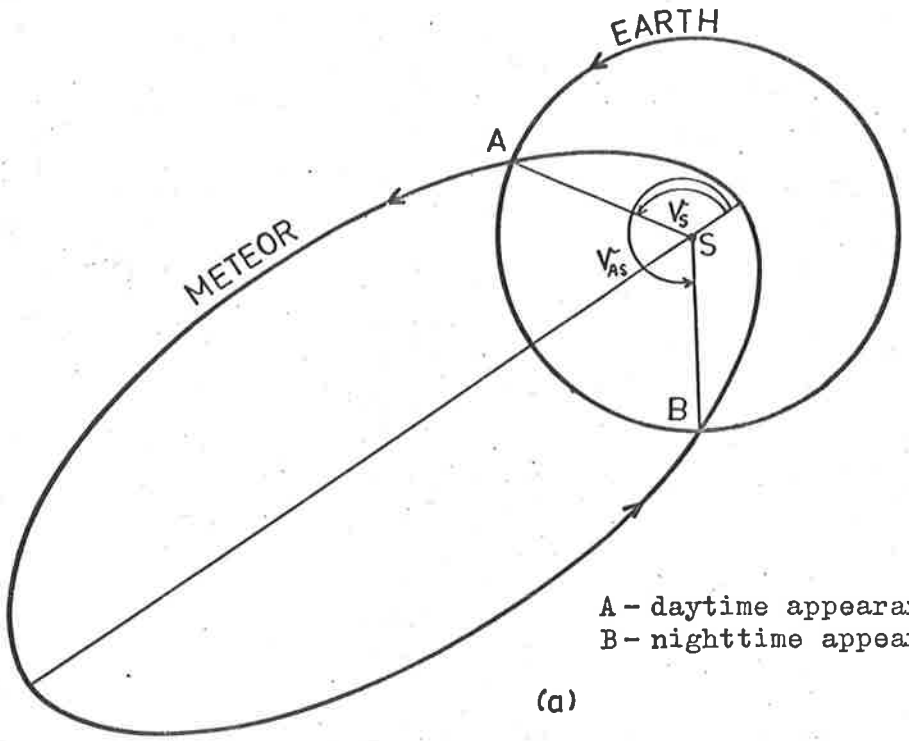
EARTH
A
METEOR
V_S
V_{AS}
S
B
A - daytime appearance
B - nighttime appearance
(a)

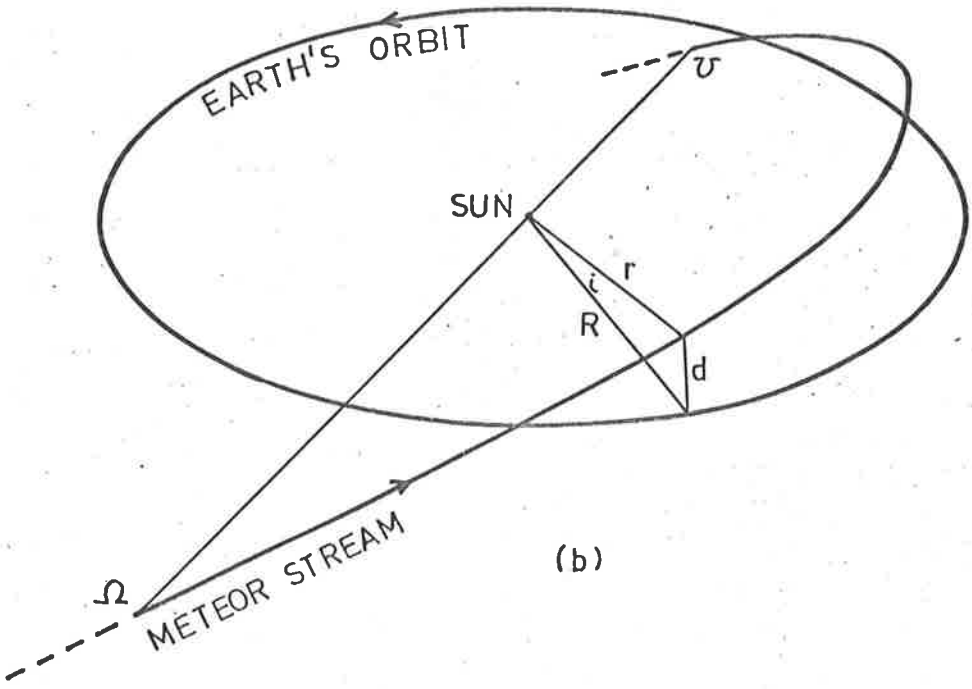
EARTH'S ORBIT
υ
SUN
r
i
R
d
Ω
METEOR STREAM
(b)

Figure 12.1

Before we examine the Adelaide results in detail for streams making two appearances, let us consider the factors that must be satisfied before classifying two groups of meteors as belonging to the same stream. The orbits must be of similar size, shape and inclination, and the theoretical time separation between showers must be satisfied. If the true anomaly of a day-time stream, i.e. a stream coming from near the sun, is ν_S, the measured true anomaly of the stream returning from aphelion passage should be given by

$$\nu_{AS} = 360^\circ - \nu_S \qquad \ldots (1)$$

assuming the Earth's orbit to be circular. With this assumption, the arc of the Earth's orbit between intersections will be given by

$$360^\circ - 2\nu_S$$

which is equivalent to a time difference of

$$52 - 0.29\,\nu_S \text{ weeks} \qquad \ldots (2)$$

For example, if a shower were observed from a low-inclination stream during the 9th week of the year with $\nu_S = 135^\circ$, we should expect its return on the 9 + 13 = 22nd week.

It must be emphasised that this time lapse between appearances has nothing to do with the time a meteor takes to traverse the orbit from A to B (Figure 1a), in fact, to observe a shower regularly twice each year is evidence of the uniformity of the distribution of meteoric matter along the orbit. If a shower only appears once and its strength fluctuates from year to year, we can draw inferences concerning its width and the uneven distribution of matter both across and along the orbit.

We can see then, that before we can say that two showers are associated with the one stream, the values of $1/a$, e, and i must be comparable, ν_{AS} must satisfy (1) and the times of occurrence must

satisfy (2).

12.2 The Daytime Streams in May and June.

In the previous chapter we considered some of the most prominent peaks in the monthly distributions of meteors with apparent heliocentric longitude relative to the apex of the Earth's Way. We found that the extra activity from the vicinity of the Sun in May was due entirely to shower meteors, as were most of the meteors comprising the very marked asymmetrical anti-Sun component from July to October. If the orbits of the two sets of meteors are examined, considering only those meteors which contribute to groups containing five or more orbits, a general similarity is immediately noticed. The bulk of the Sun orbits in May are inclined less than 20° to the ecliptic plane, and have eccentricities ranging from 0.7 to 1.0. The values of $1/a$ extend from 0.2 to 0.8, but the majority lie between 0.4 and 0.7 $a.u^{-1}$. Forty of the original 69 shower orbits in May have the true anomaly ranging from 110° to 135°. This corresponds to a period of between 13 and 20 weeks before the Earth should again intersect these orbits, i.e. the intersection should occur between August and mid-October.

An analysis of the anti-Sun component of the shower echoes over this period confirms that a large proportion of echoes have similar values for inclination, eccentricity and semi-major axis to the May Sun group. From a total of 235 shower echoes, 84 satisfied the conditions of $0.7 \leq e < 1.0$, $i < 20^{\circ}$, $0.4 \leq 1/a < 0.8$ and $225^{\circ} < \nu < 250^{\circ}$.

Thus we have shown that the May Sun group of echoes and a large part of the August to October anti-Sun group are due to an extended complex of low inclination streams with aphelia between Mars and Jupiter. A more detailed examination given below shows that these streams appear as daytime radiants in Pisces, Aries and Taurus in May and June, and nighttime radiants in the same zodiacal constellations during September and October. The variations in radiant activity from year to year shown by this complex must be due to the uneven distribution of meteoroids along the streams. The σ-Cetids, a May daytime stream delineated by Aspinall and Hawkins

(1951) are an example of this: the stream has not been detected in later years. The variations in radiant position shown by the October Taurid shower (Lovell, 1954) are also possibly due to the uneven distribution of meteoroids across the stream.

We shall now consider some aspects of the nighttime showers due to this stream. Wright and Whipple (1950) analysed 102 meteors photographed at Harvard between 1896 and 1948 covering the period October 15 to December 2. From this analysis they found two active radiants in Taurus, called the Northern and Southern Taurid streams, and two lesser centres of activity in Aries. These are likewise termed the Northern and Southern Arietids. However, there was some doubt as to the distinction between the Southern Arietids in October and Southern Taurids in November and they combined the data into one moving radiant. Data in the Adelaide radiant Table 11.2 and the detailed orbital elements of each group listed in Appendix 5 (radiants 25.1 and 29.1 respectively) support this suggestion of a single stream giving rise to these two showers. The two sets of orbits determined at Adelaide are similar in size, shape and inclination, although the values of 1/a for the Taurid meteors are a little less than those for the meteors coming from Aries in October. There is a difference of 7° in the true anomaly, but this could be characteristic of the width of the stream.

A further complication arises since both Whipple and Lovell (1954) have suggested that the Southern Arietid stream and the June daytime ζ-Perseids are either the same stream or closely related. So that the reader may follow the rather complicated pattern of names and associations, Table 12.1 has been compiled from the Adelaide data, listing the daytime radiants from near the Sun and their expected date of return. The associated radiants detected after aphelion passage, if any, are also listed. It can be seen from this table that the Adelaide data indicates a close resemblance between the ζ-Perseids (radiants 17.10 and 17.12) and the very active centre in Pisces (radiant 22.3) detected during September. The detailed orbital elements and the date of return all agree remarkably well. This survey is the first to recognise, and

TABLE 12.1

GROUPS THAT FORM COMMON STREAMS

Group	e	i	V_S	V_{AS}	Δt	t_{AS}	1/a	
14.3	.95	11	139	221	12	33	.2-.4	May Arietids
21.4	.91	6		230		32	.3-.5	S. ι-Aquarids
14.5	.85	6	126	234	16	38	.5-.6	May Arietids
17.10	.86	4	128	232	15	39	.5	June Taurids or ζ - Perseids
17.11	.85	12	125	235	16	40	.5-.6	
17.12	.79	6	124	236	16	40	.5-.7	
22.3	.82	5		235		39	.5-.6	Sept. Piscids
					ALSO			
17.13	.77	5	106	254	21	45	.4-.6	June Taurids
25.1	.80	6		245		43	.4-.6	Oct. S. Arietids
29.1	.85	9		252		46	.3-.4	Nov. S. Taurids
17.3	.98	18	158	202	6	30	.3-.5	June Arietids
17.4	.96	33	159	201	6	30	.7-.8	
17.5	.98	40	159	201	6	30	.3-.5	
21.8	.97	33		207		31	.3-.5	S. δ-Aquarids
5.2	.90	7	115	245	19	27	.2-.3	
21.1	.88	3		252		29	.2-.3	
21.1*	.87	4		250		29	.2-.4	
				POSSIBLE ASSOCIATIONS				
5.1	.86	10	138	222	12	20	.6-.8	
13.1	.88	8		236		21	.3-.5	
7.2	.82	10	134	226	13	24	.6-.8	
16.1	.81	6		243		24	.4-.6	

Group	e	i	V_S	V_{AS}	Δt	t_{AS}	l/a
14.4	.82	9	135	225	13	34	.6-.8
22.4	.85	6		222		38	.7
24.8	.79	4	111	249	20	7	.4-.6
2.1	.85	3		248		3	.3-.5

For the daytime showers:

Δt is the expected lapse of time (weeks) before the detection of any corresponding nighttime shower (in the t_{AS} week of the year).

For the nighttime showers:

t_{AS} is the actual week in which the shower is detected. This should equal the calculated value listed against the associated daytime shower.

TABLE 12.3

DAYTIME GROUPS THAT WERE NOT DETECTED AFTER APHELION PASSAGE

Group	e	i	V_S	V_{AS}	l/a	t_{AS}
7.1	.95	10	146	214	.4-.5	May 23
8.1	.82	3	116	244	.4-.5	Jul 18
8.2	.78	8	83	277	.3	Sep 26
9.2	.75	5	120	240	.6-.7	Aug 15
9.3	.82	6	116	244	.3-.4	Aug 22
19.3	.92	11	129	231	.3-.4	Nov 7
24.4	.93	8	147	213	.4-.6	Dec 5
24.5	.87	10	144	216	.8	Dec 5
24.7	.95	8	121	239	.1-.2	Jan 24
31.2	.95	6	124	236	.2	Mar 28
31.3	.81	2	96	264	.3-.4	May 23

possibly the first to see the intense activity from this quarter during September, which suggests that this activity is spasmodic or periodic in nature. In view of the previously accepted association between the ζ-Perseids and the Arietid-Taurid radiants, one immediately asks whether the new September Piscids may be part of the same stream. Certainly the values for eccentricity and inclination are similar, although the values for 1/a are greater. If one bears in mind the tendency of the October Arietid values to be slightly greater than the November Taurid values for 1/a, a discrepancy in the same sense between the Piscids and the Arietids does not exclude the former from association with the combined Arietid-Taurid stream. This infers that there is a tendency for the orbits to become larger as the Earth crosses the stream from September to November. However, this conclusion must be treated cautiously until the statistical significance of the differences is ascertained. In Section 11.2 we decided that the two September groups in Pisces, radiants 22.1 and 22.3, were from the same radiant, having been separated by a large range in the values of 1/a. If these are combined, the mean value for 1/a is 0.48 $a.u^{-1}$. If the October Arietids and November Taurids are combined, the mean value for 1/a is also 0.48 $a.u^{-1}$. Thus there may not be any significant discrepancy at all between the sizes of the orbits of the three radiants. A calculation of the correlation coefficient of 1/a for this pooled data with the position of the Earth in its orbit should answer this question.

From the data in Table 11.2 for the radiants 25.1 and 29.1 one can extrapolate the co-ordinates of the Arietid radiant in October and the Taurid radiant in November back to September 26 for comparison with the Pisces radiant. Assuming a uniform motion of the radiant with time, the right ascension and declination of the September radiant should be given by

$$\alpha = 44 - (63 - 44) \times 30/21$$
$$= 17^{\circ}$$

$$\delta = +11 - (14 - 11) \times 30/21$$
$$= +7^{\circ}$$

which is in good agreement with the radiant $17^{\circ}, +6^{\circ}$ observed for the Piscids. If we suppose the shift in true anomaly to be real over the 21 days between the Arietid and Taurid radiants, the extrapolated value for the Piscid radiant is given by

$$\nu = 245 - (252 - 245) \times 30/21$$
$$= 235^{\circ}$$

which is precisely the mean value observed. However, little weight can be placed on this result until the data have been examined statistically.

We have thus seen that there is a strong case for considering the radiants in Pisces during September, in Aries during October and in Taurus during November to belong to one and the same stream. Extending as it does over two months, it is not surprising to find that the daytime appearance of this stream is also of considerable extent. From Table 12.1 it is apparent that the group 14.5 in May is very similar to the groups 17.10 and 17.12 in June, the latter comprising the June ξ-Perseids. Another facet of this extensive stream is shown by the group 17.13. This Taurid radiant differs appreciably in right ascension and true anomaly from its closest subgroups, 17.10 and 17.12. However, the predicted return parameters for 17.13 agree quite well with those for the Southern Arietid-Taurid radiants 25.1 and 29.1, so on the basis of the previous discussion radiant 17.13 must represent a branch of the ξ-Perseids.

Further evidence of the changeable nature of the October nighttime streams comes from the list of meteor activity in the Southern Hemisphere published by Weiss (1957). In the data collected at Adelaide from 1952-1956 he observed an increase in the rate during October, but the only radiant he could isolate was at $\alpha = 102^{\circ}$, $\delta = +11^{\circ}$ with maximum activity on October 21. The

Jodrell Bank workers had also determined this radiant and given the co-ordinates as $\alpha = 98^\circ$, $\delta = +11^\circ$. There was no activity observed from this portion of the sky during the 1961 Adelaide orbit survey.

From the preceding discussion we can see that the complex picture presented by the daytime radiants in May and June is paralleled by a variable and long-enduring shower from September to November. The distribution of meteoroids must thus be decidedly non-uniform throughout the stream(s) to account for the variability in the relative strengths of the radiant groups from year to year. This variability is not surprising, for if we suppose the activity extending over two months is due to one stream, the width of the stream must be at least 70 million miles.

There are two other daytime showers in May which may be associated with nighttime showers late in the year. One of these is the group 14.4, the orbits of which resemble those of the September group 22.4. However, the predicted return is about four weeks before the detection of the latter, so the association is listed as doubtful. This may be revised when the new data groups from the analysis discussed in Section 11.3 are considered.

The group 14.3 appears to be significantly different from the ζ-Perseid/Southern Arietid group, the inclination is a little higher and the eccentricity is larger. The expected return parameters of this group of meteors coincide quite well with the Southern ι-Aquarids in August, group 21.4.

12.3 The Activity in Aquarius.

Lovell (1954) has suggested that the June daytime Arietids and the Southern δ-Aquarids in July and August are one and the same stream. The Arietid meteors referred to by Lovell have a mean radiant at $\alpha = 049^\circ$, $\delta = +27^\circ$, which corresponds to the groups 17.3, 17.4 and 17.5 in Table 11.2. These groups have accordingly been labelled the Arietids. However, there is a discrepancy in the values of inclination given by past workers when one tries to associate the δ-Aquarids with the Arietids. Lovell has quoted a value of $24^\circ \pm 5^\circ$ from the work of Miss Almond (1952) for the δ-Aquarid shower; this could be taken to agree with the lower

Arietid radiant 17.3, the mean value for the inclination of these orbits being 18°. McKinley, who also believes the daytime Arietids and the δ-Aquarids to belong to the same stream, quotes a value of 29° for the inclination of the latter, compared to 21° for the Arietids. The difference of 8° cannot be ignored, and it suggests that the streams are in fact separate. However the Adelaide data does not show this discrepancy in inclination, while retaining the hypothesis of a common stream. The Arietid groups 17.4 and 17.5 both have inclinations greater than 30°, the value for the group 17.4 of 33° agreeing very well with the mean value of 34° observed for the 52 δ-Aquarid meteors of groups 21.8.

The recent radio survey of Davies and Gill detected 35 meteors which they classed as δ-Aquarids; the mean value for inclination observed was 30°, in reasonable agreement with the Adelaide results. It is possible that the lower results of former workers are due to the inclusion of radiants closer to the ecliptic, such as the groups 21.4 and 21.6. We have identified these with the Southern ι-Aquarids. Adelaide is more favourably situated to study these southern radiants than are the Northern Hemisphere stations used in previous determinations, and the data from this survey comprises the most accurate direct orbital measurements of these meteors made to date.

It is interesting to compare the position obtained for the mean δ-Aquarid radiant with previous work in the Southern Hemisphere. Weiss (1960) made a careful study of the shower using a radar radiant equipment at Adelaide. He gave

$$\alpha = 342.2 + 0.77\ (\odot - 126.0)$$
$$\delta = -16.6 + 0.19\ (\odot - 126.0) \qquad \ldots \quad (3)$$

for the radiant co-ordinates, where $\odot$ is the solar longitude. McIntosh (1934), using visual observations made in New Zealand between 1926 and 1933, found a similar mean position for the radiant, but larger values for the mean daily motion. He determined the latter as 0.96° in α and 0.41° in δ.

A least squares fit to the data of group 21.8 gives

$$\alpha = 340.2 \pm 3.2^\circ + 0.76\ (\odot - 125.3)$$
$$\delta = -17.0 \pm 5.3^\circ + 0.27\ (\odot - 125.3) \qquad \ldots\ (4)$$

The tolerance given represents the 95% confidence level, i.e. $\pm 2\sigma\sqrt{1 - r^2}$, where σ^2 is the variance, and r is the correlation coefficient. If r is not significant at the 5% level, it is put equal to zero. In this case, the correlation with solar longitude was significant for each co-ordinate. In order to obtain the most accurate co-ordinates for the 1961 δ-Aquarid radiant, we also calculated the co-ordinates for the corresponding group of meteors that were associated into a group by the method discussed in Section 11.3. Forty-two meteors in one group were selected as belonging to the stream, 37 of which were common to both methods of selection. The mean radiant is given by

$$\alpha = 340.2 \pm 2.7 + 0.80\ (\odot - 125.6)$$
$$\delta = -16.9 \pm 5.6 + 0.35\ (\odot - 125.6) \qquad \ldots\ (5)$$

Once again, the daily motion of each co-ordinate was significant. It can be seen that the daily motion in α agrees with that given by Weiss, but the motion in δ is greater, although still less than the value given by McIntosh. The discrepancy in the absolute value of α compared to that obtained by Weiss is significant. Weiss estimated his error as $\sim 0.5^\circ$, and we can think of no obvious reason for this difference at this stage.

The mean inclination for the δ-Aquarid group corresponding to the radiant given by (5) is 32.6°, compared to 34.3° for the group 21.8. We can conclude that 33° is a representative value for this survey. The values for eccentricity and true anomaly for the δ-Aquarids agree well with the values for the daytime Arietid groups, and the mean value of 0.41 $a.u^{-1}$ for 1/a agrees reasonably with the values 0.39 and 0.47 $a.u^{-1}$ for groups 17.3 and 17.5 respectively. The mean value of 0.79 $a.u^{-1}$ for the group 17.4 was

the cause of these orbits separating from the other two groups, but as there are only three orbits it is possible that this division is invalid, and that the data should be pooled. The pooled mean value of $1/a$ for the three groups 17.3, 17.4 and 17.5 is 0.52 $a.u^{-1}$, appreciably, but not significantly, higher than that for the δ-Aquarids. The predicted date of return for the 30th week is quite compatable with the observed time of peak activity for the δ-Aquarids.

It remains to see how a stream with inclination greater than 30° could intersect the Earth's orbit at two places. The perpendicular distance from the ecliptic plane at any point in the orbit (Figure 1b) is given by

$$d = r.\sin i.\sin(\omega + \nu) \qquad \ldots \quad (6)$$

where r is the distance from the sun to the meteor. At the approach to the Earth's orbit after perihelion this can be approximated by

$$d = \sin i.\sin 2\nu_S \text{ a.u.} \qquad \ldots \quad (7)$$

which equals 0.45 a.u. for the δ-Aquarid stream. This is the distance from the Earth to the mean δ-Aquarid orbit at the time of the daytime Arietid shower in June. Now, Weiss (1960) has given the limits of detectable δ-Aquarid meteors as July 20 and August 15, a period of 26 days. The true elongation of the radiant from the Apex of the Earth's Way is 104°, therefore the width of the stream must be at least $26.1 \cdot 6.10^{6}.\sin 104^{\circ}$ miles, i.e. 42 million miles, which is 0.45 a.u. If we knew that the Earth passed through the centre of the δ-Aquarid stream, these figures would indicate that the daytime Arietids must belong to another separate stream, as the close approach distance given by (7) should be no greater than half the true width for a second intersection to take place. However, it is probable that the true width exceeds 0.45 a.u., in which case it is reasonable to assume that both showers are due to meteors from opposing sides of the stream. Thus it is quite possible that the

daytime Arietids, represented by the groups 17.3, 17.4 and 17.5, emanate from the same stream as do the δ-Aquarids. Unfortunately the Adelaide equipment only recorded over the last few days of the June Arietid activity, so it is not possible to determine the relative strengths of both portions of the stream. These figures could give a crude indication of the Earth's position with respect to the centre of this great stream, whose width must be at least half the distance between the Earth and the Sun.

We shall now consider another radiant in Aquarius, the three meteors comprising the group 5.2 in February. These could well be associated with the two meteors of radiant 21.1 in July, although the number of meteors detected is hardly significant. Confirmation of the February radiant can only come from radio data, as it is a daytime group. The list of southern radiants published by Ellyett and Roth (1955) does not include any that can be identified with radiant 5.2, neither do the lists of Weiss (1957 and 1960.a). The only other radio survey of orbits available is that of Davies and Gill, who have not published the details of the individual orbits. The list of photographic meteors of magnitude +3 recently published by McCrosky and Posen (1961) is of interest in confirming the pair 21.1 in late July. Three meteors from this list, numbers 8085, 8109 and 8110, compare favourably with the two of the Adelaide data, numbers 79747 and 84495. The five orbits are listed in Table 12.2

TABLE 12.2

	a	e	i	ω	π	q	α	δ	V_g
8085	2.5	.84	3	290	45	.39	305	-17	27.9
8109	2.8	.86	5	289	47	.39	308	-15	28.5
8110	2.6	.86	5	294	52	.36	310	-13	29.2
79747	3.3	.88	3	288	41	.39	302	-17	29.4
84495	3.5	.89	3	287	49	.39	312	-15	29.3
Mean	2.9	.87	4	290	47	.38	307	-15	28.9

McCrosky and Posen have classified meteor 8110 as a member of the Southern ι-Aquarid stream, but the value of 52° for the longitude of perihelion does not agree with the figure of 79° published by McKinley (1961), or the figure of 87° found for the group 21.4 which we have identified with this stream. Thus it seems that a minor stream does exist with a radiant at about $\alpha = 307^{\circ}$, $\delta = -15^{\circ}$ in late July. The mean parameters at the bottom of Table 12.2 are those of the pooled radio and photographic data, and have been listed in Table 12.1 as group 21.1*. They agree with those of group 5.2 better than do the parameters of the Adelaide data alone.

12.4 The Remaining Daytime Streams Observed During 1961.

Four pairs of radiants have been listed in Table 12.1 as possible associations. Although some of the parameters agree, there is sufficient discrepancy in at least one parameter to cast doubt on the association. There are twelve other daytime groups of low inclination for which there is no associated nighttime group recorded in the Adelaide data; nor do they match any of the well-known nighttime showers. These groups are listed in Table 12.3. The predicted dates of return after aphelion for two of these groups, 19.3 and 31.2, are for times during which the Adelaide equipment was not operating. Five of the remaining ten groups contain at least four meteors, and one (group 8.2) contains seven. The non-return of these groups can be taken as evidence of non-uniform distribution along the orbit.

CHAPTER 13

ASTRONOMICAL SIGNIFICANCE OF THE RESULTS

The detailed distributions of orbital elements have been presented in Chapter 10. We shall now discuss some aspects of the astronomical significance of these results, with particular regard to the results and conclusions of the other two comparable surveys, the radio survey of Davies and Gill (1960) and the photographic survey of McCrosky and Posen (1961). In order to compare these surveys it is necessary to further consider the distribution of orbits with size, shape and orientation. This leads to a discussion of the hypothesis that meteors have their origin closely linked to the short-period comets. The author concludes by suggesting that although shower meteors may originate with these comets, a large proportion of the sporadic meteors have probably originated in long-period orbits, and their origin may be related to the long-period comets.

13.1 The Magnitude of the Meteors Observed.

The photographic survey extended to a visual magnitude of +3, but the median value was +0.8. The Adelaide survey of meteors of radio magnitude +6 concerns fainter particles, while those detected by Davies and Gill at radio magnitude +8 are fainter still. The relation of radio and visual magnitude is complicated by the fact that both are dependent on velocity. McKinley has given a general formula for radio magnitudes in the range $-2 < M_r < 5$, which is

$$M_r = 36 - 2.5 \log q + 2.5 \log V \qquad \ldots \quad (1)$$

where q is the electron density along the trail*, and V is the velocity.

---

* McKinley has used the symbol q to denote electrons/metre. Previously, we have used α electrons/cm for the electron density along the trail, in accordance with the Jodrell Bank notation.

This equation was derived from combined photographic and radio observations of over 3,000 meteors, 1,400 of which were from the Perseid shower. (Millman and McKinley 1956).

The electron density q is a function of velocity. As we have seen in Chapter 8, the dependence on velocity arises from the probability that an evaporated meteor atom will produce a free electron. This probability is usually expressed as

$$\beta = \beta_o V^{\eta}.$$

Kaiser (1953) found that $\eta = 0 \pm 0.6$, and suggested that the visual brightness of a meteor may be expected to be proportional to $kv^3 \beta^{-1} \alpha_{max}$, where k(V) is the fraction of kinetic energy converted into light. Using Jacchia's assumption that $k \propto V$, Davies and Gill concluded that visual brightness varies as V^4 for constant α_{max}.

This corresponds to $\eta = 0$, which is not in agreement with the work done in America. Whipple (1955) has deduced from a comparison of photographic and radar velocity distributions that $\eta = 4$. Hawkins (1956) found that the ionization of bright Perseid and Geminid meteors indicated a value for η of 4.6, while recently the theoretical work of Lazarus (1962) showed that for velocities in excess of a threshold value of 7 km/sec, $\eta = 3.3$. These values indicate that brightness depends on a lower power of velocity than that accepted by Davies and Gill. As the exact magnitude of the meteors is not crucial to the following discussion, we shall simply note this uncertainty. The Adelaide distributions were corrected for selection for three values of η, $\eta = 0$, 2 and 4. In most

cases the form of the distribution is not markedly affected by the value chosen, and as the present evidence favours a high value, the corrected Adelaide distributions given in this chapter correspond to $\eta = 4$.

13.2 Reciprocal Semi-major Axis.

In comparing the orbital distributions obtained from the various surveys, it is convenient to begin with the distribution of meteors as a function of the size of the orbit. Figure 1 shows this distribution for four magnitude classes ranging from Whipple's bright photographic meteors to the radar results of Davies and Gill. Two facts are quickly apparent. First, the number of short period orbits increases with fainter meteors, and second, if we exclude the scattered histogram for the bright photographic meteors, the modal value for 1/a remains constant. McCrosky and Posen have also noted that in the progression to radar meteors the proportion of large orbits decreases. Whipple (1955) has suggested that rapid diffusion of the ion column of high altitude meteors inhibits their observation by radio techniques. The height of maximum ionization increases with velocity, hence the high velocity and presumably long period orbits will not be observed. The author would interpret the distributions of Figure 1 differently. In view of the constant modal value for 1/a it would seem that the decreased proportion of long period orbits in the radio data is due to the increased number of short-period orbits observed by radio techniques that do not appear in the bright photographic data.

This is made clear by comparing the distributions for the bright and faint photographic data. There can be no question of the radio echo ceiling applying to the latter, yet the proportion of long-period orbits for this data is much less than for the bright data. Apart from a small proportion of meteors with $1/a > 1.4$ a.u^{-1}, the Adelaide radio distribution is not significantly different from that of the faint photographic data. The Adelaide radio distribution given in Figure 1(c) does not include hyperbolic orbits (1/a negative in the other three distributions),

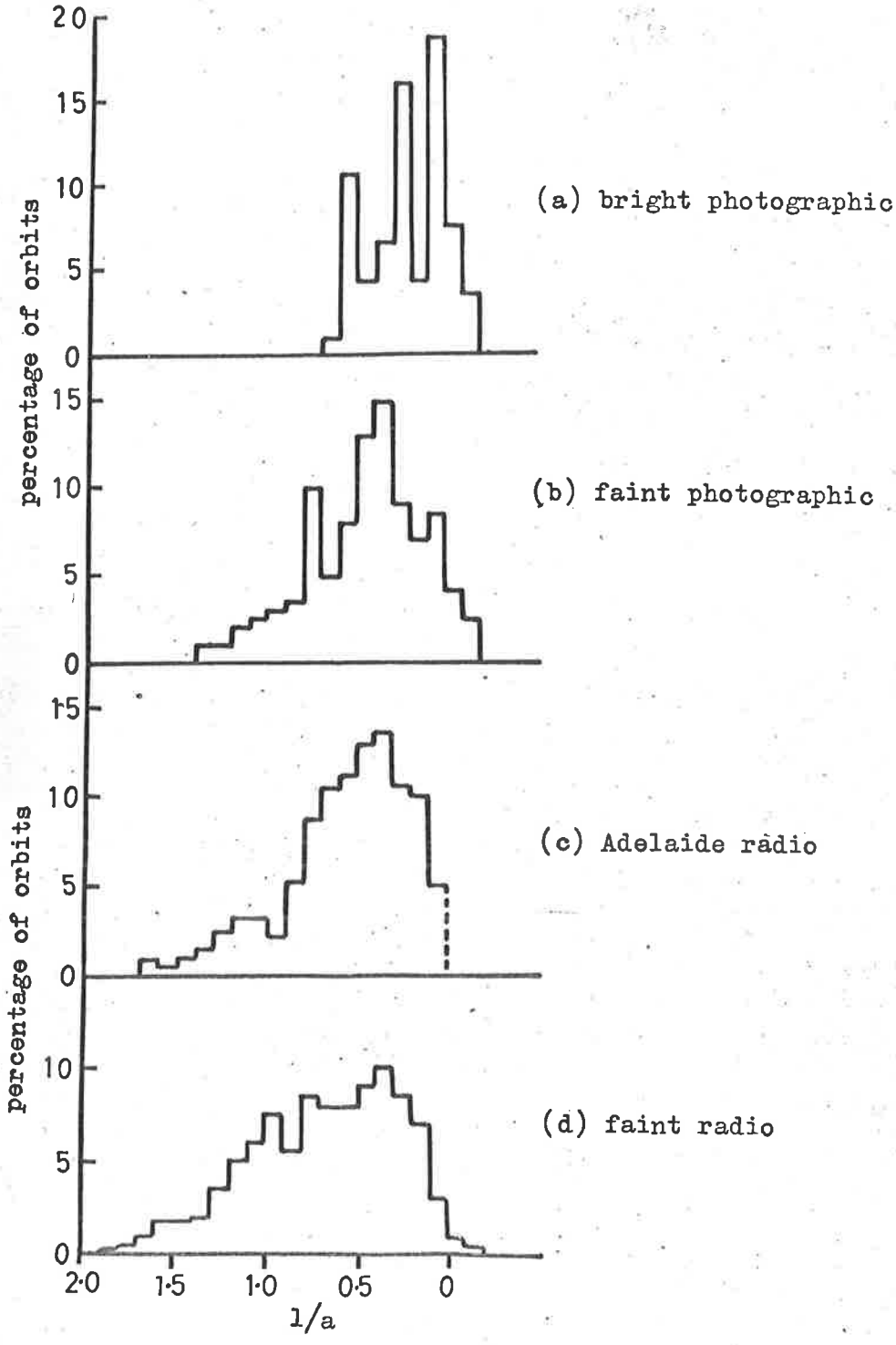

Figure 13.1 - Distribution of 1/a

but it can be seen that there is no significant difference in the distributions (b), (c) and (d) in the range $1/a < 0.5$. Had the radio echo ceiling effected the Adelaide data, the distribution for the faint radio data (d) should certainly show some evidence of this, as the height ceiling is lower for fainter magnitudes.

This is not to deny the reality of the theoretical velocity ceiling for faint meteors, however there is as yet no evidence for any serious selection imposed by this phenomenon. On the basis of the distribution with geocentric velocity observed in the Adelaide survey, we would expect a relative deficiency in the percentage of meteors with $V_g > 60$ km/sec in the surveys of fainter meteors if this mechanism were operative. Yet neither the orbital survey of Davies and Gill nor the velocity survey of McKinley (1951) show any such effect with respect to either the Adelaide radio survey or faint photographic survey. We can conclude that the lack of any significant number of hyperbolic velocities in the Adelaide data is real, and not due to observational selection.

13.3 Eccentricity.

The distribution with eccentricity is of interest. All four surveys show a very marked maximum in the vicinity of 0.9. There is a tendency for the number of orbits with low eccentricity to increase as fainter magnitudes are detected. The percentage of echoes with $e < 0.6$ for four surveys is given in the first two columns of Table 1. We have shown in Chapter 12 that all the Adelaide shower orbits have $e > 0.6$, and more than 99.5% of the faint photographic orbits likewise have $e > 0.6$, so in comparing the proportion of low eccentricity orbits in the various surveys, it is necessary to consider the percentage of shower orbits in each survey. These figures are given in the third column of Table 1.

The fact that the faint photographic data contains twice as many low eccentricity orbits as the Adelaide radio data is surprising, and cannot be explained by the quoted content of shower echoes, as the figures show that the shower percentage is similar for both surveys.

TABLE 1

	% of echoes e < 0.6		% of shower echoes
	obs.	corr.	
bright photographic	8	—	>50
faint photographic	25	25	18
Adelaide radio	12	11	22
faint radio	16	37	3

A comparison of the proportion of shower meteors is difficult, however, as the criteria used for shower membership were not the same in the different surveys. If a systematic search for echo groups in the data by Davies and Gill was made on the same basis as that outlined in Section 11.3, it is probable their figure of 3% would be increased. McCrosky and Posen believe their figure is an underestimate. There was a definite bias towards recording over shower periods during the last six months of the Adelaide survey, which would certainly raise the Adelaide percentage above normal. When these facts are considered it is reasonable to suppose a uniform decrease in the proportion of shower meteors with fainter magnitude, as has been suggested by Kaiser (1953). However, any differences in shower membership are not large enough to account for the difference between the number of low eccentricity orbits in the faint photographic data and the Adelaide radio data.

While selection factors are never above suspicion, the author cannot conceive of any that would cause this difference. Could it be that the two surveys have detected different families of meteors? An analysis of the echoes for which $e < 0.6$ confirms this suggestion. Figure 2 shows polar plots of the observed distribution of echoes with inclination for the Adelaide survey, the echoes having been divided into two groups, $e < 0.5$ and $e \geqslant 0.5$. The 1885 echoes in the latter class show the pronounced preference for low inclination direct orbits. The distribution for the 149 low eccentricity orbits is quite different. There are a few direct orbits within 10° of the ecliptic, but most of the orbits are

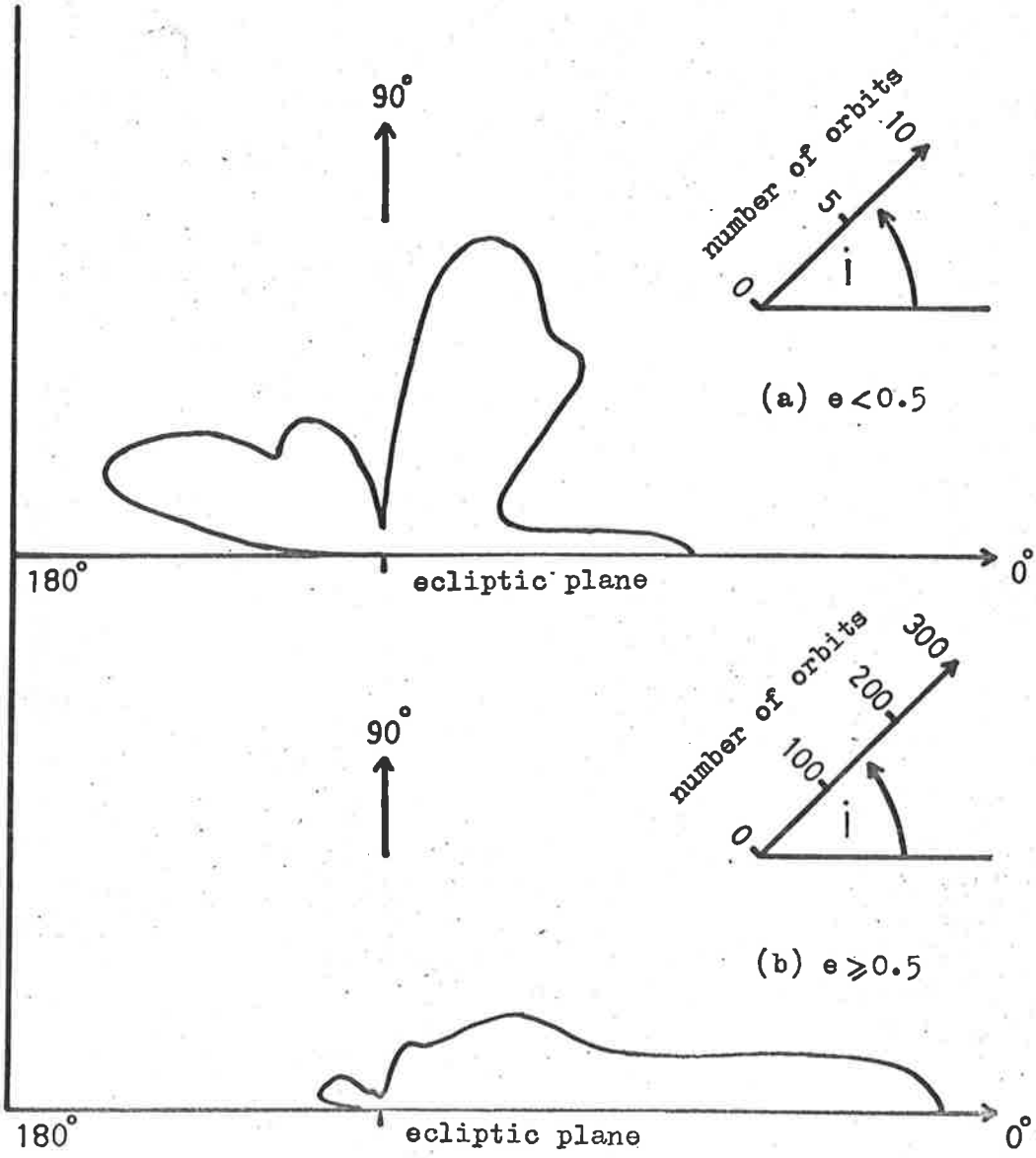

13.2 - Distribution of inclination

contained in two broad maxima centred at inclinations of 60° and 150°.

This is quite contrary to the distribution of low eccentricity orbits found for faint photographic meteors by McCrosky and Posen. The smaller and less eccentric their orbits were, the more pronounced the ecliptic concentration. The results of Davies and Gill for faint radio meteors confirms the Adelaide radio distribution. The faint radio meteors, with $e < 0.5$, show a pronounced bimodal distribution with inclination. The maxima occur at 60° and 140°. There is no doubt that the high inclination low eccentricity orbits of the Adelaide survey belong to the same family, as the distribution with aphelion distance for these orbits, given in Figure 3a, shows that all have $q' < 3$ a.u., as do the faint radio meteors. Hawkins (1962) has also found a family of low eccentricity, high inclination orbits in his current survey of faint radio meteors. He has termed these meteors the "toroidal group." His results at magnitude +8, however, do not show many retrograde orbits corresponding to the lobe at 150° in Figure 2a. The minor lobe of direct orbits centred on the ecliptic shown in Figure 2a must represent the contribution to the Adelaide data of the family of low eccentricity orbits detected by McCrosky and Posen. The fact that they did not detect the major lobes at $i = 60°$ and 150° indicates these meteors are only apparent at magnitudes fainter than +3. As the Adelaide survey corresponds approximately to visual magnitude +5, the mass distribution of these meteors must show a sharp upper limit. The Adelaide data is still being reduced for estimates of the mass of each meteor detected; it will be of great interest to see if the mass distribution obtained for these orbits displays a significant sharp cut-off at the appropriate mass level.

To examine these orbits more fully the distribution with perihelion distance q is shown in Figure 3b. This shows that the cut-off at $q' = 3$ a.u. in Figure 3a is due to the fact that we cannot detect meteors with $q > 1.0$ a.u. by earthbound techniques. These families of low eccentricity orbits probably extend out much further from the sun than 3 a.u.

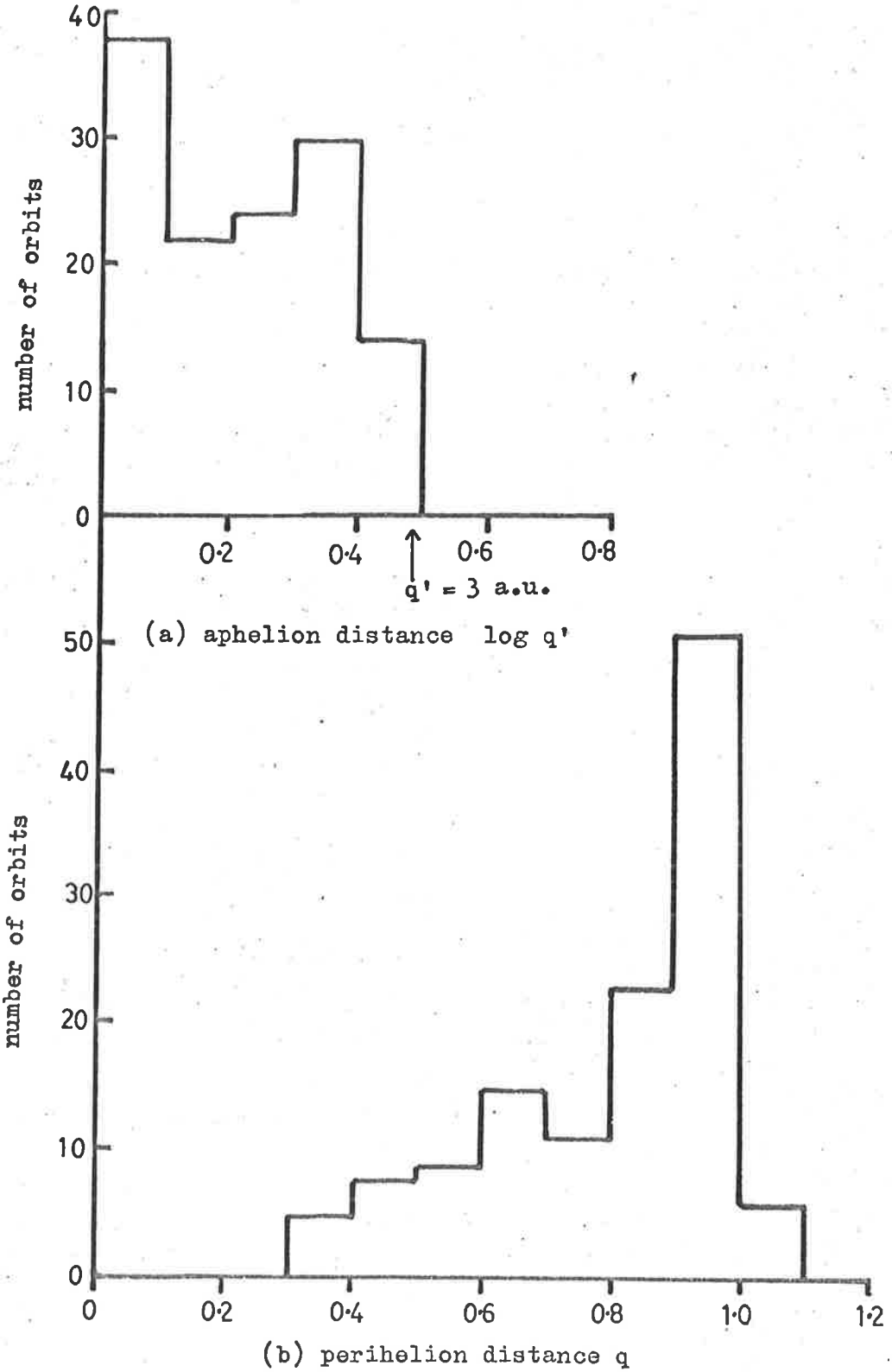

Figure 13.3 - Distributions of low eccentricity orbits, $i > 30^{\circ}$

13.4 Perihelion and Aphelion distance.

The observed distribution with aphelion distance is shown in Figure 4a. The accuracy of the data is insufficient to place much reliance on individual values of large aphelion distance, but the distribution should be valid to at least q' = 10 a.u. At this point the number of orbits is approximately 30% of the peak value which occurs at 3.6 a.u. The distribution of McCrosky and Posen for faint photographic meteors also shows a maximum at this point, although both the observed and weighted distributions fall to less than 10% of the peak value by q' = 10 a.u. Contrary to the fears that the radio data might exclude the long orbits through observational selection, this data includes more very long orbits than that of McCrosky and Posen. The true significance of this will be better known when the estimates of meteor mass are available, and the distribution has been corrected for observational and astronomical selection. The peaks of both the photographic and radio data lie inside the semi-major axis of Jupiter, which is 5.2 a.u. Beyond this distance both distributions continue to decrease. A decrease beyond Jupiter is not unexpected if the meteor distribution has evolved over sufficient time to allow the Poynting-Robertson drift to contract the orbits. This drift towards the sun results from a combination of radiation pressure and relativistic considerations, and was first considered by Poynting (1903) on a classical basis. Robertson (1937) found that the time taken for a particle of meteoric size, radius a cm, density ρ gms/cm^3, to spiral into the sun from a circular orbit, radius R a.u., is given by

$$t = 7{\cdot}0.10^6 a \rho R^2 \text{ years} \qquad \ldots \quad (1)$$

Now for a spherical particle, $a\rho$ can be simply replaced by $3/G$, where G is the surface area/mass ratio discussed in Section 6.2. The results of this survey have indicated a value of $\sim$ 25 cm^2/gm for G, hence (1) can be written

$$t = 2{\cdot}1.10^7 R^2/G \text{ years} \qquad \ldots \quad (2)$$

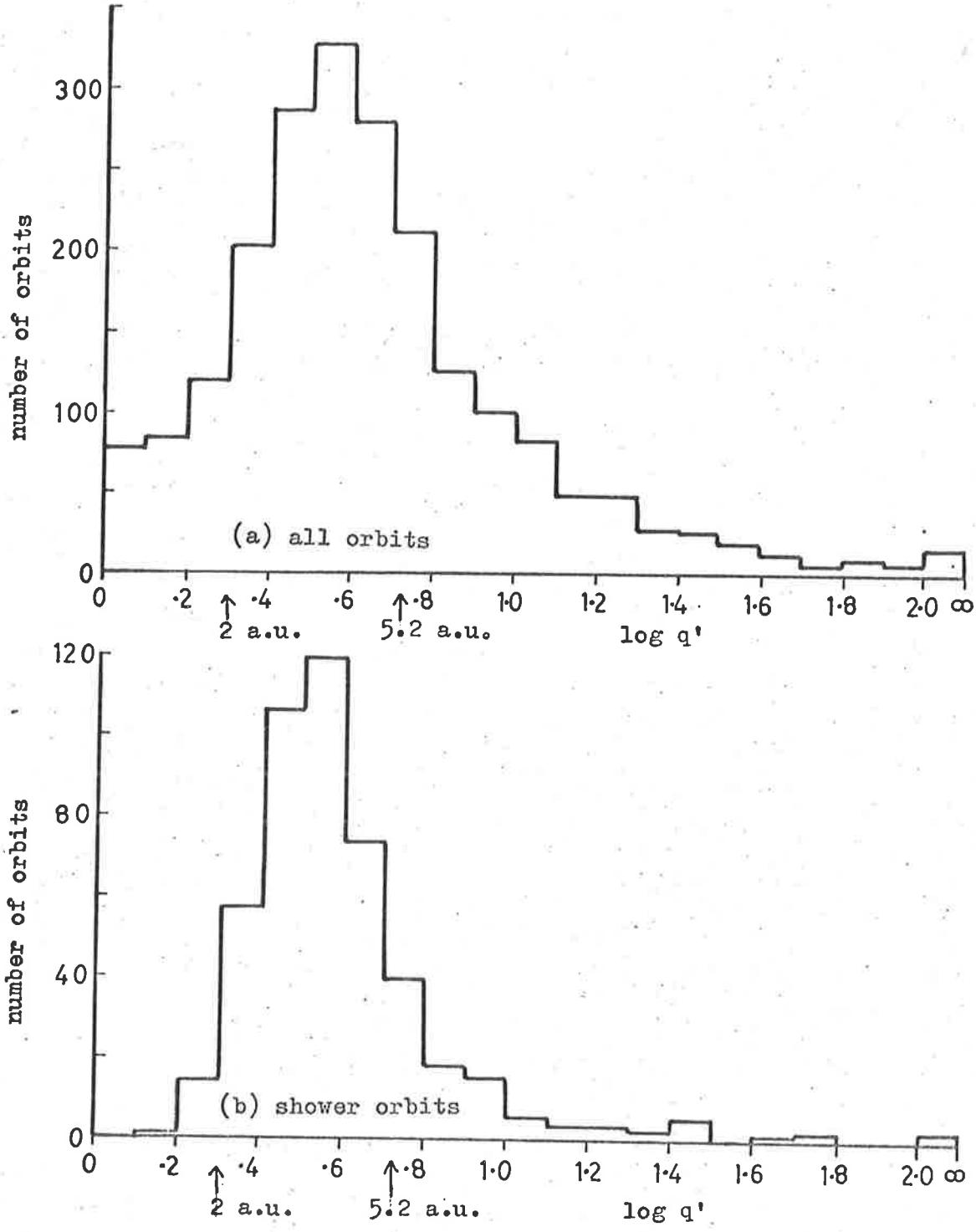

Figure 13.4 – Distribution of aphelion distance

$\simeq 10^6 R^2$ years for meteors of about radio magnitude +6.

The first effect of the drift on elliptical orbits is aphelion contraction, but gravitational attraction by Jupiter would tend to prevent the aphelia of low inclination orbits from contracting to much less than 5 a.u., thus giving rise to a family of low inclination orbits similar to that observed for the short period comets. This would apply particularly to the bright meteors, for which the Poynting-Robertson drift rate is less. However, the peak of the distribution for comets occurs at 5.2 a.u. (Porter 1952), whereas the peak of the meteor distribution is well inside Jupiter's orbit. The reason for this difference is not yet understood, but may become clear if an attempt is made to predict a steady state distribution of meteors in a manner outlined later in Section 13.7.

The distribution of aphelion distance for shower meteors only is shown in Figure 4b. It is evident that the distribution is much sharper than that for all meteors and lacks small orbits for which $q' < 2.0$ a.u., and also long orbits, for which $q' > 10$ a.u. It is possible that the lack of large orbits indicates that this section of the data is unreliable and hence groups would tend to be excluded by the association tests discussed in Section 11.3. However, this criticism cannot apply to the lack of shower orbits with small aphelia, which must represent a true difference between shower meteors and the total distribution. The sharp cut-off in the observed distribution for all echoes at $q' = 1.0$ a.u. indicates that there are many smaller orbits that lie within the earth's orbit. We would expect few of these to have high values of eccentricity, as the Poynting-Robertson drift would quickly contract any such orbits into the sun. Consideration of the orbits for which $q' < 2.0$ a.u. confirms this effect, as 44% of these echoes have $e < 0.6$, compared to an overall survey figure of 12%.

From equation (2) we can see that it would only take about one million years for a meteor of radio magnitude +6 initially travelling in an orbit similar to that of the earth of spiral into the sun. This is a very short time, astronomically speaking, and

the effects of this phenomenon should be noticable in our observed distributions. The space in the neighbourhood of the sun will not be empty, as it will be continually replenished by the contraction of larger orbits. In view of the R^2 term in (2), however, an initially uniform distribution may show some deficiency close to the sun, particularly in high eccentricity orbits. At first sight the distribution with aphelion distance for shower echoes might be taken as evidence for this effect, as these echoes all have $e > 0.6$ and there is a significant lack of orbits for which $q' < 2.0$. But we cannot necessarily assume that the shower orbits represent a random sample of high eccentricity orbits. A better approach is to study the distribution with perihelion distance for a particular range of eccentricity, such as that shown in Figure 5a for $0.8 < e < 0.9$, which includes both shower and non-shower meteors. A necessary condition for observation is $q' \geqslant 1.0$ a.u., and for any given value of e this means the minimum possible value of q is $\frac{1 - e}{1 + e}$ a.u. For $0.8 < e < 0.9$ the observational limit of q lies between 0.05 and 0.11 a.u. Thus to examine the effect of the Poynting-Robertson drift we can only study that part of the distribution for which $q > 0.11$ a.u. Figure 5a does show a peak at about 0.25 a.u., but as this distribution has not been corrected for selection it is necessary to estimate what effect this correction may have.

The correction for astronomical selection (Section 8.5) can be approximately transformed to

$$W = \frac{\sin i}{V_g} \cdot F(e,q) \qquad \ldots \quad (3)$$

where $$F^2(e,q) = 2.0 - \frac{(1-e)}{q} - q(1+e) \qquad \ldots \quad (4)$$

and W is the weighting factor.

In a simplified approach, let us consider separate ranges of perihelion distance, q. The observed median values of V_h and i are

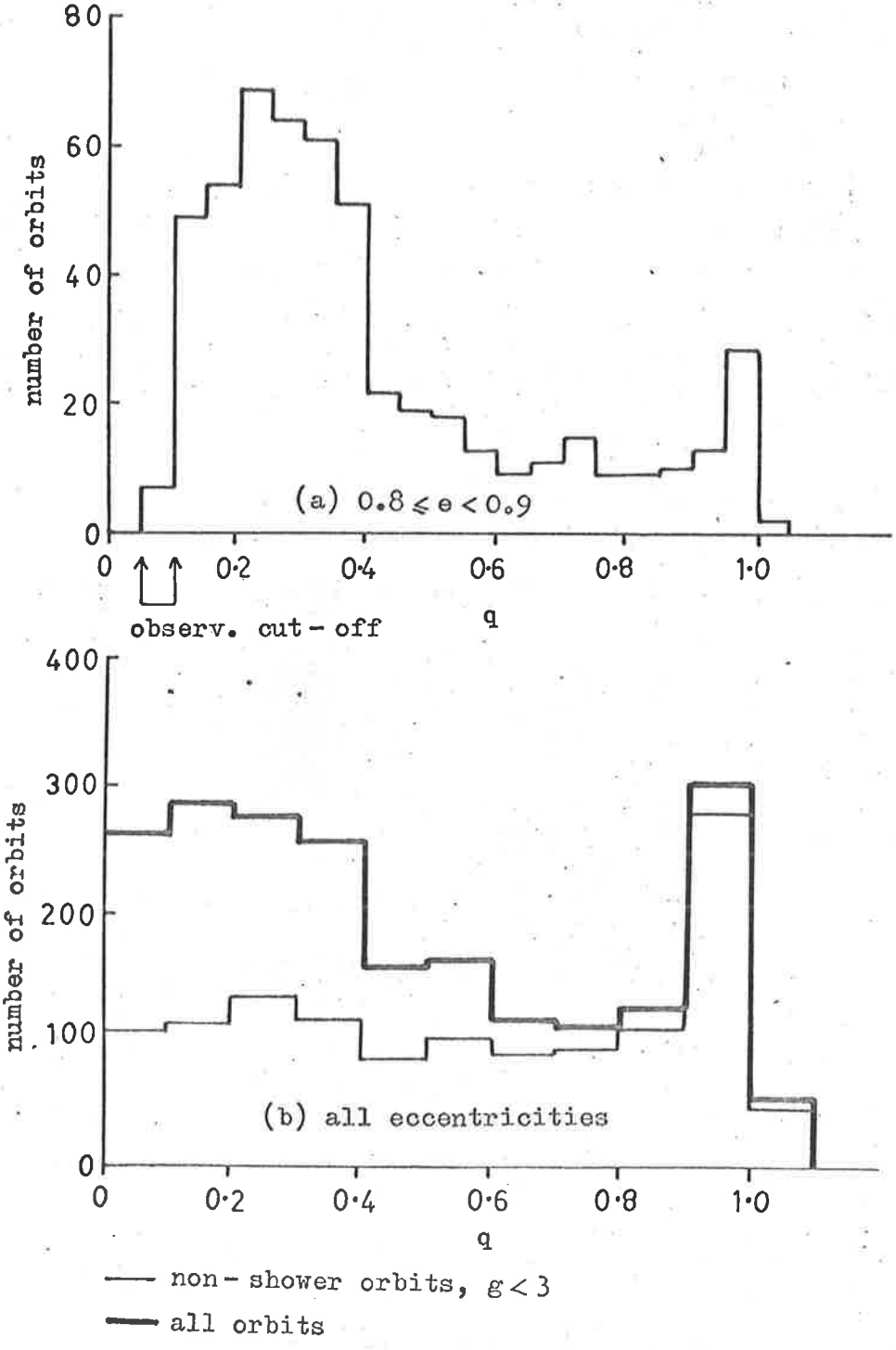

Figure 13.5 - Distributions with perihelion distance

given in Table 2.

TABLE 2.

q	V_h	i	F	W
.1-.2	31.8	20°	.85	.91
.2-.3	35.1	9°	.97	.44
.3-.4	37.2	8°	.96	.36

The values for F and the weighting function W, are calculated for q = 0.15, 0.25 and 0.35 a.u. respectively. The heliocentric velocity V_h increases with q, so that correction for observational selection will probably decrease the weighting factor still further as q increases from 0.1 to 0.4. Hence it can be seen that the decrease in the observed distribution as q is decreased from 0.25 to 0.1 a.u. can more than be accounted for by observational and astronomical selection. It would be unwise to comment further until an accurately corrected distribution is available.

The distribution for all values of eccentricity for all the meteors and non-shower meteors only is given in Figure 5b. Davies and Gill have not published their distributions with aphelion and perihelion distance, but McCrosky and Posen found that both the observed and weighted distributions are linear with q if the shower echoes are neglected. They state that this relationship holds for both long and short orbits, with a slight departure from linearity in the vicinity of Venus (0.72 a.u.). This departure does not seem significant, in view of the scatter in this distribution which is shown in Figure 6a. What is immediately noticable, of course, is that the Adelaide distribution decreases with perihelion distance, whereas both the observed and weighted distributions of McCrosky and Posen increase! Removal of the shower meteors from their data does not greatly effect the form of the distribution, although it does remove the large peak near q = 0.1 a.u. The peak in the observed distribution at q = 1.0 a.u. is due to the high probability of

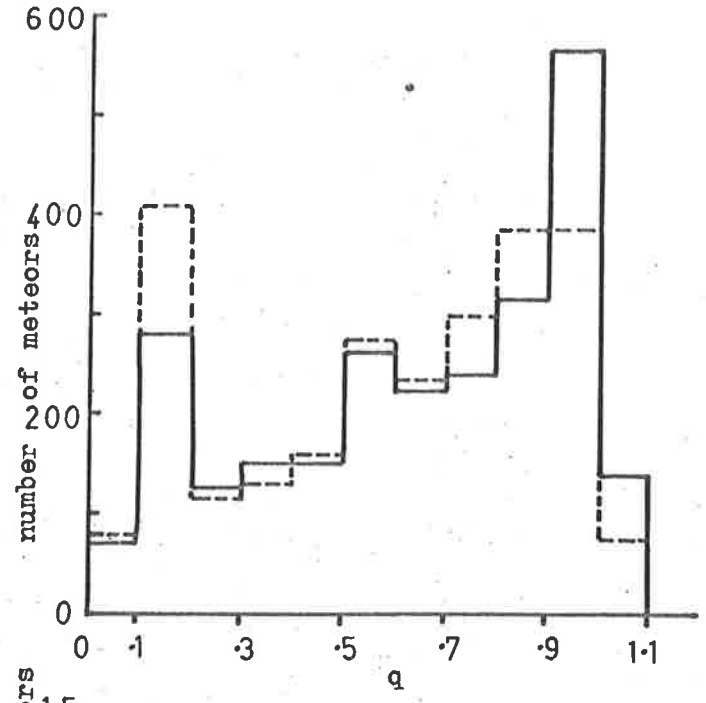

(a) faint photographic

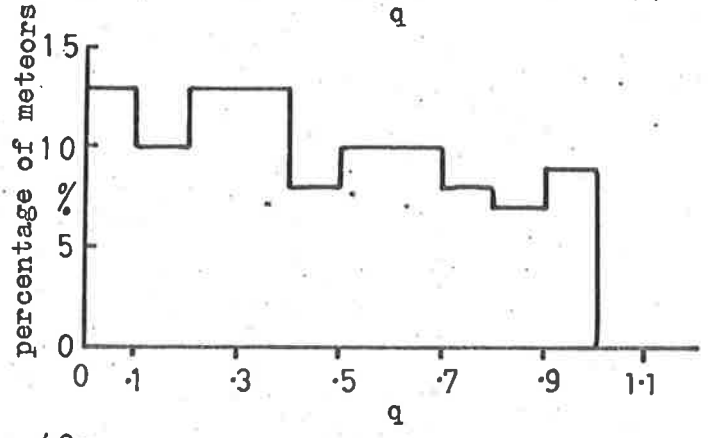

(b) Adelaide radio, weighte
non-shower orbits only

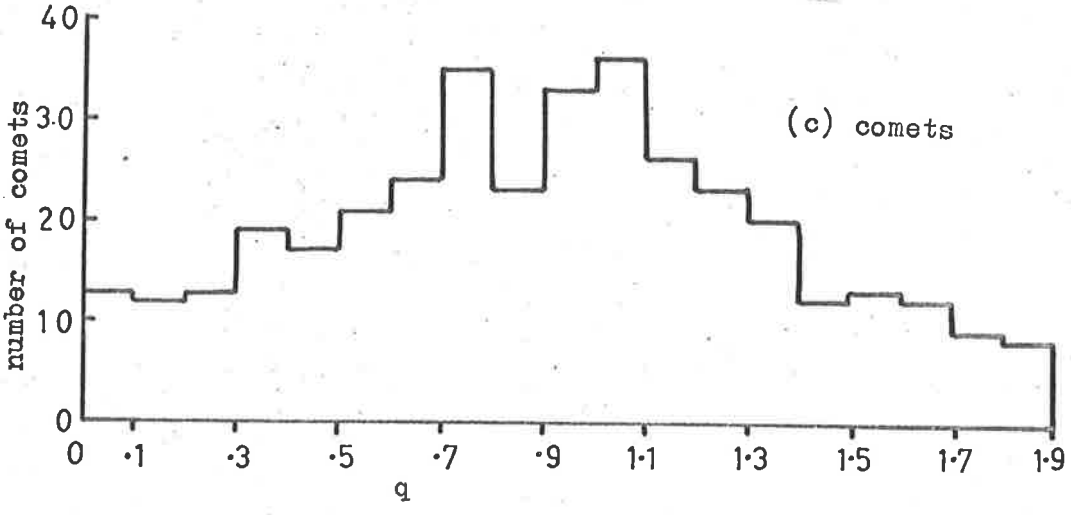

(c) comets

Figure 13.6 - Distributions with perihelion distance

detecting meteors at perihelion, and does not appear in the weighted distribution. In the case of the Adelaide data the removal of the shower echoes certainly has a significant effect on the distribution. It is obvious that shower meteors show a strong preference for small perihelion distance. However, there is still no tendency for the numbers of non-shower meteors to increase with perihelion distance.

In order to estimate the effect of astronomical selection on this distribution, the procedure previously outlined in this section, for calculating the weighting factor from equation (3) for a limited range of eccentricity, was used. The median values of e, i and V_h for each class group of q are listed in Table 3. The distribution corrected in this manner is shown in Figure 6b. It is probable that the mean values for sin i have been overestimated by use of the median value of i; this applies particularly for the groups $q > 0.5$ a.u., as the number of retrograde orbits increases with q, corresponding to the increasing number of low eccentricity orbits. However confidence in the approximate astronomical weighting procedure is given by the reduction of the peak at $0.9 < q < 1.0$ a.u. to a level which follows the general trend of the distribution, as was the case for the photographic results. It is difficult to estimate in any simple manner the probable correction for observational selection, but in view of the median values for e, i and V_h it should not be great.

We have shown that there appears significant decrease in numbers of orbits with increasing perihelion distance; however, because of the pronounced tendency for shower echoes to have small values of q, we cannot be sure that the negative slope of the distribution is not due to incomplete removal of the shower orbits. Thus, in discussing the non-shower content only, we cannot definitely say that there is any significant dependence of echo numbers on perihelion distance. Without further information it is difficult to reconcile this result with that of McCrosky and Posen. There are two possibilities: either the difference represents a real variation with meteor magnitude, or it is due to inadequate correction for

TABLE 3

q	number of orbits	e	i	V_h	W	W.N%
.0	108	.96	38	34.0	1.9	13
.1	111	.90	28	34.7	1.4	10
.2	135	.87	34	35.4	1.6	13
.3	118	.85	42	37.3	1.7	13
.4	85	.75	41	36.1	1.5	8
.5	103	.77	50	37.6	1.6	10
.6	90	.70	67	36.9	1.7	10
.7	93	.76	67	38.8	1.4	8
.8	110	.67	68	37.9	1.0	7
.9	279	.67	70	38.5	0.5	9
1.0	49	.67	54	38.2	0	0

This table gives the distribution with perihelion distance, q, approximately corrected for astronomical selection. The values of e, i and V_h given are the median values for each class interval of q. The last column, W.N%, gives the normalised product of the weighting factor, W, and the number of orbits, N.

McCrosky and Posen noted that for the photographic meteors, the trend of the distribution with perihelion distance agreed with that obtained from the observations of 369 comets with $q < 1.9$ a.u., discovered since 1800, which are listed in the Baldet and De Obaldia catalogue (1952). This distribution is shown in Figure 6c. From an analysis of cometary brightness as a function of q, they concluded that the observed distribution can be accepted as a true distribution out to 1 a.u., except for very small q.

Davies and Gill have unfortunately not published either the distribution with perihelion distance or the detailed orbital elements for each meteor, so that the data for faint radio meteors is not yet available. If their distribution with perihelion distance is similar to that obtained by this survey, and the difference between the Adelaide results and the photographic data cannot be explained by the forthcoming mass distributions for the Adelaide data, then the question of observational selection for the photographic data must come under review. It will be necessary to examine the observational procedures for bias against small perihelion distance. Any such bias could well affect the distributions for both comets and meteors, as both sets of data are obtained photographically in a nighttime sky.

When the Adelaide data are accurately corrected for observational selection, and the additional information on the mass of each meteor is included, a careful study of the way in which the numbers of meteors in different ranges of mass, inclination and other parameters vary with perihelion distance should prove of considerable value in assessing the evolutionary processes acting on the meteoric matter in the solar system.

13.5 Line of Apsides.

The distribution of orbits of meteors with the direction of the line of apsides is of considerable interest, as the data displays a completely different alignment to that of the short period comets and asteroids. Both these classes of bodies have at one time or another been proposed as the source of meteoric material, and

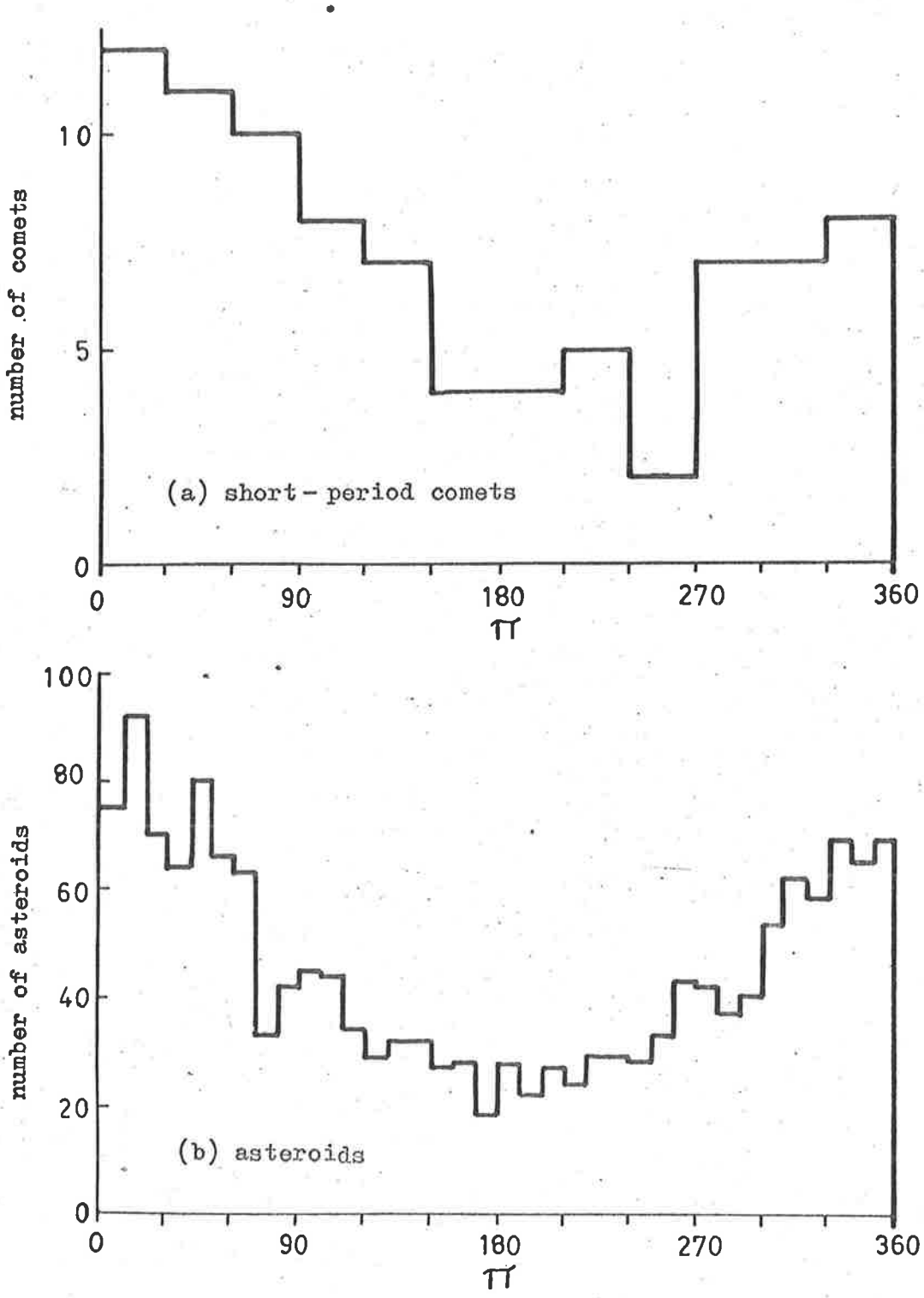

Figure 13.7 - Observed distributions of line of apsides

thus one might expect a general similarity in the alignment of the perihelia. The line of apsides is usually a difficult element to perturb, as is shown, for example, by Encke's comet and the complex Taurid stream. Whipple and Hamid (1950) have been able to show that a common origin is probable for this comet and meteor stream, although the inclination of the meteor orbits now differs by as much as 10° from that of the comet. The detailed orbital elements for the Taurid stream components and Encke's comet are given in Table 4. The values listed are those given by McKinley (1961).

TABLE 4

	P	e	i	ω	Ω	π	q
β-Taurids	3.3	.85	6	246	276	162	.34
S-Taurids	3.5	.84	5	112	45	157	.37
N-Taurids	3.1	.85	3	298	222	160	.32
1544 IX Encke	3.30	.847	12.4	185.2	334.7	159.9	.338

For low inclination orbits, the longitude of perihelion, $\pi = \omega + \Omega$ can be taken as defining the direction of the line of apsides, and it can be seen that this has remained relatively constant, although ω and Ω have changed considerably.

The distribution of longitude of perihelion for short-period comets is shown in Figure 7, together with the distribution for asteroids. The similarity is quite marked, each distribution having a minimum near 200° and a maximum coincident with the longitude of Jupiter's perihelion at 13°. The distribution for meteors is quite different. This is shown for the uncorrected Adelaide data in Figure 8, and the corrected photographic data in Figure 9. Any action of Jupiter on these distributions should be most noticeable for orbits of low inclination and aphelia of about 5 a.u. Accordingly, the distributions have been divided into three classes, all with inclination either less than 30° or greater than 150°:

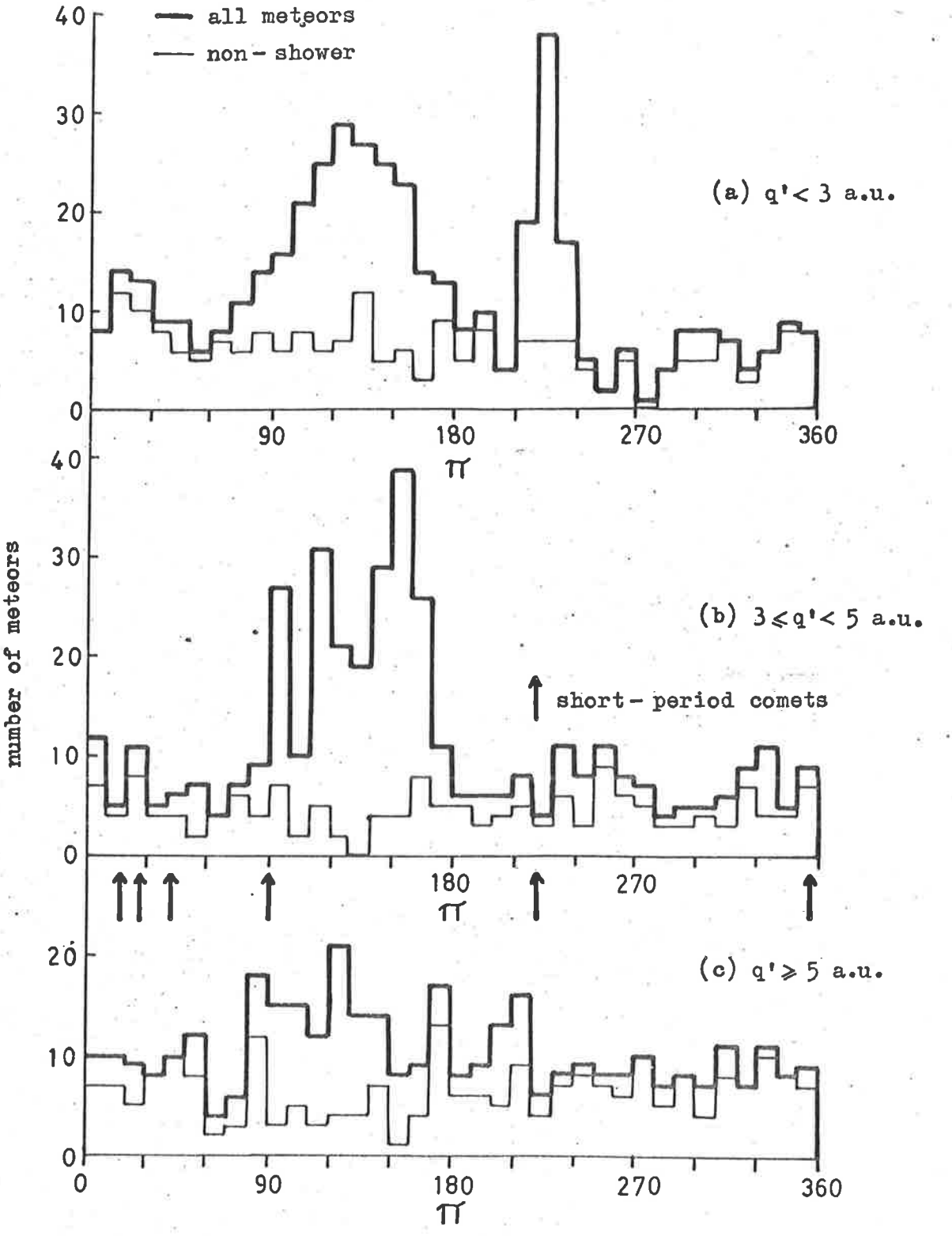

Figure 13.8 - Observed distributions of line of apsides

(1) $q' < 3$ a.u.

(2) $3 < q' < 5$ a.u.

(3) $q' > 5$ a.u.

No photographic distribution corresponding to $q' > 5$ a.u. has been published.

McCrosky and Posen went to considerable trouble to weight their distributions for observational selection. This is severe in the photographic data, as the longitude of perihelion is strongly dependent on the time of the year, and during the months June-August the observations were limited by short nights, low elevation of the ecliptic and bad weather. The Adelaide data has not yet been corrected, but although the recording was not entirely uniform throughout the year, radio observations are of course independent of the length of night and bad weather. From the theoretical response as a function of radiant declination given in Figure 10.23, it is evident that the sensitivity to low inclination meteors reaches a peak in February and October. There is certainly no excess of meteors in February, and the increased activity in October can be accounted for by the Taurid stream. The longitude of perihelion also depends on the argument of perihelion, ω. The Adelaide distribution with ω alone has been corrected for both observational and astronomical selection. The distribution is bimodal in each case with a deep minimum at 180°. As there is little difference in the corrected and uncorrected distributions with ω, we can reasonably assume that correction for selection will not alter the main features of the distribution with π.

In order to note the effect of showers on the total distributions given in Figure 8, the distributions have also been given for the non-shower meteors. It is obvious that there is no statistically significant variation with π for the uncorrected non-shower orbits. The large peaks in the total distributions for $q' < 3$ and $3 < q' < 5$ a.u. are entirely due to shower meteors. It is interesting to note that these two total distributions show little similarity with those obtained from the weighted photographic data, although both sets of data have a broad maximum in the vicinity of

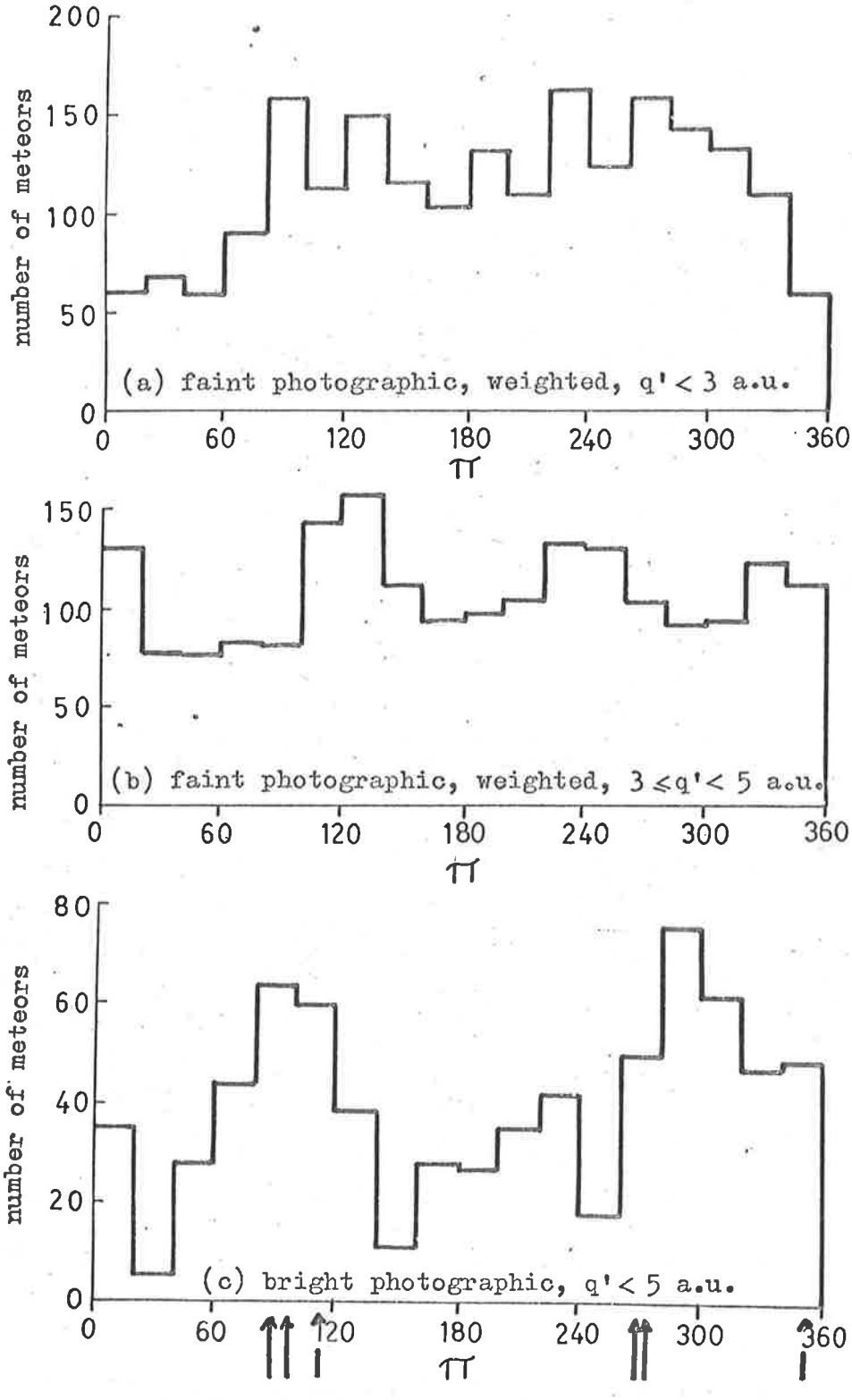

Figure 13.9 - Distributions of line of apsides

$90^\circ < \pi < 130^\circ$, and neither show a significant peak at the longitude of Jupiter's perihelion, 13°. There is a tendency for the photographic distributions to be bimodal, but the Adelaide radio data does not show this trend to any significant degree.

We have also included the distribution for 106 bright photographic meteors with $i < 30^\circ$ and $q' < 5$ a.u. accurately reduced by Jacchia. McCrosky and Posen state that this distribution, given in Figure 9c, shows the same general features as their distribution for faint meteors, and so confirms the reality of the latter. This claim is not evident from an examination of these distributions: the maxima are significantly displaced and the ratio of maximum to minimum is several times greater for the bright photographic data. This latter feature is consistent with the observation that showers are more prominent among the brighter meteors, and so will cause the distribution to display more significant peaks. The maxima for the group $3 < q' < 5$ a.u. in the faint photographic data (Figure 9b) are not significant.

The manner in which all the significant features disappear from the Adelaide radio data when the shower echoes are removed supports the hypothesis of McCrosky and Posen that the distribution by the line of apsides of meteors varies with time, and is dependent on the showers observed. They also suggest that the distribution is related to the distribution of the elements of comets that chance to approach close to the earth's orbit. In support of this they have considered the values of π for 18 short-period comets that approach within 0.1 a.u. of the earth's orbit as listed by Porter (1952). Six of these have $i < 30^\circ$ and corresponding theoretical meteor radiants north of $\delta = -20^\circ$; the values of for these are indicated with arrows in Figure 9c. For completeness we have indicated in Figure 8b the values of π for 6 close approach comets with $i < 30^\circ$ or $> 150^\circ$ with corresponding radiants that could have been detected by the 1961 Adelaide survey. Owing to the sparse nature of the cometary data, and also to the fact that the meteor data was collected over one year only, it is not surprising that no correlation exists between these values and the distribution.

Indeed, we have already noted that short-period comets show a strong perihelion alignment with Jupiter, which is not in evidence in the meteor results.

We have now discussed in some detail the distributions of lin of apsides for meteors, comets and asteroids, with the specific view of obtaining some information about the origin on meteors. Before considering the implications of these distributions, let us briefly review some of the evidence which links together the origin of shower meteors and short-period comets.

Showers have now been identified with 11 of the 19 known close approaches of short-period comets, if we accept the tentative identification of the Adelaide group 31.3 and comet Lexell 1770 I discussed in Section 11.7. Of the remaining 8 comets, 4 have predicted meteor radiants south of $\delta = -20^{\circ}$, where observations have not been made with the consistency given to the northern sky. Thus it is quite possible that more identifications will be made in the future as observations of both comets and meteors are continued.

Where there is an accepted association between a meteor shower and a comet, the two may have had a common origin, or, as in the case for Encke's comet and the Taurid stream, the meteors may have arisen from cometary ejection (Whipple and Hamid, 1950). The division and subsequent disappearance of Biela's comet after 1852, and the appearance in 1872 of a great meteor stream, subsequently named the Bielids, travelling in the same orbit has led to the belief that some showers are the result of the disintegration of a parent comet. Whatever the precise nature of the association there is no doubt that short-period comets and meteor streams are closely related.

Now consider the hypothesis that the non-shower meteors, i.e. the sporadic background, consist of a great number of unresolved minor streams. Why is the distribution of the line of apsides for these meteors not basically the same as that for the short-period comets, if these comets and meteor streams are closely related? It could be argued that as the distribution for shower meteors differs so markedly from that of the short-period comets, why should we

expect any similarity in the distribution for a great many unresolved showers forming the sporadic background? The answer to this is that the streams contributing to showers over one year are relatively few, and thus the distribution could well vary with time as suggested by McCrosky and Posen. However, the distribution for the sporadic background should follow the distribution of short-period comets much more closely due to the vastly increased number of showers used in the distribution. Therefore the lack of any agreement between the distributions of the line of apsides for short-period comets and non-shower meteors must be taken as evidence that the origin, or at least the subsequent evolution, of these meteors differs in some way to that of shower meteors.

It may be that some of these sporadic meteors have an origin associated with the long-period comets, for which there is no definite alignment of the longitude of perihelion with Jupiter. Additional evidence for this is given in the next section, where the subject of cometary association and orbit evolution is considered further.

13.6 K-index.

We have seen that the distribution of meteors in space is by no means simple. The distribution varies markedly with magnitude, and at the magnitude level of the Adelaide survey there appear to be two main classes of orbits. There are a large percentage of high eccentricity, direct short-period orbits of low inclination with aphelia just inside Jupiter. There is also a class of short-period low eccentricity orbits with inclinations centred on 60° and 150°. The latter class becomes more pronounced with fainter magnitudes; Hawkins (1962) has found evidence that this so called toroidal class is even more prominent at magnitude +11 and that the proportion of small orbits increases with fainter magnitudes.

Whipple (1954) devised a formula to aid in classifying the orbits of various bodies in the Solar system. His empirical "K" criterion is

$$K = \log_{10}\left[\frac{a(1+e)}{(1-e)}\right] - 1 \qquad \ldots \quad (5)$$

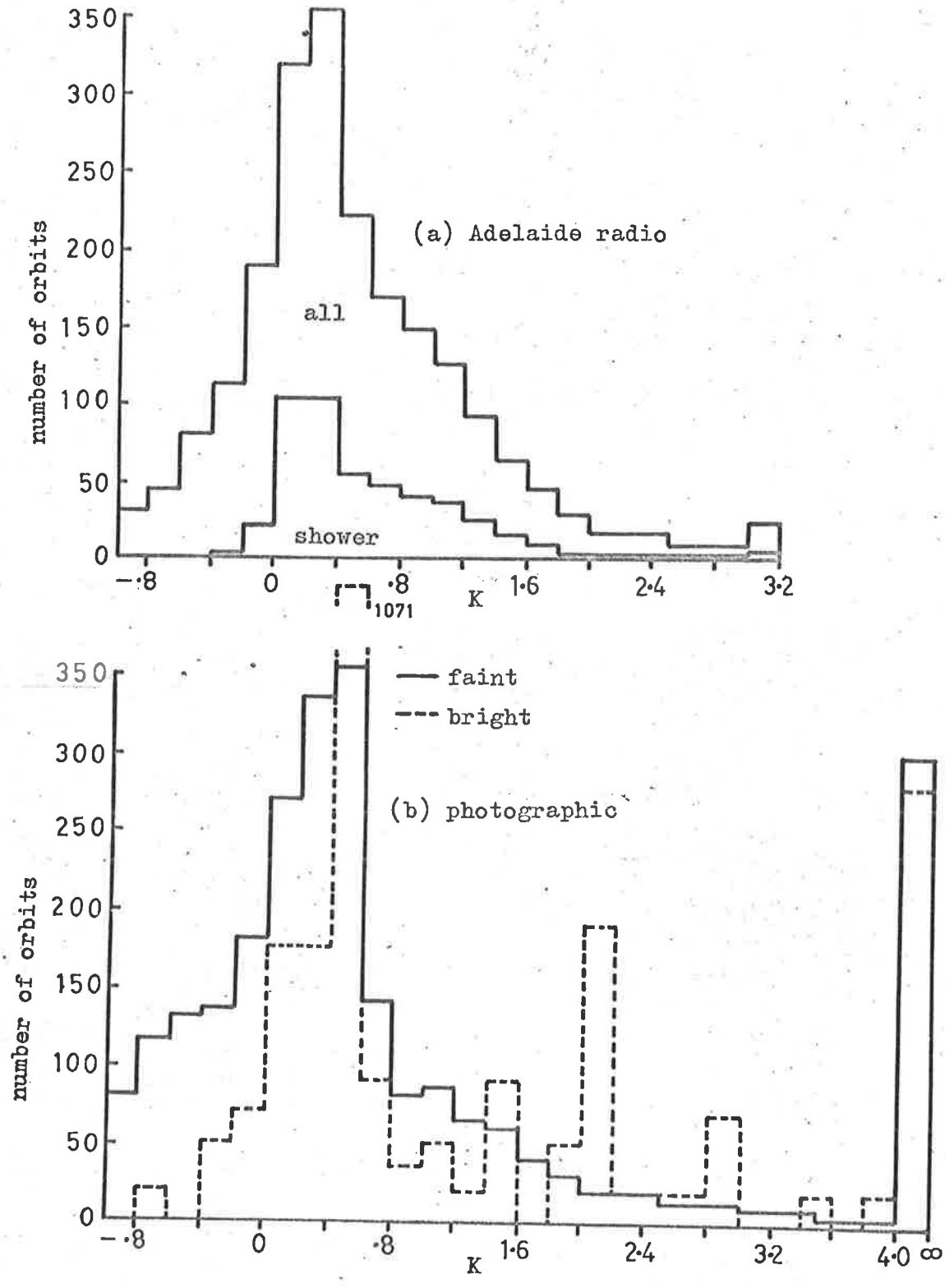

Figure 13.10 – Distribution of K – index

The bracketed quantity is the inverse square of the velocity at aphelion. Thus K tends negative for small orbits of low eccentricity. It is found that only three of the 1600 known asteroids have positive values for K. On the other hand, all of the 11 short-period comets with associated meteor streams have K positive, as do 75% of those comets with periods less than 25 years. Hence the K criterion can be used to separate between typical cometary and asteroidal type orbits. Only 5.6% of the 144 bright photographic meteors analysed by Whipple have K negative, which suggests a cometary origin for the great majority of these meteors.

McCrosky and Posen found that 25.5% of their orbits have negative K values. The figure for the Adelaide survey was comparable, 21.6% have negative K. This is a little lower than we might expect, in view of the fainter magnitude, but corresponds to a greater proportion of shower meteors observed and thus a smaller proportion of low eccentricity orbits. Only 5.3% of the 454 orbits with K negative belong to showers, and all of these have $K > -0.3$. The observed distribution with K index for all orbits and for shower orbits only is given in Figure 10a. It can be seen that the distribution for shower meteors is more asymmetric than that for all the meteors and lacks any significant number of negative K orbits. Here is further evidence of the difference between shower orbits and at least part of the sporadic background. The distribution for both bright and faint photographic meteors is shown in Figure 10b. These distributions are similar in shape to the Adelaide radio distribution, but the modal value for the latter is $K = +0.25$, compared with +0.5 for the two photographic distributions. As McCrosky and Posen have not given the distribution for shower meteors, it is difficult to determine the significance of this difference.

Although the orbits for which K is negative are generally termed "asteroidal", the K-index does not involve the orbital inclination, which obviously must be considered. Most asteroids have low inclination orbits, but the distribution with inclination given in Figure 11a shows that meteors with negative K orbits are by no means confined to the ecliptic plane. The two toroidal lobes are

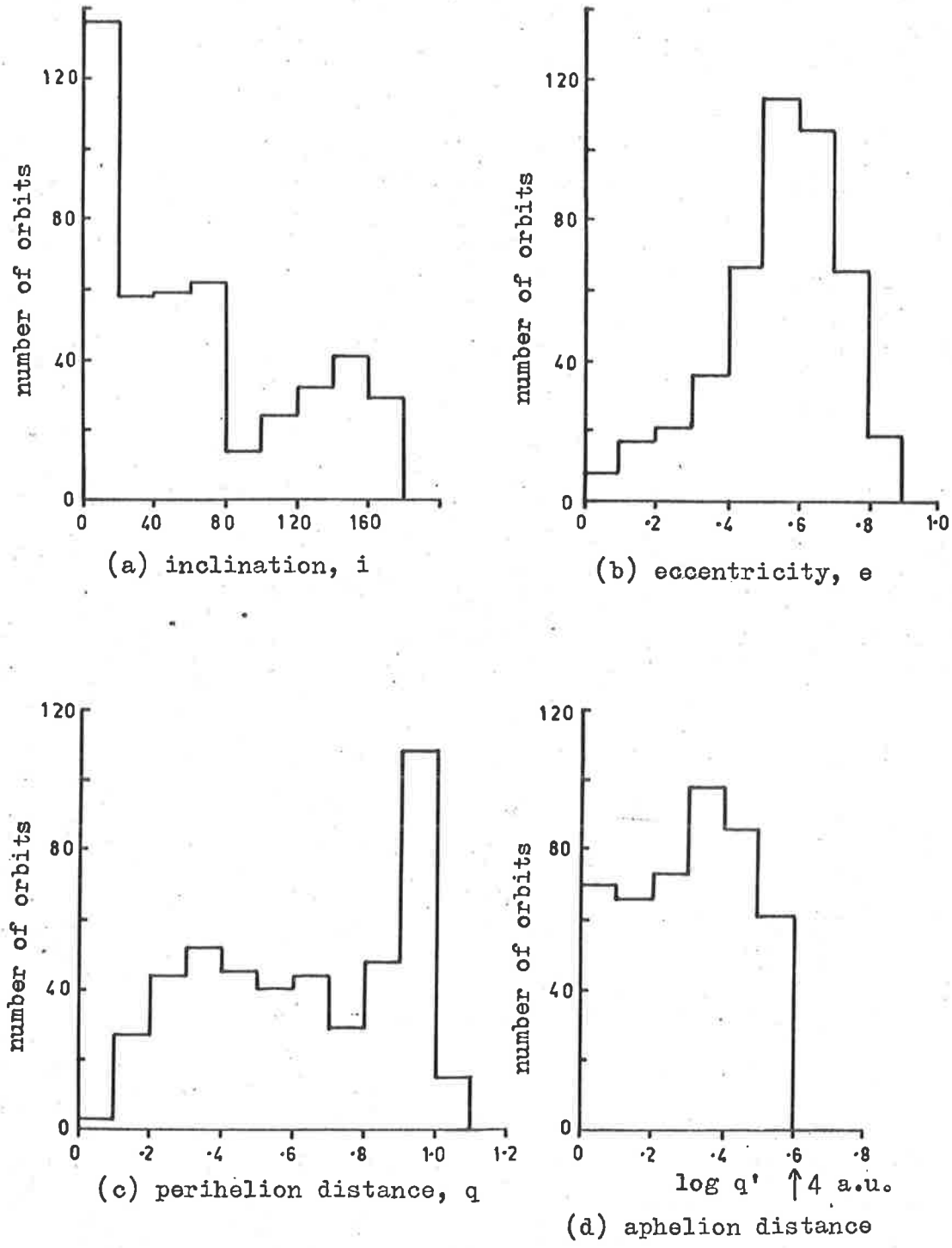

Figure 13.11 Distributions of negative-K orbits

well marked, and it is with no surprise that we find all the orbits contributing to these lobes (shown in Figure 2a) with $e < 0.5$ and $i > 30$ have K negative.

We shall now briefly consider the distributions of some of the other orbital elements for the meteors with K negative. The distribution with eccentricity (Figure 11b) has a modal value at $e = 0.55$, with no orbits for which $e > 0.9$. The observed distribution with perihelion distance (Figure 11c) shows a marked lack of orbits for which $q < 0.2$ a.u., otherwise it is reasonably uniform out to the earth's orbit. Corresponding to these distributions, there are no negative K orbits for which the aphelion distance $q' > 4$ a.u., although the observed distribution is reasonably uniform out to that limit. It is noteworthy that the distribution for shower meteors only reaches its maximum near $q' = 4$ a.u. and there are many orbits with aphelion distances out to 10 a.u.

13.7 Conclusions on the Origin of Negative-K Orbits.

We have seen in the last section that the spatial distribution of orbits with a negative K-index is quite distinct from that typical of shower meteors. The latter mostly travel in direct, low inclination orbits of high eccentricity, similar to those of the short-period comets, and typified by a positive K-index. On the other hand, the negative K orbits are generally smaller, more highly inclined, and of lower eccentricity. These meteors form part of the sporadic background and do not appear as showers. Although others have suggested an asteroidal origin for these meteors (e.g. Whipple, 1938) we shall show that a cometary origin is more plausible.

Were the meteors with negative K of an asteroidal origin, we would expect them to be solid particles with densities ~ 5 gm/cc. On the other hand, shower meteors of cometary origin are believed to mostly have much lower densities ~ 0.1 gm/cc and to consist of an agglomeration of dust particles cemented together with ices (Whipple 1951). The surface area/mass ratio G should thus be larger for shower meteors than for meteors of possible asteroidal origin. Now, measured decelerations and photographic light curves have revealed

no significant differences between the physical properties of known cometary meteors and bright meteors with negative K orbits. Both classes appear equally susceptable to fragmentation in the atmosphere during ablation. Thus we can conclude that meteors travelling in both positive and negative-K orbits have a similar physical form, possibly the fragile dust-ball construction postulated by Whipple.

Hawkins and Southworth (1958) consider that the proportion of meteors which fragment increases with fainter magnitudes. Therefore, as we have already noted that the proportion of orbits with negative K-index increases with fainter magnitudes, an asteroidal origin does not seem possible for these meteors, for if this were so, the proportion that fragment should decrease.

In seeking a cometary origin for these meteors with negative-K orbits, we must explain three facts:

(1) they do not appear as showers,

(2) the orbits have low eccentricity,

(3) the orbits may be highly inclined, e.g. the toroidal class.

Fact (2) suggests an origin which is associated with long-period orbits, so that the Poynting-Robertson effect may have time to reduce the eccentricity before the orbits are detectable at the Earth. Such an origin may also explain (1), as there would be more time for perturbations to gradually disperse any stream formation that may exist originally. Could it be that these low eccentricity orbits represent the fainter components of some streams of meteors which have been formed in long-period orbits, and perhaps contained both large and small particles of varying density? The Poynting-Robertson drift rate is proportional to the surface area/mass ratio, G. This means that for a given mass range, the low density and probably more fragile particles will suffer most from aphelion contraction until the orbits are of low eccentricity. The semi-major axis of the orbit will then decrease until the meteor spirals into the sun. During the latter stages of orbital contraction these orbits will have negative values of K. If this is so, we would expect to observe a high proportion of fragmentation among meteors of this class.

The value of G, and thus the drift rate increases with decreasing size, thus the proportion of both fragmentation and negative-K orbits should increase with fainter magnitudes. This is just what is observed by both radio and photographic techniques.

We have shown that the fact that the orbits of negative-K meteors are similar in shape to those of the asteroids is probably fortuitous. The observations are better fitted by a source associated with long-period orbits. The long-period comets are a possible source of meteoric material. Such a source would explain the last of our three facts - that the orbits may be highly inclined. The long-period comets are more uniformly distributed with inclination than those of short-period, and the high inclination members of the former may well be the source of material for the toroidal class of meteors. These meteors could not have originated with the short-period comets, as the latter show a strong preference for low inclination orbits, and perturbations by Jupiter would only further decrease the inclination of any ejected meteors.

Supposing a long-period comet did eject some meteoric material into an orbit similar to its own, the more massive component of the stream would only drift toward the sun relatively slowly compared to the smaller, less dense meteors. After a certain lapse of time the massive component will still be travelling in a high eccentricity orbit and will be recognisable as a stream, whereas the meteors of greater surface area/mass ratio, which have suffered most from Poynting-Robertson drift, will have separated from each other in space by larger absolute distances. The separation will depend on the exact value of G for each meteor. This would explain why showers are not observed amongst meteors travelling in negative-K orbits, and are more prominent among the brighter, more massive meteors.

13.8 Some Present and Future Work

The distribution in space of the sporadic background, particularly of the meteors in orbits of negative K, should be ameniable to a mathematical study in terms of the evolutionary

processes suggested in the last section. Recently Briggs (1962) set up a model for the steady state spatial distribution of particles in the solar system. This was based on the assumption that matter was being continuously injected according to a definite distribution function and continuously exhausted by the operation of the Poynting-Robertson effect alone. The steady-state density of particles at any point in space was calculated using Haug's integral (1958), which assumes a uniform distribution with the longitude of the ascending node Ω, and the longitude of perihelion π, and that the number of particles passing through perihelion per unit time is constant. The injection function was based on a random selection of 359 photographic meteors by Hawkins and Southworth (1961). Briggs assumed that particles of all sizes are continuously injected into the system with a certain mass distribution and the same spatial distribution function. One reason behind this system of injection is that comets shed both small and large particles, and that large particles themselves will eventually break up into smaller ones.

With this model, Briggs has been able to explain some of the observed features of the zodiacal light, and a mathematical study of this kind is undoubtably of great value in attempting to understand the distribution of particles in the Solar system. This work must be regarded as a major step forward. However, Briggs himself realises that many of his assumptions are not in accord with reality. For example, no allowance has been made for the perturbing action of Jupiter, which certainly plays a large part in the true spatial distribution of meteors in the Solar system. Let us consider in detail the influence of this planet. Opik (1951) has discussed the probability of collision of a meteor, in a contracting orbit, with one of the planets. The probability is much larger for Jupiter than for any other planet, and is greatest for meteors in orbits that lie near the plane of Jupiter's orbit (approximately the ecliptic plane). Further, it increases with the size of the meteor. Davies and Gill have extrapolated Opik's results, which refer to meteor orbits of low eccentricity and

inclination 10°, to include other inclinations. Their conclusions are extremely pertinent, and are given here in full.

"If the surface area/mass ratio for the radio and photographic meteors may be assumed to be 50 cm^2/gm and 5 cm^2/gm respectively, the destruction of almost all the photographic meteors with orbital inclination less than 40°, or greater than 165° will be likely by collision with Jupiter. For radio meteors, which drift more rapidly towards the Sun, the figures are 15° and 175°.

Apart from those actually captured, many more meteors will be perturbed into modified orbits. Faint meteors in orbits of inclination near 90° have the smallest chance of collision, and may often reach orbits wholly within Jupiter's after suffering only minor perturbations. The perturbations will tend to reduce the angle between the orbital plane and the ecliptic, so that the number of meteors in orbits with inclination 90° will be diminished. When their orbits have contracted further, so that collisions with the earth are possible, the meteors may be observed. The orbits will be nearly circular, and have inclinations well away from the ecliptic.

Bright meteors, and faint meteors in orbits lying closer to the plane of the ecliptic, are likely to suffer major perturbations before their orbits can contract sufficiently to escape from Jupiter's vicinity. The perturbed orbits may be expected to be predominantly direct and of low inclination, and to have aphelia near Jupiter's orbit, in the same way as do the orbits of short-period comets. If the orbits are sufficiently eccentric, so that their perihelia are within the Earth's orbit, they may be observed without further change.

In the case of the bright meteors the Poynting-Robertson drift is sufficiently slow for a 'Jupiter family' of orbits, similar to those of the comets, to be formed. The planet then retards the further contraction of the orbits, so that at any time there are likely to be few bright meteors in orbits of shorter period. Faint meteors also may be retained in the group as long

as their perihelia are far from the Sun so that their drift is slow. That these orbits are not observed probably indicates that the perihelion has to be outside the Earth's orbit for this to happen. Faint meteors in orbits with short perihelion distances will not be retained by the group, and may be observed at any stage of their subsequent contraction until their aphelia pass within the orbit of the earth.

On the basis of this model, the following orbits might thus be expected:

For bright meteors

(1) Some randomly distributed orbits of long period, which have not yet suffered close approaches to Jupiter.

(2) A group of orbits like those of the short-period comets, which have been formed from the long-period orbits by the action of Jupiter.

For faint meteors

(1) Some long-period orbits.

(2) Orbits of very short-period, that are almost circular. These should be rare at inclinations 0°, 90° and 180°.

(3) Direct orbits of low inclination and high eccentricity, many with very short periods, formed from long-period orbits after major perturbation by Jupiter. The 'Jupiter group' of orbits will not be prominent.

The main differences between the photographic and radio results thus appear to be explicable, at least quantitatively, in this way."

From these conclusions it can be seen that a model which does not include Jupiter cannot be used to predict anything but the most general features of the spatial distribution of meteors. The Poynting-Robertson effect alone cannot cause perturbations in inclination, yet the distributions with inclination for the bright and faint meteors are quite different.

There are obvious limitations in using the observed distribution for bright photographic meteors as an injection function to determine what should be the observed distribution for

meteors of all sizes. We have also mentioned the non-uniformity of both the observed and corrected distributions with the argument of perihelion for the Adelaide results. This would limit the application of Haug's integral. As a point of interest, too, it is not necessary to assume that the present observed distribution of meteors is due entirely to cometary injection. We have seen that the time taken for radio meteors of magnitude +6 to spiral into the Sun from a circular orbit of radius R a.u. is $\backsim 10^6.R^2$ years. If the age of the Solar system is assumed to be 10^{10} years, the initial radius of an orbit created with the Solar system and at present near the Sun must have been $\backsim 10^2$ a.u. This distance would be greater for fainter meteors, but Oort (1950) has suggested that the distribution of comets may extend out to distances of the order of 10^5 a.u. Thus, we cannot exclude the hypothesis that some of the faint meteors now observed travelling in near circular orbits originated at the birth of the Solar system. However, the observed distribution with eccentricity for the various magnitude ranges indicates a more recent origin for the bright meteors.

The origin of the toroidal class of low eccentricity, high inclination orbits which become more prominent with fainter magnitudes, cannot be easily explained by the theory of ejection from short-period comets. We have shown that ejection from long-period comets, however, could account for this class of meteors. Furthermore, the perihelia of these comets show no tendency to align with Jupiter, which would explain the lack of alignment observed for non-shower meteors (Section 13.5).

In view of the facts discussed in this section, it would seem better to use the observed distribution of comets as the basis for an injection function for a model of the type proposed by Briggs. With the aid of a large digital computor it should be possible to simulate the Poynting-Robertson effect and also the action of Jupiter on continuously injected meteors; then both the evolution with time of certain orbits and the steady-state spatial distribution could be studied. By varying the injection rate as a function of mass it would also be possible to study the resultant distribution for

various magnitude ranges. The necessity of this procedure is indicated by the different distributions found by the various surveys for different magnitude meteors. For example, the injectio function based on photographic meteors used by Briggs contained a term F(q) for the distribution with perihelion distance. The function used followed the trend found for photographic meteors, however we have shown that this certainly does not apply to radio meteors only a few magnitudes fainter.

To conclude, we have shown that the Adelaide survey has contributed significantly to our experimental knowledge of the distribution of meteoric particles in the Solar system. Besides adding to the detailed mapping of the streams which intersect the Earth's orbit, we have raised some important new points in regard to the distribution and origin of sporadic meteors.

REFERENCES

ALMOND, M.(1952).- Jodrell Bank Annals, 1:22

ASPINALL, A., and HAWKINS, G.S.(1951).-Mon. Not. R. Astr. Soc. 111:18

BALDET, F., and DE OBALDIA, G.(1952).-466 a 1952 Paris Obs., Sect Astrophys. de Meudon, 59 pp.

BRIGGS, R.(1962).-Astron. J.67:710

DAVIES, J.G., and GILL, J.C.(1960).-Mon. Not. R. Astr. Soc. 121:437

ELLYETT, C., and ROTH, K.(1955).-Aust. J. Phys. 8:390

HAUG, U.(1958).- Z. Astrophys. 44:71

HAWKINS, G.S.(1956).-Mon. Not. R. Astr. Soc. 116:92

HAWKINS, G.S.(1956).- Astrophys. J. 124:311

HAWKINS, G.S.(1962).- Astron. J. 67:241

HAWKINS, G.S., and PRENTICE, J.P.M.(1957).- Astron. J. 62:234

HAWKINS, G.S., and SOUTHWORTH, R.B. (1958).-Smith. Contr. to Astrophys. 2:349

HAWKINS, G.S., and SOUTHWORTH, R.B. (1961).-Smith. Contr. to Astrophys. 4:85

HERLOFSON, N.(1948).-Rep. Phys. Soc. Prog. Phys. 11:444

HUXLEY, L.G.H.(1957).- "Annals of the I.G.Y." (Pergamon Press:London.)

JACCHIA, L.G.(1949).- Harvard College Obs. and Centre of Analysis of Mass. Inst. of Tech. Rep. No.3

KAISER, T.R.(1953).- Advanc. Phys. 2:495

KAISER, T.R.(1955).- "Meteors". (Pergamon Press: London.)

LAZARUS, D., and HAWKINS, G.S.(1962).- Smith. Contr. to Astrophys. (in press)

LOVELL, A.B.C.(1954).- "Meteor Astronomy".(Clarendon Press: Oxford.)

MAINSTONE, J.S.(1958).-"Radio Measurements of Meteor Velocities". Ph.D. Thesis, Adelaide University

MAINSTONE, J.S.(1960).- Mon.Not. R. Astr. Soc. 120:517

MASS. INST. of TECH.(1953).- "Priciples of Radar" (McGraw-Hill)

McCROSKY, R.E., and POSEN, A.(1959).- Astron. J. 64:25

McCROSKY, R.E., and POSEN, A.(1961).- Smith. Contr. to Astrophys. 2:15

McKINLEY, D.W.R.(1951).- Astrophys. J. 113:225

McKINLEY, D.W.R.(1961).- "Meteor Science and Engineering". (McGraw-Hill)

McNAMARA, A.G.(1961).- Canad.J. Phys. 39:625

MEEK, M.L., and JAMES, J.C.(1959).- J. Atmos. Terr. Phys. 16:228

MILLMAN, P.M., and McKINLEY, D.W.R.(1956).- Canad. J. Phys. 34:50

MURRAY, E.L.(1961).- "An Experimental Study of the Upper Atmosphere". Ph.D. Thesis, Adelaide University.

NILSSON, C.S., and WEISS, A.A.(1962).- Aust. J. Phys. 15:1

OORT, J.H.(1950).- Bull. Astr. Inst. Netherlands, XI:91

OPIK, E.(1951).- Proc. Roy. I. Acad. 54A:165

PORTER, J.G.(1949 and 1952).- "Comets and Meteor Streams". (Chapman and Hall: London)

POYNTING, J.H.(1903).-Phil. Trans. Roy. Soc. A202:525

ROBERTSON, H.P.(1937).- Mon. Not. R. Astr. Soc. 97:423

ROBERTSON, D.S., LIDDY, D.T., and ELFORD, W.G.(1953).- J. Atmos. Terr. Phys. 4:225

VARADY, L.(1956).- Radio, Television and Hobbies, 18 Aug: 32

WEISS, A.A.(1957).- Aust. J. Phys. 10:77

WEISS, A.A.(1958).- Aust. J. Phys. 11:591

WEISS, A.A.(1959).- Aust. J. Phys. 12:116

WEISS, A.A.(1960a).- Mon. Not. R. Astr. Soc. 120:387

WEISS, A.A.(1960b).- Mon. Not. R. Astr. Soc. 121:5

WHIPPLE, F.L.(1938).- Proc. Amer. Phil. Soc. 79:499

WHIPPLE, F.L.(1951).- Astrophys. J. 113:464

WHIPPLE, F.L.(1954).- Astron. J. 59:201

WHIPPLE, F.L.(1955).- Astrophys. J. 121: 249

WHIPPLE, F.L., and HAMID, S.E.D.(1950).-Sky and Telescope, 9:248

WHIPPLE, F.L., and HAWKINS, G.S.(1959).- Handbuch der Physik, 52:519

WRIGHT, F.W., and WHIPPLE, F.L.(1950).- Tech. Rep. Harv. Coll. Obs. No. 6